NARROWING OF THE *SLES1* INTERVAL REVEALS COMPLEX EPISTATIC INTERACTIONS IN THE SUPPRESSION OF AUTOIMMUNITY

APPROVED BY SUPERVISORY COMMITTEE

Edward K. Wakeland, Ph.D

Chandra Mohan, Ph.D., M.D.

Anne Satterthwaite. Ph.D.

Andrew Zinn, Ph.D., M.D.

Nancy Olsen, M.D.

Dedicated, with grateful appreciation,

to all of my incredibly supportive friends and family,

especially my husband, Hayden, and parents, John and Nancy Bliss

And

In memory of Karis M. Hughes,

who through many years of friendship, support and intellectual discussions

greatly contributed to and improved this body of work

Narrowing of the *Sles1* Interval Reveals Complex Epistatic Interactions in the Suppression of Autoimmunity

By

Katherine Ann Belobrajdic

DISSERTATION

Presented to the Faculty of the Graduate School of Biomedical Sciences

The University of Texas Southwestern Medical Center at Dallas

In Partial Fulfillment of the Requirements

For the Degree of

DOCTOR OF PHILOSOPHY

The University of Texas Southwestern Medical Center at Dallas

Dallas, Texas

May 2010

Narrowing of the *Sles1* Interval Reveals Complex Epistatic Interactions in the Suppression of Autoimmunity

Publication No.

Katherine Ann Belobrajdic

The University of Texas Southwestern Medical Center at Dallas, 2010

Supervising Professor: Dr. Edward K. Wakeland, Ph.D.

Sle1 is a potent susceptibility locus for spontaneous systemic autoimmunity derived from the NZM2410 mouse strain. The NZW-derived suppressive modifier locus, *Sles*1, specifically prevents the spontaneous loss in tolerance mediated by the B6.*Sle1* congenic. *Sles1* had previously

been fine-mapped to a remarkably gene-rich region on murine chromosome 17 containing nearly 70 genes. A series of mouse strains were constructed with a variety of suppressive and non-suppressive variants of *Sles1* on the B6.*Sle1* genomic background which have revealed multiple layers of epistatic gene interactions within the *Sles1* interval. Phenotyping of a truncated recombinant interval mapped the *Sles1* phenotype to an approximately 638 KB segment, which combined with genomic and expression analysis, suggested *Btnl2* and the *H2* genes are strong candidates for *Sles1*. Finally, further characterization of the *Sles1* interval has revealed an allele-specific and tissue-specific reduction of major histocompatibility complex (MHC) Class II molecules on the surface of B cells, as well as a possible role for follicular helper T cells in the development of *Sle1*-mediated autoimmunity. Understanding how *Sles1* and other modifiers suppress systemic autoimmunity will reveal important insights for developing therapeutic strategies for systemic lupus eythematosus (SLE).

TABLE OF CONTENTS

PRIOR PUBLICATIONS

Limaye N, **Belobrajdic KA,** Wandstrat AE, Bonhomme F, Edwards SV, Wakeland EK. Prevalence and evolutionary origins of autoimmune susceptibility alleles in natural mouse populations. Genes and Immunity, 2008. 9(1): 61-8.

O'Shea B, Khare S, **Bliss K,** Klein P, Ficht TA, Adams LG, Rice-Ficht AC. Amplified fragment length polymorphism reveals genomic variability among *Mycobacterium avium* subsp. *paratuberculosis* isolates. *Journal of Clinical Microbiology.* 2004. 42(8): 3600-6.

Hill KK, Ticknor LO, Okinaka RT, Asay M, Blair H, **Bliss KA,** Laker M, Pardington PE, Richardson AP, Tonks M, Beecher DJ, Kemp JD, Kolsto AB, Wong AC, Keim P, Jackson PJ. Fluorescent amplified fragment length polymorphism analysis of *Bacillus anthracis, Bacillus cereus,* and *Bacillus thuringiensis* isolates. *Applied and Environmental Microbiology.* 2004. 70(2): 1068-80.

Bliss, Katherine A. Genetic diversity of *Brucella abortus* isolates as determined by amplified fragment length polymorphism (AFLP) analysis. *Undergraduate Thesis.* Texas A&M University. 2003.

Bliss, Katherine A. Evolution of virulence in Bacillus anthracis. *TAMU Undergraduate Journal of Science.* 2002. 3(1): 45-47.

LIST OF FIGURES

LIST OF TABLES

LIST OF ABBREVIATIONS

ANA anti-nuclear antibodies

APC antigen presenting cell

BCR B cell receptor

GN glomerulonephritis

ITIM immunoreceptor tyrosine-based inhibitory motif

ITSM immunoreceptor tyrosine-based stimulatory motif

MFI median fluorescence intensity

MHC major histocompatibility complex

NS not significant

SLE systemic lupus erythematosus

SNP single nucleotide polymorphism

TCR T cell receptor

T_{FH} follicular helper T cell

CHAPTER ONE

Introduction

Systemic Lupus Erythematosus

Systemic lupus erythematosus (SLE) is an autoimmune disease characterized by the production of antinuclear antibodies (ANAs), immune complex deposition and resulting systemic tissue destruction. The organs primarily affected are the cerebrovascular system and kidney (reviewed in [1, 2]). The clinical presentation of SLE is remarkably heterogenous, with an array of possible complaints including serositis, oral ulcers, non-erosive arthritis, photosensitivity, blood disorders, renal dysfunction, a wide spectrum of ANA specificity, neurological disorders, malar rash, discoid rash and other abnormal immunological features. The presence of four of the above symptoms is sufficient for a diagnosis of SLE according to the recommendations of The American College of Rheumatology [3, 4]. A positive ANA test is the most sensitive criterion, present in nearly all SLE patients, but is not the most specific criterion, as 3-5 percent of healthy people also have ANA [4]. Despite these clear guidelines, the timely diagnosis of SLE is still a challenge, as many of these complaints are non-specific and may initially be very mild.

The incidence of SLE varies widely among geographic and ethnic populations, and ranges between 1 and 11 cases per 100,000 people per year [1, 2, 5]. These population-specific differences, along with discrepancies in study designs make it difficult to clearly document the occurrence of SLE, but the rates of incidence and prevalence appear to be increasing, while morbidity is decreasing. These changes can probably be attributed to improved laboratory tests which allow for the identification of milder cases of SLE and moderate improvements in the treatment of SLE. There is a consistently strong gender bias with approximately 90% of human lupus patients being female. SLE is more common and more severe in non-Causcasians, including African-American, Afro-Caribbean, Asian, Native American and Hispanic-American populations [1, 2, 5-7].

Susceptibility to SLE is an extremely complex phenomenon with numerous gene-gene and gene-environment interactions each influencing the initiation and development of the disease. Although there are rare examples of severe single-gene defects resulting in SLE, the vast majority of susceptibility genes are inherited as a multigenic threshold liability, in which susceptibility alleles at loci scattered throughout the genome contribute to disease liability. SLE-associated polymorphisms also tend to occur in immunoregulatory genes. Mouse models of SLE have demonstrated that epistatic interactions between susceptibility, and even

suppressor, loci do occur. Furthermore, several potent murine autoimmune susceptibility alleles are very common among laboratory mouse strains, yet only cause disease when expressed in specific combinations. Together, these findings suggest that susceptibility to autoimmunity may often result from imbalances in immune regulation mediated by unfortunate combinations of “good” alleles, rather than by categorically deleterious mutations. It is not surprising then that the individual contribution of these risk alleles is often very difficult to characterize, particularly when further complicated by environmental factors implicated in SLE pathogenesis, such as ultraviolet light, exogenous sex hormones, industrial irritants, smoking, infections, and socioeconomic factors. Nonetheless, human and murine research continues to elucidate the role of genetics in this convoluted process which may identify novel therapeutic pathways.

Genetics of SLE

Human SLE Genetic Research

Single nucleotide polymorphism (SNP) association studies have primarily been used to investigate the genetic predisposition to disease in human SLE. In genome-wide association studies, SNPs are genotyped and compared in large groups of SLE patients, first degree relatives and

healthy controls. The complexity and heterogeneity of human genomes, particularly in blended ethnicities, as well as confounding non-genetic factors, significantly impede the ability of these studies to clearly identify genes contributing to SLE susceptibility. As a result, extremely large numbers of samples are required to ensure a high enough power to reliably detect SLE-associated loci. Despite advances in sequencing technology, the logistical and analytical demands of these experiments are daunting and typically require multi-institution collaborations. Recently, a new research approach called “admixture mapping” has been introduced which takes advantage of the diverse frequencies of SLE risk alleles between ancestral populations to gain power in association studies (reviewed in [8]). Once a gene is suspected of contributing to human SLE, a candidate-gene study can be completed which will more finely map the association with SLE with denser SNPs or will investigate the functional significance of risk alleles. Although improvements in study feasibility and design have begun to compensate for some of the complexity of the human genome, SLE genetic research approaches in humans remain limited.

Mouse Models of Spontaneous Lupus

To complement human SLE studies, homogenous inbred murine models of spontaneous lupus eliminate the complexity of the human genome, while enabling the use of genetic manipulation to address specific questions. In general, these models are characterized by serum antinuclear antibodies, B cell hyperactivity, splenomegaly and immune complex-mediated glomerulonephritis (GN), while displaying differences in onset age, gender bias, autoantibody specificity and organ involvement. This diversity mimics the spectrum of human lupus presentation and is consistent with the complex etiology of SLE. For most of these models, the maximum level of ANAs and circulating immune complexes occurs at the same age as a 50% mortality rate [9], suggesting that the final stages of murine SLE reflect similar cellular processes and thresholds for survival, despite differences in the initiation and development of disease. Association studies were also initially completed in a number of mouse strains prone to spontaneous lupus which identified loci for further research (reviewed in [10]).

During the derivation of the MRL strain from LG/J, AKR/J, C3H/Di and C57BL/6J mice, a subset of mice began to sponteanously develop auto-antibodies, massive lymphadenopathy and severe GN. A recessive mutation named *lpr*, was shown to be located in *fas*, a gene with a critical role in initiating cellular apoptosis [11, 12]. The *lpr*-mediated *fas*

dysfunction results in defective negative selection [13] and lymphocyte homeostasis [14], which subsequently leads to a loss of self-tolerance and the induction of autoimmunity. *Fas*^{lpr} is sufficient to produce mild lupus in multiple mouse strains, including strains that are not otherwise predisposed to develop autoimmunity [15].

The BXSB lupus model, derived from the B6 and SB/Le strains, is unusual in that males, and not females, are affected with a particularly early-onset and severe lupus-like syndrome. This atypical gender bias is due to a susceptibility loci on the Y-chromosome called *yaa*, or *Y-linked autoimmune accelerator*, which has recently been demonstrated to be a translocation of Toll-like receptor 7 (TLR7) [16-19]. This results in continuous activation of the innate immune system which exacerbates disease in numerous murine models of lupus but unlike *lpr*, is not sufficient to initiate autoimmunity in non-autoimmune mouse strains (for a review, see [20]). The phenotype of *yaa* is also characterized by massive enlargement of lymph nodes and spleen, as well as extreme monocytosis.

Unlike MRL.*Fas*^{lpr} and BXSB mice, mouse strains derived from New Zealand Black (NZB) and New Zealand White (NZW) reflect SLE as a complex disease, a multifaceted process of cooperative genetic loci and environmental factors. NZB and NZW each develop late-onset mild autoimmunity, but their F1 progeny (BWF1) have severe lupus

phenotypes at earlier ages [21]. Numerous linkage studies have cumulatively demonstrated significant associations on at least 10 autosomal chromosomes from both the NZW and NZB genome (reviewed in [10]). There are other susceptibility loci in the MRL.*Fas*^{lpr} and BXSB genomes as well. This illustrates how the interaction of genetic loci, rather than a single, deleterious gene, can result in SLE.

NZM2410, an inbred mouse strain that was further derived from BWF1 backcrossed to NZW, spontaneously develops ANAs by 4-6 months and lupus nephritis by six months [22]. Linkage analyses of (NZM2410 x B6) F1 backcrossed to NZM2410 identified numerous loci associated with disease susceptibility, termed *Sle1, Sle2,* and *Sle3,* and located on chromosomes 1, 4, and 7 respectively [23]. Additionally, heterozygosity on chromosome 17 was associated with SLE, and termed *Sle4*. These studies also clearly demonstrated a threshold liability model, in which disease incidence increased as susceptible genetic loci accumulated [22, 24]. To better understand the individual phenotypic contribution, each locus was also introgressed onto the B6 genome, generating a series of congenic strains.

As B6.*Sle1* mice age, they develop significant SLE disease pathology with a high degree of penetrance. By 9 months of age, nearly 80% of B6.*Sle1* mice make high levels of IgG ANA. Although these mice

do not develop GN, they do have mild splenomegaly and significantly increased activation of splenic B and T lymphocytes [23, 25]. Experiments with mouse models lacking in B and T cells have demonstrated that while *Sle1* B cells alone break tolerance to chromatin and *Sle1* T cells alone have heightened activation and cytokine production, *Sle1* must be present in both compartments for the production of pathogenic IgG ANAs [26]. *Sle1*-mediated autoimmunity can transition to fatal lupus with severe GN with the addition of other autoimmune prone loci, such as *Sle3/5* [24], Fas^{lpr} [27], and *yaa* [28].

Further fine-mapping revealed that a sub-locus, *Sle1b*, was able to recapitulate the majority of the *Sle1* phenotype [29]. Recent studies strongly suggest that *Ly108* is the causative gene of *Sle1b* [30, 31]. *Ly108* is a member of the *SLAM/CD2* family of receptors which, along with intracellular signaling adaptors, regulate lymphocyte-lymphocyte interactions and have been implicated in autoimmunity (reviewed in [32]). The functional effects of the *Sle1b* allele of *Ly108* will be discussed in more detail below.

Many of the SLE susceptibility loci identified in the NZM2410 backcross linkage analyses were derived from NZW, a strain with late-onset mild autoimmunity strain, suggesting the presence of suppressor loci within the NZW genome. In an attempt to find these modifying genes,

B6.*Sle1* mice were backcrossed to NZW for linkage analysis. Unfortunately, these F1 hybrid mice developed severe autoimmunity, mediated by *Sle1* homozygosity on a B6/NZW heterozygous background. This and later data would demonstrate that these NZW-derived suppressor loci act recessively. Four of these loci were identified through linkage analysis of (B6.*Sle1* x NZW) F1s backcrossed again to NZW and termed *Sles1-4*. The most potent of these intervals was *Sles1*, located on chromosome 17 near the MHC Class II complex and marker D17Mit34 in an area previously identified as *Sle4* [33]. Bi- and tri-congenic mice demonstrated that *Sles1* specifically interacts with *Sle1* to prevent the loss of tolerance to chromatin and thus subsequent phenotypes and autoimmune disease [34] even with the addition of *yaa*-mediated acceleration [19].

Fine-mapping efforts have identified successively smaller *Sles1* intervals, with the most recent interval termed $Sles1^{(28\text{-}83)}$ encompassing an approximately 1083 KB region. The $Sles1^{(28\text{-}83)}$ region (referred to as *Sles1* for the remainder of this manuscript) excludes *TNF-a*, yet includes the *H-2* gene complex, the butyrophilin-like gene family and several complement genes [35] (Figure 4B). This region is incredibly gene dense and includes 67 genes, many with known immunological functions.

Classic genetic complementation experiments have suggested that the 129 genome also contains a NZW-like suppressive *Sles1* allele [35].

Further phenotypic characterization of *Sles1* has provided insight into possible mechanistic pathways. Despite the dramatic suppression of cell surface activation markers in B lymphocytes in B6.*Sle1Sles1* mice, intracellular levels of phosphorylated ERK are elevated, suggesting that *Sles1* acts downstream of ERK to modulate B cell activation [35]. Similarly, *Sles1* has no effect on *yaa*-mediated elevated *Tlr7* expression or response to TLR7 stimulation, but potently suppresses the development of autoimmunity in B6.*Sle1yaa* mice [19]. This data illustrates the remarkable ability of *Sles1* to strongly modulate immunity in the context of dysregulated ERK and TLR7 signaling pathways. Finally, B6.*Sle1Sles1* mice do not produce either IgG or IgM ANAs [35], eliminating the simplistic and appealing theory that *Sles1* acts to limit pathogenic ANAs by drastically limiting T cell help to B cells. Despite these advances, the sheer number of immunologically relevant genes in the *Sles1* interval, along with the vast phenotypic differences between B6.*Sle1* and B6.*Sle1Sles1,* have made the identification of the causative gene(s) of *Sles1* difficult.

Sles1 can robustly suppress the development of SLE in B6 mice carrying both the *yaa* and *Sle1* loci, alleles which perturb the innate and

adaptive immune systems respectively. However, as *yaa* only accelerates autoimmunity in combination with strong SLE risk loci, and *Sles1* has no impact on proximal TLR7 signaling, it is likely that *Sles1* primarily acts to suppress *Sle1* and consequent *yaa*-mediated phenotypes as well, rather than directly affecting both susceptibility loci. Functional data suggests that *Sles1* introduces a compensatory downstream mechanism which modulates the responses of these immunological compartments, rather than the underlying genetic lesions. We will review innate and adaptive immune system genes below that have been associated with SLE to provide an understanding of the cellular environment in which *Sles1* functions.

Dysregulated Innate Immune System Signaling

The innate immune receptors are able to rapidly respond to microbes by recognizing broad classes of conserved pathogen-associated molecular patterns or PAMPs. This system allows for the immediate initiation of innate immune defenses but has a limited capacity to generate the microbe-specific immune responses that may be necessary to clear pathogens. Instead, the products of innate immune activation assist the adaptive immune system in generating a more potent and targeted immune response.

The family of Toll-Like Receptors (TLRs) is a canonical example of innate immunity. After recognition of its specific PAMP, each TLR is capable of inducing signal cascades that produce a semi-targeted, rapid, program of pro-inflammatory cytokines. For example, TLR7 recognizes a viral motif, single-stranded RNA, and initiates an anti-viral response through the production of the type I interferons, IFNa and IFNb. There has been an increasing amount of data implicating the pro-inflammatory type I interferon, IFNa, as a contributor to SLE pathogenesis (reviewed in [36]). Multiple studies have identified an IFN gene signature in peripheral blood from SLE patients, especially in patients with more severe disease [37, 38]. Others have demonstrated that sera from SLE patients can stimulate the production of IFNa [39]. Wakeland and colleagues have shown that in a murine model of spontaneous autoimmunity, IFNa exacerbated kidney nephritis [40]. In a similar mouse model, a deficiency in the type I interferon receptor significantly reduced lupus-like phenotypes in a gene-dose dependent manner [41].

The Y-chromosome autoimmune accelelerator, *yaa*, is not capable of initiating autoimmunity, but significantly enhances SLE-like phenotypes when combined with many models of murine SLE (for a review, see [20]). A translocation of TLR7 to the Y chromosome has been shown to be responsible for the majority of the *yaa*-mediated accelerated SLE

phenotype in murine models [16-19]. In addition, lupus nephritis is attenuated in TLR7-deficient MLR*Fas*^{lpr} lupus-prone mice [42]. The expression of TLR7 is also up-regulated in peripheral blood mononuclear cells (PBMCs) from SLE patients, compared with healthy controls [43]. In addition to affecting interferon expression, stimulation of TLR7 can significantly influence B cell activation [44], but in an type I interferon receptor-dependent manner [45, 46].

Tyk2, a member of the Janus tyrosine kinase (JAK) family, is constitutively associated with the cytoplasmic tail of the type I interferon receptor which is also stimulated by IL-12 and IL-23. Upon binding of type I interferon, the receptor dimerizes, which allows the JAKs to cross-phosphorylate and initiate interferon signal transduction. SNPs in *Tyk2* have been linked to human SLE in several targeted association studies [47-50], but not in two major genome-wide association studies [51, 52]. Only one of the assayed SNPs, rs2304256, was consistently associated with disease [48-50]. This non-synonymous SNP is located in the JH4 domain, a region which may be important in stabilizing the interferon receptor complex [53]. Another non-synonymous *Tyk2* polymorphism, E775K, arose spontaneously in B10.Q/J mice and resulted in an impaired Th1 immune response, susceptibility to *Toxoplasma gondii* [54], and resistance to autoimmune arthritis and experimental allergic

encephalomyelitis (EAE). However, when B10.Q/J mice were treated with pertussis toxin, a strong stimulator of the innate immune system, they were no longer resistant to autoimmunity [55]. These murine studies are consistent with a role for *Tyk2* mutations in human SLE.

Activated *Tyk2* recruits & phosphorylates STAT4, which subsequently dimerizes and translocates to the nucleus to up-regulate Th1 cytokines. A SLE-susceptible STAT4 haplotype has been associated in numerous studies of human patients representing multiple ethnicities [50-52, 56-61]. The STAT4 risk allele has been correlated with increased STAT4 expression [56, 60], increased sensitivity to IFNa signaling [58] and severe lupus nephritis [62]. In different New Zealand-derived mouse models, STAT4 deficiency has been shown to enhance [63] and, paradoxically, attenuate [64] autoimmunity. This discrepancy can most likely be attributed to differences in genetic background. Also, type I interferon activation of STAT4 is less efficient in mice than humans [65], so it may be difficult to effectively study the role of STAT4 in human SLE using murine models.

Through a separate signaling pathway, the engagement of TLR7 activates the transcription factor IRF5, which then up-regulates the expression of pro-inflammatory cytokines including type I interferons. SNPs in IRF5 were very strongly associated with human SLE in multiple

ethnic populations [51, 52, 66-68]. However, numerous studies have revealed a very complicated picture of the role of IRF5 polymorphisms in human SLE risk. Collectively, up to eight different polymorphisms form a significant SLE risk haplotype with only minor effects observed for each individual allele [66, 67, 69-72]. The level of cellular IRF5 is increased by two polymorphisms: the risk allele of a promoter indel increases the expression of IRF5 mRNA [72], while a SNP in the polyA signal sequence increases the stability of IRF5 mRNA [70, 71]. The other two polymorphisms affect isoform expression patterns: the T allele at rs2004640 introduces a new donor splice affecting the usage of exon 1A or 1B [69], while an indel in exon 6 generates isoforms with or without a 30bp in-frame insertion [71]. Overall, a total of nine human IRF5 isoforms have been detected, each with different patterns of expression, regulation and transcriptional response [73]. As many of these isoforms are co-expressed, it has been difficult to determine the overall contribution to SLE risk of any one isoform. In addition to risk alleles, one study identified a protective effect with an IRF5 polymorphism [67]. Synergistic susceptibility effects of the IRF5 risk haplotype with STAT4 [56, 60] and Tyk2 [48] polymorphisms have also been observed. This suggests an epistatic interaction as IRF5 and STAT4/Tyk2 are each part of discrete signaling cascades.

The contribution of TLR7 to SLE risk has often been studied along with another toll-like receptor: TLR9, which recognizes hypomethylated CpG DNA motifs common in bacterial DNA. In mouse models of susceptible B cells, BCR signaling, combined with signaling from TLR7 [18, 74] or TLR9 [75-77] is sufficient for the activation of autoreactive B cells. This process is also enhanced by IFNa [74, 78]. But while the TLR7 has consistently been linked to SLE risk [17, 42, 79], TLR9 has also been associated with SLE resistance in both human and murine studies that do not exclusively consider B cells [42, 74, 80-84]. The demonstrated ability of repetitive TLR9 signaling to induce hypo-responsive human pDCs [80] and murine macrophages [85] may contribute to this phenomenon.

IRAK1 is downstream of both TLR7 and TLR9, and after phosphorylation, IRAK1 influences NFkB/MAPK activation, inflammatory cytokine production and activates IRF7 (for review, see [86]). IRAK1 deficient mice have been demonstrated to be resistant to induced EAE, a nervous system autoimmune disorder, but have no detectable T-cell intrinsic defects [87]. A very recent study has strongly associated IRAK1 SNPs with human SLE and demonstrated that IRAK1 deficient autoimmune

GENE	Affected Processes	Murine SLE	Human SLE
TLR7	Production of pro-inflammatory cytokines; B cell activation	[16-19, 42, 74, 79]	[43]
TYK2	Production of pro-inflammatory cytokines		[47-50]
STAT4	Production of pro-inflammatory cytokines	[63, 64]	[51, 52, 56-62]
IRF5	Production of pro-inflammatory cytokines		[48, 51, 52, 56-59, 66-72]
TLR9	Production of pro-inflammatory cytokines; B cell activation	[42, 74-77, 79]	[80-84]
IRAK1	Production of pro-inflammatory cytokines	[87, 88]	[88]
MyD88	Production of pro-inflammatory cytokines; B cell class switching	[28, 89-91]	

Table 1. SLE-Associated Genes Affecting Innate Immune Signaling

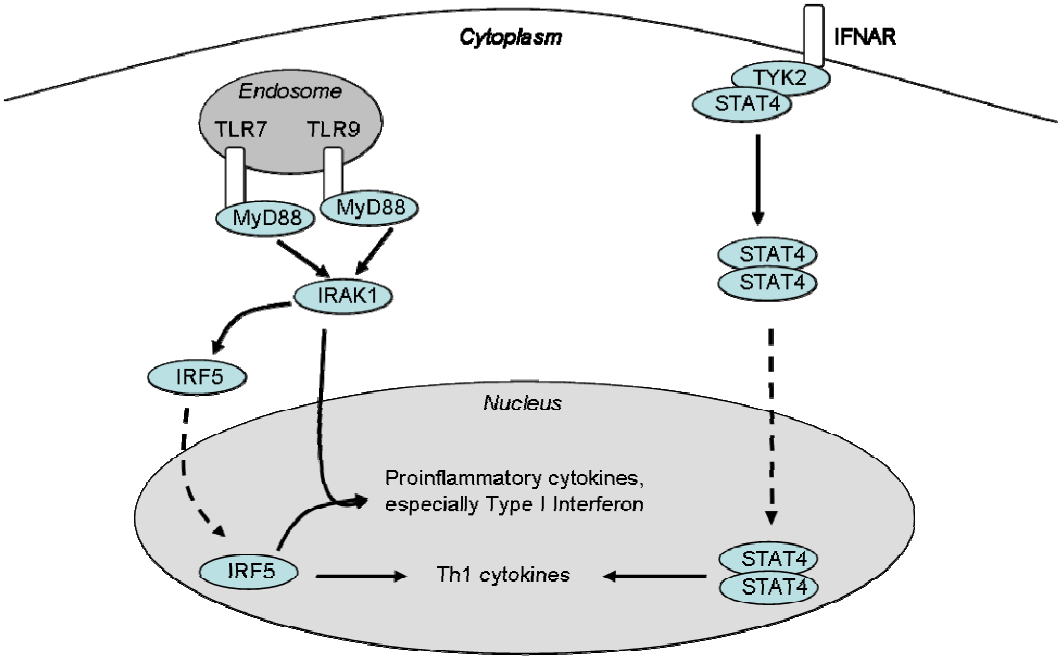

Figure 1. Diagram of SLE-associated Genes Affecting Innate Immune Signaling. After engagement of TLR7 with ssRNA or TLR9 with CpG motifs, the adaptor molecule MyD88 initiates signal transduction pathways including the activation of IRAK1 and the NFkB pathway resulting in the upregulation of proinflammatory cytokines. Also, the transcription factor IRF5 is activated and translocates to the nucleus where it mediates the exression of proinflammatory and Th1 cytokines. Meanwhile, engagement of the Type I Interferon receptor (IFNAR) with extracellular type I interferon at the cell surface activates the constiutively associated Tyk2 adaptor, leading to the recruitment, phosphorylaton and dimerazation of Stat4, which then translocates to the nucleus and upregulates Th1 cytokines.

prone B6.*Sle1* and B6.*Sle3* do not develop lupus-like symptoms [88]. IRAK1 is located on the X-chromosome which may contribute to the SLE female bias [88].

Perhaps the most essential adaptor for TLR signaling is MyD88. Except for TLR3, MyD88 is a component of the signaling complex which associates with the cytoplasmic tail of all TLRs. This facilitates several downstream signal transduction pathways, such as IRAK1 and IRF5, resulting in the production of pro-inflammatory cytokines. MyD88 deficiency was shown to significantly reduce or eliminate lupus nephritis in the *Ptpn6*^{spin} [92], MRL/*lpr* [90], *Lyn*$^{-/-}$ [91] and *Fcgr2b*-/- [89] murine models of SLE. In the latter two studies, MyD88 was required for B cell class switching to pathogenic immunoglobulin subclasses IgG2a and IgG2b [89, 91] which explains the large role of nucleic-acid sensing TLRs and MyD88 in the development of GN. Other experiments with lupus-prone transgenic mouse models have demonstrated MyD88-dependent but T cell-independent spontaneous autoimmunity [93, 94], suggesting that in the prescence of TLR signaling, T cell signaling may not necessarily be required for autoimmunity. In further support of the contribution of TLR signaling to SLE pathogenesis, a negative regulator of TLR signaling, *Tir8/Sigirr*, has been shown to inhibit autoimmunity in lupus-prone B6.*lpr* mice [95].

Dysregulated Adaptive Immune System Signaling

Specificity, potency and memory are defining and crucial characteristics of the adaptive immune response. However, when natural regulatory mechanisms are perturbed, these same traits may contribute to chronic, progressive autoimmune disease. Vast repertoires of the adaptive immune receptors, the T cell receptor (TCR) and the B cell receptor (BCR), are produced to enable the detection of an extremely diverse array of potential pathogens. As a necessary by-product of this process, auto-reactive lymphocytes are generated, but must be inactivated or eliminated to maintain self-tolerance. A variety of mechanisms contribute to limit the activation of auto-reactive lymphocytes, but all of them rely on signaling thresholds & cascades to discriminate between auto-reactive lymphocytes and non-auto-reactive lymphocytes. Antigen recognition, together with numerous receptors & adaptors, transmit a cumulative signal, initiating a lymphocyte activation program. This signal can be both quantitatively and qualitatively modified by other specialized receptors and adaptors. Thus, it is not surprising that polymorphisms resulting in small changes in immune signaling genes can establish significant potential for SLE, as well as possibly influence resistance to specific pathogens.

Central tolerance occurs in the thymus and bone marrow, respectively for T cells and B cells. For T cells, this is achieived through a process called negative selection, in which thymocytes that receive a strong stimulation in the absence of foreign antigen (and are thus auto-reactive) are eliminated through apoptosis. In a similar manner, developing B cells with a strong response to self will also be deleted. However, autoreactive B cells also have the opportunity to undergo secondary Ig chain rearrangement (receptor editing), possibly producing a non-autoreactive and viable BCR. These processes are not perfect though, allowing auto-reactive lymphocytes to escape and mature in the periphery.

Consequently, a second layer of protection acts in the periphery, where simultaneous signaling through multiple types of stimulatory receptors, including the antigen-specific receptor (TCR or BCR), is necessary for lymphocyte activation. The requirement of co-stimulatory signaling limits the activation of auto-reactive lymphocytes because cell-surface levels of these co-stimulatory receptors are only significantly up-regulated following stimulation of the innate immune system. Stimulation of the innate immune response by the presence of pathogens and/or tissue damage is therefore a crucial requirement for an effective adaptive

immune response by effectively legitimizing the need for an immune response.

The SLAM family of co-receptors has been associated with autoimmunity. The SLAM gene cluster are the key candidates in the potent SLE-predisposing sub-loci, *Sle1b*, which in B6 mice results in a spontaneous loss of tolerance to chromatin and moderate systemic autoimmunity [31]. The autoimmune-prone *Sle1b* allele results in higher expression of an alternate isoform of SLAMF6/Ly108, termed *Ly108-1*, on lymphocytes [31, 96]. In T-cells, increased levels of *Ly108-1* decrease signaling thresholds, resulting in hyper-responsive T cells [97]. Compared to the alternative isoform, *Ly108-1* has an additional immunoreceptor tyrosine based stimulatory motif (ITSM) in its cytoplasmic tail [98] which is partially responsible for this increased sensitivity [97]. In support of the mouse research, SNPs within the SLAM family have been associated with human SLE [99]. Extensive polymorphisms in the SLAM family of genes have been documented in both laboratory and diverse wild mouse strains [31, 100]. Many of these mutations occur in critical domains suggesting that selective pressure favors the functional diversification of these genes and their effect on immune responses [100].

In T cells, after ligand engagement, many of the SLAM family receptors recruit the SLAM-associated protein, SAP, adaptor to the TCR

signaling complex. SAP then recruits other molecules that are crucial for downstream signaling events. SAP was originally identified as the causative gene in X-linked lymphoproliferative (XLP) disease, a rare human disorder which results in a defective immune response to Epstein-Barr virus (EBV) [101]. In rheumatoid arthritis patients, decreased SAP expression has been observed in peripheral T cells [102]. The *Ly108-1* mediated decreased signaling threshold in T cells has been demonstrated to be SAP-dependent [97], highlighting the role of SAP in transducing SLAM family co-stimulatory signals. Other studies in mouse models have shown that SAP expression in T cells is essential for stable T-B cell interactions leading to germinal centre formation [103] so it is not surprising that the *Sle1b*-mediated production of ANAs is also SAP-dependent [104]. Perhaps the most striking illustration of the impact of SAP on SLE is the observation that a de novo mutation resulting in defective SAP thymocyte expression significantly attenuated systemic autoimmunity in the murine MRL-*Fas*^{lpr} model of spontaneous SLE [105].

While increased expression of the *Ly108-1* isoform lowers signal thresholds in mature lymphocytes [96, 97], it has been shown to increase signal thresholds and impair central tolerance in developing lymphocytes [96, 106]. The discrepancy between these studies may be explained by the presence of alternative adaptors in different cell types that qualitatively

change the end result of *Ly108-1* signaling. For example, in B cells, the SLAM family has been shown to interact with EAT-2, rather than SAP, while the presence of an unidentified additional adaptor has been suggested in thymocytes [106]. Similarly, up-regulation of Ly108-1 has been demonstrated to affect B cell peripheral tolerance [96].

In addition to co-stimulatory molecules, there are also inhibitory receptors and adaptors associated with SLE. In B cells, after BCR stimulation, *Lyn*, a src family protein tyrosine kinase associated with the BCR, is activated & recruits other adaptor molecules in both activating and inhibiting signaling cascades. *Lyn*-deficient B cells have been demonstrated to be hyper-responsive and capable of breaking peripheral self-tolerance, despite being subject to enhanced negative selection [107]; this results in a SLE phenotype of circulating auto-antibodies and severe GN [108]. However, in *Lyn*-deficient mice, these SLE phenotypes are dependent on endogenous levels of Bruton's tyrosine kinase (*Btk*), another component of BCR signal transduction [109] and MyD88, a crucial molecule in innate immune signaling pathways [91]. In subsets of human SLE patients, *Lyn* expression or recruitment/retention to lipid rafts is decreased in B cells [110, 111]. In addition, SNPs within *Lyn* have also been associated with human SLE in a large genome-wide association

study [51] and with European female SLE patients in a SNP-dense Lyn-focused study [112] .

Although other *src* family kinases can compensate for the lack of *Lyn* in many signaling cascades, *Lyn* is absolutely required for the CD22/SHP-1 inhibitory pathway [107]. CD22/Siglec-2 is a B-cell restricted sialic acid-binding adhesion receptor that also functions as a BCR co-receptor. After BCR cross-linking, the cytoplasmic tail of CD22 tail is tyrosine-phosphorylated which then recruits and activates the Src homology domain 1 containing phosphatase SHP-1 via Lyn [107]. Similar to the SLAM family of genes, numerous polymorphisms in CD22 have been observed in both humans [113] and mice [114, 115]. Two mouse alleles, CD22a and CD22c, have been identified in autoimmune-prone mouse strains, NZW and BXSB, respectively, while a third allele, CD22b, is found in autoimmune-resistant strains like B6 and BALB/c [114, 115]. Although CD22-deficiency in mouse models is sufficient to produce hyper-responsive B cells [116] and spontaneous auto-antibodies [117], it is not sufficient to mediate severe autoimmunity disease phenotypes such as kidney nephritis [117]. Also, mice with half of the normal cell surface levels of CD22 (knock-out heterozygotes) are not able to generate spontaneous auto-antibodies without epistatic interaction with *yaa* [118]. In humans, the Q152E polymorphism in CD22 has been shown to non-

significantly associate with SLE patients in an early study [113] while an increase of CD22+ cells has been correlated with an improvement in disease activity [119]. Epratuzumab, a humanized anti-CD22 monoclonal antibody, which induces rapid CD22 internationalization, was able to decrease disease symptoms and B cell levels but had no impact on auto-antobody levels or T cell levels for SLE patients in its first clinical trial [120]. In *ex vivo* human B cells, epratuzumab was demonstrated to inhibit proliferation in specifically SLE cells, compared to normal controls, in response to IL-2, IL-10, and CD40-CD40L signaling [121].

Once its ITIM motif is phosphorylated, SHP-1 inhibits cell activation by dephosphorylating cell signaling intermediates. SHP-1 has been of interest in autoimmunity research since Tsui and colleagues demonstrated in 1993 that mutations in SHP-1 were responsible for the *motheaten* mutation in mice and led to systemic early-onset and fatal autoimmunity [122]. However, a B cell-specific knock-out of *Ptpn6*, the gene that codes for SHP-1, was also sufficient to develop systemic autoimmunity and immune-complex mediated kidney nephritis [123]. Another variation of SHP-1, termed s*pin*, was discovered in an ENU mutagenesis screen, and results in MyD88-dependent mild autoimmunity and auto-inflammatory phenotypes [92]. SHP-1 activity is decreased in the spleen and lymph nodes of autoimmune MRL/*Fas*^{lpr} mice compared to MRL wild-type mice

[124]. Dysregulated SHP-1 expression has also been observed ex vivo in human SLE B cells [125].

Another molecule downstream of *Lyn* is *Fcgr2b*, which modulates B cell activation through an immunoreceptor tyrosine-based inhibitory motif (ITIM). A human SLE-associated *Fcgr2b* functional polymorphism in the transmembrane domain of *Fcgr2b* results in decreased retention/recruitment of *Fcgr2b* into lipid rafts, leading to decreased *Fcgr2b*-mediated inhibition of BCR signaling [126]. Another SLE-associated SNP in the promoter of *Fcgr2b* results in decreased expression of *Fcgr2b* in activated human B cells [127]. In mice, *Fcgr2b* deficiency in B cells can mediate the production of ANAs and fatal GN in the B6 strain, but not in the Balb/c strain [128]. Further studies with the *Fcgr2b* knock-out mouse have demonstrated that multiple B6 loci contribute to this strain sensitivity and modifier genes can enhance (*Yaa*) or attenuate (*lpr*) *Fcgr2b*-deficiency-mediated autoimmunity [129].

Programmed death receptor 1, also known as *PCDC1* and *PD-1*, transmits an inhibitory signal via an ITIM when simultaneously engaged with one of its ligands, either PD-L1 or PD-L2, and the TCR or BCR [130]. The *PD-1.3A* allele has been associated with SLE susceptibility in European and Hispanic-American populations, yet also with SLE resistance in Spanish populations [131, 132]. This SNP is located in an

enhancer-like domain in intron 4 of PD-1 and the risk allele disrupts the binding of the RUNX-1 transcription factor [133]. In a recent study, there was decreased basal and induced expression of PD-1 on activated CD4+ T cells in SLE patients homozygous for the *PD1-1.3A allele*, compared to heterozygote and *PD-1.3G* (the protective allele) homozygote SLE patients. Futhermore, despite no detectable difference when optimally stimulated, *PD-1* inhibition of T cell function was significantly decreased in *PD-1.3A* homozygote SLE patients at levels of suboptimal stimulation [134]. The role of PD-1 in tolerance has also been established in mouse models as B6.*PD-1*$^{-/-}$ mice display a lupus-like autoimmune disorder [135]. In the BXSB mouse model, exogenous PD-1 can ameliorate autoimmunity, but full suppression requires simultaneous treatment with a blocking antibody to ICOS, a T cell co-stimulatory receptor [136]. Together, these treatments shift the signaling milieu from a stimulatory state to an inhibitory environment. PD-1 also contributes to maintaining ocular immunological privilege and fetal-maternal tolerance [130].

PTPN22/LYP is a negative regulator of the TCR signaling complex which encodes a lymphoid-specific phosphatase (LYP). PTPN22 inhibits T cell activation by dephosphorylating components of the TCR signaling complex [137]. In human SLE, a *PTPN22* functional polymorphism, R260W, has been strongly & repeatedly associated with human SLE risk

and other autoantibody-associated diseases [51, 66, 138] while another functional variant, R263Q, has demonstrated a weak, protective effect [139] in human SLE. In a knock-out model of the mouse PTPN22-homolog, *Pep*, on a B6 non-autoimmune background, T cell signaling is enhanced in double positive thymocytes undergoing positive selection and effector/memory T cells but there is no effect on thymocytes undergoing negative selection, naïve T cells or B cells [137]. This results in hyper-responsive & expanded effector/memory T cells, an increase in spontaneous germinal B centers, and increased serum Ig, but no autoantibodies; thereby demonstrating that *Pep*-deficiency alone is not sufficient to break self-tolerance [137]. However, when the CD45 E613R mutant, which is also not sufficient to break tolerance on a B6 non-autoimmune background, and the $Pep^{-/-}$ are combined, a severe lupus-like disease develops [140], illustrating the epistatic interaction common in SLE susceptibility genes. Interestingly, although the PTPN22 R620W variant generates hyper-responsive T cells [137], a recent study demonstrated that this same variant results in hypo-responsive B cells [141].

Finally, TNFRSF4/OX40/CD134 which is expressed on activated CD4+ T cells and its corresponding ligand, TNFSF4/OX40L/CD134L, which is found on activated B cells, activated dendritic cells, and vascular

endothelial cells have been linked to SLE. In CD4+ T cells, CD134 signaling contributes to Th2 differentiation and late-stage survival signals, potentially amplifying autoimmunity. It has been demonstrated that signals thru CD134 can restore normal effector functions to anergic, autoreactive, peripheral T cells [142, 143]. A risk haplotype of CD134L is associated with human SLE [144, 145] and produces 6.7 fold increase in expression in EBV-transformed cell lines [144]. A greater proportion of CD134+ CD4+ T cells in peripheral blood has been associated with human SLE, as well as increased disease activity and lupus nephritis [146]. This is consistent with the observation that patients with proliferative lupus nephritis have increased levels of CD134L on the epithelial cells of the glomerular capillary wall [147].

The strongest genetic locus associated with SLE is the extended HLA region [52, 148] containing the major histocompatibility genes, 132 other immunoregulatory genes and numerous housekeeping genes [149]. In addition to its remarkable gene density, this locus also represents an extraordinary frequency of polymorphisms. The sheer diversity, both in genes and alleles, of the immune response which can be generated from this region is staggering and may explain why this locus is associated with over one hundred human diseases. For human SLE, the most consistent associations are with the MHC Class II genes, especially *HLA-DR3* and

HLA-DR2 alleles, but in a population-specific manner [150]. There is also an unusually high degree of linkage disequilibrium throughout this area which has impeded efforts to identify the effects of individual genes [149]. High-density SNP screenings of the HLA region, only recently feasible, have repeatedly suggested that there are multiple, independent disease susceptibility loci within this genomic interval [51, 151, 152].

Within this region, it is the MHC Class II genes that associate most strongly with diseases. This is not surprising as the successful presentation of antigens by MHC Class II molecules is a critical component of lymphocyte development and immune responses, processes that also play major roles in autoimmunity. In mice, the MHC Class II family is historically grouped into two loci: I-A containing the *H2-Ab*, *H2-Aa*, and *H2-Eb* genes, and I-E containing the *H2-Ea* gene (reviewed in [153]). The molecules in the I-A region are highly polymorphic while only minor variations have been identified within *H2-Ea*. All of these genes are within the *Sles1* interval.

Many *H2* alleles, including B6 (*b*) and NZW (*z*) variants, have been strongly associated with murine autoimmune phenotypes (reviewed in [10]). H2 heterozygosity has been linked to murine SLE [154, 155], which may be partially explained by individual alleles predisposing to distinct auto-antigens [154]. Some studies have found $H2^z$ alleles to be

associated with disease susceptibility [156], while others with SLE resistance [157, 158]. *H2*^{b} has also been linked to autoimmunity [158]. It is important to note that the B6 haplotype does not generate *H2-Ea* molecules, due to a promoter defect, and *H2-Eb*^{b} molecules remain in the cytoplasm as partially glycosylated precursors [159]. However, the NZW haplotype does produce functional *H2-Ea*^{z} and *H2-Eb*^{z} molecules. Attempts to identify specific contributions of NZW-like functional or B6-like non-functional *H2-Ea* alleles to autoimmunity have also produced contradictory results [155, 156]. The discrepancies in these studies are probably due to several factors. First of all, different genome backgrounds may introduce modifier or epistatic loci. Secondly, a common methodology is to use *H2*-congenic mice which often carry flanking donor strain contamination. The extremely high density of immunologically relevant genes in the extended H2 region therefore may hinder the correct interpretation of these experiments. As a result, the mechanism of the association of *H2* with murine SLE has not been well established.

Insights into Dysregulated Immunoregulation and SLE

Immunoregulatory signaling thresholds and cascades are extraordinarily complex, much like SLE pathogenesis. A vast number of molecules make up this network of receptors, adaptors, signal transducers

and transcription factors; each with the ability to enhance, modulate or inhibit the end result of the signaling pathway. Additionally, many of these intermediates are at least partially redundant and/or active in multiple pathways making it very difficult to determine precise, individual contributions. Many of these genes, like the SLAM family, CD22, and IRF5 are also remarkably polymorphic with various alleles and isoforms, each with subtle functional differences. Mohan and colleagues recently demonstrated that genetically diverse spontaneous models of murine SLE result in similar downstream signaling patterns in B cells, suggesting that a variety of polymorphisms lead to nearly the exact same end result [160]. Many positionally-cloned SLE-susceptible loci turn out to be several concatenated sub-loci because it is easier to initially detect the total, synergistic phenotype. In much the same way, nearly every model of spontaneous autoimmunity has been demonstrated to have epistatic gene interactions or dependencies. For example, the well-studied B6.*Sle1* murine model breaks tolerance to nuclear antigens, but only develops significant, severe fatal lupus with the addition of other loci like *Sle3* or y*aa*, which are not capable of developing lupus-like disease without the underlying *Sle1* dysfunction. Also, the further addition of the *Sles1* locus suppresses all disease even in the severe B6.*Sle1yaa* model. Another study showed that the activation of auto-reactive B cells can be

suppressed through the simultaneous engagement of the *Fcgr2b* and CD22 inhibitory receptors [161] illustrating that sufficient negative signal regulation can compensate for other SLE-predisposing mutations. Overall, a cumulative net change in adaptive and innate immune signaling must occur to potentiate SLE susceptibility.

Adaptive immune signaling genes have the unique ability to affect central tolerance, in addition to contributing to the maintenance of peripheral tolerance. In general, hypo-responsive lymphocytes, such as *Sle1b* thymocytes and immature B cells, have defective central tolerance, while hyper-responsive lymphocytes, like $Lyn^{-/-}$ B cells and $Ptpn22^{-/-}$ T cells, have defective peripheral tolerance. B cell signaling defects seem to be a central theme in SLE susceptibility, which is not surprising considering their role of producing anti-nuclear antibodies, the hallmark of SLE. In many artificial models, auto-reactive B cells are able to break tolerance with appropriate signals from either T cells or innate immune stimuli, but may not be sufficient to produce pathogenic ANAs. Conversely, T cell dysregulated signaling seems to assist and amplify SLE development and pathogenesis.

Innate immune signaling predominantly affects peripheral tolerance and end-organ tissue damage. TLR signaling is capable of stimulating auto-reactive B cells, while TLR-mediated production of inflammatory

cytokines creates an autoimmune and pro-inflammatory cellular environment, as best evidenced by the *yaa* TLR7 translocation. The most compelling evidence for the strong role of innate immune signaling in SLE development is from studies of *MyD88*, a crucial signaling intermediate for nearly all TLR pathways. *MyD88* deficiency eliminates or drastically reduces lupus phenotypes in many diverse mouse models of autoimmunity. In humans with virtually no intact TLR-signaling cascade (deficient in *MyD88*, *IRAK1*, and *UNC-93B*), there is no evidence of autoimmune disease, despite defective central and peripheral tolerance resulting in the accumulation of large numbers of auto-reactive mature naïve B cells in peripheral blood [162]. Also, *Ptpn6*^{spin} mutant mice only spontaneously develop autoimmunity disease when housed in conventional animal housing, versus gnotobiotic conditions [92]. Together, this data suggests that even normal levels of innate immune signaling, combined with flawed adaptive tolerance mechanisms, may lead to the development of autoimmunity.

There are several caveats that must be considered when interpreting studies of immune signaling genetic determinants of SLE. First, there are other processes which have significant contributions to autoimmune development and pathogenesis, including apoptosis, auto-antigen clearance, complement, and end-organ targeting. Secondly,

many immune signaling genes affect multiple cell types. Examples include adaptive immune-signaling genes *Ly108* and *Ptpn2*2 in T and B cells and innate immune-signaling gene *TLR9*. Therefore, only examining the effect of a polymorphism in one cell type or making systemic knock-outs may not be sufficient for understanding a particular gene's role in SLE. Finally, many naturally occurring SLE-associated immune signaling gene variants result in very subtle functional changes that may not be approximated by knock-out models.

Although precise mechanistic details are often elusive, an overall picture of SLE risk has emerged in which a dysregulatated, yet functioning, immune system is driven into autoimmunity by excessive immune system stimulation, either as a result of environmental factors and/or further cellular dysfunction.

Identifying the Causative Gene of Sles1

Overall, the sheer number of immunologically relevant genes in the *Sles1* interval, as well as the significant phenotypic differences between B6.*Sle1* and B6.*Sle1Sles1* mice have made the identification of the causative gene of *Sles1* difficult. The current body of knowledge suggests that *Sles1* functions by rebalancing the autoimmune-prone immune system of B6.*Sle1* or B6.*Sle1yaa* mice by introducing a compensatory

immuno-modulating allele. The potency of *Sles1* suggests that it may operate at the level of central tolerance, preventing the initiation of any autoimmune disease and thus all subsequent pathology, yet B cells from B6.*Sle1Sles1* mice display cytoplasmic evidence of activation. The mechanism of the autoimmune-prone *Sle1b* isoform of *Ly108* suggests that *Sles1* may balance lymphocyte signaling by altering either the signaling threshold or downstream signaling pathways.

This report will detail our efforts to identify the causative gene of *Sles1* through further fine-mapping and characterization of this interval. We analyzed several NZW-derived *Sles1* intervals, including a newly generated truncated recombinant of the $Sles1^{(28\text{-}83)}$ region. We also developed congenic mice to further investigate the $Sles1^{129}$ allele, previously shown to complement the suppressive *Sles1* allele. Finally, we completed preliminary systemic genomic and expression analysis of the *Sles1* interval and strong candidate genes.

GENE	Affected Processes	Murine SLE	Human SLE
LY108	T cell signaling threshold, B cell signal threshold & receptor editing	[31, 96, 97, 106]	
SAP	T cell signal transduction, germinal centre formation	[97, 104, 105]	
LYN	Inhibition of B cell signal transduction	[107, 108]	[51, 110-112]
CD22	Inhibition of B cell signal transduction	[115-117, 163]	[113, 119, 121, 124]
SHP-1	Inhibition of B cell signal transduction	[92, 122-124]	[125]
FCGR2B	Inhibition of B cell signal transduction	[128, 129]	[51, 126, 127, 164]
PD-1	Inhibition of T & B cell signal transduction, induction of apoptosis	[135, 136]	[131-134]
PTPN22	Modulation of T & B cell signal transduction	[137, 140]	[51, 138, 139, 141]
CD134	Th2 differentiation, late-stage T cell survival	[142, 143]	[144-147]
MHCII	T cell development, antigen presentation	[154-158]	[51, 52, 148, 150]

Table 2. SLE-Associated Genes Affecting Adaptive Immune Signaling

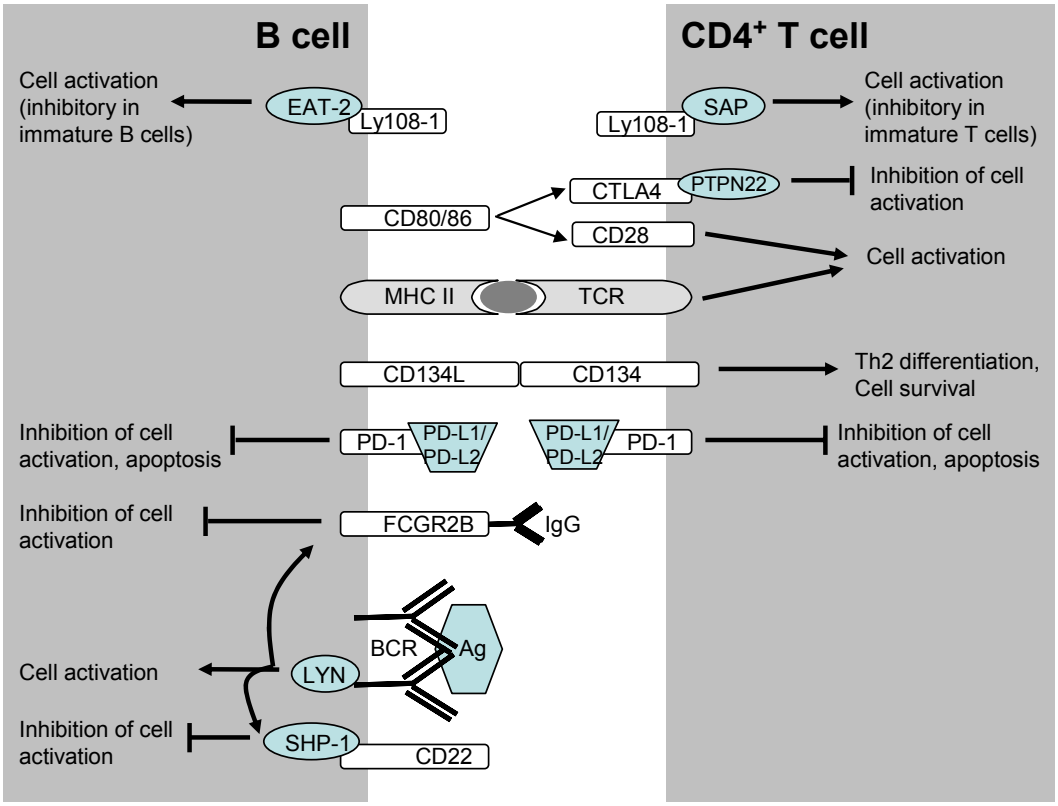

Figure 2. Diagram of SLE-associated Genes Affecting Adaptive Immune Signaling as Modeled in B cell-T cell Interaction. In B cells, after cross-linking of the BCR with antigen, the adaptor Lyn is phosphorylated, leading to the cell activation. Negative regulatory pathways of B cell activation include the engagement of FCGR2B with IgG and the engagement of the BCR co-receptor CD22 with sialic acid-bearing ligands. In CD4+ T cells, simultaneous engagement of the TCR with a peptide-MHC complex and CD28 with either CD80 or CD86 on APCs leads to T cell activation, while the engagement of CD134 with CD134L on B cells leads toTh2 differentiation and late-stage survival signals. The engagement of CTLA4 with CD80 or CD86 initiates a negative regulatory pathway of cellular activation via PTPN22. On either B or T cells, the simultaneous engagement of PD-1 with either the BCR or TCR and a PD-1 ligand (either PD-L1 or PD-L2) inhibits cell activation and promotes apoptosis. Also, the engagement of Ly108-1 leads to an ecreased signaling threshold on mature lymphocytes, but an increased signaling threshold in immature lymphocytes.

CHAPTER TWO

Materials and Methods

Mice

All mice were housed in The University of Texas Southwestern Medical Center at Dallas (UTSW) Animal Resource Center's specific pathogen free (SPF) facility under the supervision of Dr. Jose Casco and with the approval of the Institutional Animal Care and Use Committtee (IACUC) of UTSW.

C57Bl/6J (B6) mice were originally obtained from The Jackson Laboratory (Bar Harbor, Maine) and maintained in our colony and UTSW Mouse Breeding Core for use in these experiments.

The generation of B6 congenic mice carrying the NZW-derived (via NZM2410) *Sle1* and *Sles1* intervals has been previously described [22, 33]. The boundaries of the *Sle1* interval are defined by the microsatellite markers D1Mit202 and D1Mit17. Multiple *Sles1* intervals were generated for these studies by intercrossing *Sles1* heterozygotes (B6/NZW) to create truncated recombinant intervals, identified through PCR screening with microsatellite markers, and subsequently bred to homozygosity on a B6.*Sle1yaa* background. These intervals, from largest to smallest, are B6.*Sle1Sles1*$^{81\text{-}22}$, B6.*Sle1Sles1*$^{(28\text{-}83)}$, and B6.*Sle1Sles1*^{KB1} (see Figure 4A

for a schematic). Female mice carrying these intervals were used in these experiments at 2 months, 7 months and 9 months of age. Refer to Table 4, Microsatellite Marker Information, for details on breakpoint microsatellite markers and strain abbreviation used throughout this document.

B6 mice carrying the BXSB-derived y-chromosome *yaa* loci were obtained from The Jackson Laboratory and are referred to as B6.*yaa*. Male B6.*yaa* mice were then bred to female B6.*Sle1* mice and bred to homozygosity. In a similar fashion, *yaa* was also added to each *Sles1* congenic strain. Male mice were used in these experiments at 2 months, 4 months and 6 months of age. Refer to Table 3. Mouse Strain Information, for strain abbreviation used throughout this document.

The B6.*Sle1Sles1*^{129} congenic mice were initially generated by intercrossing (B6.*Sle1* x 129) F1 mice. The resulting F2 progeny were screened with polymorphic MIT markers, D17Mit135 and D17Mit24 (see Table 4), which flank the *Sles1*$^{(28\text{-}83)}$ to select breeders to be backcrossed to B6.*Sle1yaa* mice. Subsequent generations were also screened and backcrossed to B6.*Sle1yaa* mice. After five generations, breeders were screened with the Illumina Mouse Low Density SNP panel (Illumina, Inc., San Diego, California) to identify any remaining contaminating areas of 129-derived genome. MIT markers were identified for each of these regions and used to screen and select breeders for the remaining

Full Strain Name	Abbreviation[1]	Chr 1: Sle1/b[2]			Chr 17: Sles1[3]				Chr X: yaa[4]
C57Bl/6	B6	*b*	*b*	*b*	*b*	*b*	*b*	*b*	n/a
B6.*yaa*	B6.*yaa*	*b*	*b*	*b*	*b*	*b*	*b*	*b*	*yaa*
B6.*Sle1*^{NZW}	B6.*Sle1*	*z*	*z*	*z*	*b*	*b*	*b*	*b*	n/a
B6.*Sle1yaa*	B6.*Sle1yaa*	*z*	*z*	*z*	*b*	*b*	*b*	*b*	*yaa*
B6.*Sle1Sles1*^{zKB1}	B6.*Sle1KB1*	*z*	*z*	*z*	*b*	*b*	*z*	*b*	n/a
B6.*Sle1Sles1*^{zKB1}*yaa*	B6.*Sle1KB1yaa*	*z*	*z*	*z*	*b*	*b*	*z*	*b*	*yaa*
B6.*Sle1Sles1*$^{z(28-83)/B6}$	B6.*Sle1Sles1het*	*z*	*z*	*z*	*b*	*b/z*	*b/z*	*b*	n/a
B6.*Sle1Sles1*$^{z(28-83)/B6}$*yaa*	B6.*Sle1Sles1hetyaa*	*z*	*z*	*z*	*b*	*b/z*	*b/z*	*b*	*yaa*
B6.*Sle1Sles1*$^{z(28-83)}$	B6.*Sle1Sles1*	*z*	*z*	*z*	*b*	*z*	*z*	*b*	n/a
B6.*Sle1Sles1*$^{z(28-83)}$*yaa*	B6.*Sle1Sles1yaa*	*z*	*z*	*z*	*b*	*z*	*z*	*b*	*yaa*
B6.*Sle1Sles1*$^{z(81-22)/B6}$	B6.*Sle1(81-22het)*	*z*	*z*	*z*	*b/z*	*b/z*	*b/z*	*b/z*	n/a
B6.*Sle1Sles1*$^{z(81-22)/B6}$*yaa*	B6.*Sle1(81-22het)yaa*	*z*	*z*	*z*	*b/z*	*b/z*	*b/z*	*b/z*	*yaa*
B6.*Sle1Sles1*$^{z(81-22)}$	B6.*Sle1(81-22)*	*z*	*z*	*z*	*z*	*z*	*z*	*z*	n/a
B6.*Sle1Sles1*$^{z(81-22)}$*yaa*	B6.*Sle1(81-22)yaa*	*z*	*z*	*z*	*z*	*z*	*z*	*z*	*yaa*
B6.*Sle1Sles1*^{129}	B6.*Sle1Sles1(129)*	*z*	*z*	*z*	*bc*	*bc*	*bc*	*bc*	n/a
B6.*Sle1Sles1*^{129}*yaa*	B6.*Sle1Sles1(129)yaa*	*z*	*z*	*z*	*bc*	*bc*	*bc*	*bc*	*yaa*
129/SvJ	129		*z*		*bc*	*bc*	*bc*	*bc*	n/a
(129xB6.*Sle1*) F1	(129xB6.*Sle1*) F1		*z*		*bc/b*	*bc/b*	*bc/b*	*bc/b*	n/a
129.*Sles1*^{B6}	129.*Sles1(B6)*		*z*		*b*	*b*	*b*	*b*	*b* *yaa*

Table 3. Mouse Strain Information

A schematic (not to scale) of relevant nested SLE-associated loci per chromosome is shown above a table itemizing each mouse strain used in these studies and their respective haplotypes for each loci. Boundary microsatellite markers for each interval are listed in the footnotes below. See Table 3 for more information on these markers.

[1] The abbreviated form of the strain name used in figures and text

[2] *Sle1b* is bounded by D1Mit113. *Sle1* is bounded by D1Mit202 and D1Mit17. *z* haplotype = NZW, *b* haplotype = B6. 129 genome contains identical haplotype to NZW for *Sle1b*.

[3] *Sles1*$^{81-22}$ was historically bounded by D17Mit81 and D17Mit22. *Sles1*$^{28-83}$ was originally bounded by D17Mit28 and D17Mit83. Later, fine-mapping of the breakpoints established 204/ms4 and 49/ms7 was microsatellite boundaries for this interval. *Sles1*^{KB1} is bounded by markers kb13 and 49/ms7. *z* haplotype = NZW, *b* haplotype = B6, *bc* = 129, *b/z* = NZW/B6 heterozygote.

[4] Only male mice carry the *yaa* loci. n/a indicates that female mice were used for this group.

backcross generations. Finally, mice were intercrossed to generate a B6.*Sle1yaa* line with a homozygous 6.45 MB region derived from the 129 genome which contained the entire *Sles1*$^{(28\text{-}83)}$ interval. B6.*Sle1Sles1*^{129} mice were again screened with the Illumina Mouse Low Density SNP panel (Illumina, Inc., San Diego, California) to ensure that all other contaminating 129-derived genome intervals had been eliminated. In a similar manner, 129.*Sles1*^{B6} mice were also generated. 129.*Sles1*^{B6} mice are homozygous for the NZW haploype of *Sle1b*, as the 129 genome has an identical haplotype for this region [31].

PCR Genotyping

Tail clips were obtained at weaning and used to prepare crude lysates. Briefly, 250ul of tail lysis buffer (50mM Tris, ph 8.0, 50mM KCl, 2.5mM EDTA, 0.45% NP-40, 0.45% Tween-20) with 0.4mg/ml Proteinase K (Roche Applied Science, Indianapolis, Indiana) were added to each tail clip and incubated for at least 20 hours in a 55ºC water bath. Tail lysates were then vortexed and spun down at 14000 rpm for 10 minutes and subsequently stored at -20 ºC.

Typically, 0.5ul of crude tail lysate supernatant was used in a 20ul polymerase chain reaction, along with 330nM of each forward and reverse primer. Cycling conditions included an initial 3 minute denaturing step at

Name	Forward Sequence	Reverse Sequence	Position[#]	Polymorphism
Chromosome 1 – *Sle1*				
D1Mit202	CCATAAGCCTCCTCTTTCCC	AAAATGAACTCAGCGGGTTG	158971080	B6>NZW=129
D1Mit113	CCTCAAAATCAGGATTAAAAGGG	ACATGGGGTGGACTTGTGAT	173634611	NZW>B6=129
D1Mit17	GTGTCTGCCTTTGCACCTTT	CTGCTGTCTTTCCATCCACA	191395133	NZW>B6>129
Chromosome 17 – *Sles1*				
D17Mit164	AGGCCCTAACATGTAGCAGG	TATTATTGAGACTGTGGTTGTTGTTG	03824615	B6 > 129
D17Mit156	ATACTGAAACAATTGCACATGACA	TAAATTTGGTCTTTTTGACCTATGC	11080463	B6 > 129
D17Mit174	GCACCTGTTTCTCTTCAGGC	TGGAGTGCTGGGATTAAAGG	26295589	129 > B6
D17Mit135	CATAGATCAGATAGTCGCACGC	TCTCAGGAAGGCAGGACAGT	31064214	129 > B6
D17Mit175	TGGAAATCGGAGCCTCTG	TTGGAAAAGGTTGAGAGTAGATCA	31879623	B6 > 129
204/ms4	ATCCCCTGGTTTCACTCCTT	TCATGCTCAAAGAAGCAACAA	34060807	B6 > NZW
D17Mit28	ACTCAGGACTCAGAATGAAGATCC	ATTCCTAGATGAAAAGTCTGTGGC	34037681	B6 > NZW
kb1	ACCATCCTGACTGCCTTGTT	TGCACCCTTTTAGGAAGGAA	34421700	B6 > NZW
kb7	AGTAGCAGGGAGATGGCTCA	CGTGAGGTTTTGGTTGGACT	34454146	NZW > B6
kb10	TCAACTAGGGCCTGCTATGG	TTCGACTTCTTGCCACAATG	34698604	B6 > NZW
kb13	GGATCAGCCAAAGAGGACAG	TCCAGCATCCCTCTGCTACT	34707437	B6 > NZW
kb14	TCCACATGAAGGGATGTGTG	CAGAACAGCCTCCAAGATGAG	34713906	B6 > NZW
kb11	CGTCTGCGCATGAAATAAAG	CGACCCTCCTCTCACTTCAG	34786681	NZW > B6
kb6	AGGGACCATACCTGTGGTTG	AGCCTTGTCCTTTCCTACCC	34819622	B6 > NZW
D17Mit34	TGTTGGAGCTGAATACACGC	GGTCCTTGTTTATTCCCAGTACC	34780998	NZW > B6
D17Mit83	GTTACAGTCTTTCTTAAGGTAATTGCG	CAGTGCTGCTCCCAACATTA	34993786	NZW > B6
49/ms7	GCAACACATGTTCTTGATAATCACT	GTTACAACTTTTGCTGGTTAGATTT	35143976	NZW > B6
D17Mit24	ACCTCCACCTCTCTCTGTG	TGGAGAGACGTCCTATGATG	37519109	B6 > 129
D17Mit115	GATGACAGGCCTGCTCTCTT	AGGAAGAGCCAGTGAAAGAGG	47611568	B6 > 129

Table 4. Microsatellite Markers – Primer Information.
DxMITxxx markers are standard markers, with more information available at online mouse genomic resources.
[#] Indicates position along chromosome in basepairs, according to University of California – Santa Cruz mouse genome browser, mm9 build (based on NCBI build m37) (http://www.genome.ucsc.edu).

95ºC, followed by 40 cycles of 30 seconds at 95ºC, 30 seconds at the annealing temperature (ranging from 50-65ºC), 45 seconds at 72ºC, and a final 5 minute extension period at 72ºC. Entire PCR reactions, along with 5ul loading dye (40% sucrose, 0.25% bromophenol blue) were run on 2-5% agarose gels at 150V for 0.75-2 hours to resolve the polymorphic bands. Information on standard microsatellite (MIT) markers was obtained from the Ensemble Mouse Genome Assembly (http://www.ensembl.org) and Mouse Genome Informatics Database (http://www.informatics.jax.org/).

In the absence of an appropriate microsatellite marker, published sequence with known microsatellite repeats was accessed from the Ensembl Mouse Genome Assembly (http://www.ensembl.org). Repetitive elements were masked by RepeatMasker software (http://www.repeatmasker.org) before primers flanking target sequences were generated by Primer3 software (http://frodo.wi.mit.edu/primer3/) and screened for non-specific hybridization with NCBI Blast (http://blast.ncbi.nlm.nih.gov).

Sequencing

Sequencing primers were designed in a similar method as described above for designing microsatellite marker primers. To generate

a PCR product, 250 ng of purified DNA was used in a 100ul polymerase chain reaction, along with 300nM of each forward and reverse primer. Cycling conditions included an initial 3 minute denaturing step at 95ºC, followed by 40 cycles of 30 seconds at 95ºC, 30 seconds at the annealing temperature (ranging from 50-65ºC), 60-90 seconds at 72ºC, and a final 5 minute extension period at 72ºC. PCR products were then purified using High Pure PCR Purification Kit (Roche Applied Science, Indianapolis, Indiana) and/or, if necessary, Qiagen Gel Purification Kit (Qiagen, Germantown, Maryland) and quantified on a Nanodrop spectrophotometer (Thermo Scientific, Wilmington, Delaware). Samples were submitted for sequencing in the UTSW Sequencing Core, in accordance with their guidelines.

Quantitative Real-time RT-PCR

Thymi were harvested and ground between frosted glass slides to generate single cell suspensions. Cells were washed once with FACS buffer (PBS, 2% FCS, 1% HEPES) and resuspended in 1mL of Trizol (Invitrogen, Carlsbad, California) before being stored at -80ºC for up to one week. RNA was isolated using Qiagen RNA Isolation Kit (Qiagen, Germantown, Maryland) and quantified on a Nanodrop spectrophotometer (Thermo Scientific, Wilmington, Delaware). RNA expression was

analyzed using Taqman Gene Expression Assays (Applied Biosystems, Inc., Foster City, California), specific for *Btnl2* (Mm01281666_m1), *Notch4* (Mm00440525_m1) and *B2M* (Mm00437762_m1). Absolute MAX QRT-PCR Mix (Thermo Scientific, Wilmington, Delaware) was used for amplification, as per manufacturer's instructions. An ABI 7300 Real Time System, using Sequence Detection Software (Applied Biosystems, Inc., Foster City, California) was used for amplification and analysis. The message levels of *Btnl2* and *Notch4* were expressed after normalization to *B2M* expression levels.

Serology

Mice were bled via retro-orbital bleeding or cardiac puncture at 5, 7, and 9 months for females and 4 and 6 months for male mice carrying the *yaa* loci. The whole blood was incubated at 4ºC overnight, before being spun down at 14000 rpm for 5 minutes, allowing for the sera to be separated and stored long-term at -20ºC. ELISA assays were used to detect IgM and IgG autoantibodies (autoAbs) specific for chromatin and dsDNA. Briefly, Immunolox HB 96-well plates (Dynatech, Chantilly, California) were precoated with 50µl/well of methylated bovine serum albumin (mBSA), 50µl/well of 50µg/mL dsDNA (Sigma-Aldrich; dissolved in PBS) and 50µl/well of 50µg/mL total histones (Roche Applied Science,

Indianapolis, Indiana). All coating steps were for 30 minutes at 37ºC followed by two washes in PBS. Once coated, ELISA plates were incubated overnight at 4ºC with 200µl/well of ELISA Blocking Buffer (PBS, 0.1% gelatin, 3% BSA, 3mM EDTA). Sera were added at a final dilution of 1:800 in Serum Diluent (PBS, 0.1% gelatin, 2% BSA, 3mM EDTA, 0.05% Tween-20) and incubated for two hours at room temperature. Bound IgG or IgM was detected using alkaline phosphatase conjugated goat anti-mouse IgG or IgM (Roche Applied Science, Indianapolis, Indiana) and p-nitrophenyl phosphate (Sigma-Aldrich, St. Louis, Missouri) as the substrate. OD450 was measured by an Elx800 Automated Microplate Reader (Bio-Tek Instruments, Winooski, Vermont) and the raw optical densities (ODs) were converted to arbitrary normalized units (ANU) using a six-point standard curve generated by a monoclonal IgG antibody derived from a NZM2410 mouse [165] or a pooled sera IgM standard. A 1:250 dilution of this supernatant was set at 1000 ANU/mL. Samples were considered “ANA positive” if their ANA level was greater than the average + 4 standard deviations of the ANA levels of the age-matched control group (B6 for females or B6.*yaa* for males).

Flow Cytometric Analysis and Antibodies

For splenocyte single cell suspensions, spleens were harvested, weighed, and crushed with a 10cc syringe plunger. For thymocyte single cell suspensions, thymi were harvested and ground between two frosted slides. Cells were washed once and resuspended in 5-10 mLs of FACS buffer (PBS, 2% FCS, 1% HEPES) before being counted. Cells (1.2×10^6 per well) were then stained on ice in 96-well plates. Cells were blocked with 40ul of 2.4G2 (American Type Tissue Collection, Rockville, MD) before 40ul of 2X antibody cocktails were added. Ten to twelve color combinations of optimized dilutions of the following antibodies were used: FITC-CD25 (7D4), FITC-Ly9 (30C7), FITC-MHCII (2G9), FITC-CD86 (GL1), PE-CD127 (SB/199), PE-CD138 (Syndecan), PerCP-Cy5.5-CD69 (H1.2F3), PerCP-Cy5.5-IgM (RP-60.2), PE-Cy7-CD8 (53-6.7), PE-Cy7-NK1.1 (PK136), PECy7-CD45 (30-F11), PE-Cy7-B220 (RA36B2), APC-CD5 (53-7.3), Alexa700-CD4 (RM4-5), APC-Cy7-CD4 (GK1.54), APC-Cy7-Gr1 (RB6-8C5), APCCy7-B220 (RA36B2), Bio-CXCR5 (2G8), Bio-CD25 (7D4), Bio-CD69 (H1.2F3) (BD Biosciences, San Jose, California), FITC-PD-1 (J43), PE-ICOS (7E.17G9), PE-MHCII (M5/114.14.2), PE-Ly108 (13G3-19D), PE-Cy5-CD8 (53-6.7), PE-Cy5-F4/80 (BM8), PE-Cy7-CD23 (B3B4), APC-CD45 (30F11), APC-CD44 (1M7), APC-CD11b (M1/70), Alexa700-CD19 (1D3), Alexa700-CD3 (500A2), Alexa700-CD11b

(M1/70), PacBlue-CD3 (17A2), PacBlue-CD11b (M1/70), PacBlue-CD11b (N418), PacBlue-CD21/35 (4E3), Bio-Ly108 (13G3-19D), Bio-CD86 (GL1), Bio-CD45 (30F11) (eBiosciences, San Diego, California), PE-TexasRed-CD62L (MEL-14), PE-TexasRed-CD19 (6D5), PETexasRed-CD4 (RM4-5) (Invitrogen, Carlsbad, California), PE-Neu (7/4) (Serotec, Raleigh, North Carolina) and Bio-mPDCA (Miltenyi Biotec, Bergisch Gladbach, Germany). After two washes in FACS buffer, cells stained with biotin-conjugated antibodies were stained with Streptavidin-QDot655 (Invitrogen, Carlsbad, California). After a single wash, red blood cells were depleted with a very brief incubation in 10% Fix and Lyse Buffer (BD Biosciences, San Jose, California) and followed immediately by two washes in FACS buffer. Cells were then fixed in 1% paraformaldehyde and stored up to 24 hours at 4ºC. Just prior to data collection, cells were washed twice, resuspended in FACS buffer and filtered through nylon mesh. Data was collected on LSR II with FacsDiva software (BD Biosciences, San Jose, California). Dead cells and cell clusters were excluded on the basis of forward and side scatter properties. For each fluorochrome in each antibody panel, a single antibody was used to stain cell aliquots to generate compensation controls. Flow cytometry data was analyzed using FlowJo (Tree Star, Ashland, OR).

Renal Pathology

Longitudinal kidney sections from 6 month old male mice carrying the *yaa* locus were fixed in 10% neutral-buffered formalin (Sigma-Aldrich, St. Louis, Missouri) before being embedded in paraffin, cut into 3μm sections and stained with hemotoxylin and eosin with periodic acid-Schiff. In a blind manner, the sections were then blind examined for evidence of disease pathology in the glomeruli, tubules or interstitial areas by Dr. Xin J. Zhou (Department of Pathology, UTSW). The GN severity was graded on a scale of 0 to 4, where 0 indicates normal and 4 indicates significant evidence of disease.

Microarray

B cells and T cells were sorted from splenic single cell suspensions from three each B6.*Sle1* and B6.*Sle1Sles1* female 6-8 week old mice using the MoFlow Flow Cytometer (DakoCytomation) using antibodies against FITC-B220 (GL1) and PE-CD4 (H129.19) (BD Biosciences, San Jose, California). Purity achieved was greater than 95%. RNA was isolated from the sorted cells and hybridized to the Illumina Sentrix 48K Beadarray (Illumina, Inc., San Diego, California) by the UTSW Microarray Core. Illumina Beadstudio software (Ilumina, Inc., San Diego, California) was used to subtract background and normalize data using a cubic spline

algorithm. Genes were considered significantly differentially expressed when the change was greater than 2-fold.

Large Lupus Association Study 1 (LLAS1) Human SLE SNP Association

In collaboration with Oklahoma Medical Research Foundation (OMRF), DNA samples from 5023 SLE patients and 5238 healthy controls, representing African-American, Asian, European-American, Gullah and Hispanic populations, were genotyped on Illumina iSelect multisample genotyping BeadChip (Illumina, Inc., San Diego, California). After hybridization to the BeadChip, SNPs were extended by single-labeled nucleotides and read on an Illumina Bead Array Station (Illumina, Inc., San Diego, California). Normalized fluorescent intensity data for each sample was converted into SNP genotype with Illumina BeadStudio 3.1 software (Illumina, Inc., San Diego, California).

Statistical Analysis

Data was analyzed using non-parametric Mann-Whitney test in GraphPad Prism (Graphpad Software, San Diego, California). Error bars represent SEMs.

CHAPTER THREE

Fine-Mapping of *Sles1* to ~638 KB

Introduction

Complex interactions between genetic and environmental factors affect the initiation and development of SLE. Decades of human and murine research have identified numerous genetic loci associated with SLE susceptibility. Mouse models of spontaneous lupus have made possible experiments to identify the individual and combinatorial contributions of these SLE-associated genetic loci.

Our previous studies have focused on the congenic dissection and characterization of disease-associated loci identified from murine models of spontaneous SLE. Each locus, such as the NZW-derived *Sle1*, contribute unique phenotypes and specific combinations of these loci can recapitulate lupus-like disease on a non-autoimmune B6 genetic background. For this study, we have focused on female B6.*Sle1* congenic mice which spontaneously develop mild autoimmunity characterized by a loss in tolerance to chromatin, IgG autoantibody production, hyperactivation of B and T cells, and mild splenomegaly [23]. In male B6.*Sle1* congenic mice, the addition of the BXSB-derived y-chromosome loci, *yaa,* dramatically enhances these phenotypes and also mediates the

development of kidney glomerulonephritis. Disease is also drastically accelerated in B6.*Sle1yaa* males versus B6.*Sle1* females with significant disease occurring around 3-6 months of age versus 9-12 months of age, respectively [28].

Sle1, as well as other potent SLE susceptibility loci, are derived from the non-autoimmune NZW strain, suggesting the presence of modifier loci in the NZW genome. Linkage analysis of the NZW strain identified several suppressive loci; the strongest of which was termed *Sles1* (*SLE suppressor 1*) and mapped to the MHC region on mouse chromosome 17 [33]. Congenic dissection and characterization has demonstrated that *Sles1* specifically interacts with *Sle1* to prevent the loss of tolerance to chromatin and thus subsequent phenotypes and autoimmune disease, even in the accelerated B6.*Sle1yaa* male model [19]. Previous studies have narrowed the *Sles1* locus to a ~1083 KB interval termed $Sles1^{(28\text{-}83)}$, excluding *TNF-a*, yet including the MHC region and several complement genes [35].

In this study, we demonstrate that the causative *Sles1* gene maps to a ~638 KB interval representing the proximal portion of the $Sles1^{(28\text{-}83)}$ interval but terminating just after the butyrophilin-like gene complex in exon 3 of *Notch4*. The genes in the telomeric portion of $Sles1^{(28\text{-}83)}$, represented by the non-suppressive *Sles1* truncated recombinant, termed

Sles1^{KB1}*,* are now excluded from consideration as *Sles1* causal gene candidate. Therefore, the strongest remaining non-MHC candidate for the *Sles1* causative gene is *Btnl2* (*butyrophilin-like 2*).

Results

Sles1^{KB1}*,* a Truncated Recombinant, Represents the Terminal ~445 KB of *Sles1*$^{(28\text{-}83)}$

Similar to our previous studies of *Sles1*, a truncated recombinant strategy was used to further fine-map *Sles1,* as illustrated in Figure 3*.* Briefly, B6.*Sle1Sles1*$^{B6/(28\text{-}83)}$ heterozygote mice were intercrossed to generate truncated recombinants. Truncated recombinant intervals were identified through PCR screening of tail clip lysate with polymorphic microsatellite markers spanning the *Sles1*$^{(28\text{-}83)}$ interval. Recombinant mice were backcrossed to B6.*Sle1Sles1*$^{(28\text{-}83)}$*yaa* and resulting progeny carrying the recombinant were then intercrossed to generate a homozygous line. B6.*Sle1* females and B6.*Sle1yaa* males homozygous for this recombinant were then aged and phenotyped to determine whether the *Sles1* suppressive phenotype mapped in or out of the truncated interval.

One truncated recombinant interval, termed *Sles1*^{KB1}, was identified via screening 2586 progeny with microsatellite markers. This frequency is

significantly less than expected (intercrossed heterozygotes should have produced one recombinant per one hundred mice over this 0.5 CM interval, $X^2 = 22.0; p < 0.005$), suggesting the *Sles1*$^{(28\text{-}83)}$ region is a recombinational coldspot in strong linkage disequilibrium (LD). In an earlier, larger *Sles1* interval, we identified a recombinational hotspot between an area slightly proximal of *Sles1*$^{(28\text{-}83)}$ [35]. This is consistent with high-resolution human studies demonstrating that the genomic organization of the extended MHC region consists of blocks of very strong LD punctuated by recombinational hotspots [166, 167].

The recombinant breakpoints of the ~445 KB *Sles1*^{KB1} interval was determined through PCR screening with polymorphic microsatellite markers spanning the *Sles1*$^{(28\text{-}83)}$ region. Once the breakpoint interval was narrowed between polymorphic published MIT microsatellite markers, primers were designed that flanked known microsatellites and used for further screening. In this manner, the proximal recombination breakpoint for *Sles1*^{KB1} was identified to be within an 8.8 KB interval between designed markers “kb10” and “kb13” (see Table 4 for more marker information) surrounding the gene *Notch4*. Sequence analysis of *Notch4* later revealed that the breakpoint occurs within exon 3. The distal recombinational breakpoint of *Sles1*^{KB1} was the same as *Sles1*$^{(28\text{-}83)}$. Figure 4B shows the genomic organization and breakpoint intervals of

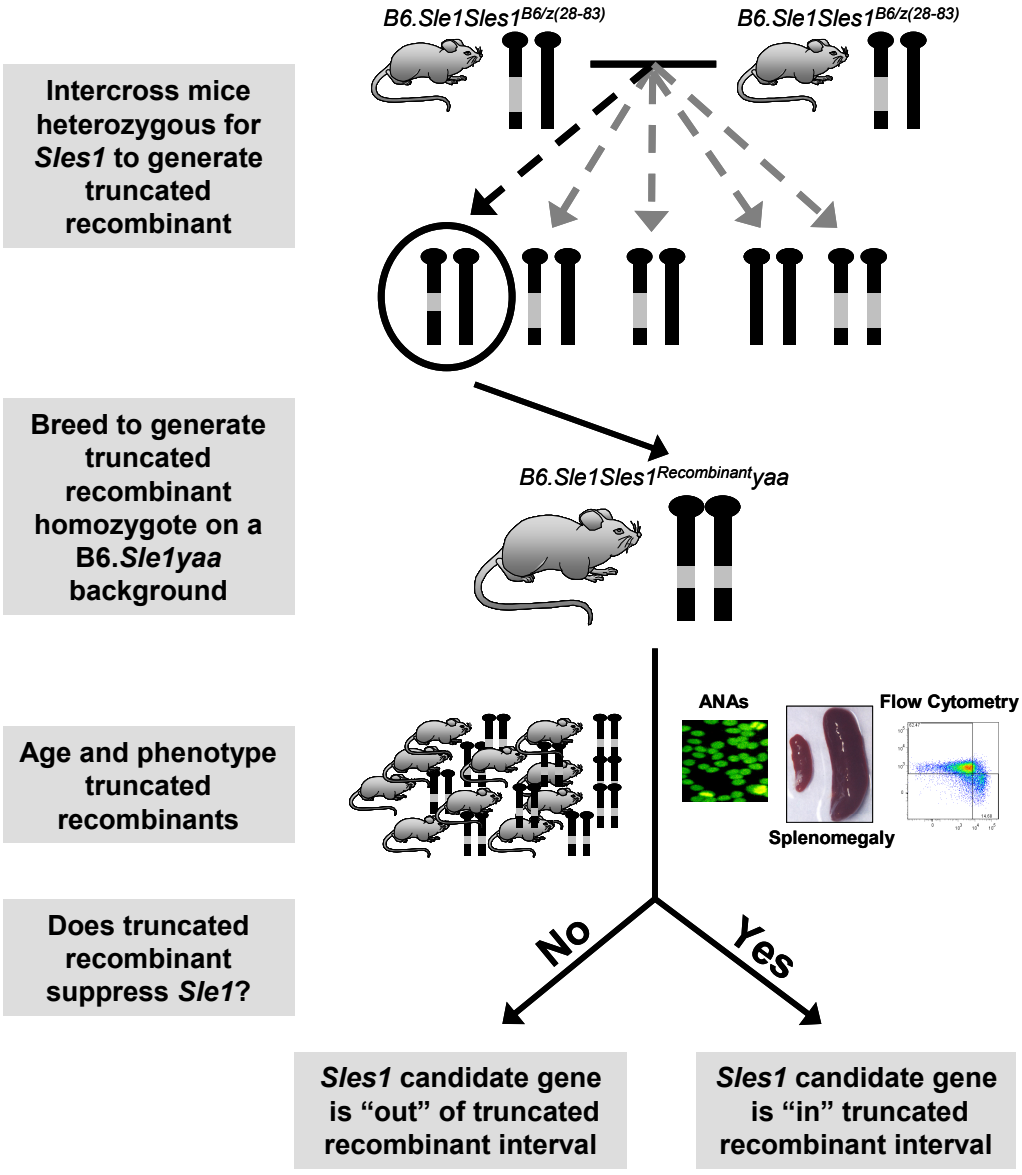

Figure 3. Truncated recombinant strategy to fine-map *Sles1*. B6.*Sle1* mice heterozygous for *Sles1* were intercrossed and progeny screened for truncated recombinants using microsatellite markers. Once identified, the truncated recombinant was back-crossed to B6.*Sle1Sles1*$^{(28\text{-}83)}$*yaa* and subsequently intercrossed to generate a homozygous line. Mice were then aged and assayed for suppression of *Sle1*.

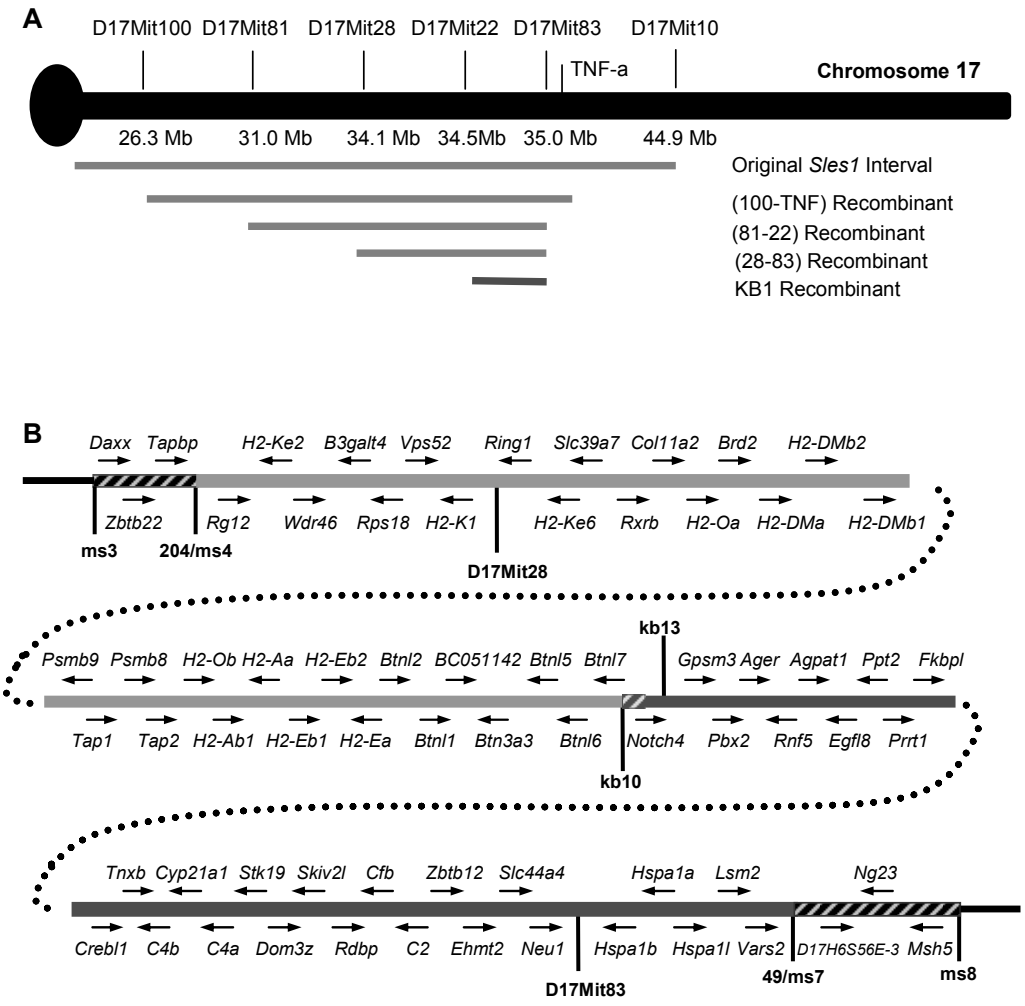

Figure 4. Genomic organization of *(28-83)* and *KB1 Sles1* intervals
A. Physical map of historical and current *Sles1* intervals on chromosome 17.
B. Detailed map of current Sles1 intervals, (28-83) and KB1, showing microsatellite markers (heavy vertical lines) flanking breakpoint regions (hatched thick horizontal lines) and genes (italicized names). Transcription orientation is indicated by arrows. Gene information and marker location were obtained from Ensembl 52

Sles1$^{(28\text{-}83)}$ and *Sles1*^{KB1}. For the remainder of this manuscript, *Sles1*$^{(28\text{-}83)}$ may be termed simply *Sles1* while *Sles1*^{KB1} will be termed *KB1*.

Sles1^{KB1} Does Not Suppress *Sle1*-mediated Disease in Female Mice

We comprehensively evaluated *Sle1*-mediated disease in age- and sex- matched B6, B6.*Sle1*, B6.*Sle1Sles1*and B6.*Sle1KB1* female mice to determine if the *Sles1* suppressive phenotype mapped to the *Sles1*^{KB1} interval. In addition to assaying humoral autoimmunity and splenomegaly, flow cytometry characterization of splenic cell subpopulations and cellular activation was completed.

Suppression of *Sle1*-mediated humoral autoimmunity was determined through ELISAs detecting antinuclear IgG at various ages. In 9 month old females, B6.*Sle1KB1* mice demonstrated no capacity for suppression and their ANA levels were indistinguishable from B6.*Sle1* mice ANA levels (898.0 ± 152.1 vs. 894.8 ± 132.4, respectively). B6.*Sle1Sles1* mice had significantly lower ANA levels (96.90 ± 21.22) than either B6.*Sle1KB1* ($p < 0.0001$) or B6.*Sle1* ($p < 0.0001$) (Figure 5A). However, in 12 month old females, B6.*Sle1KB1* mice had slightly lower ANA levels than B6.*Sle1* mice (1398.0 ± 177.2 vs. 2008.0 ± 178.6, $p = 0.0146$), but dramatically higher ANA levels than B6.*Sle1Sles1* mice (151.1 ± 59.41, $p < 0.0001$). These results map the potent *Sles1*

suppressive phenotype to the proximal non-*KB1* interval of *Sles1*$^{(28\text{-}83)}$, while suggesting the presence of a very weak modifier locus in the *Sles1*^{KB1} interval.

As shown in Figure 6, the comparison of 12 month old mouse spleen weights demonstrated a similar pattern. While B6.*Sle1KB1* mice had slightly less splenomegaly compared to B6.*Sle1* mice (206.9 ± 16.6 mg vs. 259.7 ± 18.8 mg, respectively, p =0.0399), B6.*Sle1Sles1* mice had much smaller spleens (131.2 ± 8.9 mg) than either B6.*Sle1KB1* mice (p = 0.0003) or B6.*Sle1* mice ($p < 0.0001$). These results also localize the strong *Sles1* phenotype out of *Sles1*^{KB1}, but are consistent with a weak suppressive effect within *Sles1*^{KB1}.

Extensive 10-12 color flow cytometry analysis was completed on 12 month old female splenocytes to fully evaluate the suppressive capacity of *Sles1*^{KB1} in sub- phenotypes (for details, see *Materials and Methods*). Of the 24 splenic cell parameters with quantitative differences between B6.*Sle1* and B6.*Sle1Sles1* mice, 20 were also significantly different between B6.*Sle1Sles1*and B6.*Sle1KB1* while none were significantly different between B6.*Sle1* and B6.*Sle1KB1* (Table 5). This contrasts with the ANA and splenomegaly data, which show small differences between B6.*Sle1* and B6.*Sle1KB1.*

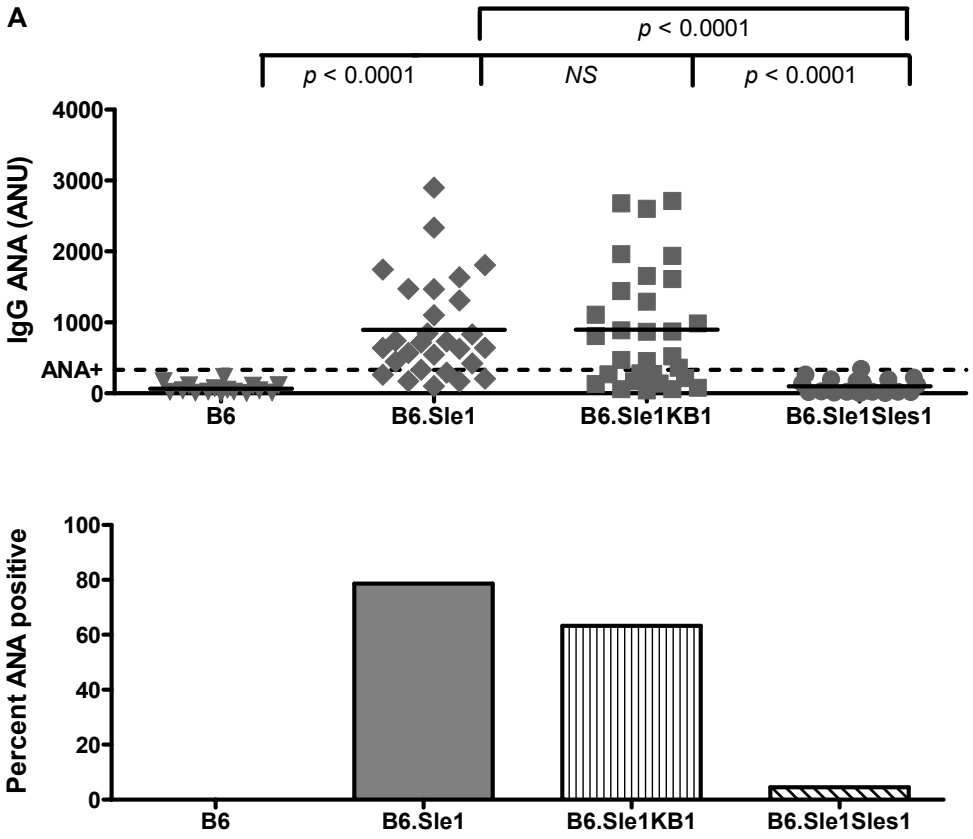

Figure 5A. *Sle1*-mediated humoral autoimmunity is not suppressed in 9 month B6.*Sle1Sles1*^{KB1} females. Top panel shows IgG ANA levels and bottom panel shows penetrance of ANA positivity. Mice were considered ANA positive when the level was 4 standard deviations above the B6 group mean. n = 16-30 mice per genotype.

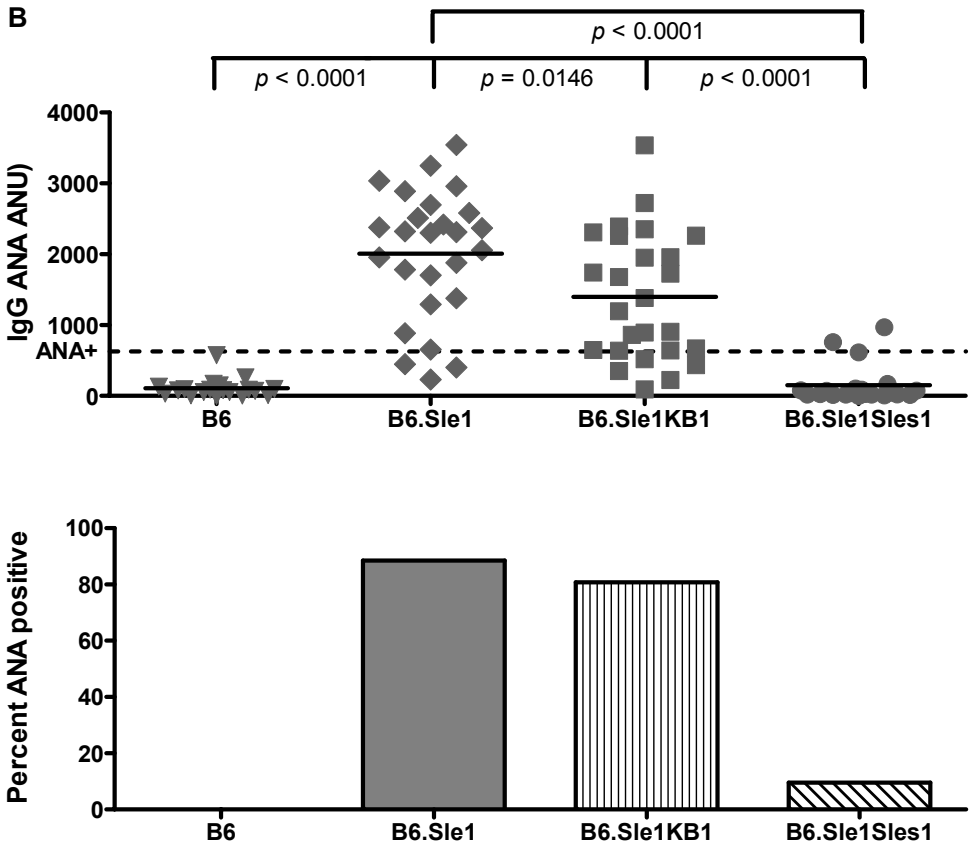

Figure 5B. *Sle1*-mediated humoral autoimmunity is slightly suppressed in 12 month B6.*Sle1Sles1*^{KB1} females. Top panel shows IgG ANA levels and bottom panel shows penetrance of ANA positivity. Although *Sles1*^{KB1} mice had slightly lower ANA levels, they did have not decreased ANA penetrance. Mice were considered ANA positive when the level was 4 standard deviations above the B6 group mean. n = 19-26 mice per genotype.

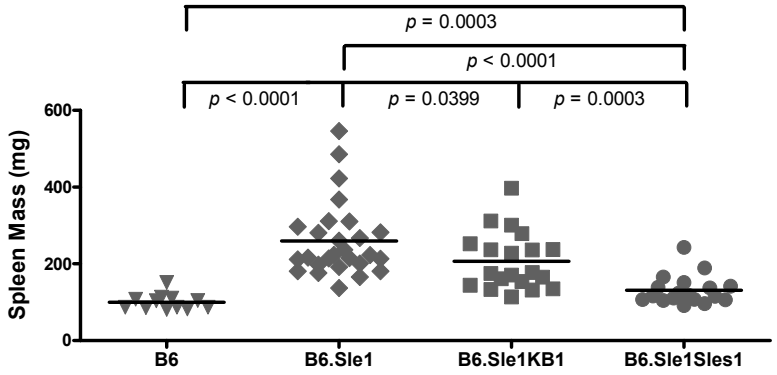

Figure 6. *Sle1*-mediated splenomegaly is slightly less in 12 month B6.*Sle1Sles1*^{KB1}females. n = 12-27 mice per genotype.

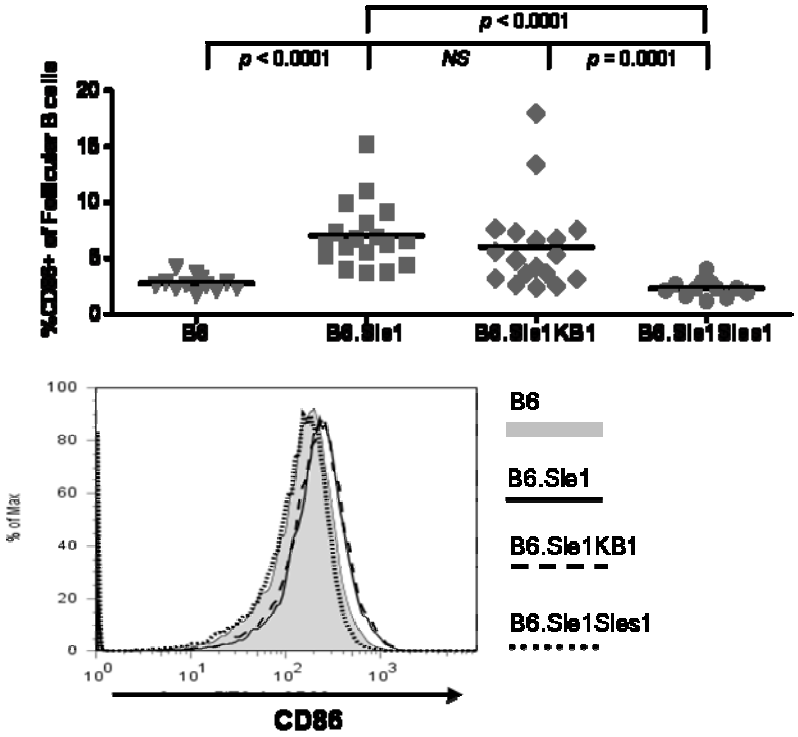

Figure 7. *Sle1*-mediated follicular B cell hyper-activation is not affected in 12 month B6.*Sle1Sles1*^{KB1} females. Top panel shows percentages of follicular B cells (B220$^+$CD23$^+$CD21$^+$IgM$^+$) that are CD86+. Bottom panel is a representative CD86 histogram overlay of follicular B cells. n = 12-18 mice per genotype.

Sle1 induces hyper-activation of lymphocytes, as shown by increased expression of the activation marker CD86 on follicular B cells ($B220^+CD23^+CD21^+IgM^+$) and activation marker CD69 on helper T cells ($CD3^+CD4^+$). Figure 7 demonstrates that while the percentage of $CD86^+$ follicular B cells is indistinguishable between B6.*Sle1* and B6.*Sle1KB1* mice (7.03 ± 0.68 vs. 6.04 ± 0.95, respectively), it is dramatically reduced in B6.*Sle1Sles1* mice so to be comparable to follicular B cell activation levels in B6 mice (2.34 ± 0.22 vs. 2.79 ± 0.19, respectively) (Table 5). In a similar fashion, B6.*Sle1* and B6.*Sle1KB1* again have equivalent percentages (35.33 ± 2.82 vs. 31.61 ± 2.83) of CD69+ helper T cells which are significantly higher than in B6.*Sle1Sles1* mice (11.03 ± 2.04, both $p < 0.0001$). In contrast to activated B cells, B6.*Sle1Sles1* mice actually have significantly less $CD69^+$ activated T cells than B6 mice (Table 5) demonstrating the remarkable capacity of *Sles1* to regulate the immune response. These phenotypes are also reflected in the cell-surface density of these activation markers as determined by median fluorescence intensity (MFIs) (bottom panel of Figure 7 and right panel of Figure 8A). Therefore, $Sles1^{KB1}$ is not sufficient to restore normal lymphocyte activation levels in B6.*Sle1* mice, unlike $Sles1^{(28\text{-}83)}$.

Sle1 also mediates striking changes in subpopulations of helper T cells, reflecting the hyperactivity of this cellular compartment. Specifically,

there is an increase in memory helper T cells ($CD62L^{lo}CD44^{hi}CD4^{+}CD3^{+}$), a corresponding decrease in naïve helper T cells ($CD62L^{hi}CD44^{lo}CD4^{+}CD3^{+}$), and an increase in follicular helper T cells ($ICOS^{+}CXCR5^{+}CD4^{+}CD3^{+}$). B6.*Sle1* mice and B6.*Sle1KB1* mice each had greater than 2-fold increases in the percentages of memory helper T cells, compared to B6.*Sle1Sles1* mice (71.41 ± 2.90 and 63.67 ± 3.50 vs. 27.59 ± 3.00, both $p < 0.0001$) (Table 5 and Figure 8B).

Similarly, there is a marked increase in the percentage of follicular helper T cells in B6.*Sle1* and B6.*Sle1KB1* but not in B6.*Sle1Sles1* splenocytes (33.34 ± 2.09 and 26.81 ± 2.30 vs. 7.28 ± 1.20, both $p < 0.0001$) (Table 5 and Figure 8C). This is also reflected in the cell-surface densities of ICOS, CXCR5, and PD-1, all markers of follicular helper T cells [168, 169] (bottom panel of Figure 8C). B6.*Sle1Sles1* mice had even lower percentages than B6 mice of memory (27.59 ± 3.00 vs. 38.81 ± 2.71, $p = 0.0304$) and follicular (7.28 ± 1.20 vs. 14.60 ± 1.52, $p = 0.0007$) helper T cells (Figure 8B-C, Table 5). This may reflect an intrinsic effect of *Sles1* or an epistatic interaction of *Sles1* with *Sle1*. Thus, B6.*Sle1Sles1* mice, but not B6.*Sle1KB1* mice, can suppress the skewing of helper T cell sub-populations, not only compared to B6.*Sle1* mice, but also when compared to B6 mice.

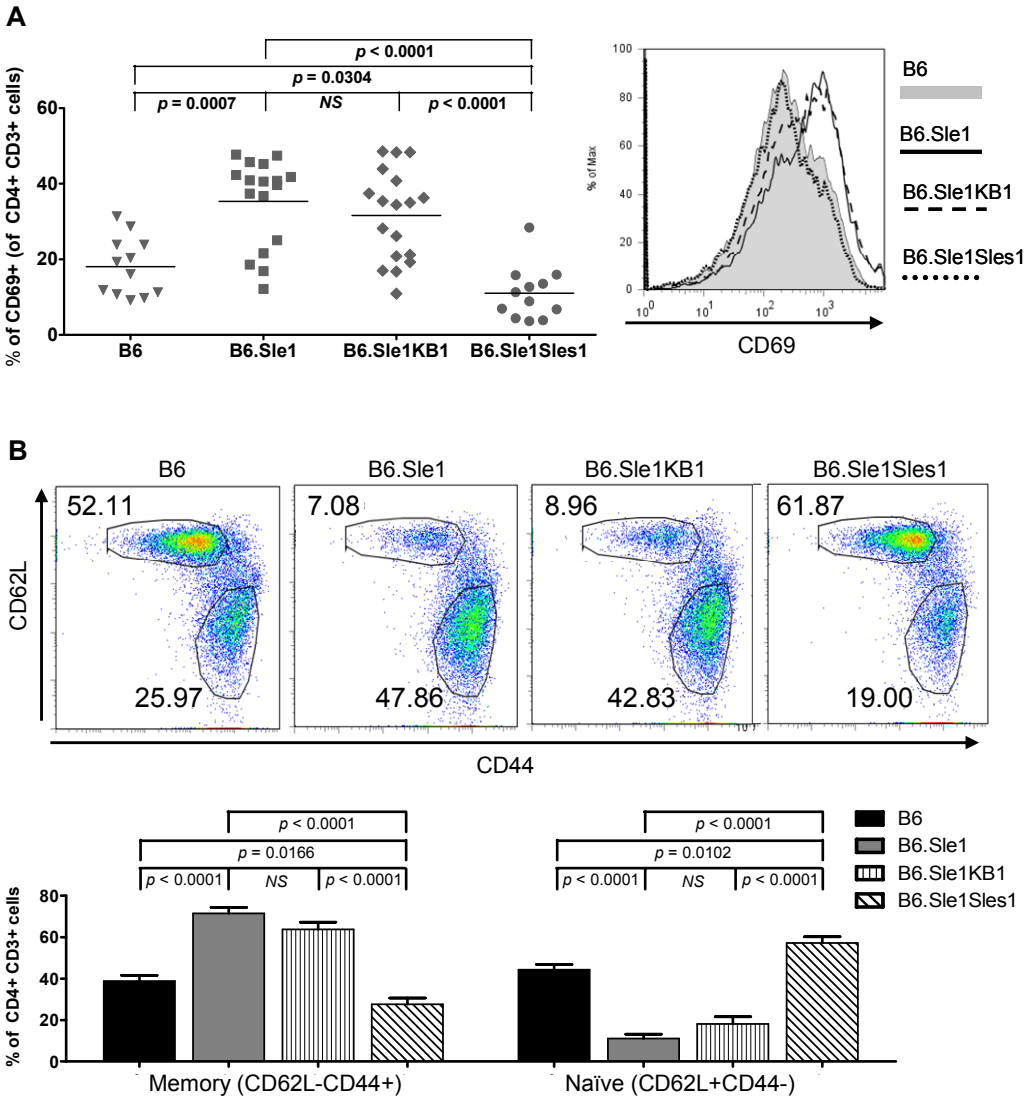

Figure 8A-B. *Sle1*-mediated T cell activation is not suppressed in 12 month B6.*Sle1Sles1*^{KB1}females. **A.** Left panel, percent of CD4^{+} CD3^{+} T cells that are CD69+. Right panel, representative CD69 histogram overlay of CD4+ CD3+ T cells. **B**. Top panel, representative dot plots of memory vs. naïve CD4^{+}CD3^{+} T cells. Bottom panel, percentages of CD4^{+}CD3^{+} T cells that are memory (left) and naïve (right). n = 12-18 mice per genotype.

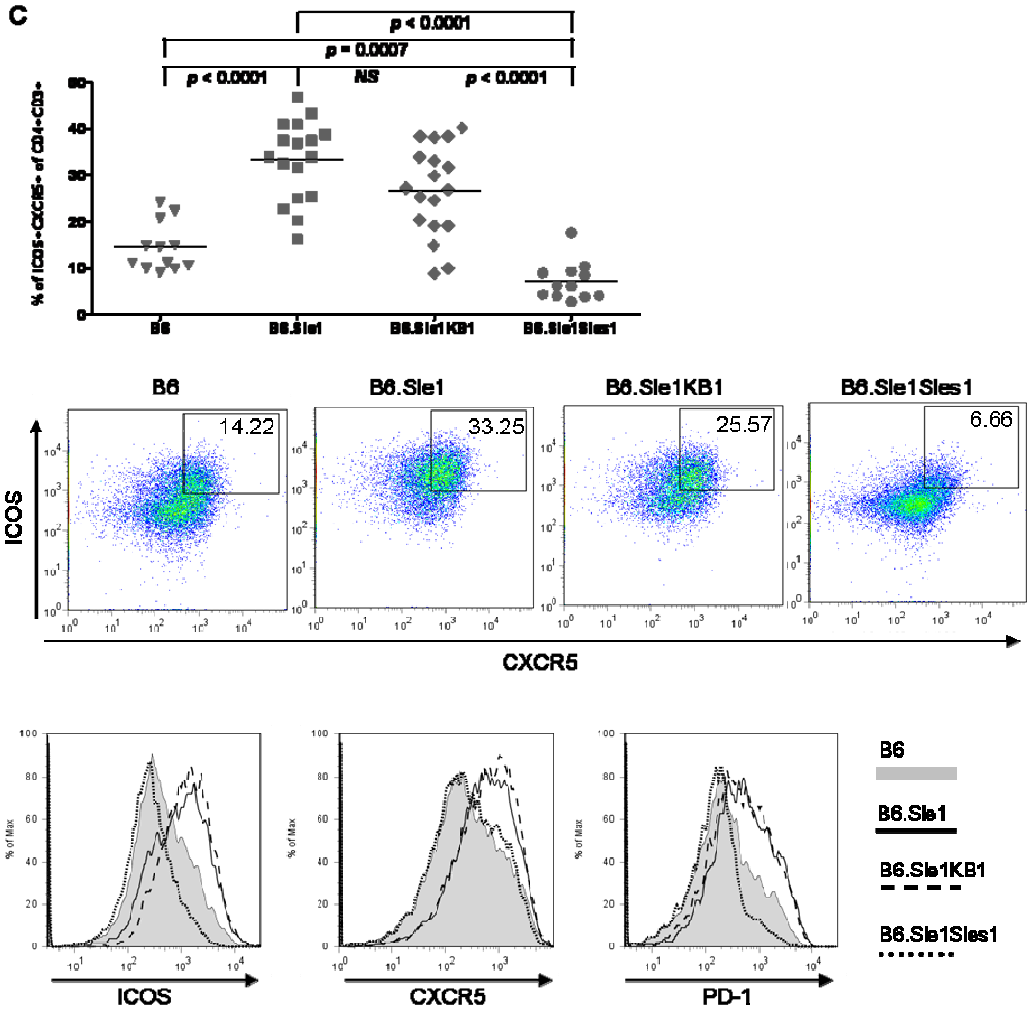

Figure 8C. *Sle1*-mediated follicular helper T cell expansion is not suppressed in 12 month B6.*Sle1Sles1*^{KB1}females. Top panel, percentages of CD4+ CD3+ T cells are follicular helper T cells (ICOS^{+}CXCR5^{+}). Middle panel, representative dot plots of follicular helper CD4+CD3+ T cells. Bottom panel, representative histogram overlay of CD4^{+} CD3^{+} T cells showing expression of ICOS (left), CXCR5 (middle) and PD-1 (right). n = 12-18 mice per genotype.

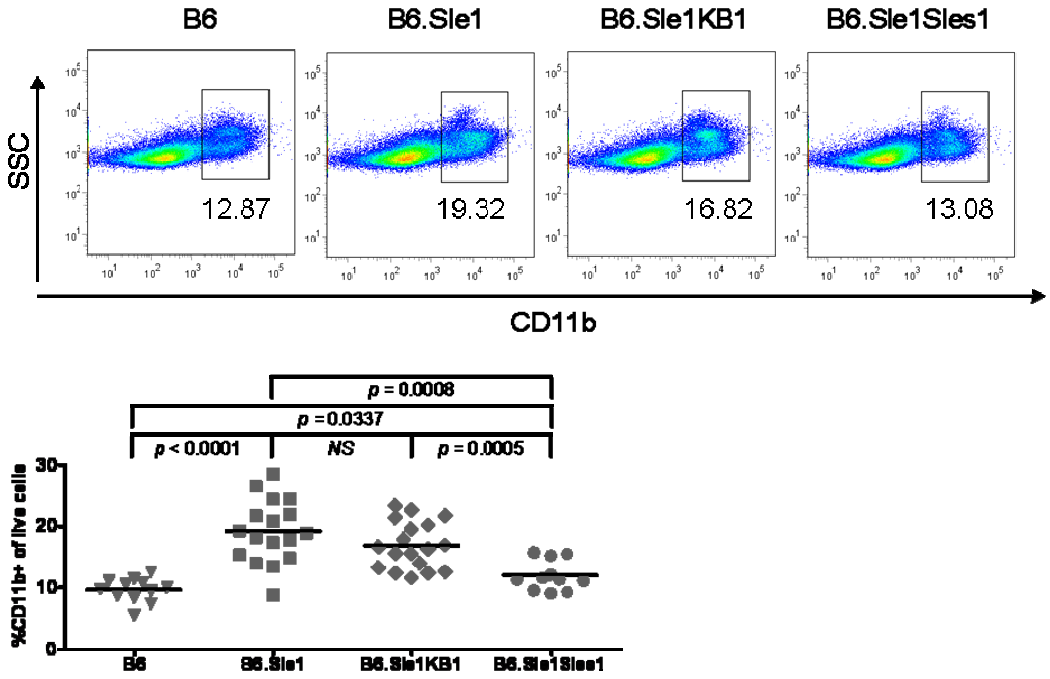

Figure 9. *Sle1*-mediated monocytosis is not suppressed in 12 month B6.*Sle1Sles1*^{KB1} females. Top panel, representative dot plots of CD11b^{+} cells (of live). Bottom panel, percentages of CD11b+ (of live). n = 12-18 mice per genotype.

Table 5. Splenic cell populations in B6, B6.*Sle1*, B6.*Sle1KB1*, and B6.*Sle1Sles1* 12 month females

Population[1]	B6 (n=12)	B6.*Sle1* (n=18)	B6.*Sle1KB1* (n=18)	B6.*Sle1Sles1* (n=12)	B6 vs B6.*Sle1*	B6.*Sle1* vs. B6.*Sle1KB1*	B6.*Sle1* vs B6.*Sle1Sles1*	B6.*Sle1KB1* vs B6.*Sle1Sles1*
B220/CD19+	48.76 ± 1.70	40.62 ± 1.70	41.15 ± 1.18	45.23 ± 1.51	***P* = 0.0056**	NS	NS	NS
Number of cells	74188 ± 2443	66540 ± 3483	68066 ± 2331	73123 ± 3513	***P* = 0.0056**	NS	**NS**	**NS**
CD86+	4.74 ± 0.37	6.00 ± 0.48	5.70 ± 0.64	4.78 ± 0.57	***P* < 0.0001**	NS	***P* < 0.0001**	***P* = 0.0001**
T1 ($CD23^-CD21^-IgM^+$)	6.20 ± 0.45	3.86 ± 0.29	4.59 ± 0.31	6.67 ± 0.42	***P* = 0.0008**	NS	***P* < 0.0001**	***P* = 0.0010**
T2 ($CD23^+CD21^{hi}IgM^{hi}$)	1.87 ± 0.31	1.79 ± 0.24	1.58 ± 0.28	1.85 ± 0.22	NS	NS	NS	NS
Follicular[2]	36.12 ± 1.42	24.54 ± 1.58	26.18 ± 1.47	36.35 ± 0.84	***P* < 0.0001**	NS	***P* < 0.0001**	***P* < 0.0001**
CD86+	2.79 ± 0.19	7.03 ± 0.68	6.04 ± 0.95	2.34 ± 0.22	***P* < 0.0001**	NS	***P* < 0.0001**	***P* = 0.0001**
MZ ($CD23^-CD21^+IgM^+$)	8.54 ± 0.66	9.91 ± 0.80	10.34 ± 0.85	9.42 ± 0.59	NS	NS	NS	NS
B1a ($CD5^+CD23^-B220^+$)	4.15 ± 0.46	5.96 ± 0.51	6.01 ± 2.48	4.14 ± 0.44	***P* = 0.0262**	NS	***P* = 0.0235**	***P* = 0.0325**
B1b ($CD5^-CD23^-B220^{lo}$)	6.29 ± 1.12	5.70 ± 0.86	5.81 ± 1.00	6.10 ± 0.87	NS	NS	NS	NS
B2 ($CD5^-CD23^+B220^+$)	19.46 ± 3.65	9.01 ± 1.44	8.50 ± 0.90	16.67 ± 2.29	***P* = 0.0210**	NS	***P* = 0.0063**	***P* = 0.0043**
Plasma ($CD19^-CD138^+$)	0.88 ± 0.06	1.57 ± 0.15	1.47 ± 0.18	0.74 ± 0.22	***P* = 0.0005**	NS	***P* < 0.0001**	***P* = 0.0002**
CD3+	32.30 ± 1.27	26.09 ± 1.06	26.75 ± 0.68	33.31 ± 1.55	***P* = 0.0007**	NS	***P* = 0.0024**	***P* = 0.0014**
Number of cells	31913 ± 1253	24428 ± 987.8	25957 ± 727.6	29616 ± 1548	***P* < 0.0001**	NS	***P* = 0.0323**	**NS**
CD4+	52.37 ± 0.88	64.14 ± 2.21	61.82 ± 2.47	54.67 ± 0.69	***P* = 0.0007**	NS	***P* = 0.0084**	***P* = 0.0490**
CD69+	18.05 ± 2.23	35.33 ± 2.82	31.61 ± 2.83	11.03 ± 2.04	***P* = 0.0007**	NS	***P* < 0.0001**	***P* < 0.0001**
CD25+CD69-	4.51 ± 0.41	4.94 ± 0.40	5.72 ± 0.48	6.45 ± 0.36	***P* = 0.0004**	NS	***P* = 0.0324**	NS
CD69+CD25+	4.29 ± 0.66	8.24 ± 0.27	7.50 ± 0.50	3.87 ± 0.45	***P* = 0.0008**	NS	***P* = 0.0324**	***P* = 0.0015**
CD69+CD25-	17.74 ± 2.48	34.15 ± 1.88	28.69 ± 2.79	12.56 ± 1.65	***P* = 0.0009**	NS	***P* = 0.0005**	***P* = 0.0017**
$CD62L^{hi}CD44^{lo}$	44.26 ± 2.56	11.10 ± 2.05	18.11 ± 3.44	57.20 ± 3.00	***P* < 0.0001**	NS	***P* < 0.0001**	***P* < 0.0001**
$CD62L^{lo}CD44^{hi}$	38.81 ± 2.71	71.41 ± 2.90	63.67 ± 3.50	27.59 ± 3.00	***P* < 0.0001**	NS	***P* < 0.0001**	***P* < 0.0001**
Follicular Helper[3]	14.60 ± 1.52	33.34 ± 2.09	26.81 ± 2.30	7.28 ± 1.20	***P* < 0.0001**	NS	***P* < 0.0001**	***P* < 0.0001**
CD8+	37.76 ± 0.93	26.11 ± 2.18	27.77 ± 2.69	36.54 ± 0.73	***P* = 0.0008**	NS	***P* = 0.0032**	***P* = 0.0401**
CD69+	8.58 ± 1.78	22.16 ± 3.63	18.80 ± 2.71	6.74 ± 1.47	***P* = 0.0008**	NS	***P* = 0.0032**	***P* = 0.0037**
CD11b+	9.67 ± 0.56	19.21 ± 1.24	16.90 ± 0.90	12.02 ± 0.74	***P* < 0.0001**	NS	***P* = 0.0080**	***P* = 0.0005**
Number of cells	11085 ± 1189	20254 ± 1848	15849 ± 1066	12948 ± 859.5	***P* = 0.0002**	NS	***P* = 0.0025**	**NS**
Neutrophils[4]	2.84 ± 0.42	6.28 ± 0.69	5.10 ± 0.48	3.16 ± 0.46	***P* = 0.0010**	NS	***P* = 0.0025**	***P* = 0.0277**
Inflammatory Monocytes[5]	1.60 ± 0.30	4.05 ± 0.32	3.69 ± 0.42	2.65 ± 0.30	***P* < 0.0001**	NS	***P* = 0.0051**	NS
Resident Monocytes[6]	0.91 ± 0.13	2.27 ± 0.26	1.97 ± 0.24	1.57 ± 0.15	***P* < 0.0001**	NS	NS	NS
Macrophages[7]	2.02 ± 0.14	3.68 ± 0.31	3.62 ± 0.37	2.56 ± 0.29	***P* = 0.0002**	NS	***P* = 0.0373**	NS
CD11c+	4.33 ± 0.24	8.24 ± 0.63	7.25 ± 0.34	5.07 ± 0.31	***P* < 0.0001**	NS	***P* = 0.0005**	***P* = 0.0004**
NK1.1+	2.71 + 0.21	1.72 ± 0.16	1.89 ± 0.14	2.43 ± 0.19	***P* = 0.0164**	NS	***P* = 0.0164**	NS

Table 5. Splenic cell populations in B6, B6.*Sle1*, B6.*Sle1KB1*, and B6.*Sle1Sles1* 12 month females

[1] Ten to eleven color flow cytometry was completed on splenocytes as detailed in Materials and Methods. Shown values represent mean ± SEM. Indented subsets indicate that the listed percentages are of the indicated parent population. All other percentages are of live cells, as determined by forward and side scatter profiles. NS = not significant.

[2] $B220^{+}CD23^{+}CD21^{+}IgM^{+}$

[3] $CD3^{+}CD4^{+}ICOS^{+}CXCR5^{+}$

[4] $CD11b^{+}Gr1^{+}SSC^{hi}$

[5] $CD11b^{+}Gr1^{+}Neu7/4^{+}SSC^{lo}$

[6] $CD11b^{+}Gr1^{-}Neu7/4^{+}$

[7] $CD11b^{+}F4/80^{+}$

Sle1 also produces a mild monocytosis when added to the B6 genomic background as measured by the significant increase in the percentage of $CD11b^+$ splenocytes (19.21 ± 1.24 vs. 9.67 ± 0.56, respectively, $p < 0.0001$). This phenotype is partially corrected by B6.*Sle1Sles1* mice (12.02 ± 0.74, $p = 0.0008$ vs. B6.*Sle1* and $p = 0.0337$ vs. B6), but not by B6.*Sle1KB1* (16.90 ± 0.90, $p = 0.0005$ vs. B6.*Sle1Sles1*).

In conclusion, despite extensive assaying, B6.*Sle1KB1* 12mo old female mice failed to demonstrate a *Sle1*-suppressing phenotype which is in stark contrast to age- and sex-matched B6.*Sle1Sles1* mice. This data maps the causative gene of *Sles1* into the proximal portion of the $Sles1^{(28\text{-}83)}$ interval that is not represented by $Sles1^{KB1}$. There were very slight, yet consistent, non-significant reductions of *Sle1*-disease by B6.*Sle1KB1* mice which could merely reflect natural variations in mouse handling and processing or perhaps an extremely weak suppressive effect.

$Sles1^{KB1}$ Does Not Suppress *Sle1*-mediated Disease in Male Mice with *Yaa*

To investigate the possibility of a slight suppressive phenotype contained within the $Sles1^{KB1}$ region, we also comprehensively evaluated *Sle1*-mediated disease in age- and sex- matched 4-6 month old B6.yaa,

B6.*Sle1yaa*, B6.*Sle1Sles1yaa* and B6.*Sle1KB1yaa* male mice. The *yaa* loci accelerates and amplifies autoimmune disease in male mice making B6.*Sle1yaa* is an extremely robust model of lupus. Like in the female B6.*Sle1* model above, we assayed humoral autoimmunity, splenomegaly, and splenic cell population markers.

Sle1-mediated humoral autoimmunity was determined through ELISAs detecting antinuclear IgG at various ages. In 4 month old males, B6.*Sle1KB1yaa* mice actually demonstrated increased ANA levels compared to B6.Sle1yaa (491.7 ± 83.28 vs. 213.5 ± 37.66, $p = 0.0108$) while B6.Sle1Sles1yaa mice had dramatically lower ANA levels than either diseased group (32.96 ± 5.69, both $p < 0.0001$) (Figure 10A). However, in 6 month old males, B6.*Sle1KB1yaa* mice were indistinguishable from B6.*Sle1yaa* mice in ANA levels (512.0 ± 100.3 vs. 421.0 ± 59.16). B6.*Sle1Sles1* mice again had much lower ANA levels (40.13 ± 11.74, $p < 0.0001$) (Figure 10B). These results map the potent *Sles1* suppressive phenotype to the proximal non-*KB1* interval of $Sles1^{(28\text{-}83)}$. Additionally, the existence of a very weak modifier locus (or loci) in the $Sles1^{KB1}$ interval is suggested. This modifier may further accelerate the generation of ANAs, but only in B6.*Sle1yaa* mice, as this effect was not evident in the B6.*Sle1* female model.

As shown in Figure 11, the comparison of 6 month old mouse spleen weights demonstrated a similar pattern. While B6.*Sle1KB1yaa* mice had

comparable degrees of splenomegaly as B6.*Sle1yaa* mice (566.0 ± 60.5 mg vs. 504.4 ± 58.63 mg), B6.*Sle1Sles1yaa* mice had much smaller spleens (82.58 ± 3.64 mg) than either B6.*Sle1KB1yaa* or B6.*Sle1yaa* mice (both $p < 0.0001$) (Figure 11). These results also localize the strong *Sles1* phenotype out of the $Sles1^{zKB1}$ interval.

Extensive 10-12 color flow cytometry analysis was completed on 6 month old male splenocytes to fully evaluate the suppressive capacity of $Sles1^{KB1}$ in sub-phenotypes (for details, see *Materials and Methods*). Of the 27 splenic cell parameters with quantitative differences between B6.*Sle1yaa* and B6.*Sle1Sles1yaa* mice, 24 were also significantly different between B6.*Sle1Sles1yaa* and B6.*Sle1KB1yaa.* Only six of these parameters were significantly different between

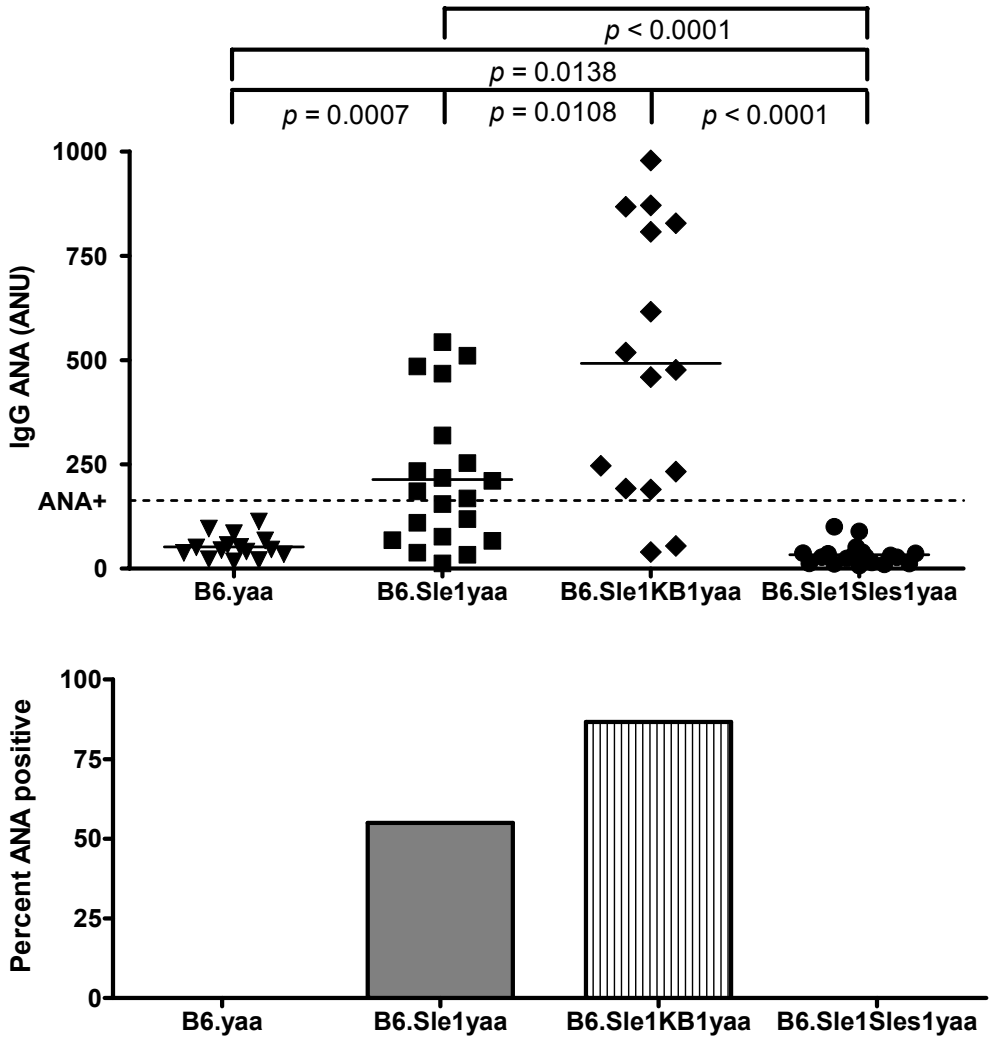

Figure 10A. *Sle1*-mediated humoral autoimmunity is enhanced in 4 month B6.*Sle1Sles1*^{KB1}*yaa* males. Top panel shows IgG ANA levels and bottom panel shows penetrance of ANA positivity. Mice were considered ANA positive when the level was 4 standard deviations above the B6.*yaa* group mean. n = 15-20 mice per genotype.

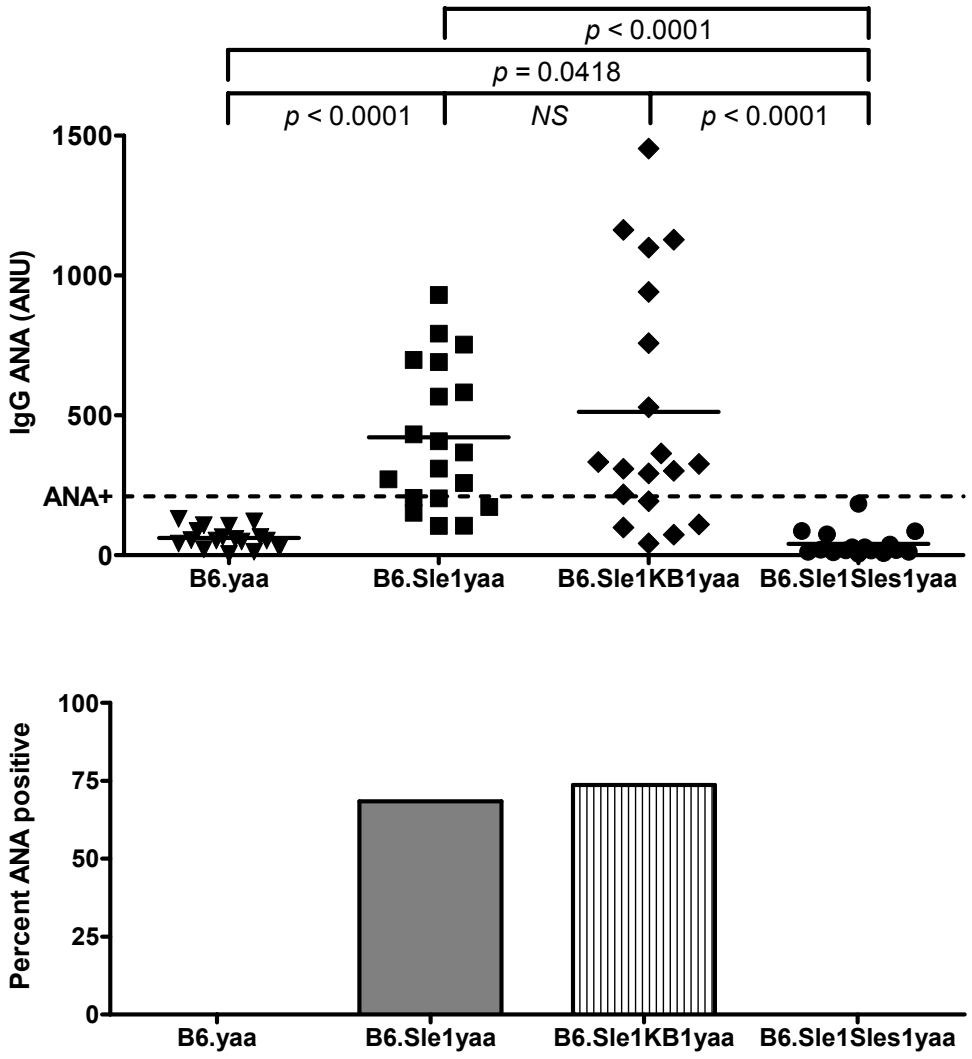

Figure 10B. *Sle1*-mediated humoral autoimmunity is enhanced in 4 month B6.*Sle1Sles1*^{KB1}*yaa* males. Top panel shows IgG ANA levels and bottom panel shows penetrance of ANA positivity. Mice were considered ANA positive when the level was 4 standard deviations above the B6.*yaa* group mean. n = 15-20 mice per genotype.

B6.*Sle1yaa* and B6.*Sle1KB1yaa,* four of which reflect increased disease in B6.*Sle1KB1yaa* mice (Table 6).

Sle1 induces hyper-activation of lymphocytes, as shown by increased expression of the activation marker CD86 on follicular B cells ($B220^+CD23^+CD21^+IgM^+$) and activation marker CD69 on helper T cells ($CD3^+CD4^+$). Figure 12 demonstrates that while the percentage of $CD86^+$ follicular B cells is statistically indistinguishable between B6.*Sle1yaa* (11.85 ± 1.46), B6.*Sle1KB1yaa,* (12.82 ± 2.32) and B6.*Sle1Sles1yaa* mice (7.42 ± 0.74), there is a trend towards less activation in the B6.*Sle1Sles1yaa* group (Figure 12, top panel). A representative histogram overlay of CD86 on follicular helper B cells also demonstrates that the suppressive phenotype is exclusive to B6.*Sle1Sles1yaa* mice (Figure 12, bottom panel). This is more clearly shown in the T cell compartment. B6.*Sle1yaa* and B6.*Sle1KB1yaa* have equivalent percentages of $CD69^+$ helper T cells (27.52 ± 1.69 vs. 27.58 ± 2.80) which are significantly higher than in B6.*Sle1Sles1yaa* mice (10.00 ± 0.59, both $p < 0.0001$) (Figure 13A and Table 6). In contrast to activated B cells, B6.*Sle1Sles1yaa* mice actually have significantly less $CD69^+$ activated T cells than B6 mice (Table 6) demonstrating the remarkable capacity of *Sles1* to regulate the immune response. This phenotypes is also reflected in the cell-surface density of $CD69^+$ on helper T cells as determined by

MFIs (right panel of Figure 13A). Therefore, *Sles1*^{KB1} is not sufficient to restore normal lymphocyte activation levels in B6.*Sle1yaa* mice, unlike *Sles1*$^{(28\text{-}83)}$.

Sle1 also mediates striking changes in subpopulations of helper T cells, reflecting the hyperactivity of this cellular compartment. Specifically, there is an increase in memory helper T cells ($CD62L^{lo}CD44^{hi}CD4^{+}CD3^{+}$), a corresponding decrease in naïve helper T cells ($CD62L^{hi}CD44^{lo}CD4^{+}CD3^{+}$), and an increase in follicular helper T cells ($ICOS^{+}CXCR5^{+}CD4^{+}CD3+$). B6.*Sle1KB1yaa* had slightly increased percentages of memory helper T cells, compared to B6.*Sle1yaa* mice (83.72 ± 2.46 vs. 74.19 ± 3.42, $p = 0.0119$), both of which were roughly 4-fold higher than the percentages of memory helper T cells in B6.*Sle1Sles1yaa* mice (19.54 ± 0.81, both $p < 0.0001$) (Table 6 and Figure 13B). There is a marked increase in the percentage of follicular helper T cells in B6.*Sle1yaa* and B6.*Sle1KB1yaa* but not in B6.*Sle1Sles1yaa* splenocytes (17.17 ± 2.20 and 19.72 ± 2.48 vs. 3.12 ± 0.50, $p < 0.0001$ and $p = 0.0003$, respectively) (Table 6 and Figure 13C). This is also reflected in the cell-surface densities of ICOS, CXCR5 and PD-1 (bottom panel of Figure 13C). B6.*Sle1Sles1yaa* mice had even lower percentages than B6.*yaa* mice of memory (19.54 ± 0.81 vs. 32.87 ± 2.10, $p < 0.0001$) and follicular (3.12 ± 0.50 vs. 6.64 ± 1.15, p = 0.0066)

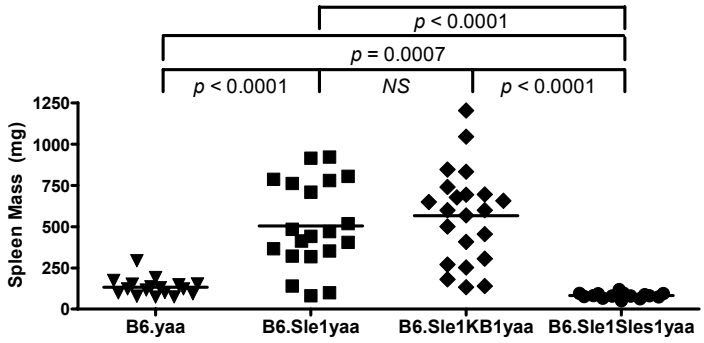

Figure 11. *Sle1*-mediated splenomegaly is not suppressed in 6 month B6.*Sle1Sles1*^{KB1}*yaa* males. n = 17-22 mice per genotype.

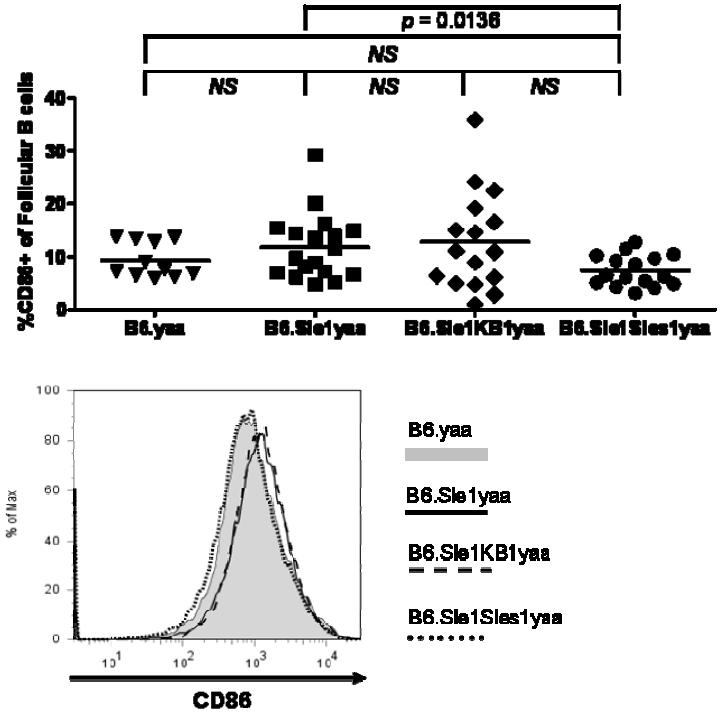

Figure 12. *Sles1*-mediated follicular B cell hypo-activation is not recapitulated in 6 month B6.*Sle1Sles1*^{KB1}*yaa* males. Top panel shows percentages of follicular B cells (B220^{+}CD23^{+}CD21^{+}IgM^{+}) that are CD86^{+}. Bottom panel is a representative CD86 histogram overlay of follicular B cells. n = 11-16. mice per genotype.

helper T cells (Figure 13B-C, Table 6). Thus, B6.*Sle1Sles1yaa* mice, but not B6.*Sle1KB1yaa* mice, can prevent the skewing of helper T cell sub-populations, not only compared to B6.*Sle1yaa* mice, but also when compared to B6.*yaa* mice.

The addition of *yaa* to B6.*Sle1* results in extreme monocytosis as measured by the significant increase in the percentage of $CD11b^+$ splenocytes. This phenotype is corrected by B6.*Sle1Sles1yaa* mice, compared to B6.*Sle1*yaa mice (12.37 ± 0.60 vs. 39.72 ± 3.84, $p < 0.0001$), but statistically not by B6.*Sle1KB1* (29.57 ± 3.75, $p = 0.0004$ vs B6.*Sle1Sles1*) despite a trend towards less disease. We looked more carefully at the monocyte compartment to see if this trend could be explained by differences in subpopulations. Within in the $CD11b^+$ cell population, B6.*Sle1KB1yaa* and B6.*Sle1Sles1yaa* mice had similar percentages of inflammatory monocytes ($Gr1^+Neu7/4^+SSC^{lo}$) and neutrophils ($Gr1^+SSC^{hi}$), which were
significantly lower than in B6.*Sle1yaa* mice (Figure 14B). This could reflect an overall decrease in these populations or a lack in migration to the spleen in B6.*Sle1KB1yaa* mice. It also suggests that increased numbers of splenic monocytes probably do not play a critical role in late-stage SLE as 6 month old B6.*Sle1KB1yaa* males have significant disease pathology.

B6.*Sle1yaa* 6 month old male mice also have dramatic GN as determined by the blinded examination of stained longitudinal kidney sections by an independent investigator (for more details, see *Materials and Methods*). B6.*Sle1Sles1yaa* mice had very little GN (overall pathology score, mean 0.50 ± 0.34), comparable to B6.*yaa* mice (0.63 ± 0.13), which was significantly less kidney damage than in either B6.*Sle1yaa* or B6.*Sle1KB1yaa* mice (3.40 ± 0.37 and $p = 0.0109$, 3.20 ± 0.16 and $p = 0.0012$, respectively) (Figure 15).

Despite extensive assaying, B6.*Sle1KB1yaa* 6mo old male mice failed to demonstrate a *Sle1*-suppressing phenotype which is in stark contrast to age- and sex-matched B6.*Sle1Sles1*yaa mice. This data supports the mapping of the causative gene of *Sles1* into the proximal portion of the $Sles1^{(28\text{-}83)}$ interval that is not represented by $Sles1^{KB1}$. Unlike B6.*Sle1KB1* females, B6.*Sle1KB1*yaa mice did not demonstrate a trend towards less disease, with the exception of monocytosis. B6.*Sle1KB1* mice actually showed significant increases in ANA levels at 4 months and skewing of the memory and naïve T cell subpopulations at 6 months (Figures 10A and 13B). This suggests a weak epistatic interaction between $Sles1^{KB1}$ and *yaa*.

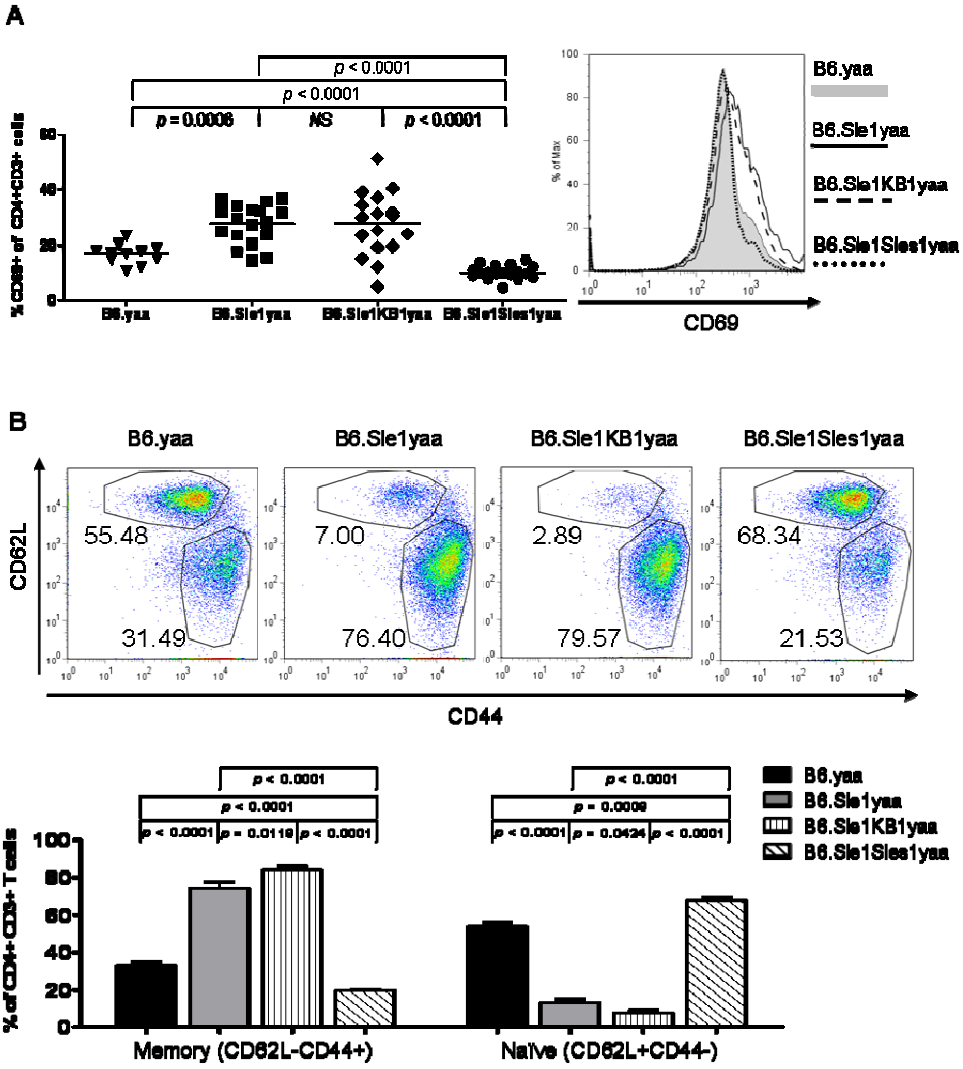

Figure 13A-B. *Sle1*-mediated T cell activation is not suppressed in 6 month B6.*Sle1Sles1*^{KB1}*yaa* males. **A.** Left panel, percentages of $CD4^+$ $CD3^+$ T cells that are $CD69^+$. Right panel, representative CD69 histogram overlay of $CD4^+$ $CD3^+$ T cells. **B**. Top, representative dot plots of memory vs naïve $CD4^+CD3^+$ T cells. Bottom panel, percentages of $CD4^+CD3^+$ T cells that are memory (left) and naïve (right). n = 10-22 mice per genotype.

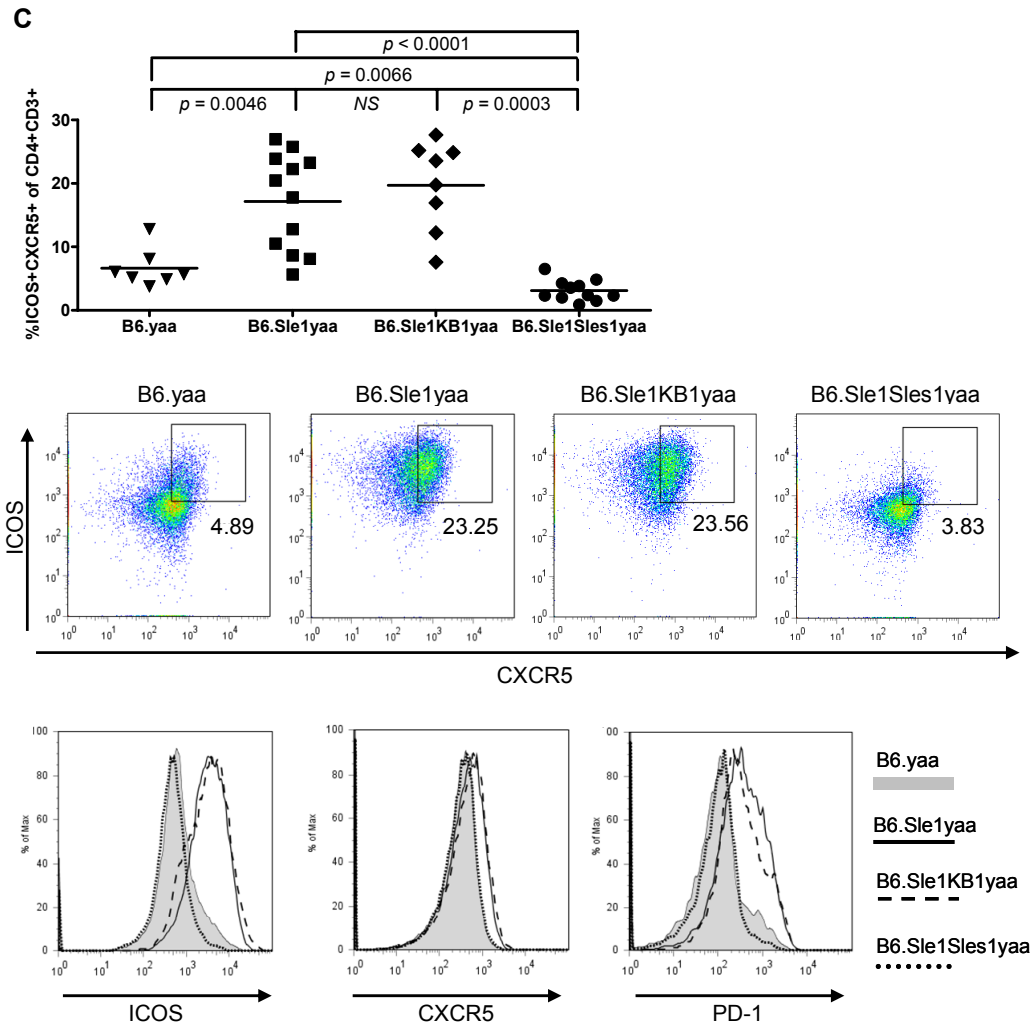

Figure 13C. *Sle1*-mediated follicular helper T cell expansion is not suppressed in 6 month B6.*Sle1Sles1*^{KB1}*yaa* males. Top panel, percentages of CD4$^+$ CD3$^+$ T cells are follicular helper T cells (ICOS$^+$CXCR5$^+$). Middle, representative dot plots of follicular helper CD4$^+$CD3$^+$ T cells. Bottom, representative histogram overlay of CD4$^+$ CD3$^+$ T cells showing expression of ICOS (left), CXCR5 (middle) and PD-1 (right). n = 7-12 mice per genotype.

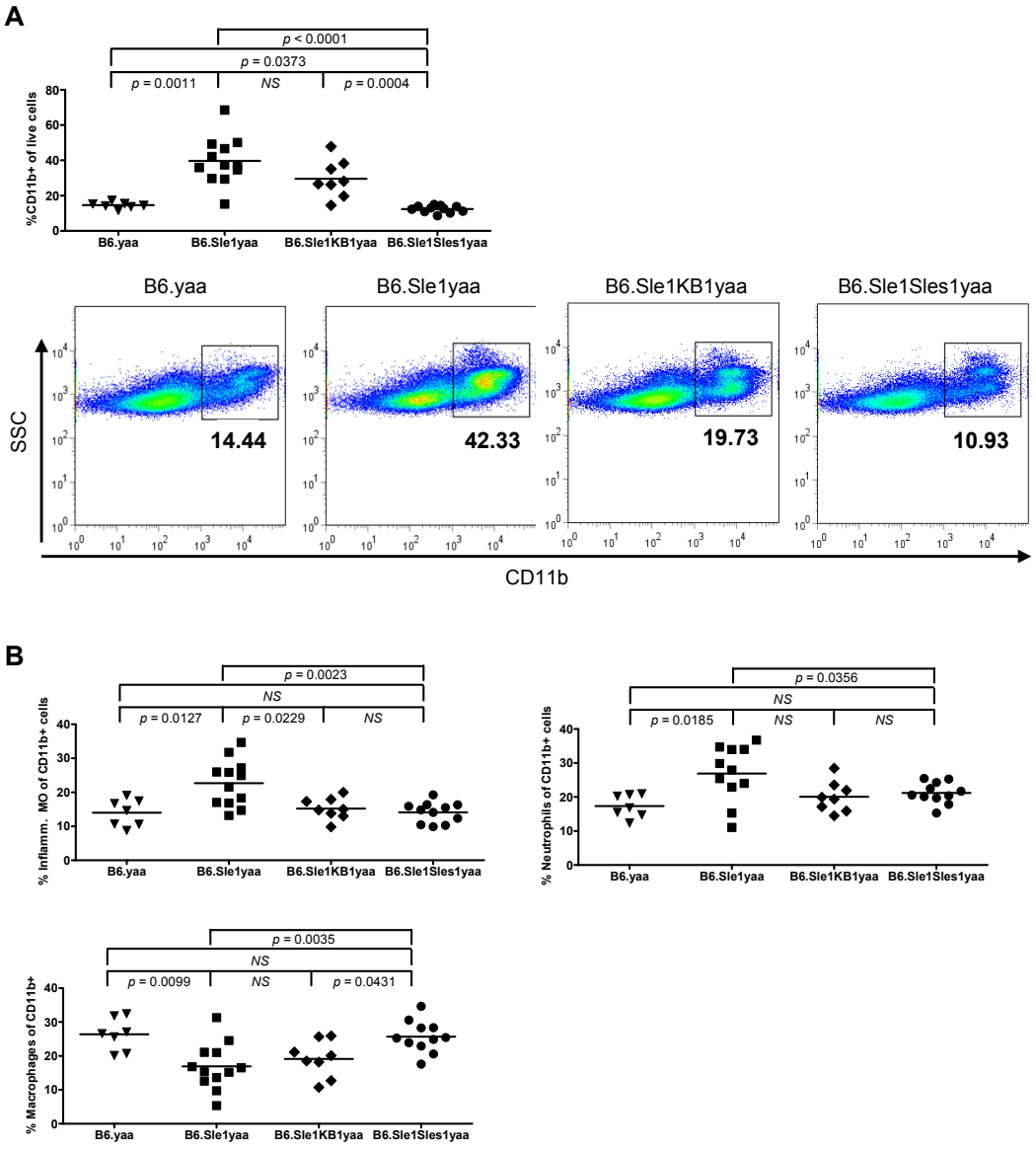

Figure 14. *Sle1*-mediated monocytosis is partially suppressed in 6 month B6.*Sle1Sles1*^{KB1}*yaa* males. **A.** Top panel, representative dot plots of CD11b+ cells (of live). Bottom panel, percentages of CD11b^{+} (of live cells). **B.** Percentages of inflammatory monocytes (Gr1^{+}Neu7/4^{+}SSC^{lo}), neutrophils (Gr1^{+}SSC^{hi}) and macrophages (F4/80^{+}) gated through live CD19/3^{-} CD11b^{+} cells. n = 7-12 mice per genotype.

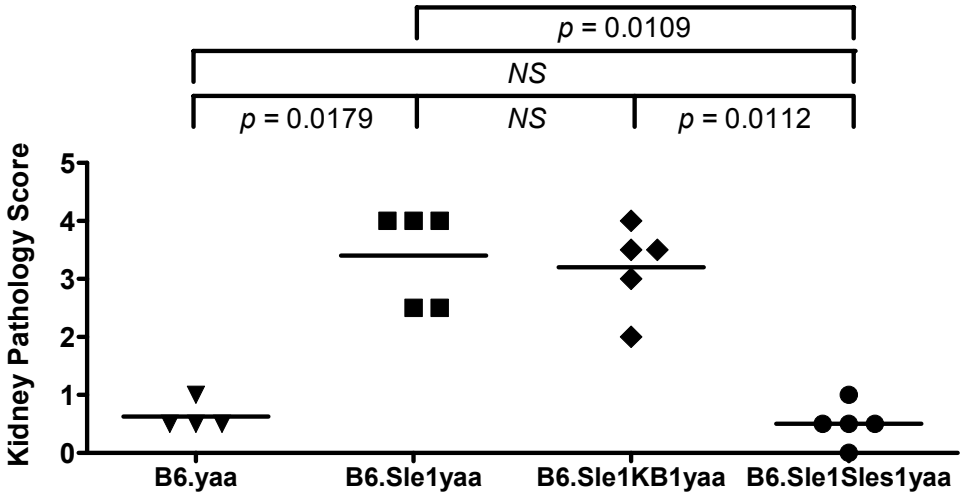

Figure 15. *Sle1*-mediated glomerulnephritis is not suppressed in 6 month B6.*Sle1Sles1*^{KB1}*yaa* males. Stained longitudinal kidney sections were blind examined for evidence of disease pathology in the glomeruli, tubules or interstitial areas by Dr. Xin J. Zhou (Department of Pathology, UTSW). The GN severity was graded on a scale of 0 to 4, where 0 indicates normal and 4 indicates significant evidence of disease. See *Materials and Methods* sections for more details.

Table 6. Splenic cell populations in B6.yaa, B6.*Sle1yaa*, B6.*Sle1KB1yaa*, and B6.*Sle1Sles1yaa* 6 month males

Population[1]	B6 (n=7-20)	B6.*Sle1* (n=12-24)	B6.*Sle1KB1* (n=8-22)	B6.*Sle1Sles1* (n=11-24)	B6 vs B6.*Sle1*	B6.*Sle1* vs. B6.*Sle1KB1*	B6.*Sle1* vs B6.*Sle1Sles1*	B6.*Sle1KB1* vs B6.*Sle1Sles1*
B220/CD19+	39.27 ± 2.33	25.04 ± 2.16	29.36 ± 2.86	44.96 ± 2.05	***P* = 0.0003**	NS	***P* < 0.0001**	***P* = 0.0006**
Number of cells	45211 ± 2526	27429 ± 2614	31507 ± 4022	47884 ± 1711	***P* = 0.0004**	NS	***P* < 0.0001**	***P* = 0.0070**
CD86+	15.07 ± 1.08	18.09 ± 1.30	18.53 ± 2.32	12.54 ± 0.92	NS	NS	***P* = 0.0020**	***P* = 0.0249**
T1 ($CD23^-CD21^-IgM^+$)	10.56 ± 1.22	14.40 ± 2.31	19.11 ± 3.14	7.15 ± 1.05	NS	NS	NS	***P* = 0.0006**
T2 ($CD23^+CD21^{hi}IgM^{hi}$)	1.18 ± 0.19	0.88 ± 0.19	0.42 ± 0.07	3.10 ± 0.36	NS	***P* = 0.0284**	***P* < 0.0001**	***P* < 0.0001**
Follicular[2]	45.78 ± 2.22	32.33 ± 2.34	36.38 ± 2.25	45.90 ± 1.62	***P* < 0.0001**	NS	***P* < 0.0001**	***P* = 0.0036**
CD86+	9.36 ± 1.00	11.85 ± 1.46	12.82 ± 2.32	7.42 ± 0.74	NS	NS	***P* = 0.0136**	NS
MZ ($CD23^-CD21^+IgM^+$)	2.74 ± 0.38	2.24 ± 0.37	1.50 ± 0.58	5.26 ± 0.29	NS	NS	***P* = 0.0002**	***P* < 0.0001**
B1a ($CD5^+CD23^-B220^+$)	1.12 ± 0.22	1.19 ± 0.11	0.98 ± 0.08	0.66 ± 0.08	NS	NS	***P* = 0.0014**	***P* = 0.0232**
B1b ($CD5^-CD23^-B220^{lo}$)	3.93 ± 0.17	5.36 ± 0.32	7.05 ± 0.63	3.82 ± 0.11	***P* = 0.0015**	***P* = 0.0186**	***P* = 0.0003**	***P* = 0.0003**
B2 ($CD5^-CD23^+B220^+$)	38.91 ± 2.52	20.85 ± 2.21	23.85 3.52	40.10 ± 2.22	***P* = 0.0011**	NS	***P* = 0.0002**	***P* = 0.0044**
Plasma ($CD19^-CD138^+$)	1.02 ± 0.13	2.86 ±0.25	3.43 ± 0.28	0.94 ± 0.16	***P* = 0.0006**	NS	***P* = 0.0001**	***P* = 0.0003**
CD3+	30.98 ± 1.06	18.15 ± 1.42	16.57 ± 1.73	35.29 ± 1.31	***P* < 0.0001**	NS	***P* < 0.0001**	***P* < 0.0001**
Numbr of cells	30758 ± 1364	17448 ± 1852	16074 ± 2173	34486 ± 1291	***P* = 0.0001**	NS	***P* < 0.0001**	***P* < 0.0001**
CD4+	48.47 ± 2.04	59.03 ± 1.78	66.37 ± 1.70	48.29 ± 1.04	***P* = 0.0004**	NS	***P* < 0.0001**	***P* < 0.0001**
CD69+	16.79 ± 1.09	27.52 ± 1.69	27.58 ± 2.80	10.00 ± 0.59	***P* = 0.0006**	NS	***P* < 0.0001**	***P* < 0.0001**
CD25+CD69-	9.12 ± 0.40	10.38 ± 0.70	16.38 ± 1.44	9.09 ± 0.49	***P* = 0.0162**	NS	***P* = 0.0012**	***P* = 0.0001**
CD69+CD25+	3.79 ± 0.49	7.58 ± 0.96	8.88 ± 0.95	2.98 ± 0.41	NS	***P* = 0.0006**	NS	***P* < 0.0001**
CD69+CD25-	11.29 ± 1.17	16.48 ± 1.47	17.72 ± 2.44	6.14 ± 0.76	***P* = 0.0232**	NS	***P* < 0.0001**	***P* = 0.0005**
Mem. ($CD62L^{lo}CD44^{hi}$)	32.87 ± 2.10	74.19 ± 3.42	83.72 ± 2.46	19.54 ± 0.81	***P* < 0.0001**	***P* = 0.0119**	***P* < 0.0001**	***P* < 0.0001**
Naïve ($CD62L^{hi}D44^{lo}$)	53.43 ± 2.67	12.78 ± 2.36	7.36 ± 1.78	67.32 ± 1.94	***P* < 0.0001**	***P* = 0.0424**	***P* < 0.0001**	***P* < 0.0001**
Follicular Helper[3]	6.64 ± 1.15	17.17 ± 2.20	19.72 ± 2.48	3.12 ± 0.50	***P* = 0.0046**	NS	***P* < 0.0001**	***P* = 0.0003**
CD8+	37.71 ± 0.95	25.88 ± 1.56	23.24 ± 2.07	41.15 ± 0.68	***P* < 0.0001**	NS	***P* < 0.0001**	***P* < 0.0001**
CD69+	6.34 ± 0.80	12.87 ± 1.29	8.08 ± 1.12	4.71 ± 0.49	***P* = 0.0021**	***P* = 0.0112**	***P* < 0.0001**	***P* = 0.0302**
CD11b+	14.60 ± 0.66	39.72 ± 3.84	29.57 ± 3.75	12.37 ± 0.60	***P* = 0.0011**	NS	***P* < 0.0001**	***P* = 0.0004**
Number of cells	14497 ± 658.6	39435 ± 3791	29428 ± 3748	12283 ± 599.8	***P* = 0.0011**	NS	***P* < 0.0001**	***P* = 0.0006**
Neutrophils[4]	2.13 ± 0.22	7.04 ± 1.14	4.19 ± 0.48	2.45 ± 0.15	***P* = 0.0086**	NS	***P* = 0.0039**	***P* = 0.0093**
Inflammatory Monocytes[5]	1.65 ± 0.11	8.06 ± 1.52	3.19 ± 0.40	1.61 ± 0.10	***P* = 0.0005**	***P* = 0.0122**	***P* < 0.0001**	***P* = 0.0008**
Resident Monocytes[6]	0.98 ± 0.13	1.92 ± 0.38	1.68 ± 0.41	0.98 ± 0.14	***P* = 0.0470**	NS	***P* = 0.0042**	NS
Macrophages[7]	3.34 ± 0.54	5.36 ± 0.88	3.97 ± 0.50	2.99 ± 0.28	***P* = 0.0311**	NS	***P* = 0.0015**	NS
CD11c+	5.45 ± 0.49	8.62 ± 1.22	7.91 ± 1.63	3.43 ± 0.33	NS	NS	***P* = 0.0005**	***P* = 0.0149**
NK1.1+	2.69 ± 0.21	1.95 ± 0.20	2.03 ± 0.38	2.91 ± 0.16	***P* = 0.0384**	NS	***P* = 0.0009**	***P* = 0.0431**

Table 6. Splenic cell populations in B6.*yaa*, B6.*Sle1yaa*, B6.*Sle1KB1yaa*, and B6.*Sle1Sles1yaa* 6 month males

[1] Ten to eleven color flow cytometry was completed on splenocytes as detailed in Materials and Methods. Shown values represent mean ± SEM. Indented subsets indicate that the listed percentages are of the indicated parent population. All other percentages are of live cells, as determined by forward and side scatter profiles. NS = not significant.

[2] $B220^{+}CD23^{+}CD21^{+}IgM^{+}$

[3] $CD3^{+}CD4^{+}ICOS^{+}CXCR5^{+}$

[4] $CD11b^{+}Gr1^{+}SSC^{hi}$

[5] $CD11b^{+}Gr1^{+}Neu7/4^{+}SSC^{lo}$

[6] $CD11b^{+}Gr1^{-}Neu7/4^{+}$

[7] $CD11b^{+}$F4/80+

Genomic and Expression Analysis of *Sles1* Genes

We conducted interval-wide genomic and expression analysis experiments to identify the strongest non-MHC Class II candidates for the causative gene of *Sles1*. At this point, the MHC Class II family was not under consideration as *Sles1* causative genes due to complementation data suggesting the presence of a suppressive *Sles1* allele in the 129 genome, which has identical MHC Class II molecules as the non-suppressive B6 allele of *Sles1* [35].

We participated in the Large Lupus Association Study (LLAS1) which included the genotyping of 76 SNPs across the *Sles1*$^{(28\text{-}83)}$ interval in over 5000 each of human SLE patients and healthy controls from diverse racial populations. Significant association in at least one population was identified for 49 of these SNPs, representing 15 genes (Table 7). Of these genes, only four were located in the remaining non-*KB1 Sles1* candidacy interval: *Wdr46, Ring1, Tap2* and *Btnl2. Wdr46 (WD repeat domain 46)* had five SNPs weakly associated with disease (*p*-values ranged from 0.040621 to 0.000228). *Ring1 (ring finger protein 1)* had only one SNP associated with SLE in Asians (rs2854028, $p = 0.000267$). *Tap2 (transporter 2, ATP-binding cassette, sub-family B*) had eight SNPs associated with lupus in African-Americans, Asians, and European-Americans (*p*-values ranged from 0.00597 to 5.76×10^{-7}). *Btnl2*

SNP	Gene	AA[1]	Asians	EA[2]	Gullah	Hispanic
rs3130349	*AGER*			1.34E-19		
rs3132965	*AGER*	0.000763	0.001366	9.62E-15		
rs3134940	*AGER*			1.40E-19		
rs8365	*AGER*			3.97E-19		
rs1980493	***BTNL2***			**4.85E-28**		
rs2076529	***BTNL2***		**0.000166**	**2.04E-21**		
rs2076530	***BTNL2***		**5.02E-08**	**1.53E-20**		
rs2076533	***BTNL2***		**5.08E-05**	**9.44E-22**		**0.002389**
rs2294880	***BTNL2***			**5.96E-08**		
rs2294884	***BTNL2***			**3.12E-06**		**0.001692**
rs3117116	***BTNL2***			**1.56E-07**		**0.011865**
rs3129954	***BTNL2***				**0.038361**	
rs3763305	***BTNL2***		**7.86E-08**	**0.001341**		**0.001797**
rs3793126	***BTNL2***			**1.75E-08**		
rs3793127	***BTNL2***			**0.000217**		
rs3817966	***BTNL2***			**2.90E-09**		
rs1042663	*C2*			0.002754		
rs7746553	*C2*			0.003191		
rs2734318	*C4B*		0.003490	6.82E-15		4.75E-07
rs4151657	*CFB*			1.24E-08		
rs537160	*CFB*			3.31E-20		
rs7756934	*CYP21A2*	0.000601	0.000224	1.10E-09		
rs13118	*NEU1*		0.000267			
rs3134942	***NOTCH4***	**0.008564**		**1.44E-34**		
rs1035798	*PBX2*	0.000590		0.000714		
rs2070600	*PBX2*			0.000487		0.017488
rs3131300	*PBX2*			4.20E-19	0.018998	
rs2269425	*PPT2*			3.66E-07		
rs3134950	*PPT2*		0.002678			0.001918
rs2854028	***RING1***		**0.000267**			
rs9469089	*RNF5*			4.13E-05		
rs1015166	***TAP2***			**0.000156**		
rs1044043	***TAP2***		**5.76E-07**			
rs2239701	***TAP2***	**0.004027**				
rs241436	***TAP2***	**0.001331**				
rs241437	***TAP2***		**2.39E-05**	**0.005967**		
rs241440	***TAP2***	**0.000207**	**5.23E-06**	**3.17E-06**		
rs4148870	***TAP2***	**0.005776**				
rs4148871	***TAP2***		**1.09E-05**			
rs1009382	*TNXB*			1.79E-05		2.80E-09
rs17421133	*TNXB*	1.70E-05		1.86E-08		
rs185819	*TNXB*	0.000814		1.00E-17		
rs204883	*TNXB*	1.21E-06		5.06E-13		
rs429150	*TNXB*		0.005244	4.38E-13	0.011822	
rs462093	***WDR46***		**0.000474**			
rs463260	***WDR46***		**0.000505**			
rs465151	***WDR46***	**0.001743**		**0.000398**		
rs469064	***WDR46***		**0.000228**			
rs6906691	***WDR46***	**0.005006**			**0.040621**	

Table 7. Summary of Non-MHC Class II *Sles1*$^{(28\text{-}83)}$ LLAS1 Human SLE SNP Associations. Bolded genes remain are not excluded by the KB1 interval. p-values are indicated for the association of each SNP within diverse racial groups. For more details, see *Materials and Methods*. AA = African Americans, EA = European Americans

(butyrophilin-like 2, class II associated) had the strongest associations of the non-*KB1* genes with 12 SNPs variably associated with all of the populations except African-Americans. Nine of these SNPs had extremely significant *p*-values in European-Americans (*p*-values ranged from $3.12x10^{-6}$ to $4.85x10^{-28}$). Finally, the strongest single association ($p = 1.44x10^{-34}$) was for rs3134942, located in *Notch4,* in European Americans. This SNP also had a weak association ($p = 0.00856$) in African Americans (Table 7). Although the breakpoint between non-*KB1* and *KB1 Sles1* intervals occurs early in the *Notch4* gene (in the latter half of exon 3) excluding *Notch4* from consideration, it is possible that this reflects a bystander association to a causal variation in either the early portion or promoter of *Notch4*. This "bystander" effect must also be taken into account when interpreting these results as the three genes with the strongest associations *Tap2, Btnl2* and *Notch4*, are also the three genes most closely located near the MHC Class II genes, known to be the most strongly associated loci with SLE [51, 52]. However, recent high-density SNP screens across this interval provide evidence for multiple, independent susceptibility loci [51, 151, 152].

To systematically identify any *Sles1*-mediated gene expression dsyregulation, a microarray assay was completed on RNA isolated from purified splenic B and T cells from 2 month old B6.*Sle1* and B6.*Sle1Sles1*

Gene	Location [1]	LLAS1 Human SNP Association [2]					Mouse Microarray [3]	
		AA	Asian	EA	Gullah	Hisp.	B cells	T cells
Wdr46	**34077641**	**+**	**++**	**++**	**+**		↓↓	↓↓
B3Galt4	**34087089**						↓	↓
Ring1	**34158029**		**++**					
Brd2	**34250877**							↓
Psmb9	**34319169**						↓↓	↓↓
Tap2	**34341488**	**++**	**+++**	**+++**			↑↑	↑
Btnl2	**34493167**		**+++**	**+++**	**+**	**+**		
Notch4	**34701227**	**+**		**+++**				
Pbx2	34729416	++		+++	+	+	↑	↑
Ager	34734787	++	+	+++				
Rnf5	34738100			+++				
Ppt2	34753698		+	+++		+	↓↓	↓↓
Tnxb	34807501	+++	+	+++	+	+++		
C4b	34865326		+	+++		+++		
Cyp21a1	34938293	++	++	+++				
Stk19	34960938						↑	
Dpm3z	34973964							↑
Cfb	34993324			++				
C2	34999552			+				
Zbtb12	35031647						↓↓	nd
Neu1	35068212		++				↑	

Table 8. Summary of Genomic and Expression Analysis of *Sles1*$^{(28-83)}$ Non-MHC Class II Genes. Bolded genes are located in the non-*KB1 Sles1* interval.

[1] Indicates position along chromosome in basepairs, according to University of California – Santa Cruz mouse genome browser, mm9 build (based on NCBI build m37) (http://www.genome.ucsc.edu).

[2] Plus signs indicate at least one SNP within the gene was associated with human SLE in racial sub-group. AA = African Americans, EA = European Americans, Hisp. = Hispanic. For more details, see *Materials and Methods*. +, p = 0.002 - 0.05;
++, p = 0.0002-0.001; +++, $p < 0.001$.

[3] Arrow signs indicate the direction of gene dysregulation in B cells and/or T cells isolated from 6-8 week old B6.*Sle1Sles1* female mice, compared to age- and sex- matched B6.*Sle1* mice. For more details, see Materials and Methods. nd = probe not detected. One arrow, p = 0.05 – 0.01; two arrows, $p < 0.001$

```
      [---------Leader---------][---------------------------------
B6     MVDCPRYSLSGVAASFLFVLLTIKHPDDFRVVGPNLPILAKVGEDALLTCQLLPKRTTAH 60
NZW    MVDCPRYSLSGVAASFLFVLLTIKHPDDFRVVGPNLPILAKVGEDALLTCQLLPKRTTAH 60
       ************************************************************

       ----------------------------IgVa---------------------------
B6     MEVRWYRSDPDMPVIMYRDGAEVTGLPMEGYGGRAEWMEDSTEEGSVALKIRQVQPSDDG 120
NZW    MEVRWYRSDPAMPVIMYRDGAVVTGLPMEGYGGRAEWMEDSTEEGSVALKIRQVQPSDDG 120
       ********** ********** ************************************

       ---------------------][---------------------------------------
B6     QYWCRFQEGDYWRETSVLLQVAALGSSPNIHVEGLGEGEVQLVCTSRGWFPEPEVHWEGI 180
NZW    QYWCRFQEGDYWRETSVLLQVAALGSSPNIHVEGLREGEVQLVCTSRGWFPEPEVHWEGI 180
       ********************************** ***********************

       ----------------------IgCa-------------------------------][Hep-
B6     WGEKLMSFSENHVPGEDGLFYVEDTLMVRNDSVETISCFIYSHGLRETQEATIALSGQRL 240
NZW    WGEKLMSFSENHVPGEDGLFYVEDTLMVRNDSVETISCFIYSHGLRETQEATIALSGQRL 240
       ************************************************************

       tad][-------------------------------------------------------
B6     QTELASVSVIGHSQPSPVQVGENIELTCHLSPQTDAQNLEVRWLRSRYYPAVHVYANGTH 300
NZW    QTELASVSVIGHSQPSPVQVGENIELTCHLSPQTDAQNLEVRWLRSRYYPAVHVYANGTH 299
       ************************************************************

       ---------------------IgVb----------------------------------]
B6     VAGEQMVEYKGRTSLVTDAIHEGKLTLQIHNARTSDEGQYRCLFGKDGVYQEARVDVQVM 360
NZW    VAGEQMVEYKGRTSLVTDAIHEGKLTLQIHNARTSDEGQYRCLFGKDGVYQEARVDVQVM 359
       ************************************************************

       [-----------------------------------IgCb------------------
B6     AVGSTPRITREVLKDGGMQLRCTSDGWFPRPHVQWRDRDGKTMPSFSEAFQQGSQELFQV 420
NZW    AVGSTPRITREVLKDGGMQLRCTSDGWFPRPHVQWRDRDGKTMPSFSEAFQQGSQELFQV 419
       ************************************************************

       --------------------------------][---Transmembrane--][------
B6     ETLLLVTNGSMVNVTCSISLPLGQEKTARFPLSDSKIALLWMTLPVVVLPLAMAIDLIKV 480
NZW    ETLLLVTNGSMVNVTCSISLPLGQEKTARFPLSDSKIALLWMTLPVVVLPLAMAIDLIKV 479
       ************************************************************

       ---Intracellular-----------------]
B6     KRWRRTNEQTHSSNQENNKNDENHRRRLPSDERLR- 515
NZW    KRWRRTNEQTHSSNQENNKNDENHRRRLPSDERLR- 515
       ********************************
```

Figure 16. *Btnl2* protein sequence alignment between B6 and NZW alleles. Asterisks below the alignment indicate consensus. Domains are indicated above alignment. Three SNPs in *Btnl2* result in three non-synonymous substitutions: D71A, E82V, G156R. Two are in the IgVa domain and one is in the IgCa domain.

female mice. Five genes in the non-*KB1 Sles1* interval demonstrated changes in gene expression: *Wdr46, B3Galt4, Brd2, Psmb9* and *Tap2 (*Table 8*).* It should be noted that the microarray assay did not contain any probes specific for *Btnl2*, but did include *Notch4*-specifc probes.

As *Tap2* is involved in processing antigens for MHC I, thus probably having a limited role in autoimmunity, we further investigated sequence and expression

differences between the B6 and NZW alleles of the most likely non-MHC Sles1 candidates, *Btnl2* and *Notch 4*. Three SNPs were detected in *Btnl2* and each translated into a significant non-synonymous mutation: D71A and E82V both replaced a negatively charged amino acid with a non-polar amino acid, while G156R replaced a non-polar amino acid with a positively charged amino acid (Figure 16). All of these polymorphisms occurred in the extracellular Ig domains (Figure 16), which are predicted to mediate receptor binding [170]. Real-time PCR expression analysis also demonstrated a non-significant, but strong trend toward down-regulation of *Btnl2* in the thymus of B6.*Sle1Sles1*, versus B6.*Sle1*, two month old female mice (Figure 17, left panel). The non-suppressive phenotype of *Sles1*^{KB1} eliminates the majority of the *Notch4* gene from consideration, but one synonymous polymorphism was detected in codon 67 in exon 3. The promoter region of *Notch4* remains in the candidate interval, but no

expression dysregulation was evident in the thymus of 2 month old B6.*Sle1Sles1* mice (Figure 17, right panel). Together, this data supports *Btnl2*, but not *Notch4*, as a strong candidate for *Sles1*.

Discussion

The data presented here clearly demonstrate that the causative gene of *Sles1* is located in the proximal ~638 KB of the $Sles1^{(28\text{-}83)}$ interval, or the region that is not within the truncated recombinant, $Sles1^{KB1}$. This reduces the number of candidate genes from 67 to 35. Among the remaining genes, the strongest non-MHC II candidate for *Sles1* is *Btnl2* (Figure 18).

Btnl2 was originally identified through high homology to the butyrophilin family member, which is closely related to the B7 gene family [171]. The canonical members of this group are the B7 co-stimulatory molecules, CD80 and CD86, which provide crucial second-signals to T cells via CD28, as well as inhibitory signals through CTLA4 (reviewed in [172]). Other members of the B7 family interact with ICOS to deliver stimulation to T cells [173] and PD-1 to induce T cell apoptosis [130]. The butyrophilin-like family has four members in humans (*Btnl2, 3, 8* and *9*), but has expanded to seven members in mice (*Btnl1, 2, 4, 5, 6, 7,* and *9*), although murine *Btnl4-6* may be psuedogenes. Human and murine

BTNL2 proteins have 63% of their amino acids conserved [174]. Mouse BTNL2 has been detected in mucosal, particularly in dendritic-like cells, and lymphoid tissues, including B cells, T cells and macrophages [174, 175]. A murine splice variant, lacking one of the IgV domains, has also been detected [175]. Murine BTNL2 contains two each of variable and constant immunoglobulin domains (IgV and IgC), a typical butyrophilin heptad repeat, a transmembrane domain and a short cytoplasmic tail [171, 174]. However, the relatively short cytoplasmic tail does not include any signaling motifs [171, 174], suggesting that BTNL2 does not receive and transmit cell signals. Instead, BTNL2 may deliver signals to cells expressing its receptor or act as decoy receptor.

Functional studies have identified an immunoregulatory role for BTNL2. Experiments with a soluble BTNL2-Ig fusion protein have demonstrated that the unknown BTNL2 receptor is constitutively expressed on B cells and up-regulated upon activation of T cells but is not one of the known B7 family receptors: CD28, CTLA4, ICOS, PD-1, HVEM or BTLA. However, only $CD4^+$ T cells, and not B cells, displayed inhibited activation-induced proliferation in the presence of plate-bound BTNL2-Ig fusion [174, 175]. Additionally, BTNL2 has been shown to be expressed on dendritic-like cells of the intestine, where it also negatively regulates $CD4^+$ T cells [175]. Overall, this inhibitory immunoregulatory function, as

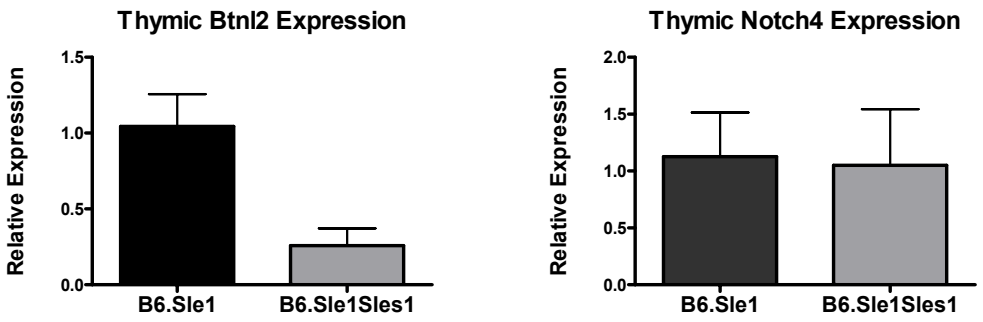

Figure 17. *Btnl2*, but not *Notch4*, is downregulated in B6.*Sle1Sles1* thymus tissue, compared to B6.*Sle1*.

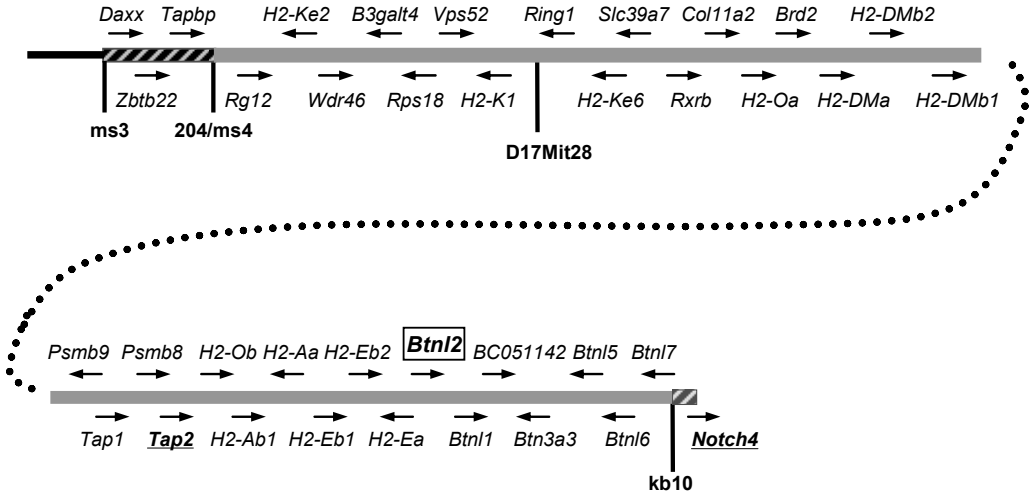

Figure 18. *Sles1* Non-MHC Class II Strongest Candidate Gene Schematic

Detailed map of remaining non-*KB1* portion of *Sles1*$^{(28\text{-}83)}$ interval, showing microsatellite markers (heavy vertical lines) flanking breakpoint regions (hatched thick horizontal lines) and genes (italicized names). The strongest Sles1 candidate genes are denoted by boxes, and lesser candidates by underlining. Transcription orientation is indicated by arrows. Gene information and marker location were obtained from Ensembl 52 (www.ensembl.org/Mus_musculus/) based on NCBI build m37.

well as the high homology to B7 co-stimulatory molecules and human autoimmune disease associations, support BTNL2 as a candidate gene for *Sles1*.

The slight opposing differences in the phenotypes of *Sles1*^{KB1} in females and males with *yaa* illustrate the complex interaction between genes in autoimmunity, albeit on a very small scale. In females, B6.*Sle1KB1* mice demonstrate a consistent trend towards slight disease reduction, occasionally reaching significance, while in males, B6.*Sle1KB1yaa* mice do not have a trend towards suppression and occasionally have significantly worse disease than B6.*Sle1yaa* mice. This phenomenon does not occur in mice carrying *Sles1*$^{(28\text{-}3)}$, an interval which contains *Sles1*^{KB1} in its entirety, which displays consistent and potent suppression in both female and male *yaa* models of autoimmunity. Together, these observations are consistent with multiple interacting genes, in both the non-*KB1* portion of the *Sles1*$^{(28\text{-}83)}$ and *Sles1*^{KB1} intervals, producing different overall phenotypic effects, dependent on *yaa*-mediated increased innate immune stimulation. Although these subtle phenotypic differences illustrate the complexity of both this interval and autoimmunity, the magnitude of these particular effects are too small to warrant further investigation.

CHAPTER FOUR

Characterizing Differences Between Heterozygous *Sles1*$^{(28\text{-}83)}$ and *Sles1*$^{(81\text{-}22)}$ Intervals

Introduction

Earlier work by Morel [33] and colleagues on *Sles1* demonstrated that this interval operates in a recessive manner. It was originally identified through a backcross of (B6.*Sle1* x NZW) F1 to NZW, and heterozygotes have been repeatedly shown to develop autoimmunity at levels similar to B6.*Sle1* mice [33, 35]. Therefore, it was very surprising that during the most recent phase of the *Sles1* fine-mapping investigations, it became apparent that *Sles1* heterozygotes had significant suppressive capacity. This loss of recessive character could only be affected by two possible factors: the continual reduction of the *Sles1* interval had eliminated undetected modifier genes and/or the gradual transfer of the animal colony to a new and cleaner vivarium had subtly altered the environment and consequent immune system stimulation.

Efforts to reduce the *Sles1* interval and identify the causative gene had resulted in a series of nested *Sles1* intervals. The current interval is

Figure 19. Genomic organization of *(81-22)* and *(28-83) Sles1* intervals. Physical map of historical and current *Sles1* intervals on chromosome 17. Marker location were obtained from Ensembl 52 (www.ensembl.org/Mus_musculus/) based on NCBI build m37.
* D17Mit22 currently maps into the middle of the $Sles1^{(28\text{-}83)}$ interval, but it has been determined that the $Sles1^{(81\text{-}22)}$ interval extends at least as far as the distal breakpoint of $Sles1^{(28\text{-}83)}$.

Sles1$^{(28\text{-}83)}$, ~1183 KB flanking the MHC Class II cluster on chromosome 17. The precursor interval is *Sles1*$^{(81\text{-}22)}$, of at least 4000 KB and encapsulating the entire *Sles1*$^{(28\text{-}83)}$ region. Both of these intervals have identical homozygote phenotypes (personal communication, Dr. Srividya Subramanian). However, clear knowledge of their heterozygote phenotypes had not been obtained and the possibility exists that a modifier loci has been lost by the current *Sles1* interval.

Alternatively, it has been well-documented that innate immune signaling can affect the initiation and development of SLE [18, 40, 41, 74, 76-79, 176]. Croker and colleagues have described a murine model of autoimmunity in which disease only occurs when the mice are exposed to pathogens, rather than a gnotobiotic facility [92]. However, there is no knowledge at this time, or in the foreseeable future, as to the environmental differences that may or may not exist between the NA or NG vivariums at UTSW.

These non-mutually exclusive options to explain this change in the transmission of the *Sles1* phenotype are reminiscent of the complex gene-environment interactions that are common in complex diseases like SLE. To determine the contribution of genetics to this phenomenon, we phenotyped homozygotes and heterozygotes of each *Sles1*$^{(28\text{-}83)}$ and

Sles1$^{(81\text{-}22)}$ in both females and males, with the latter also carrying the *yaa* susceptibility locus.

Results

Sles1$^{(28\text{-}83)het}$ and _Sles1_$^{(81\text{-}22)het}$ suppress _Sle1_-mediated autoimmunity in a comparable, non-recessive manner.

We comprehensively evaluated *Sle1*-mediated disease in age- and sex- matched B6, B6.*Sle1*, B6.*Sle1Sles1*^{het}, B6.*Sle1Sles1, B6.Sle1(81-22)*^{het} and B6.*Sle1(81-22)* aged female mice to determine any differences in the heterozygote phenotype of these two nested *Sles1* intervals. In this manner, we could clearly characterize whether they operate in a recessive or dominant manner. In addition to assaying humoral autoimmunity and splenomegaly, flow cytometry was completed to identify changes in splenic leukocyte subpopulations and cellular activation.

Sle1-mediated humoral autoimmunity was determined by measuring antinuclear IgG at 7 months of age using ELISAs as described earlier. B6.*Sle1Sles1*^{het} mice demonstrated no statistically significant difference in ANA levels, compared to B6.*Sle1(81-22*^{het}*)* mice (105.9 ± 54.24 vs. 216.4 ± 163.5). ANA levels for both heterozygote groups, despite a slight trend towards increased levels, were also not statistically significantly different from their respective homozygote groups (*Sles1*,

51.16 ± 12.81; (*81-22)*, 79.73 ± 42.06). However, ANA levels for both heterozygote groups were significantly different than those of the autoimmune B6.*Sle1* group (565.4 ± 94.33, $p < 0.0001$ vs. B6.*Sle1Sles1*^{het} and $p = 0.0026$ vs. B6.*Sle181-22*^{het}) (Figure 19). These results indicate that *Sle1*-mediated humoral autoimmunity is similarly reduced in both heterozygote and homozygotes of *Sles1* and *(81-22)*. Thus, this data demonstrates that in contrast to previous studies, both *Sles* and *(81-22)* intervals behave in a dominant fashion.

As shown in Figure 21, the comparison of 12 month old mouse spleen weights demonstrated a similar pattern. B6.*Sle1* mice had significantly elevated spleen weights (175.7 ± 10.18 mg vs. B6, 115.4 ± 2.51), compared to both heterozygote groups (*Sles1*^{het}, 140.9 ± 9.61 mg, $p = 0.0138$; *81-22*^{het}, 113.90 mg ± 5.20 mg, $p = 0.0070$). Splenomegaly in neither heterozygote group statistically differed from each other or their respective homozygote group. However, *Sles1*^{het} mice, but not the (*81-22)*^{het} mice, had non-significant splenomegaly, with a mean spleen weight intermediate between the B6.*Sle1* and B6.*Sle1Sles1* groups, suggesting a co-dominant character unique to *Sles1* (Figure 21).

Surprisingly, despite a slight increase, there was no significant difference in the activation of follicular B cells ($B220^+CD23^+CD21^+IgM^+$), as defined by CD86 positivity, between B6.*Sle1* and B6 mice (10.90 ±

1.15 vs. 8.52 ± 0.64, respectively). Other data sets have demonstrated an approximately 2-fold increase in B6.*Sle1* mice (Figures 7 and 33, Tables 5 and 11). This is probably a result of subtle differences in immunological stimulation affecting these particular experiments. Nonetheless, there is also no difference in B cell (B220+) activation between any of the *Sles1*^{het} and (*81-22)*^{het} groups. Like the splenomegaly data, there is a slight trend towards increased B cell activation only in the *Sles1*^{het} group, with a mean percentage of CD86^{+} cells of 9.14 ± 0.82, a value which is intermediate between B6.*Sle1* (10.90 ± 1.15) and B6.*Sle1Sles1* (7.81 ± 0.81) mice (Figure 22, Table 9).

Sle1 mediates CD4^{+} T cell hyper-activation, assayed by the percentage of cells that were positive for CD69 (24.44 ± 1.10 vs. B6, 20.19 ± 0.88, p = 0.0102). Both *Sles1*^{het} and *(81-22)*^{het} demonstrated comparable reduced CD4^{+} T cell *Sle1*-mediated hyper-activation (*Sles1*^{het}, 16.06 ± 1.94, p = 0.0021; *81-22*^{het}, 15.97 ± 2.61, p = 0.0014) (Figure 23A, Table 9). Like the ANA data, both *Sles1* and *(81-22)* are dominant for the CD4^{+} T cell hyper-activation sub-phenotype.

The percentages of CD4+ T cell sub-populations also reflect *Sle1*-mediated increased activation. B6.*Sle1* mice have an approximately 2-fold increase in the percentages of memory helper T cells (CD62L^{lo}CD44^{hi}CD4^{+}CD3^{+}), compared to B6.*Sle1Sles1* mice (76.72 ±

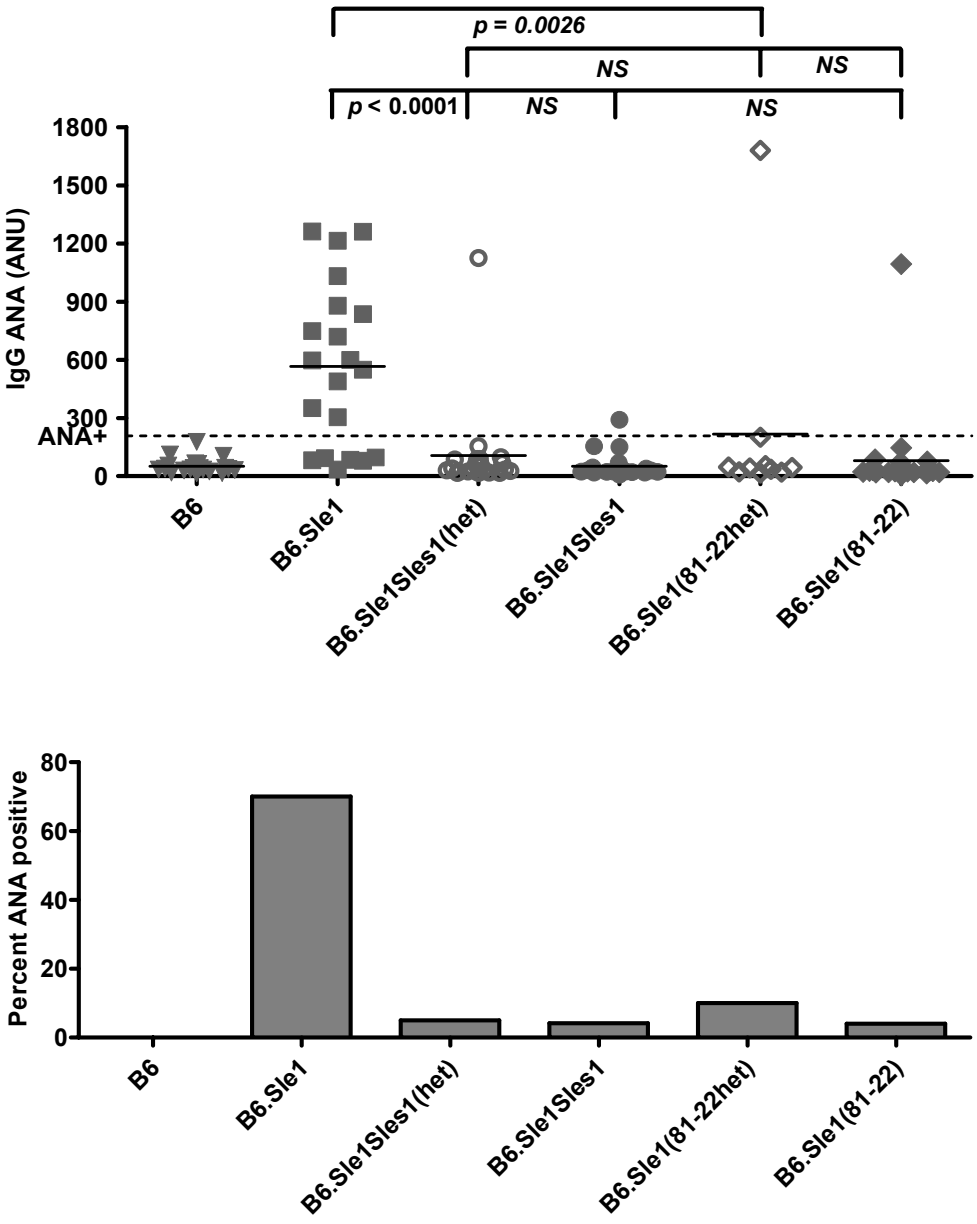

Figure 20. *H*umoral autoimmunity is suppressed in 7 month female B6.*Sle1* mice heterozygous for either *Sles1* or *(81-22)*. Top panel shows IgG ANA levels and bottom panel shows penetrance of ANA positivity. Mice were considered ANA positive when the level was 4 standard deviations above the B6 group mean. n = 10-25 mice per genotype.

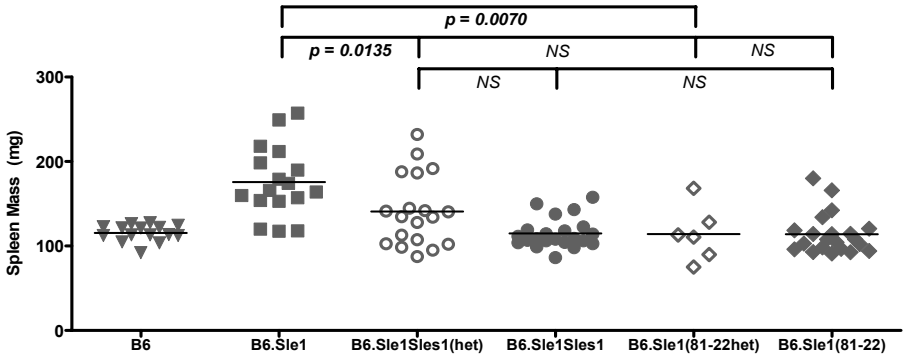

Figure 21. *Sle1*-mediated splenomegaly is suppressed in both *Sles1* and *(81-22)* heterozygous 12 month old female mice. Although not significant, *Sles1* heterozygotes demonstrate a trend of only partial suppression. n = 6-22 mice per genotype.

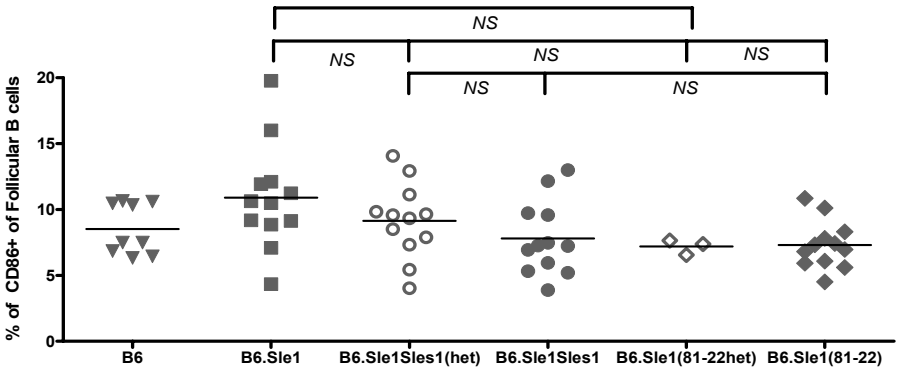

Figure 22. Both *Sles1* and *(81-22)* heterozygous 12 month old female mice demonstrate a non-significant trend towards suppressing *Sle1*-mediated B-cell hyper-actiation. Top panel shows percentages of follicular B cells ($B220^+CD23^+CD21^+IgM^+$) that are $CD86^+$. n = 3-12 mice per genotype.

0.33 vs. 38.83 ± 2.20, $p < 0.0001$) and a corresponding decrease in the percentage of naïve helper T cells ($CD62L^{hi}CD44^{lo}CD4^{+}CD3^{+}$) (14.70 ± 2.71 vs. 52.14 ± 2.27, $p < 0.0001$) (Figure 23B, Table 9). Both *Sles1*^{het} and *(81-22)*^{het} mice demonstrate similar partial reduction of *Sle1*-mediated expansion of memory CD4+ T cells (*Sles1*^{het}, 56.43 ± 4.97, $p = 0.0056$ vs. B6.*Sle1*; *(81-22)*^{het}, 54.67 ± 3.73, $p = 0.0019$ vs. B6.*Sle1*) and contraction of naïve $CD4^{+}$ T cells (*Sles1*^{het}, 34.98 ± 4.88, $p = 0.0037$; *(81-22)*^{het}, 37.46 ± 4.35, $p = 0.0024$) (Figure 23B, Table 9).

There is also a marked increase in the percentage of follicular helper T cells ($ICOS^{+}CXCR5^{+}CD4^{+}CD3^{+}$) in B6.*Sle1* compared to B6.*Sle1Sles1* or B6.*Sle1(81-22)* (18.44 ± 1.40 vs. 4.39 ± 0.62 or 6.38 ± 1.04, $p < 0.0001$). Both heterozygote intervals demonstrate comparable partial suppression, significantly different from both B6.*Sle1* and their respective homozygotes (B6.*Sle1Sles1*^{het}, 9.79 ± 1.75, $p = 0.0021$ vs B6.*Sle1*, $p = 0.0025$ vs B6.*Sle1Sles1*; B6.*Sle1(81-22)*^{het}, 11.11 ± 2.50, $p = 0.0014$ vs B6.*Sle1*, $p = 0.0215$ vs. B6.*Sle1(81-22)* (Figure 23B, Table 9). This is consistent with a similar co-dominant character of both *Sles1* and *(81-22)*.

In conclusion, both B6.*Sle1Sles1*^{het} and B6.*Sle1(81-22)*^{het} mice suppress *Sle1*-mediated phenotypes in a non-recessive manner. Both heterozygote intervals operate in a similar dominant fashion for ANA

levels, splenomegaly and lymphocyte hyper-activation, while they operate in a similar co-dominant fashion for T cell sub-population skewing. There were slight, non-significant, trends that B6.*Sle1Sles1*^{het} mice, and not B6.*Sle1(81-22)*^{het} mice, may be co-dominant for splenomegaly and B cell hyper-activation. This may reflect an actual phenotypic difference between the *Sles1* and *(81-22)* intervals, suggesting the loss of a weak modifier loci.

Sles1$^{(28-83)het}$ and _Sles1_$^{(81-22)het}$ suppress _Sle1yaa_-mediated autoimmunity in a recessive manner.

As the female data suggested the possibility of a subtle difference between the *Sles1* and *(81-22)* intervals, we also comprehensively evaluated *Sle1*-mediated disease in age- and sex- matched B6.*yaa*, B6.*Sle1yaa*, B6.*Sle1Sles1*^{het}*yaa,* B6.*Sle1Sles1yaa, B6.Sle1(81-22)*^{het}*yaa* and B6.*Sle1(81-22)yaa* male mice to see if the *yaa* environment of increased immune stimulation could enhance this difference.

Suppression of *Sle1*-mediated humoral autoimmunity was determined through ELISAs detecting antinuclear IgG at 4 and 6 months of age. At 4 months of age, B6.*Sle1Sles1*^{het}*yaa* mice did not have significantly different ANA levels compared to B6.*Sle1(81-22)*^{het}*yaa* mice (80.29 ± 22.83 vs. 75.94 ± 10.69). Both heterozygote groups were

significantly different than B6.*Sle1yaa* (213.5 ± 37.66, p = 0.0012 vs. B6.*Sle1Sles1*^{het}yaa, p = 0.0348 vs. B6.*Sle1(81-22)*^{het}*yaa*) and their respective homozygotes (vs. B6.*Sle1Sles1yaa*, 32.96 ± 5.70, p = 0.0140; vs. B6.*Sle1(81-22)yaa*, 27.60 ± 4.27, p = 0.0010). At 6 months of age, B6.*Sle1Sles1*^{het}*yaa* mice still did not have significantly different ANA levels compared to B6.*Sle1(81-22)*^{het}*yaa* mice (417.5 ± 119.5 vs. 315.0 ± 87.82). The ANA levels of both heterozygote groups approached the ANA levels of the B6.*Sle1yaa* group, compared to at 4 months, but only B6.*Sle1Sles1*^{het}*yaa* mice remained significantly different than B6.*Sle1yaa* (619.9 ± 134.5, p = 0.0432 vs. B6.*Sle1Sles1*^{het}yaa). Both heterozygote groups remained significantly different from their respective homozygotes (vs. B6.*Sle1Sles1yaa*, 68.76 ± 46.20, p < 0.0001; vs. B6.*Sle1(81-22)yaa*, 100.3 ± 72.30, p = 0.0004). Although the means of the B6.*Sle1Sles1*^{het}*yaa* and B6.*Sle1(81-22)*^{het}*yaa* groups were very similar, there did appear to be a different distribution of ANA levels within each heterozygote group. B6.*Sle1Sles1*^{het}*yaa* mice had a large cluster of samples with very low ANA levels, and a smaller number of samples with a wide range of ANA levels, while B6.*Sle1(81-22)*^{het}*yaa* mice have a more even distribution of ANA levels across a smaller range of values (Figure 24A-B). These results indicate that *Sle1*-mediated humoral autoimmunity is suppressed in a co-dominant manner by both B6.*Sle1Sles1*^{het}*yaa* and

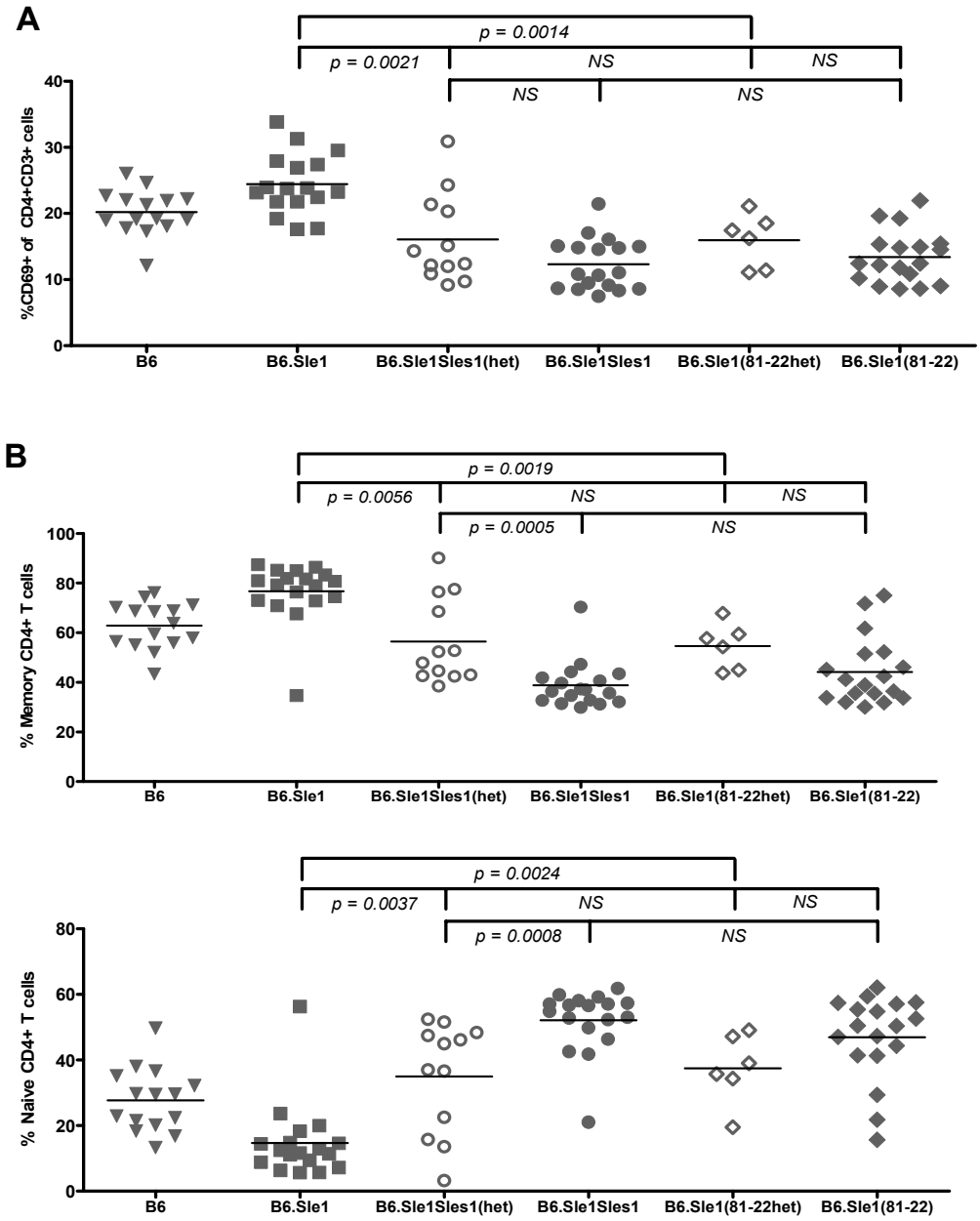
A
p = 0.0014
p = 0.0021
NS
NS
NS
NS
%CD69+ of CD4+CD3+ cells
40
30
20
10
0
B6
B6.Sle1
B6.Sle1Sles1(het)
B6.Sle1Sles1
B6.Sle1(81-22het)
B6.Sle1(81-22)
B
p = 0.0019
p = 0.0056
NS
NS
p = 0.0005
NS
% Memory CD4+ T cells
100
80
60
40
20
0
B6
B6.Sle1
B6.Sle1Sles1(het)
B6.Sle1Sles1
B6.Sle1(81-22het)
B6.Sle1(81-22)
p = 0.0024
p = 0.0037
NS
NS
p = 0.0008
NS
% Naive CD4+ T cells
80
60
40
20
0
B6
B6.Sle1
B6.Sle1Sles1(het)
B6.Sle1Sles1
B6.Sle1(81-22het)
B6.Sle1(81-22)

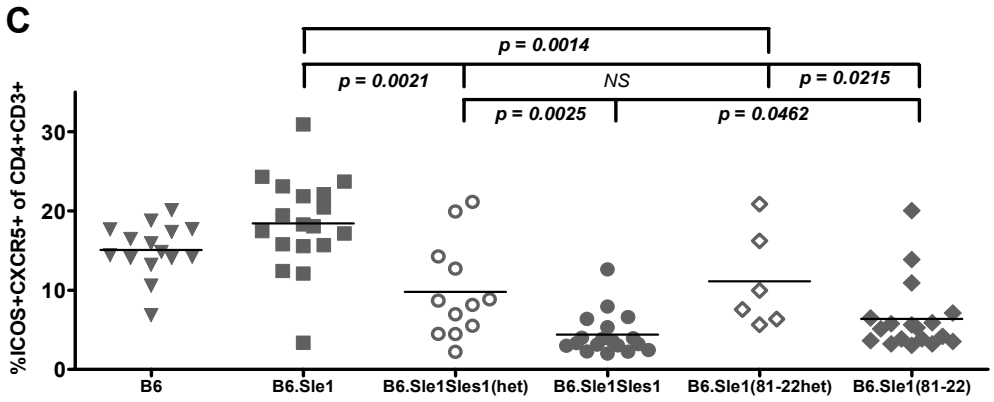

Figure 23. Both *Sles1* and *(81-22)* heterozygous 12 month old female mice only partially suppress *Sle1*-mediated T cell phenotypes, compared to homozygotes. **A**. Percentages of $CD4^+$ $CD3^+$ T cells that are $CD69^+$. **B.** Percentages of $CD4^+CD3^+$ T cells that are memory (top) and naïve (middle). Although (81-22) heterozygotes are not significantly different than (81-22) homozygotes, this is likely due to a low sample number for the heterozygotes, as there is a strong trend towards partial suppression. **C**. Percentages of $CD4^+$ $CD3^+$ T cells that are follicular helper T cells ($ICOS^+CXCR5^+$). n = 6-18 mice per genotype.

Table 9. Splenic cell populations in B6.*Sle1Sles1*^{het}, B6.*Sle1Sles1*, B6.*Sle1(81-22*^{het}*)*, and B6.*Sle1(81-22)* 12 month females

Population[1]	B6 (n=9-15)	B6.*Sle1* (n=11-18)	B6.*Sle1Sles1(het)* (n=12-18)	B6.*Sle1Sles1* (n=12-18)	B6.*Sle (81-22het)* (n=3-12)	B6.*Sle (81-22)* (n=12-18)
B220/CD19+	41.33 ± 3.16	36.05 ± 1.70	42.91 ± 2.32	35.90 ± 2.61	36.82 ± 3.71	32.99 ± 2.94
Number of cells	49564 ± 2403	39025 ± 1880	49467 ± 1283	40116 ± 2793	25383 ± 4840	40292 ± 3713
CD86+	6.50 ± 0.69	7.31 ± 0.60	6.06 ± 0.39	6.06 ± 0.46	4.26 ± 0.44	6.10 ± 0.53
T1 ($CD23^-CD21^-IgM^+$)	5.68 ± 0.61	5.45 ± 0.79	4.40 ± 0.31	4.60 ± 0.48	4.00 ± 0.26	6.01 ± 1.26
T2 ($CD23^+CD21^{hi}IgM^{hi}$)	2.53 ± 0.21	2.11 ± 0.18	2.45 ± 0.16	2.88 ± 0.20	2.23 ± 0.12	2.66 ± 0.27
Follicular[2]	50.09 ± 2.42	42.06 ± 2.20	50.38 ± 2.84	52.60 ± 2.35	51.15 ± 3.25	54.50 ± 1.85
CD86+	8.52 ± 0.64	10.90 ± 1.15	9.14 ± 0.82	7.81 ± 0.81	7.20 ± 0.33	7.31 ± 0.52
MZ ($CD23^-CD21^+IgM^+$)	7.70 ± 0.90	7.22 ± 0.76	7.94 ± 0.52	8.17 ± 0.55	4.63 ± 0.78	6.37 ± 0.88
B1a ($CD5^+CD23^-B220^+$)	1.50 ± 0.20	2.22 ± 0.56	1.33 ± 0.21	0.99 ± 0.15	0.48 ± 0.12	1.01 ± 0.14
B1b ($CD5^-CD23^-B220^{lo}$)	5.59 ± 0.42	5.92 ± 0.34	5.45 ± 0.43	4.79 ± 0.36	3.46 ± 0.50	4.86 ± 0.45
B2 ($CD5^-CD23^+B220^+$)	28.43 ± 2.41	20.24 ± 1.56	28.43 ± 2.90	26.38 ± 2.13	12.86 ± 2.52	26.93 ± 2.52
Plasma ($CD19^-CD138^+$)	1.23 ± 0.13	1.87 ± 0.23	1.35 ± 0.22	0.92 ± 0.14	1.20 ± 0.11	0.81 ± 0.07
CD3+	24.13 ± 1.09	19.90 ± 1.14	21.82 ± 1.69	23.08 ± 1.36	18.76 ± 1.69	23.42 ± 1.50
Number of cells	26466 ± 765.0	21849 ± 805.3	27323 ± 913.7	23766 ± 1432	18947 ± 2935	25746 ± 1492
CD4+	48.36 ± 1.98	58.21 ± 2.26	50.50 ± 3.07	46.68 ± 1.41	43.04 ± 0.71	51.29 ± 1.49
CD69+	20.19 ± 0.88	24.44 ± 1.10	16.06 ± 1.94	12.31 ± 0.92	15.97 ± 1.63	13.39 ± 0.94
CD25+CD69-	10.32 ± 0.69	11.09 ± 0.94	10.61 ± 0.86	11.73 ± 0.73	11.49 ± 1.77	11.18 ± 0.60
CD69+CD25+	6.86 ± 0.30	7.22 ± 0.33	6.95 ± 0.65	6.42 ± 0.59	7.23 ± 0.28	5.84 ± 0.46
CD69+CD25-	18.29 ± 0.90	20.89 ± 1.30	12.93 ± 1.68	11.49 ± 1.18	15.05 ± 2.61	12.63 ± 1.24
$CD62L^{hi}CD44^{lo}$	27.73 ± 2.51	14.70 ± 2.71	34.98 ± 4.88	52.14 ± 2.27	37.46 ± 4.35	46.97 ± 3.07
$CD62L^{lo}CD44^{hi}$	62.88 ± 2.41	76.72 ± 2.81	56.43 ± 4.97	38.83 ± 2.20	54.67 ± 3.73	44.18 ± 3.19
Follicular Helper[3]	15.09 ± 0.86	18.44 ± 1.40	9.79 ± 1.75	4.39 ± 0.62	11.11 ± 2.50	6.38 ± 1.04
CD8+	29.57 ± 1.57	22.36 ± 2.03	34.36 ± 2.58	33.19 ± 1.71	33.28 ± 3.38	31.89 ± 2.08
CD69+	11.21 ± 0.65	14.68 ± 1.09	10.80 ± 1.44	10.41 ± 0.64	11.00 ± 0.98	10.23 ± 0.61
CD11b+	7.35 ± 0.39	10.21 ± 0.82	8.62 ± 0.46	8.98 ± 0.47	8.99 ± 1.87	8.40 ± 0.46
Number of cells	7990 ± 455					
Neutrophils[4]	1.72 ± 0.39	1.56 ± 0.27	0.67 ± 0.20	1.82 ± 0.29	1.03 ± 0.55	1.48 ± 0.33
Inflammatory Monocytes[5]	0.65 ± 0.11	0.62 ± 0.06	0.45 ± 0.10	0.94 ± 0.14	0.47 ± 0.16	0.75 ± 0.14
Resident Monocytes[6]	0.29 ± 0.02	0.40 ± 0.04	0.30 ± 0.04	0.39 ± 0.04	0.26 ± 0.05	0.35 ± 0.05
Macrophages[7]	1.46 ± 0.14	1.94 ± 0.17	1.87 ± 0.17	2.35 ± 0.18	2.32 ± 0.40	1.88 ± 0.13
CD11c+	9.14 ± 0.53	8.78 ± 0.38	7.80 ± 0.41	8.96 ± 0.47	8.82 ± 0.85	8.56 ± 0.51
NK1.1+	3.30 ± 0.42	2.21 ± 0.15	2.52 ± 0.14	4.43 ± 0.69	3.31 ± 0.65	3.47 ± 0.53

Table 9, continued. Splenic cell populations in B6.*Sle1Sles1*^{het}, B6.*Sle1Sles1*, B6.*Sle1(81-22*^{het}*)*, and B6.*Sle1(81-22)* 12 month females

Population[1]	B6.*Sle1* vs B6.*Sle1Sles1(het)*	B6.*Sle1* vs B6.*Sle1(81-22het)*	B6.*Sle1Sles1(het)* vs B6.*Sle1Sles1*	B6.*Sle1(81-22het)* vs. B6.*Sle1(81-22)*	B6.*Sle1Sles1(het)* vs B6.*Sle1(81-22het)*	B6.*Sle1Sles1* vs. B6.*Sle1(81-22)*
B220/CD19+	***P* = 0.0292**	NS	NS	NS	NS	NS
Number of cells	***P* = 0.0004**	***P* = 0.0497**	***P* = 0.0143**	NS	***P* = 0.0127**	NS
CD86+	NS	***P* = 0.0103**	NS	NS	***P* = 0.0169**	NS
T1 ($CD23^-CD21^-IgM^+$)	NS	NS	NS	NS	NS	NS
T2 ($CD23^+CD21^{hi}IgM^{hi}$)	NS	NS	NS	NS	NS	NS
Follicular[2]	***P* = 0.0414**	NS	NS	NS	NS	NS
CD86+	NS	NS	NS	NS	NS	NS
MZ ($CD23^-CD21^+IgM^+$)	NS	NS	NS	NS	***P* = 0.0364**	NS
B1a ($CD5^+CD23^-B220^+$)	NS	***P* = 0.0076**	NS	***P* = 0.0492**	***P* = 0.0046**	NS
B1b ($CD5^-CD23^-B220^{lo}$)	NS	***P* = 0.0030**	NS	NS	***P* = 0.0218**	NS
B2 ($CD5^-CD23^+B220^+$)	***P* = 0.0162**	***P* = 0.0482**	NS	***P* = 0.0231**	***P* = 0.0174**	NS
Plasma ($CD19^-CD138^+$)	NS	NS	NS	***P* = 0.0364**	NS	NS
CD3+	NS	NS	NS	NS	NS	NS
Number of cells	***P* = 0.0001**	NS	***P* = 0.0489**	NS	***P* = 0.0430**	NS
CD4+	NS	***P* = 0.0017**	NS	***P* = 0.0043**	***P* = 0.0087**	***P* = 0.0288**
CD69+	***P* = 0.0021**	***P* = 0.0014**	NS	NS	NS	NS
CD25+CD69-	NS	NS	NS	NS	NS	NS
CD69+CD25+	NS	NS	NS	NS	NS	NS
CD69+CD25-	***P* = 0.0033**	NS	NS	NS	NS	NS
$CD62L^{hi}CD44^{lo}$	***P* = 0.0037**	***P* = 0.0024**	***P* = 0.0008**	NS	NS	NS
$CD62L^{lo}CD44^{hi}$	***P* = 0.0056**	***P* = 0.0019**	***P* = 0.0005**	NS	NS	NS
Follicular Helper[3]	***P* = 0.0025**	***P* = 0.0357**	***P* = 0.0025**	***P* = 0.0215**	NS	***P* = 0.0462**
CD8+	***P* = 0.0016**	***P* = 0.0180**	NS	NS	NS	NS
CD69+	***P* = 0.0400**	NS	NS	NS	NS	NS
CD11b+	NS	NS	NS	NS	NS	NS
Number of cells	NS	NS	NS	NS	NS	NS
Neutrophils[4]	***P* = 0.0439**	NS	***P* = 0.0124**	NS	NS	NS
Inflammatory Monocytes[5]	NS	NS	***P* = 0.0253**	NS	NS	NS
Resident Monocytes[6]	NS	NS	NS	NS	NS	NS
Macrophages[7]	NS	NS	NS	NS	NS	NS
CD11c+	NS	NS	NS	NS	NS	NS
NK1.1+	NS	NS	***P* = 0.0089**	NS	NS	NS

Table 9. Splenic cell populations in B6, B6.*Sle1*, B6.*Sle1Sles1*^{het}, B6.*Sle1Sles1*, B6.*Sle1(81-22*^{het}*)* and B6.*Sle1(81-22)* 12 month females

[1] Ten to eleven color flow cytometry was completed on splenocytes as detailed in Materials and Methods. Shown values represent mean ± SEM. Indented subsets indicate that the listed percentages are of the indicated parent population. All other percentages are of live cells, as determined by forward and side scatter profiles. NS = not significant.

[2] $B220^{+}CD23^{+}CD21^{+}IgM^{+}$

[3] $CD3^{+}CD4^{+}ICOS^{+}CXCR5^{+}$

[4] $CD11b^{+}Gr1^{+}SSC^{hi}$

[5] $CD11b^{+}Gr1^{+}Neu7/4^{+}SSC^{lo}$

[6] $CD11b^{+}Gr1^{-}Neu7/4^{+}$

[7] $CD11b^{+}F4/80^{+}$

B6.*Sle1(81-22)*^{het}*yaa* mice at 4 months of age, but transitions to a mostly recessive mode by 6 months of age. There is also the suggestion of interval-specific mechanistic differences.

Six month old B6.*Sle1yaa* mice had dramatically elevated spleen weights (515.8 ± 42.11 mg vs. B6.*yaa*, 102.7 ± 10.08 mg), which were not significantly different from either heterozygote mice (B6.*Sle1Sles1*^{het}*yaa*, 414.5 ± 64.87 mg; B6.*Sle1*(*81-22)*^{het}*yaa*, 610.5 ± 108.7 mg). Splenomegaly in each heterozygote group was also very different from their respective homozygote group (B6.*Sle1Sles1yaa*, 93.86 ± 11.22, p = 0.0034; B6.*Sle1(81-22)yaa*, 114.7 ± 19.16, p = 0.0128). Again, there are slight differences within each heterozygote group: in B6.*Sle1Sles1*^{het}*yaa* mice, the majority of their samples are below the mean, while in B6.*Sle1(81-22)*^{het}*yaa* mice, the majority of their samples are above the mean (Figure 25). Overall, this data is consistent with both *Sles1* and *(81-22)* intervals operating in a recessive fashion.

Sle1 also induces hyper-activation of lymphocytes, as shown by increased expression of the activation marker CD86 on follicular B cells ($B220^+CD23^+CD21^+IgM^+$) and activation marker CD69 on helper T cells ($CD3^+CD4^+$). Figure 26 and Table 10 demonstrate that while the percentage of $CD86^+$ follicular B cells is indistinguishable between B6.*Sle1yaa* (14.66 ± 1.41), B6.*Sle1Sles1*^{het}*yaa* (16.26 ± 1.69) and

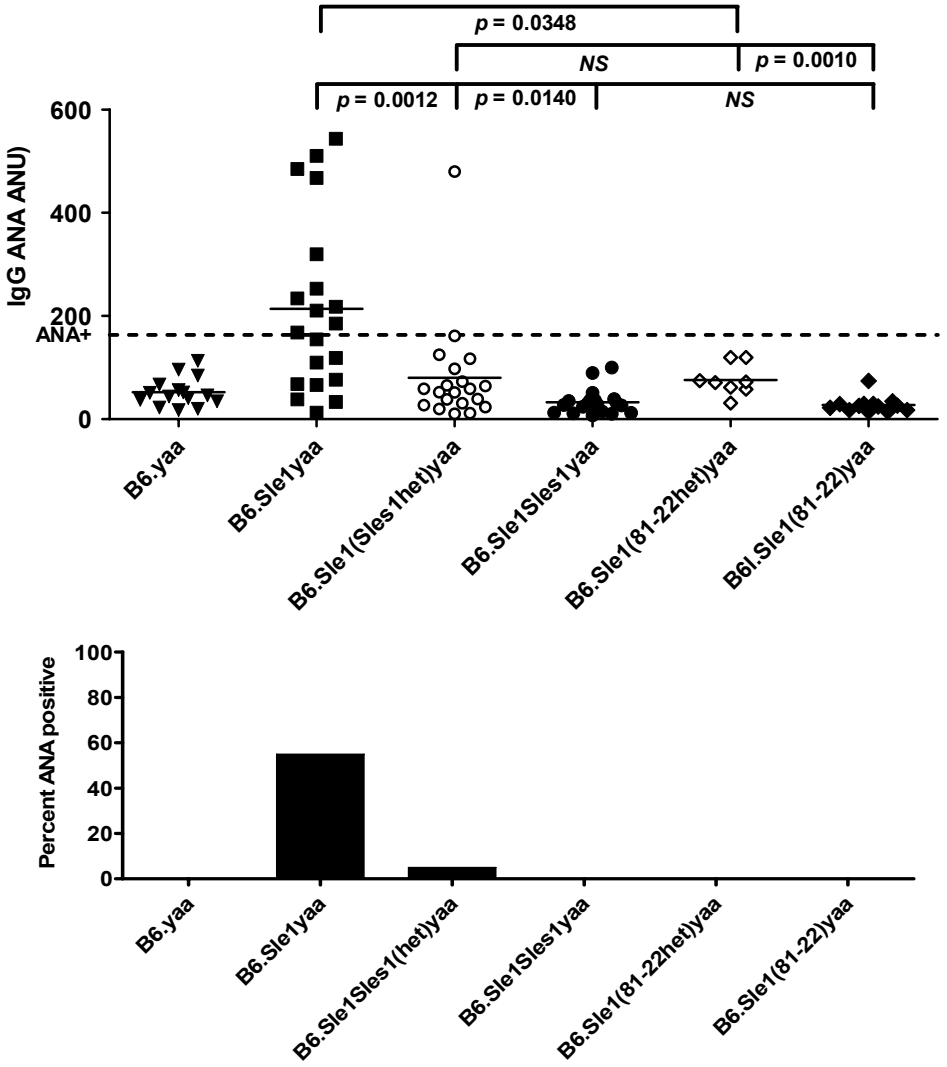

Figure 24A. Both *Sles1* and *(81-22)* heterozygous 4 month old B6.*Sle1yaa* male mice display only partial suppression of *Sle1*-mediated humoral autoimmunity, compared to homozygotes. Although the means are similar between *Sles1* and *(81-22)* heterozygotes, there is a slightly different distribution within each group; the *Sles1* heterozygote group has a wider range of ANA levels, but more samples with very low ANA levels. Top panel shows IgG ANA levels and bottom panel shows penetrance of ANA positivity. Mice were considered ANA positive when the level was 4 standard deviations above the B6.*yaa* group mean. n = 8-20 mice per genotype.

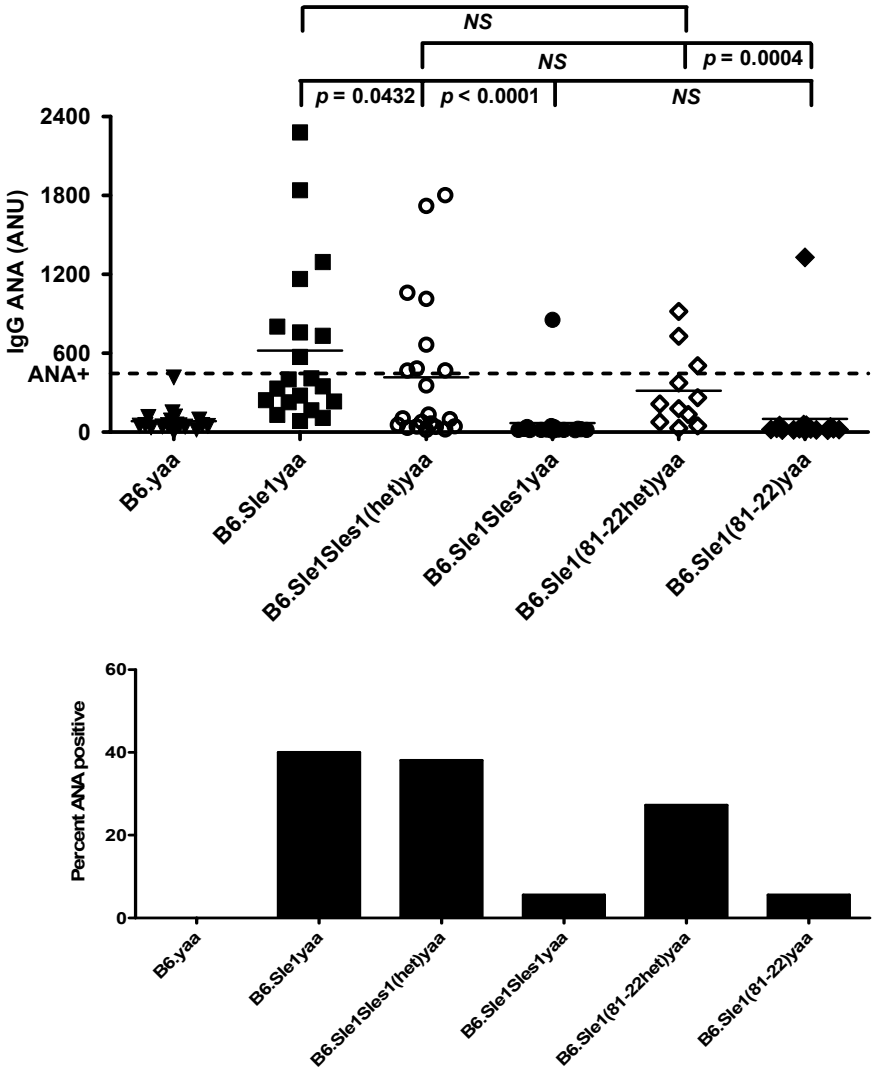

Figure 24B. Both *Sles1* and *(81-22)* heterozygous 6 month old B6.*Sle1yaa* male mice display only partial suppression of *Sle1*-mediated humoral autoimmunity, compared to homozygotes. Although the means are similar between *Sles1* and *(81-22)* heterozygotes, there is a slightly different distribution within each group; the *Sles1* heterozygote group has a wider range of ANA levels, but more samples with very low ANA levels. Top panel shows IgG ANA levels and bottom panel shows penetrance of ANA positivity. Mice were considered ANA positive when the level was 4 standard deviations above the B6.*yaa* group mean. n = 11-21 mice per genotype.

B6.*Sle1(81-22)*^{het}*yaa* mice (15.33 ± 1.12), it is reduced in B6.*Sle1Sles1yaa* mice (9.88 ± 0.58, $p = 0.0034$ vs. B6.*Sle1Sles1*^{het}*yaa*) and B6.*Sle1(81-22)yaa* mice (11.21 ± 0.74, $p = 0.0128$ vs. B6.*Sle1(81-22)hetyaa*). In a similar fashion, B6.*Sle1,* B6.*Sle1Sles1*^{het}*yaa,* and B6.*Sle1(81-22)*^{het}*yaa* have equivalent percentages of CD69+ helper T cells (25.70 ± 1.45 vs. 22.04 ± 1.44 vs. 24.97 ± 1.67) which are significantly higher than either B6.*Sle1Sles1yaa* mice (11.25 ± 1.07, $p < 0.0001$) or B6.*Sle1(81-22)yaa* mice (10.46 ± 0.72) (Figure 27A and Table 10). These phenotypes are also reflected in the cell-surface density of these activation markers as determined by MFIs (bottom panels of Figure 26 and Figure 27A). Again, this data demonstrates that on a *yaa* background, both *Sles1* and *(81-22)* intervals act recessively.

The percentages of $CD4^+$ T cell sub-populations also reflect *Sle1*-mediated increased activation. B6.*Sle1yaa* mice have an approximately 3-fold increase in the percentages of memory helper T cells ($CD62L^{lo}CD44^{hi}CD4^+CD3^+$), compared to B6.*Sle1Sles1yaa* mice (79.88 ± 1.60 vs. 26.60 ± 2.40, $p < 0.0001$) and a corresponding decrease in the percentage of naïve helper T cells ($CD62L^{hi}CD44^{lo}CD4^+CD3^+$) (7.88 ± 1.44 vs. 57.28 ± 3.58, respectively, $p < 0.0001$) (Figure 27B, Table 10). Both B6.*Sle1Sles1*^{het}*yaa* and B6.*Sle1(81-22)*^{het}*yaa* mice demonstrate statistically equivalent B6.*Sle1yaa*-like percentages of memory $CD4^+$ cells

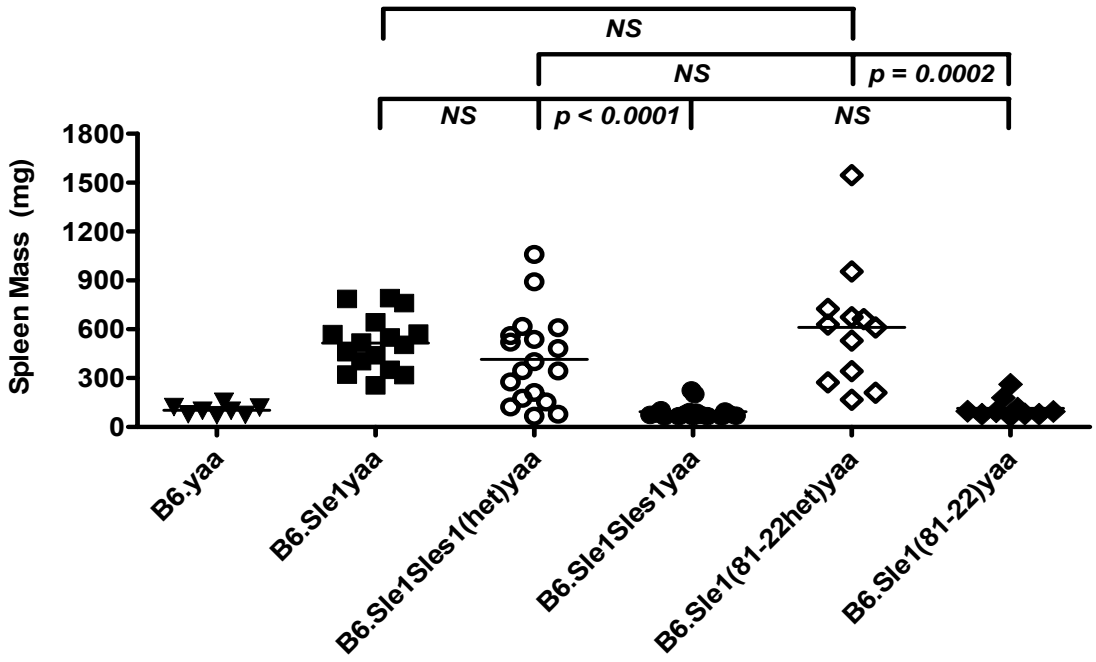

Figure 25. *Sle1*-mediated splenomegaly is not suppressed in either *Sles1* or *(81-22)* heterozygous 6 month old males. n = 8-18 mice per

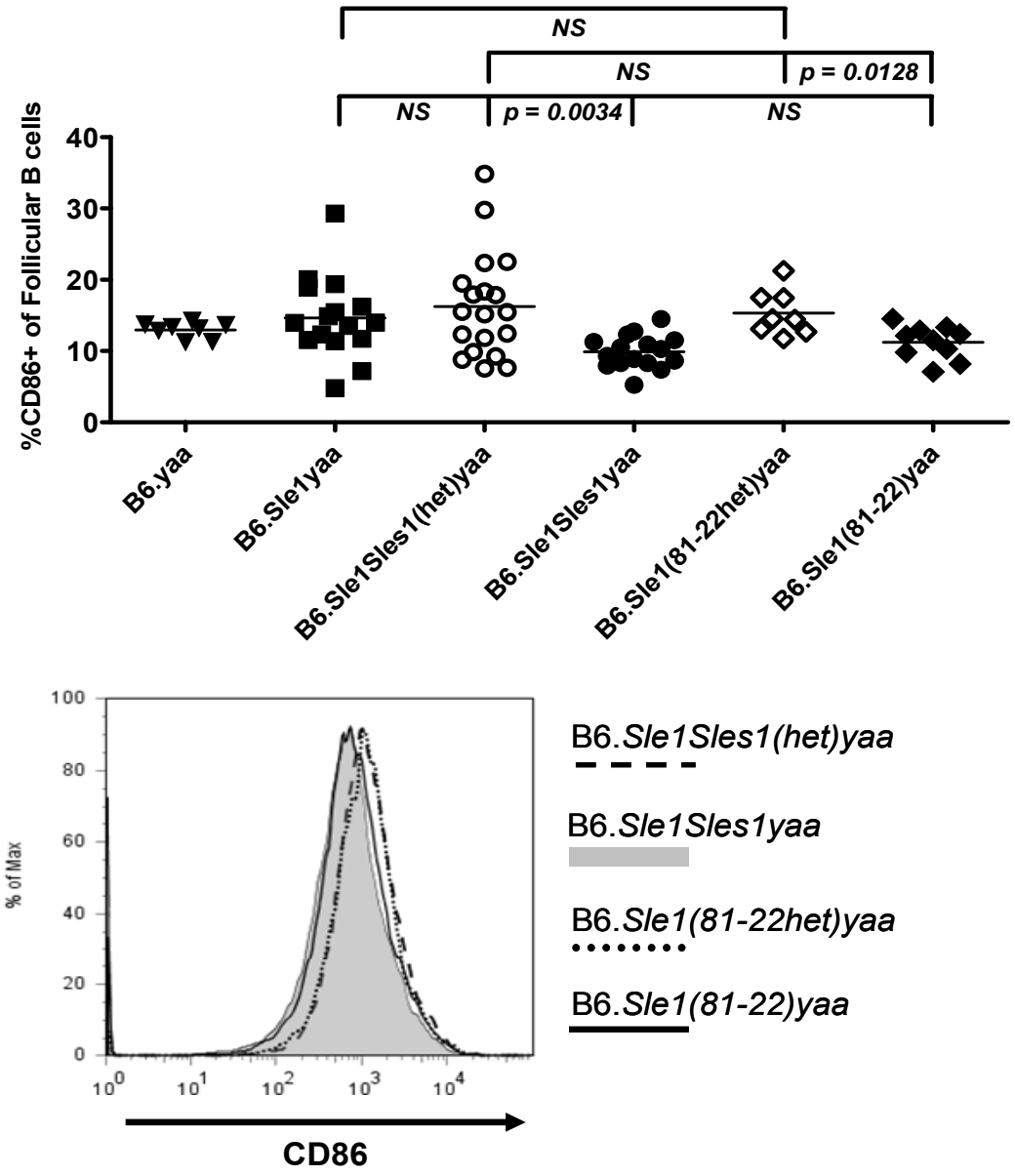

Figure 26. *Sle1*-mediated B-cell hyperactivation is not suppressed in either *Sles1* or *(81-22)* heterozygous 6 month old males. Top panel shows percentages of follicular B cells ($B220^+CD23^+CD21^+IgM^+$) that are $CD86^+$. Bottom panel is a representative CD86 histogram overlay of follicular B cells.
n = 8-18 mice per genotype.

(63.70 ± 5.05 and 74.96 ± 3.95), though there is slight trend towards partial suppression in the B6.*Sle1Sles1*^{het}*yaa* mice. Also, both heterozygote groups have dramatically expanded memory CD4$^+$ T cell populations, compared to their respective homozygote groups (B6.*Sle1Sles1yaa*, 26.60 ± 2.40, $p < 0.0001$; B6.*Sle1(81-22)yaa*, 24.62 ± 0.89, $p < 0.0001$). A similar pattern is observed with the percentages of naïve CD4$^+$ T cells. Also, B6.*Sle1(81-22)yaa*, compared to B6.*Sle1Sles1yaa*, have a smaller range of values of memory and naïve helper T cell percentages (Figure 27B and Table 10).

In addition, B6.*Sle1yaa,* B6.*Sle1Sles1*^{het}*yaa*, and B6.*Sle1(81-22)*^{het}*yaa* all have increased percentages of follicular helper T cells (ICOS$^+$CXCR5$^+$CD4$^+$CD3$^+$) (20.89 ± 0.98, 18.00 ± 1.98, and 20.3 ± 1.28, respectively) compared to B6.*Sle1Sles1* or B6.*Sle1(81-22)* (5.20 ± 0.82 and 4.89 ± 0.66, all $p < 0.0001$). There is a slight trend towards less disease in the B6.*Sle1Sles1*^{het}*yaa*, but not the B6.*Sle1(81-22)*^{het}*yaa* mice (Figure 27C and Table 10). Both heterozygous intervals also have increased cell-surface density of ICOS, CXCR5 and PD-1, compared to the both homozygous intervals, as shown in the representative histogram overlays (Figure 27C, bottom panel). Together, this data illustrates that in the T cell compartment, both *Sles1* and *(81-22)* act in recessive manner,

but there may be slight *Sles1*^{het}-specific suppression, suggesting the loss of a modifier loci in the encapsulating *(81-22)* interval.

The addition of yaa to B6.*Sle1* results in extreme monocytosis as measured by the percentage of CD11b^{+} splenocytes. This phenotype is corrected by B6.*Sle1Sles1yaa* and B6.*Sle1(81-22)yaa* mice, compared to B6.*Sle1*yaa mice (12.12 ± 0.82 and 15.40 ± 2.98 vs. 31.32 ± 3.00, $p <$ 0.0001 and $p = 0.0024$, respectively). Both B6.*Sle1Sles1*^{het}*yaa* and B6.*Sle1(81-22)*^{het}*yaa* have similar percentages of CD11b^{+} cells (18.18 ± 1.63 and 21.55 ± 3.28) but with small changes in sample distribution so that only the former is statistically different from B6.*Sle1yaa* ($p = 0.0018$). The B6.*Sle1Sles1*^{het}*yaa* mice are also different from the B6.*Sle1Sles1yaa* homozygotes mice ($p = 0.0052$). Also, the B6.*Sle1(81-22)yaa* homozygote mice display a trend towards reduced *Sle1yaa*-mediated myeloid expansion so that the B6.*Sle1(81-22)*^{het}*yaa* mice are not statistically different (Figure 28 and Table 10). This data demonstrates a co-dominant behavior for *Sles1*, and probably *(81-22)* as well, although the latter is confounded by lesser suppression of the homozygote interval.

Finally, B6.*Sle1yaa* 6 month old male mice also have dramatic GN as determined by the blinded examination of stained longitudinal kidney sections by an

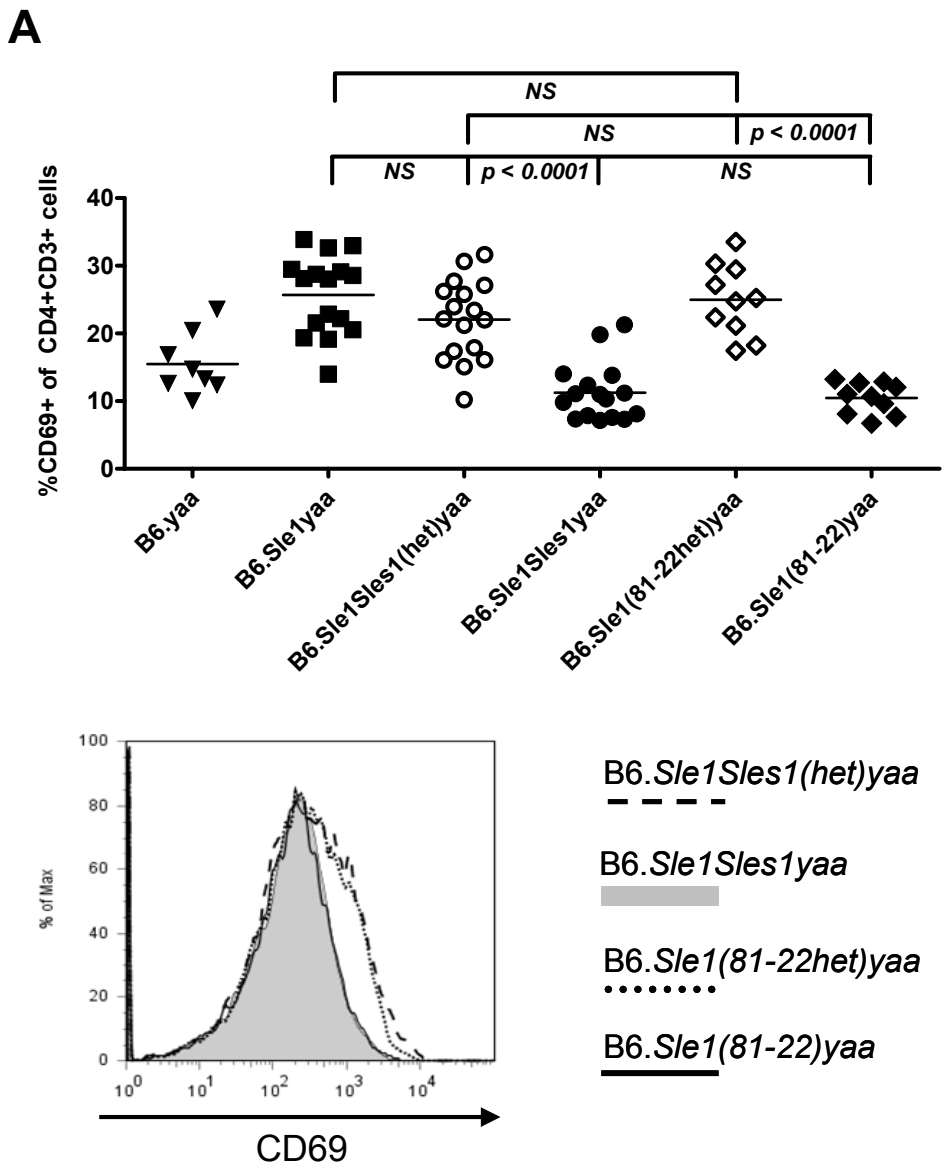

Figure 27A. *Sle1*-mediated T-cell hyperactivation is not suppressed in either *Sles1* or *(81-22)* heterozygous 6 month old males. A. Top panel, percentages of $CD4^+$ $CD3^+$ T cells that are CD69+. Bottom panel, representative CD69 histogram overlay of $CD4^+$ $CD3^+$ T cells. n = 8-18 mice per genotype.

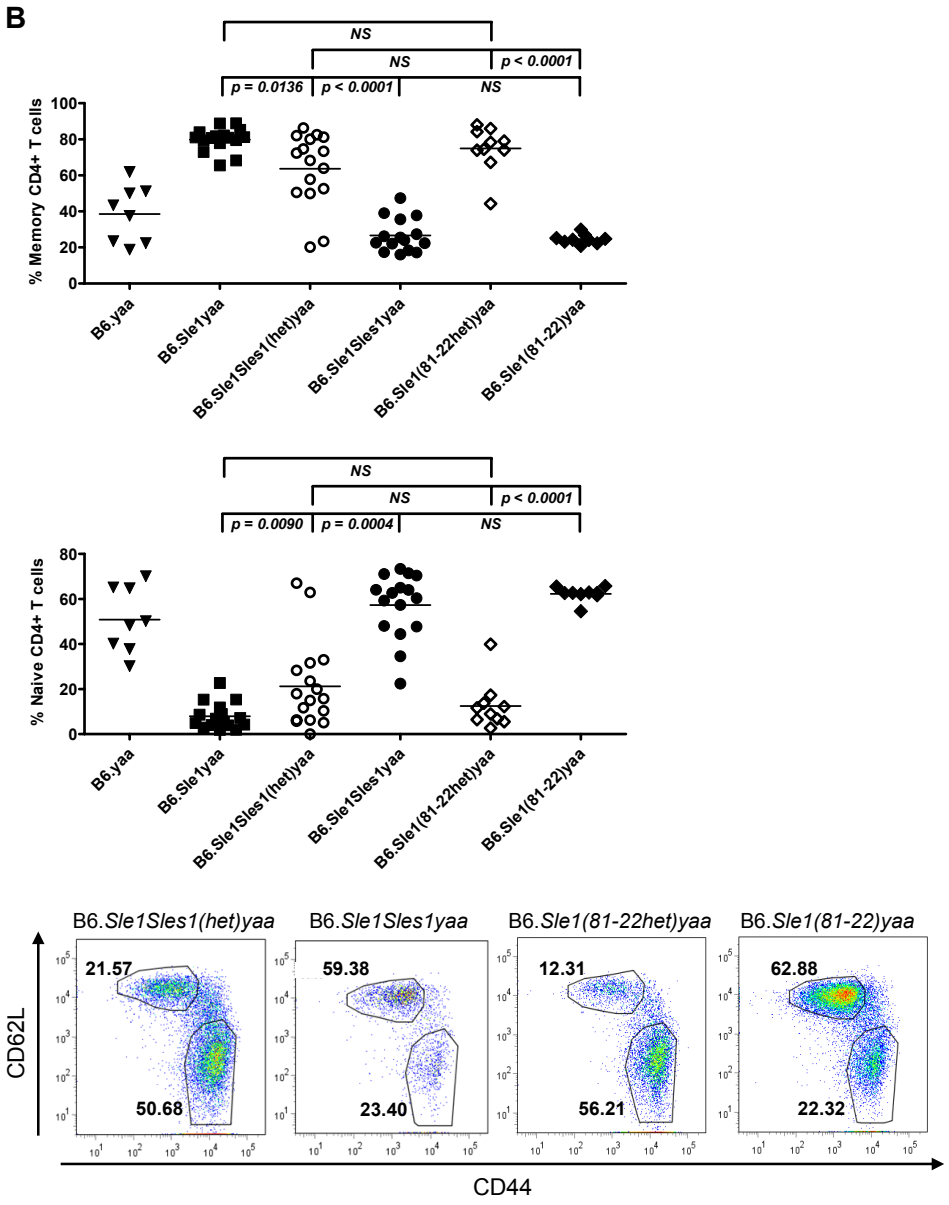

Figure 27B. *Sles1* heterozygous 6 month old male mice with *yaa* have a statistically significant slight suppression of *Sle1*-mediated skewing of CD4+ T cell memory and naïve populations, while *(81-22)* heterozygotes only have a trend towards slight suppression. Top and middle panels, percentages of CD4+CD3+ T cells that are memory (top) and naïve (middle). Bottom panel, representative dot plots of memory vs naïve CD4+CD3+ T cells. n = 8-18 mice per genotype.

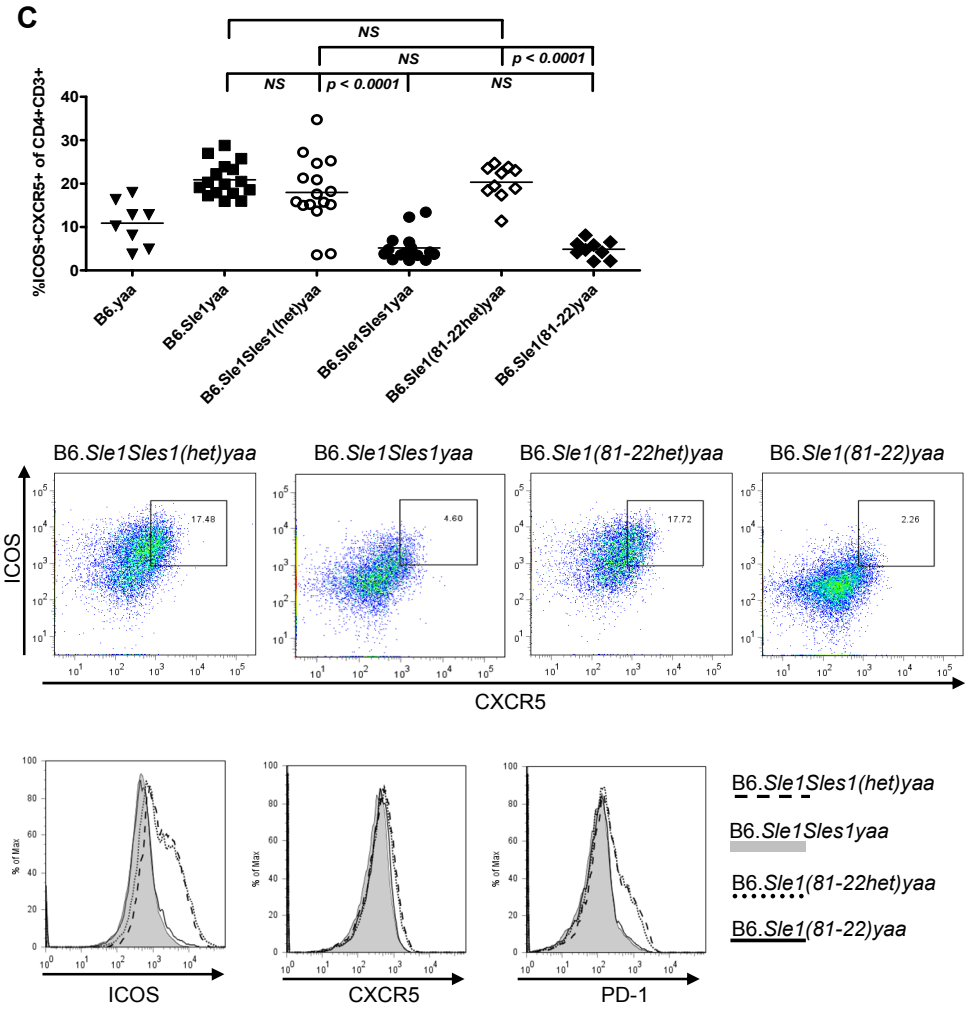

Figure 27C. Neither *Sles1* or *(81-22)* heterozygous 6 month old males have suppressed the *Sle1*-mediated follicular helper T cell expansion. Top panel, percentages of CD4+ CD3+ T cells are follicular helper T cells (ICOS+CXCR5+). Middle, representative dot plots of follicular helper CD4+CD3+ T cells. Bottom, representative histogram overlay of CD4+ CD3+ T cells showing expression of ICOS (left), CXCR5 (middle) and PD-1 (right). n = 8-18 mice per genotype.

independent investigator (for more details, see *Materials and Methods* section). Figure 29 shows the overall pathology score for each experimental group. B6.*Sle1Sles1*^{het}*yaa* mice have significantly reduced GN, compared to B6.*Sle1yaa* mice (1.10 ± 0.37 vs. 3.40 ± 0.37, p = 0.0109), but a non-significant trend towards increased GN, compared to B6.*Sle1Sles1yaa* (0.50 ± 0.16). Although this experiment is hampered by low sample numbers, it seems highly likely B6.*Sle1(81-22)*^{het}*yaa* mice have GN scores (2.50 ± 0.50) intermediate between scores of B6.*Sle1yaa* and B6.*Sle1Sles1yaa* mice.

In conclusion, *Sles1* and *(81-22)* act in recessive manner for most *Sle1yaa*-mediated phenotypes. Both intervals act in a co-dominant manner for monocytosis and ANA levels, although the latter seems to progress towards more recessive character as the mice age from four to six months. There were very slight, but consistent trends towards less disease in B6.*Sle1Sles1*^{het}*yaa* mice, but not in B6.*Sle1(81-22)*^{het}*yaa* mice despite both heterozygote groups being statistically indistinguishable in every phenotype. However, B6.*Sle1(81-22)*^{het}*yaa*, but not B6.*Sle1Sles1*^{het}*yaa*, mice failed to be statistically different than B6.*Sle1* mice for several parameters (6 month ANA levels, percentages of memory and naïve helper T cell sup-populations, and monocytosis). This suggests the possibility of weak modifier loci in *Sles1*$^{(81-22)}$ interval which are no

longer in the current *Sles1 i*nterval. As this phenomenon is not seen in the female B6.*Sle1* model, these modifier loci probably interact specifically with *yaa* to amplify autoimmunity.

Discussion

As the recessive character of *Sles1* had been thoroughly established through both the initial identification of the loci in an NZW backcross of female (B6.*Sle1* x NZW) F1s and many years of experiments, it is quite surprising that *Sles1* is now clearly acting in a co-dominant or dominant fashion on a B6.*Sle1* female model of autoimmunity. Over the recent years, when hints of this phenomenon appeared, only two things had changed that could possibly account for this startling discrepancy: the further reduction of the *Sles1* interval from the previous and larger interval, *(81-22)*, and the transfer of the mouse colony into a new vivarium. This work now clearly shows that *(81-22)* also behaves in a co-dominant/dominant manner on a B6.*Sle1* female model. This suggests that environmental variation, rather than different genetic content of these two intervals, is more likely to account for this change in *Sles1* behavior.

Surprisingly, both *Sles1* and *(81-22)* intervals behaved in recessive and/or co-dominant fashion on a B6.*Sle1yaa* male model of accelerated

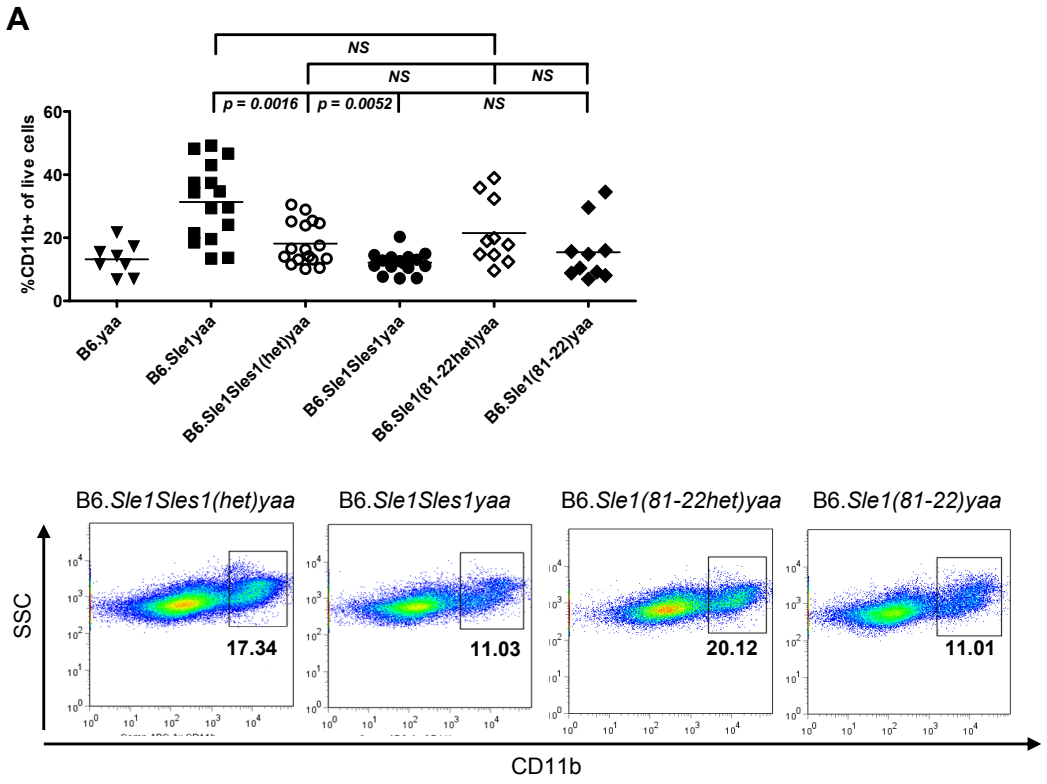

Figure 28. Both *Sles1* and *(81-22)* heterozygous 6 month old males have suppressed *Sle1*-mediated monocytosis. A. Top panel, representative dot plots of CD11b+ cells (of live). Bottom panel, percentages of CD11b+ (of live). n = 8-18 mice per genotype.

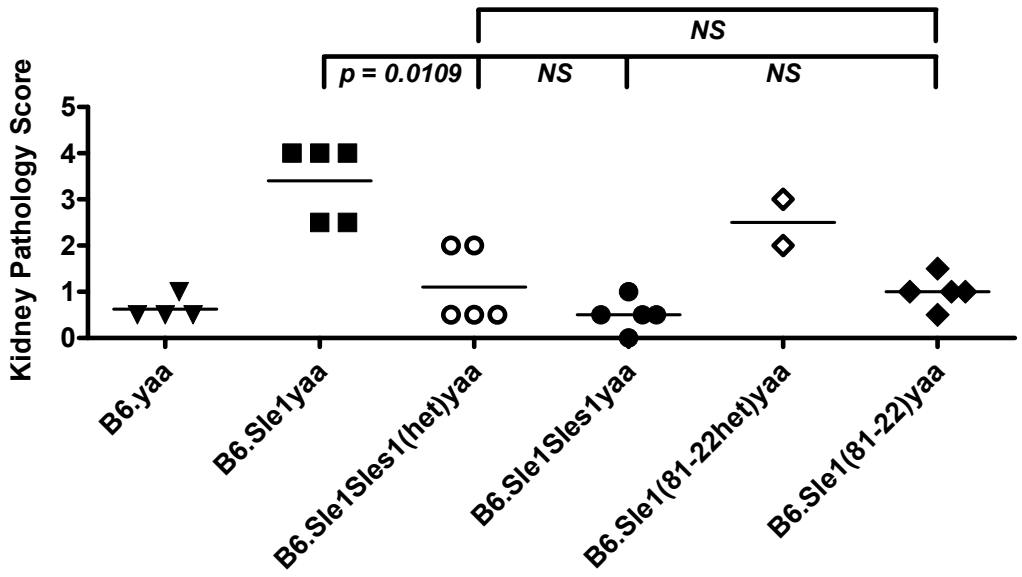

Figure 29. Only *Sles1* heterozygotes, and not *(81-22)* heterozygotes, have suppressed *Sle1*-mediated glomerulonephritis in 6 month old B6.*Sle1yaa* males. However, these results must be considered preliminary until more results for (81-22) heterozygotes are obtained. Stained longitudinal kidney sections were blind examined for evidence of disease pathology in the glomeruli, tubules or interstitial areas by Dr. Xin J. Zhou (Department of Pathology, UTSW). The GN severity was graded on a scale of 0 to 4, where 0 indicates normal and 4 indicates significant evidence of disease. See *Materials and Methods* sections for more

Table 10. Splenic cell populations in B6.*Sle1Sles1*^{het}*yaa*, B6.*Sle1Sles1yaa*, B6.*Sle1(81-22*^{het}*)yaa*, and B6.*Sle1(81-22)yaa 6* month males

Population[1]	B6.*yaa* (n=9-15)	B6.*Sleyaa1* (n=11-18)	B6.*Sle1Sles1(het)*yaa (n=12-18)	B6.*Sle1Sles1yaa* (n=12-18)	B6.*Sle1 (81-22het)*yaa (n=3-12)	B6.*Sle1 (81-22)*yaa (n=12-18)
B220/CD19+	37.69 ± 4.22	28.10 ± 1.73	36.04 ± 4.34	46.72 ± 1.95	28.27 ± 4.07	44.25 ± 3.56
Number of cells	48890 ± 3121	27752 ± 2285	45221 ± 3797	51318 ± 1524	28859 ± 6104	47834 ± 4071
CD86+	19.05 ± 0.60	20.34 ± 1.42	19.92 ± 1.54	15.82 ± 0.68	21.84 ± 2.12	18.61 ± 0.85
T1 ($CD23^-CD21^-IgM^+$)	4.55 ± 0.51	5.11 ± 0.76	4.49 ± 0.56	4.08 ± 0.35	4.47 ± 0.84	3.56 ± 0.30
T2 ($CD23^+CD21^{hi}IgM^{hi}$)	2.66 ± 0.53	2.09 ± 0.41	2.85 ± 1.25	5.90 ± 0.64	2.35 ± 0.48	4.89 ± 0.94
Follicular[2]	48.41 ± 1.59	38.35 ± 1.44	44.35 ± 3.31	53.24 ± 1.72	41.74 ± 3.69	49.04 ± 1.91
CD86+	12.95 ± 0.40	14.66 ± 1.41	16.26 ± 1.69	9.88 ± 0.58	15.33 ± 1.12	11.21 ± 0.74
MZ ($CD23^-CD21^+IgM^+$)	3.10 ± 0.65	1.83 ± 0.37	2.89 ± 0.71	5.34 ± 0.67	2.78 ± 0.84	5.31 ± 0.55
B1a ($CD5^+CD23^-B220^+$)	0.91 ± 0.10	0.99 ± 0.09	0.82 ± 0.10	0.67 ± 0.08	0.77 ± 0.14	0.56 ± 0.07
B1b ($CD5^-CD23^-B220^{lo}$)	4.28 ± 0.23	5.44 ± 0.51	4.49 ± 0.68	3.75 ± 0.39	5.30 ± 1.05	3.99 ± 0.31
B2 ($CD5^-CD23^+B220^+$)	42.13 ± 3.28	20.06 ± 2.26	32.47 ± 3.96	39.31 ± 3.87	22.69 ± 5.18	38.19 ± 3.70
Plasma ($CD19^-CD138^+$)	1.05 ± 0.17	2.57 ± 0.24	2.13 ± 0.28	0.72 ± 0.08	2.97 ± 0.56	1.38 ± 0.43
CD3+	28.06 ± 2.19	19.21 ± 0.95	21.97 ± 2.13	32.35 ± 1.21	18.67 ± 2.14	28.77 ± 2.67
Number of cells	33247 ± 950.9	20060 ± 974.8	26775 ± 2151	35282 ± 791.8	17930 ± 3234	27534 ± 3403
CD4+	52.05 ± 1.17	64.61 ± 1.94	55.15 ± 3.77	51.39 ± 1.38	59.56 ± 3.65	50.57 ± 1.64
CD69+	15.49 ± 1.61	25.70 ± 1.45	22.04 ± 1.44	11.25 ± 1.07	24.97 ± 1.67	10.46 ± 0.74
CD25+CD69-	9.29 ± 0.26	8.15 ± 0.55	10.26 ± 0.52	10.16 ± 0.29	7.95 ± 0.62	10.48 ± 0.72
CD69+CD25+	4.40 ± 0.51	6.95 ± 0.70	6.48 ± 0.70	3.84 ± 0.31	5.43 ± 0.46	3.10 ± 0.41
CD69+CD25-	12.71 ± 1.27	18.52 ± 1.48	17.66 ± 1.29	9.04 ± 0.88	17.64 ± 1.88	7.22 ± 1.02
CD62L+CD44-	50.83 ± 5.16	7.88 ± 1.44	21.21 ± 4.63	57.28 ± 3.58	12.53 ± 3.33	62.28 ± 1.07
CD62L-CD44+	38.58 ± 5.53	79.88 ± 1.60	63.71 ± 5.05	26.60 ± 2.40	74.96 ± 3.95	24.62 ± 0.89
Follicular Helper[3]	10.87 ± 1.80	20.89 ± 0.98	18.00 ± 1.98	5.20 ± 0.82	20.31 ± 1.28	4.89 ± 0.66
CD8+	36.56 ± 1.69	24.49 ± 1.61	30.21 ± 1.83	38.67 ± 1.54	28.30 ± 2.88	40.37 ± 1.67
CD69+	6.48 ± 0.46	14.25 ± 0.67	9.66 ± 0.75	5.21 ± 0.43	10.71 ± 0.69	4.97 ± 0.39
CD11b+	13.24 ± 1.79	31.32 ± 3.00	18.18 ± 1.63	12.12 ± 0.82	21.55 ± 3.28	15.40 ± 2.98
Number of cells	14619 ± 1188	30179 ± 3460	17398 ± 1903	12258 ± 705.6	18073 ± 3749	16227 ± 3655
Neutrophils[4]	1.78 ± 0.21	6.85 ± 127	3.96 ± 0.51	2.78 ± 0.29	5.40 ± 1.57	4.75 ± 1.84
Inflammatory Monocytes[5]	1.15 ± 0.22	4.68 ± 0.69	1.90 ± 0.26	1.20 ± 0.17	3.17 ± 0.71	2.18 ± 0.68
Resident Monocytes[6]	0.51 ± 0.05	1.39 ± 0.19	0.97 ± 0.15	0.63 ± 0.08	1.45 ± 0.40	0.56 ± 0.06
Macrophages[7]	2.05 ± 0.23	3.30 ± 0.58	2.76 ± 0.49	2.14 ± 0.16	2.28 ± 0.35	2.54 ± 0.19
CD11c+	6.45 ± 0.46	10.63 ± 1.06	8.41 ± 0.89	5.23 ± 0.51	9.10 ± 0.69	4.90 ± 0.40
NK1.1+	2.57 ± 0.23	1.98± 0.16	2.00 ± 0.15	2.97 ± 0.16	1.93 ± 0.29	2.61 ± 0.15

Table 10, continued. Splenic cell populations in B6.*Sle1Sles1^{het}yaa*, B6.*Sle1Sles1yaa*, B6.*Sle1(81-22^{het})yaa*, and B6.*Sle1(81-22)yaa* 6mo month males

Population[1]	B6.Sle1Sles1(het)yaa vs B6.*Sle1Sles1yaa*	B6.*Sle1(81-22het)yaa* vs. B6.*Sle1(81-22)yaa*	B6.Sle1Sles1(het)yaa vs B6.*Sle1(81-22het)yaa*	B6.*Sle1Slesyaa1* vs. B6.*Sle1(81-22)yaa*	B6.*Sle1yaa* vs. B6.*Sle1(Sles1het)yaa*	B6.*Sle1yaa* vs. *B6.Sle1(81-22het)yaa*
B220/CD19+	NS	***P* = 0.0147**	NS	NS	NS	NS
Number of cells	***P* = 0.0029**	NS	NS	***P* = 0.0140**	***P* = 0.0384**	NS
CD86+	***P* = 0.0418**	NS	NS	***P* = 0.0190**	NS	NS
T1 ($CD23^-CD21^-IgM^+$)	NS	NS	NS	NS	NS	NS
T2 ($CD23^+CD21^{hi}IgM^{hi}$)	***P* = 0.0006**	NS	NS	NS	NS	NS
Follicular[2]	***P* = 0.0081**	NS	NS	NS	NS	NS
CD86+	***P* = 0.0034**	***P* = 0.0128**	NS	NS	NS	NS
MZ ($CD23^-CD21^+IgM^+$)	***P* = 0.0030**	***P* = 0.0191**	NS	NS	NS	NS
B1a ($CD5^+CD23^-B220^+$)	NS	NS	NS	NS	NS	NS
B1b ($CD5^-CD23^-B220^{lo}$)	NS	NS	NS	NS	NS	NS
B2 ($CD5^-CD23^+B220^+$)	NS	***P* = 0.0401**	NS	NS	***P* = 0.0034**	NS
Plasma ($CD19^-CD138^+$)	***P* < 0.0001**	***P* = 0.0021**	NS	***P* = 0.0153**	NS	NS
CD3+	***P* = 0.0011**	***P* = 0.0143**	NS	NS	NS	NS
Number of cells	***P* = 0.0086**	NS	***P* = 0.0033**	NS	***P* = 0.0351**	***P* = 0.0250**
CD4+	***P* = 0.0202**	NS	NS	NS	***P* = 0.0202**	NS
CD69+	***P* < 0.0001**	***P* < 0.0001**	NS	NS	NS	NS
CD25+CD69-	NS	***P* = 0.0172**	***P* = 0.0129**	NS	***P* = 0.0044**	NS
CD69+CD25+	***P* = 0.0018**	***P* = 0.0039**	NS	NS	NS	NS
CD69+CD25-	***P* < 0.0001**	***P* = 0.0007**	NS	NS	NS	NS
CD62L+CD44-	***P* = 0.0004**	***P* < 0.0001**	NS	NS	***P* = 0.0090**	NS
CD62L-CD44+	***P* < 0.0001**	***P* < 0.0001**	NS	NS	***P* = 0.0136**	NS
Follicular Helper[3]	***P* < 0.0001**	***P* < 0.0001**	NS	NS	NS	NS
CD8+	***P* = 0.0021**	***P* = 0.0076**	NS	NS	***P* = 0.0293**	NS
CD69+	***P* < 0.0001**	***P* < 0.0001**	NS	NS	***P* = 0.0002**	***P* = 0.0032**
CD11b+	***P* = 0.0052**	NS	NS	NS	***P* = 0.0016**	NS
Number of cells	***P* = 0.0051**	NS	NS	NS	NS	NS
Neutrophils[4]	NS	NS	NS	NS	***P* = 0.0351**	NS
Inflammatory Monocytes[5]	***P* = 0.0383**	NS	NS	NS	***P* = 0.0002**	NS
Resident Monocytes[6]	NS	***P* = 0.0028**	NS	NS	NS	NS
Macrophages[7]	NS	NS	NS	NS	NS	NS
CD11c+	***P* = 0.0026**	***P* = 0.0002**	NS	NS	NS	NS
NK1.1+	***P* = 0.0006**	***P* = 0.0232**	NS	NS	NS	NS

Table 10. Splenic cell populations in B6.*Sle1Sles1^{het}yaa*, B6.*Sle1Sles1yaa*, B6.*Sle1(81-22^{het})yaa*, and B6.*Sle1(81-22)yaa* 6 month males.

[1] Ten to eleven color flow cytometry was completed on splenocytes as detailed in Materials and Methods. Shown values represent mean ± SEM. Indented subsets indicate that the listed percentages are of the indicated parent population. All other percentages are of live cells, as determined by forward and side scatter profiles. NS = not significant.

[2] $B220^{+}CD23^{+}CD21^{+}IgM^{+}$

[3] $CD3^{+}CD4^{+}ICOS^{+}CXCR5^{+}$

[4] $CD11b^{+}Gr1^{+}SSC^{hi}$

[5] $CD11b^{+}Gr1^{+}Neu7/4^{+}SSC^{lo}$

[6] $CD11b^{+}Gr1^{-}Neu7/4^{+}$

[7] $CD11b^{+}$F4/80+

autoimmunity. This is in stark contrast to the B6.*Sle1* female data, but consistent with historical data. As both the males and females for these experiments were litter-mates, and thus aged simultaneously, it seems likely that any subtle extrinsic environmental variations would have affected both groups equally. Therefore, the *yaa* locus, which accelerates autoimmunity through increased expression of TLR7 and consequent potent and sustained enhanced innate immune stimulation, is probably responsible for this phenomenon. Although *yaa* results in artificial immune system activation, real environmental immune stimulants would act through similar pathways and could conceivably drive *Sles1* from a dominant character to a recessive character. This supports the theory that subtle environmental variations have resulted in the discrepancies in the behavior of *Sles1*.

Despite the vivarium move, there were no detectable changes in the environment of the animal colony. This suggests that very subtle environmental variations may be sufficient to promote significant phenotypic changes, particularly in genes susceptible to innate immune system perturbations. It also highlights that the suppressive capacity of *Sles1* may rely on a delicate immunoregulatory balance, sensitive to environmental stimulation. Finally, this data suggests that investigators

with long-term immunological mouse studies should be aware of the impact of even small environmental fluctuations on their phenotypes.

CHAPTER FIVE

Investigating the Capacity of the 129 Genome to Suppress SLE

Introduction

In the process of characterizing the NZW-derived autoimmune-prone allele of *Sle1b*, it was determined that the mouse strain 129 contained the same autoimmune-prone haplotype. Furthermore, a B6 congenic carrying the $Sle1b^{129}$ allele developed spontaneous ANAs by nine months of age, similar to B6.$Sle1b^{NZW}$ congenic, while none of the parental strains (B6, NZW and 129) developed significant levels of ANAs [31]. As this was reminiscent of the original discovery of *Sles1*, classic genetic complementation studies were completed in which (129xB6.*Sle1*) F1s, but not (129XB6) F1s and (129xB6.*Sle1Sles1*) F1s, developed a lupus-like disease with high levels of ANAs, splenomegaly, and significant GN [35]. Both (129xB6.*Sle1*) F1s and (129xB6.*Sle1Sles1*) F1s had equivalent heterozygous B6/129 genomic backgrounds, but were homozygous for a $Sle1b^{NZW}$-like haplotype (one derived from each B6 and 129). However, they differed in their phenotype and at the *Sles1* locus, with the former group diseased and heterozygous between B6 and 129,

while the latter group was healthy and heterozygous between 129 and NZW. This strongly suggested that the 129 genome contained a suppressive *Sles1* allele, complementing *Sles1*^{NZW}.

There is also support in the literature for B6- and 129-derived loci modifier loci. Botto and colleagues have identified and characterized 129 loci on chromosomes 1 and 7, and B6 loci on chromosomes 3 and 13, which are associated with the development of autoimmunity disease on a mixed B6 and 129 genomic background [177, 178]. The 129 locus identified on chromosome 1, termed *Sle16,* overlaps with the *Sle1b* interval and has displayed extremely similar phenotypes [179, 180], so it is likely that they are both the same allele.

The confirmation of a SLE suppressing phenotype for *Sles1*^{129,} but with high homology to B6, would provide significant advantages for future studies of *Sles1* candidate genes. For example, of the 650 SNPs with data for both B6 and 129 in the Mouse Phenome SNP Database, less than 1% or a mere two SNPs, are polymorphic for those two strains. In contrast, 37% of the 2589 SNPs with data for B6 and NZW are polymorphic for these strains (http://phenome.jax.org). If *Sles1*^{129} and *Sles1*^{B6} have divergent phenotypes, the number of candidate genetic variations would be significantly fewer than those between *Sles1*^{NZW} and *Sles1*^{B6}. In particular, a suppressive *Sles1*^{129} allele would also eliminate

the 129-derived but B6-like MHC Class II molecules from *Sles1* candidacy. This would also establish a B6-histocompatible suppressive allele of *Sles1*, enabling bone marrow transplant experiments which have not been possible yet. In this study, we generated and phenotyped B6.*Sle1Sles1*^{129} congenic mice to confirm the presumed suppressive behavior of *Sles1*^{129}.

Results

Generation of *B6.Sle1Sles1*^{129}*yaa* Congenic Strain

The B6.*Sle1Sles1*^{129} congenic mice were initially generated by intercrossing (B6.*Sle1* x 129) F1 mice. The resulting F2 progeny were screened with polymorphic MIT markers, flanking *Sles1*$^{(28\text{-}83)}$, to select breeders to be back-crossed to B6.*Sle1yaa* mice. Subsequent generations were also screened and backcrossed to B6.*Sle1yaa* mice. Finally, mice were intercrossed to generate a B6.*Sle1yaa* line with a homozygous 6.45 MB region derived from the 129 genome but containing the entire *Sles1*$^{(28\text{-}83)}$ interval. B6.*Sle1Sles1*^{129} mice were screened with a SNP panel to ensure that there were no other contaminating intervals of 129-derived genome. An overview of this process is shown in Figure 30. For more details, see *Materials and Methods* section.

Sles1^{129} Partially Suppresses *Sle1*-mediated Disease in Female Mice

We comprehensively evaluated *Sle1*-mediated disease in age- and sex- matched B6, B6.*Sle1*, B6.*Sle1Sles1*^{129} and B6.*Sle1Sles1* female mice to determine if the 129 allele of *Sles1* was also suppressive, as preliminary data suggested. In addition to assaying humoral autoimmunity and splenomegaly, flow cytometry characterization of splenic leukocytel subpopulations cellular activation was completed.

Sle1-mediated humoral autoimmunity was determined through ELISAs detecting antinuclear IgG at various ages. In 9 month old females, B6.*Sle1Sles1*^{129} mice demonstrated no capacity for suppression and their ANA levels were indistinguishable from B6.*Sle1* mice ANA levels (642.6 ± 152.3 vs. 520.3 ± 110.9). B6.*Sle1Sles1* mice had significantly lower ANA levels (79.01 ± 26.21) than either B6.*Sle1Sles1*^{129} (p = 0.0002) or B6.*Sle1* (p < 0.0001) (Figure 31A). However, in 12 month old females, despite an intermediate ANA level mean, B6.*Sle1Sles1*^{129} mice were still not significantly different from B6.*Sle1* mice (875.7 ± 268.9 vs. 1473.0 ± 156.0) and remained statistically different from B6.*Sle1Sles1* mice (159.7 ± 69.98, p < 0.0023) (Figure 31B). Although *Sles1*^{129} clearly does not recapitulate the potent *Sles1* phenotype, these results suggest a possible weak suppressive effect.

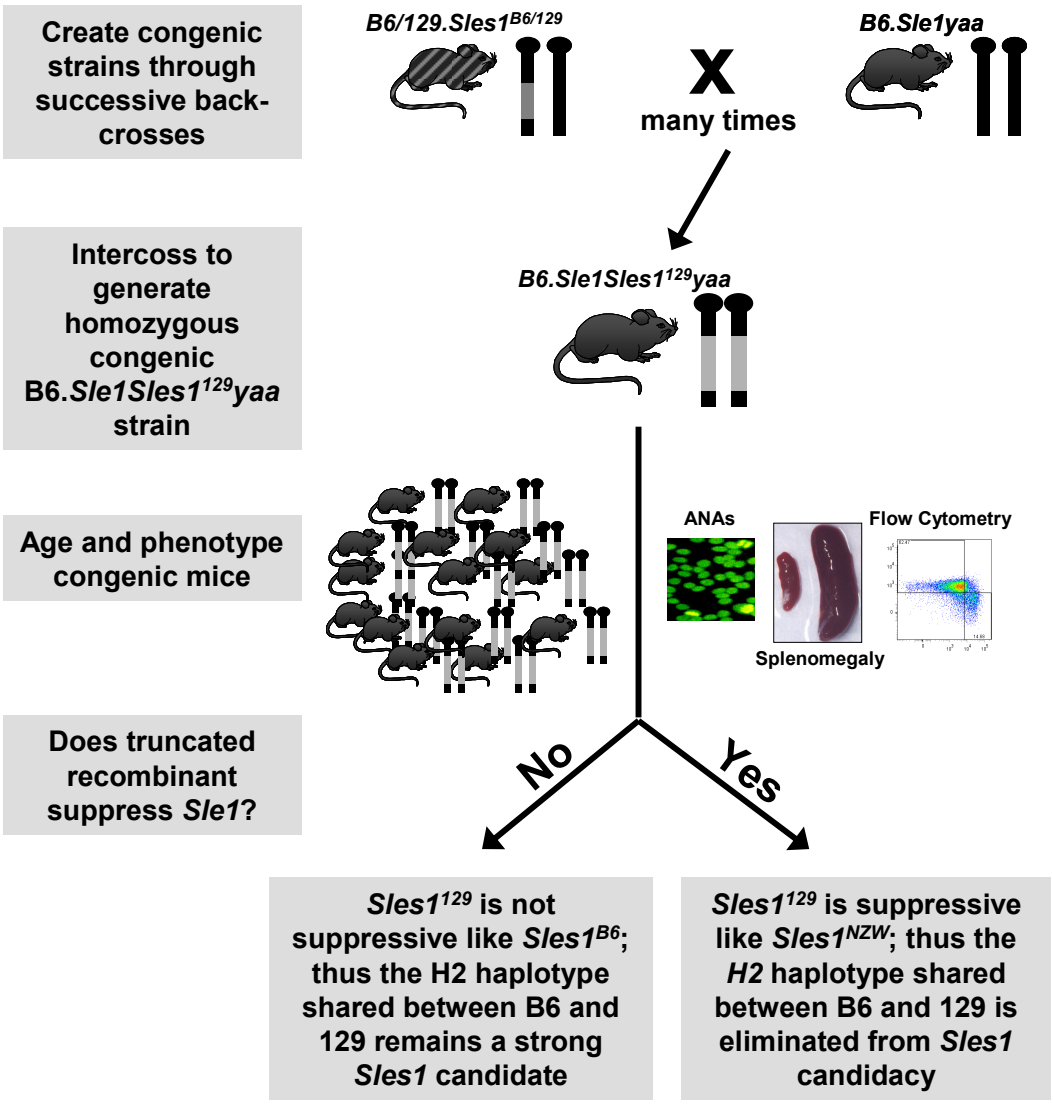

Figure 30. Generation of B6.*Sle1Sles1^{129}yaa* congenic mice.
Mice heterozygous for *Sles1* (B6/129) on a mixed B6 and 129 genome were successively backcrossed to B6.*Sle1yaa* mice, while maintaining *Sles1* as heterozygous. Eventually, progeny were intercrossed to generate a homozygous congenic strain, B6.*Sle1Sles1^{129}yaa*. Mice were then aged and assayed for suppression of *Sle1*.

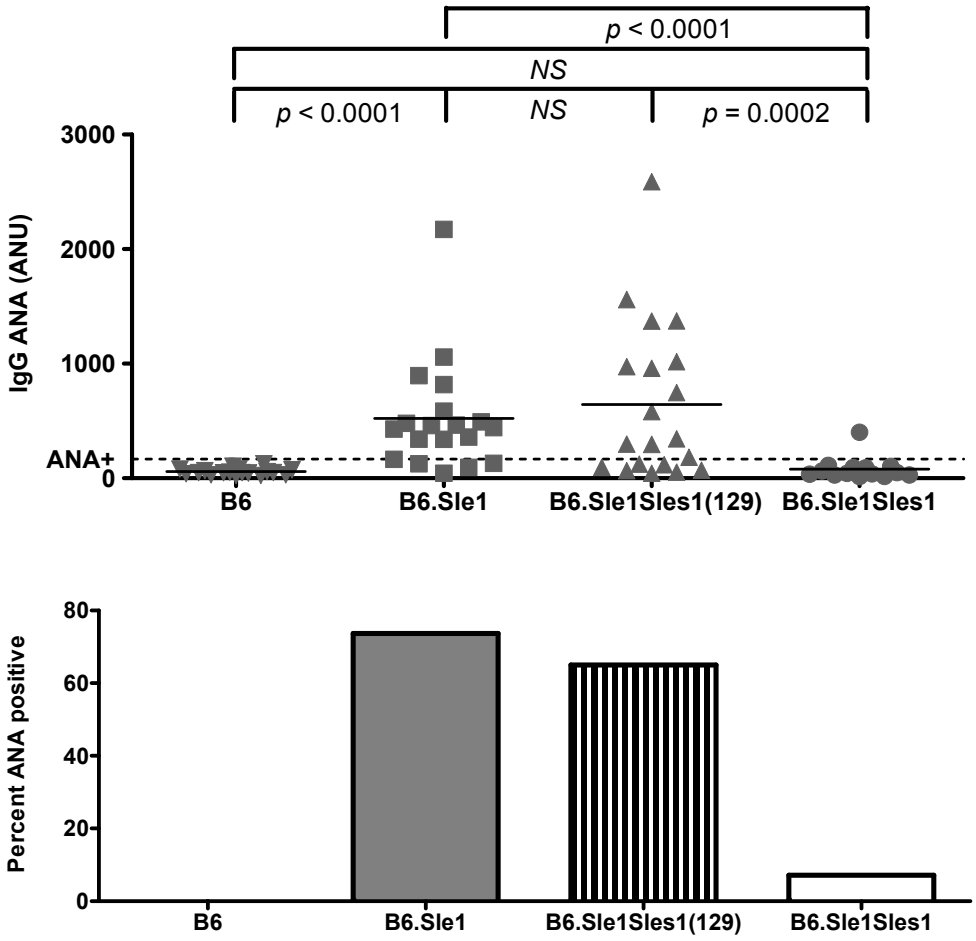

Figure 31A. *Sle1*-mediated humoral autoimmunity is not suppressed in 9 month B6.*Sle1Sles1*^{129} females. Top panel shows IgG ANA levels and bottom panel shows penetrance of ANA positivity. Mice were considered ANA positive when the level was 4 standard deviations above the B6 group mean. n = 14-20 mice per genotype.

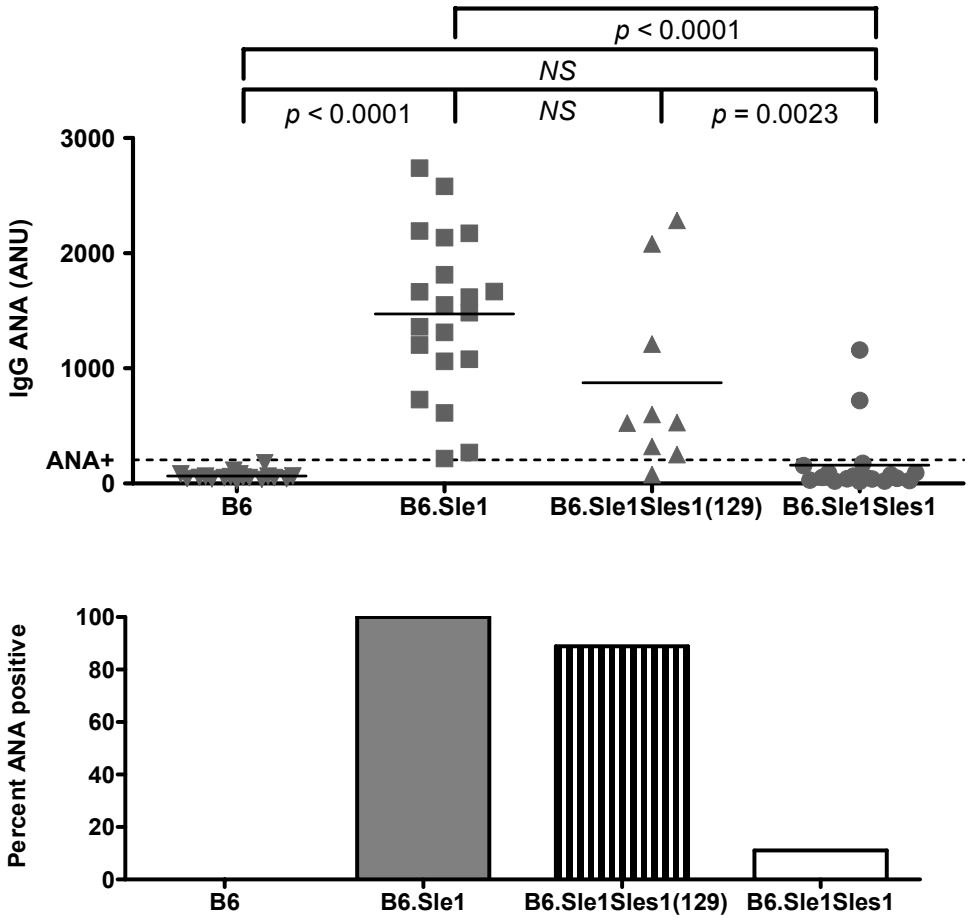

Figure 31B. *Sle1*-mediated humoral autoimmunity is not suppressed in 12 month B6.*Sle1Sles1*^{129} females. There is a non-significant trend towards suppression in B6.*Sle1Sles1*^{129} mice, but that may be an artifact of disparate sample numbers between the groups. Top panel shows IgG ANA levels and bottom panel shows penetrance of ANA positivity. Mice were considered ANA positive when the level was 4 standard deviations above the B6 group mean. n = 9-20 mice

As shown in Figure 32, the comparison of 12 month old mouse spleen weights demonstrated a similar pattern. While B6.*Sle1Sles1*^{129} mice had slightly reduced splenomegaly, compared to B6.*Sle1* mice (168.7 ± 15.41 mg vs. 200.8 ± 10.92 mg, p = 0.0498), B6.*Sle1Sles1* mice had still smaller spleens (123.2 ± 3.72 mg, p = 0.0024). These results also confirm a slightly suppressive phenotype of *Sles1*^{129}.

Extensive 10-12 color flow cytometry analysis was completed on 12 month old female splenocytes to fully evaluate the suppressive capacity of *Sles1*^{129} in sub-phenotypes (for details, see *Materials and Methods*). Of the 22 splenic cell parameters with quantitative differences between B6.*Sle1* and B6.*Sle1Sles1* mice, 14 were also significantly different between B6.*Sle1* and B6.*Sle1Sles1*^{129} while 10 were significantly different between B6.*Sle1Sles1* and B6.*Sle1Sles1*^{129} (Table 11).
This is consistent with the ANA and splenomegaly data, which show an intermediate phenotype for *Sles1*^{129}.

Sle1 induces hyper-activation of follicular B cells ($B220^+CD23^+CD21^+IgM^+$) as shown by increased expression of the activation marker CD86. Figure 33 demonstrates that while the percentage of $CD86^+$ follicular B cells is indistinguishable between B6.*Sle1Sles1* and B6.*Sle1Sles1*^{129} mice (4.04 ± 0.55 vs. 4.64 ± 1.20), much lower than in B6.*Sle1* mice (8.43 ± 1.13, p = 0.0040 vs. *Sles1* and p

= 0.0258 vs. *Sles1*^{129}) (Table 11). This phenotype is also reflected in the cell-surface density of CD86 as determined by MFIs (bottom panel of Figure 33). This conflicts with the ANA and splenomegaly data, in that *Sles1*^{129} fully recapitulates typical *Sles1* suppression of B cell activation.

Sle1 also mediates striking changes in the helper T cell ($CD4^+CD3^+$) compartment, including hyper-activation and sub-population proportions. B6.*Sle1Sles1* mice have lower percentages of activated $CD69^+$ helper T cells than B6.*Sle1Sles1*^{129} mice (12.86 ± 1.11 vs. 20.16 ± 1.60, $p = 0.0010$). The latter group had slightly less activated helper T cells than B6.*Sle1* mice (23.08 ± 1.01, both $p = 0.0497$). This is also illustrated by the cell-surface density of CD69 as determined by MFIs (Figure 34A).

Sle1 also induces an increase in memory helper T cells ($CD62L^{lo}CD44^{hi}CD4^+CD3^+$), a corresponding decrease in naïve helper T cells ($CD62L^{hi}CD44^{lo}CD4^+CD3^+$), and an increase in follicular helper T cells ($ICOS^+CXCR5^+CD4^+CD3^+$). Although B6.*Sle1Sles1*^{129} had a slight reduction in memory helper T cells, compared to B6.*Sle1* (70.66 ± 2.53 vs. 78.81 ± 2.07, $p = 0.0192$), both of these groups had approximately twice the percentage of memory helper T cells as B6.*Sle1Sles1* mice (36.89 ± 1.71, $p = 0.0004$ and $p < 0.0001$, respectively) (Table 11 and Figure 34B).

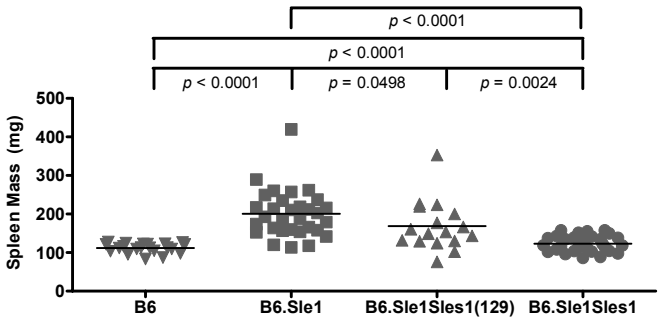

Figure 32. *Sle1*-mediated splenomegaly is slightly suppressed in 12 month B6.*Sle1Sles1*^{129} females. n = 14-26 mice per genotype.

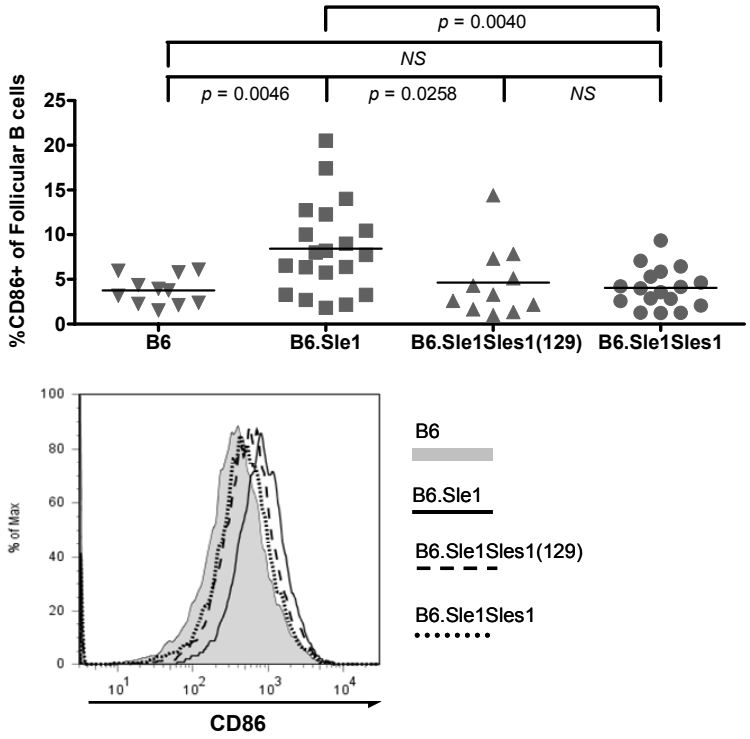

Figure 33. *Sle1*-mediated follicular B cell hyper-activation is suppressed in 12 month B6.*Sle1Sles1*^{129} females. Top panel shows percentages of follicular B cells (B220+CD23+CD21+IgM+) that are CD86+. Bottom panel is a representative CD86 histogram overlay of follicular B cells. n = 11-20 mice per genotype.

Similarly, there is a small decrease in the percentage of follicular helper T cells in B6.*Sle1Sles1*^{129} mice, compared to B6.*Sle1* mice (18.44 ± 2.69 vs. 24.35 ± 2.64, $p = 0.0086$). B6.*Sle1Sles1* mice have dramatically less follicular helper T cells than either of these groups (2.24 ± 0.26, $p = 0.0007$ and $p < 0.0001$, respectively) (Table 11). This is also reflected in the cell-surface densities of ICOS, CXCR5 and PD-1, (Figure 34C). Together, *Sles1*^{129} is capable of partially reducing *Sle1*-mediated T cell dysregulation.

Sle1 also produces a mild monocytosis when added to the B6 genomic background as measured by the significant increase in the percentage of CD11b^{+} splenocytes (14.77 ± 0.82 vs. 8.19 ± 0.49, $p < 0.0001$). This phenotype is partially corrected by both B6.*Sle1Sles1* (11.29 ± 0.75, $p = 0.0031$) and B6.*Sle1Sles1*^{129} mice (11.63 ± 1.03, p = 0.0017) (Figure 35 and Table 11).

In conclusion, B6.*Sle1Sles1*^{129} female mice display an intermediate phenotype, between both B6.*Sle1* and B6.*Sle1Sles1* female. For some parameters, like helper T cell activation and monocytosis, *Sles1*^{129} is indistinguishable from *Sles1*. As the B6 and 129 genomes share identical MHC Class II molecules, yet represent both non-suppressive and partially-suppressive *Sles1* alleles, it suggests that a non-MHC Class II gene may

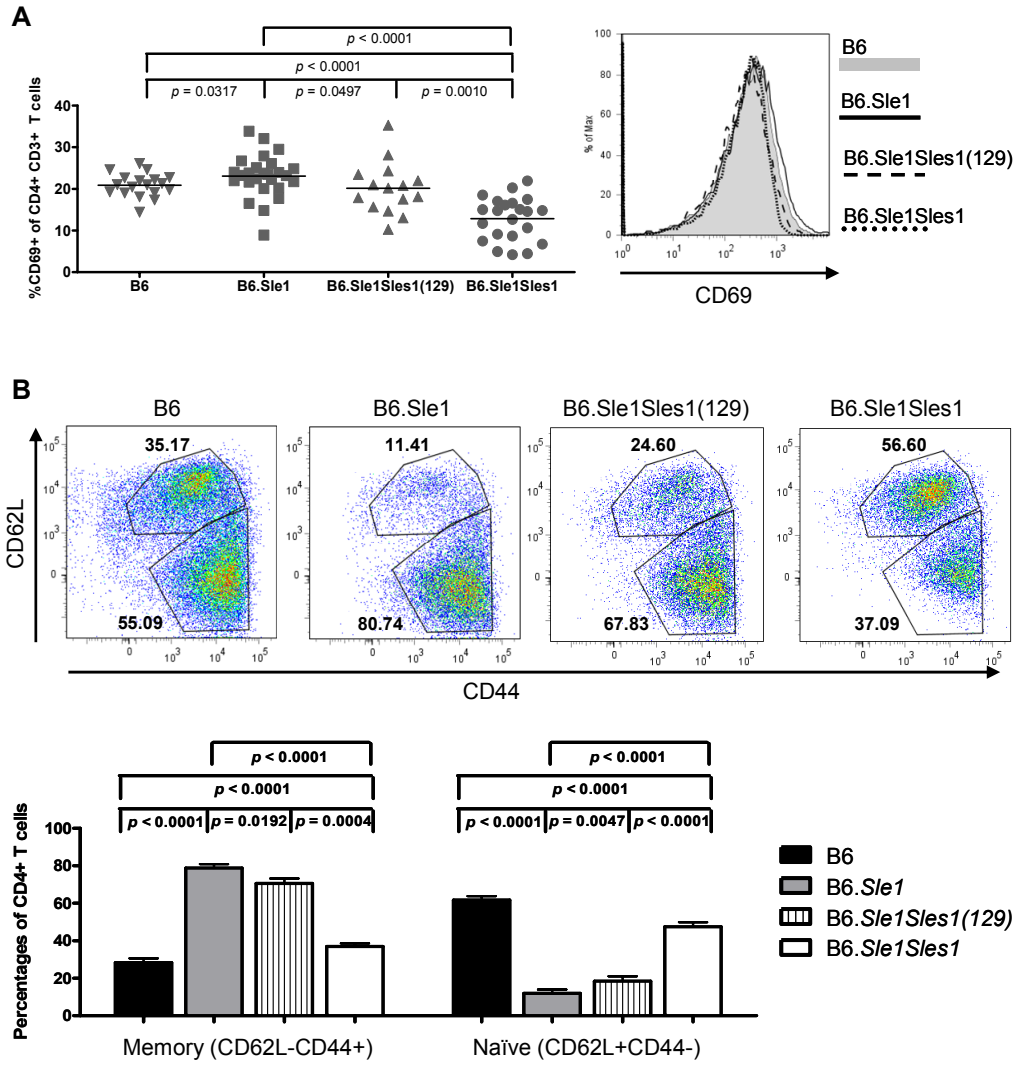

Figure 34A-B. *Sle1*-mediated T cell activation is slightly suppressed in 12 month B6.*Sle1Sles1*^{129} females. A. Left panel, percentages of CD4+ CD3+ T cells that are CD69+. Right panel, representative CD69 histogram overlay of CD4+ CD3+ T cells. B. Top, representative dot plots of memory vs naïve CD4+CD3+ T cells. Bottom panel, percentages of CD4+CD3+ T cells that are memory (left) and naïve (right). n = 14-26 mice per genotype.

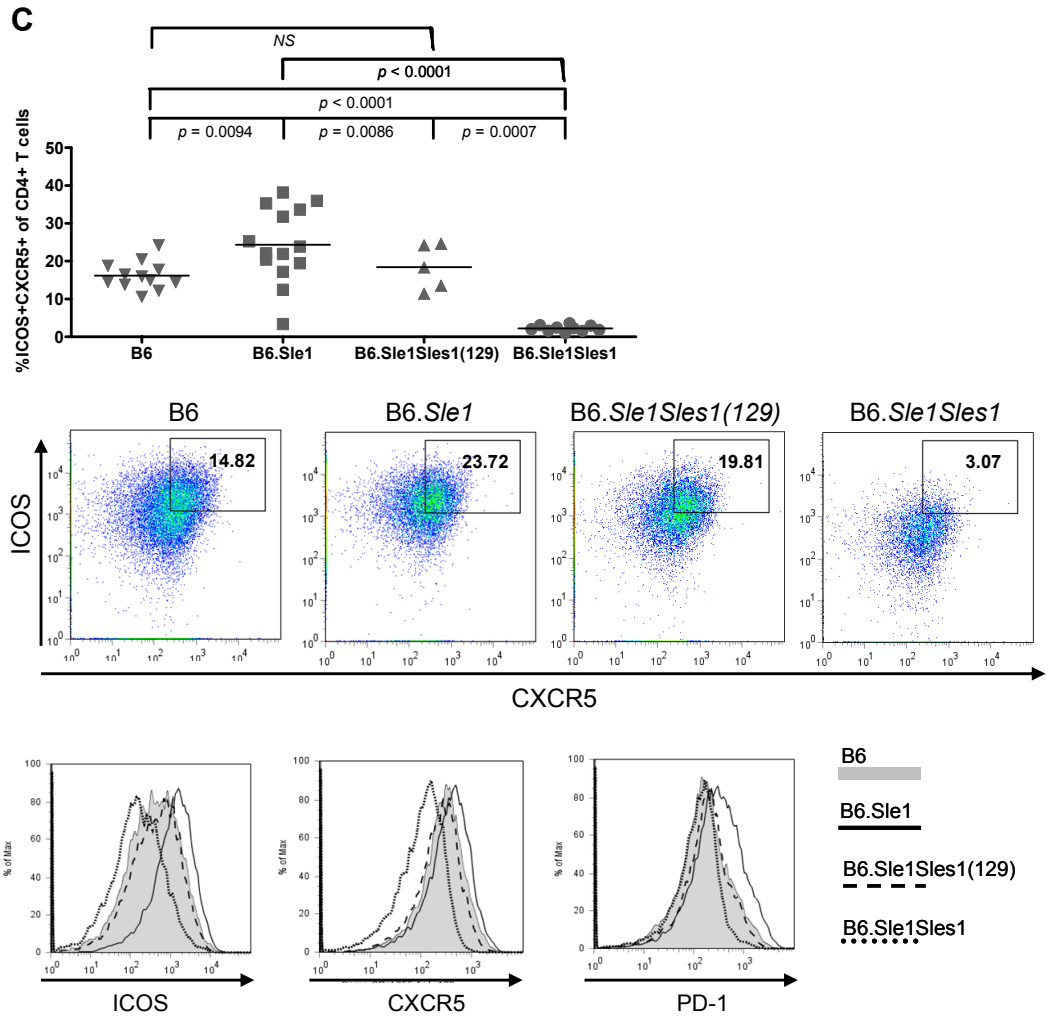

Figure 34C. Follicular helper T cell expansion is slightly suppressed in 12 month B6.*Sle1Sles1*^{129} females, compared to B6.*Sle1Sles1* females. However, B6.*Sle1Sles1* mice show a dramatic decrease in follicular helper T cells even compared to B6 mice, which is not recapitulated by B6.*Sle1Sles1*^{129} mice. Top panel, percentages of CD4+ CD3+ T cells are follicular helper T cells (ICOS+CXCR5+). Middle, representative dot plots of follicular helper CD4+CD3+ T cells. Bottom, representative histogram overlay of CD4+ CD3+ T cells showing expression of ICOS (left), CXCR5 (middle) and PD-1 (right). n = 5-14 mice per genotype.

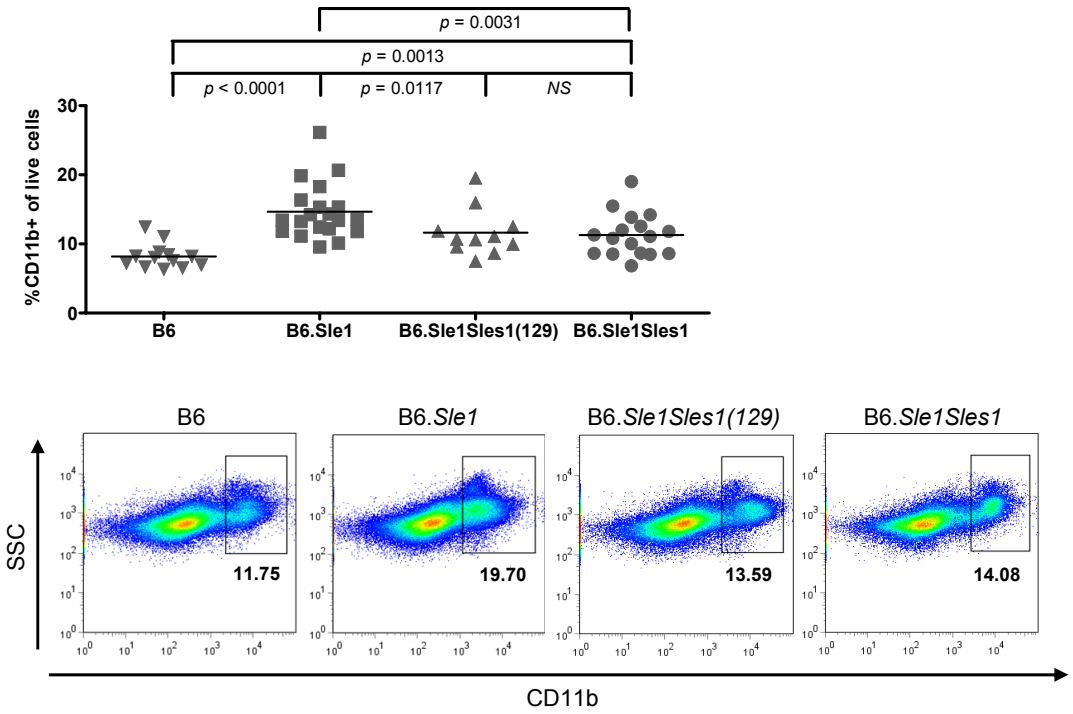

Figure 35. *Sles1*-mediated suppression of monocytosis is recapitulated by *Sles1*^{129} in 12 month old females. Top panel, percentages of CD11b+ (of live). Bottom panel, representative dot plots of CD11b+ cells (of live cells). n = 11-20 mice per genotype.

Table 11. Splenic cell populations in B6, B6.*Sle1*, B6.*Sle1Sles1*$^{(129)}$, and B6.*Sle1Sles1* 12 month females

Population[1]	B6 (n=7-12)	B6.*Sle1* (n=14-20)	B6.*Sle1Sles1*^{129} (n=9-12)	B6.*Sle1Sles1* (n=11-19)	B6 vs. B6.*Sle1Sles1*	B6.*Sle1* vs. B6.*Sle1Sles1*^{129}	B6.*Sle1* vs. B6.*Sle1Sles1*	B6.Sle1Sles1^{129} vs. B6.*Sle1Sles1*
B220/CD19+	54.30 ± 1.36	40.48 ± 2.08	45.42 ± 1.93	48.12 ± 1.45	***P* = 0.0003**	NS	***P* = 0.0020**	NS
Number of cells	53600 ± 1345	39960 ± 2054	44285 ± 1998	47495 ± 1430	***P* < 0.0001**	NS	***P* = 0.0020**	NS
CD86+	5.89 ± 0.72	9.98 ± 0.71	7.51 ± 0.77	6.91 ± 0.58	NS	***P* = 0.0097**	***P* = 0.0018**	NS
T1 ($CD23^-CD21^-IgM^+$)	4.54 ± 0.41	4.56 ± 0.46	3.85 ± 0.44	3.81 ± 0.27	NS	NS	NS	NS
T2 ($CD23^+CD21^{hi}IgM^{hi}$)	4.05 ± 0.22	3.46 ± 0.30	2.98 ± 0.25	4.46 ± 0.28	NS	NS	***P* = 0.0232**	***P* = 0.0011**
Follicular[2]	54.01 ± 2.50	41.50 ± 2.13	49.86 ± 2.63	56.06 ± 0.71	NS	***P* = 0.0219**	***P* < 0.0001**	***P* = 0.0385**
CD86+	3.76 ± 0.50	8.43 ± 1.13	4.64 ± 1.20	4.04 ± 0.55	NS	***P* = 0.0258**	***P* = 0.0040**	NS
MZ ($CD23^-CD21^+IgM^+$)	8.75 ± 0.75	11.16 ± 1.25	7.16 ± 1.13	11.92 ± 0.65	***P* = 0.0022**	***P* = 0.0272**	NS	***P* = 0.0041**
B1a ($CD5^+CD23^-B220^+$)	1.87 ± 0.21	2.82 ± 0.37	2.63 ± 0.24	1.82 ± 0.17	NS	NS	***P* = 0.0399**	***P* = 0.0122**
B1b ($CD5^-CD23^-B220^{lo}$)	5.50 ± 0.45	6.03 ± 0.40	4.61 ± 0.43	4.83 ± 0.30	NS	***P* = 0.0219**	***P* = 0.0197**	NS
B2 ($CD5^-CD23^+B220^+$)	36.30 ± 1.60	21.28 ± 1.90	29.35 ± 2.40	34.02 ± 1.23	NS	***P* = 0.0197**	***P* < 0.0001**	NS
Plasma ($CD19^-CD138^+$)	1.48 ± 0.36	3.11 ± 0.45	2.34 ± 0.36	1.19 ± 0.19	NS	NS	***P* = 0.0005**	***P* = 0.0110**
CD3+	26.31 ± 0.73	21.79 ± 0.74	26.95 ± 1.06	24.96 ± 1.01	NS	***P* = 0.0004**	***P* = 0.0082**	NS
Number of cells	24757 ± 2945	22439 ± 1040	27990 ± 1169	24879 ± 695.9	NS	***P* = 0.0033**	NS	***P* = 0.0350**
CD4+	54.59 ± 1.82	60.97 ± 1.42	55.01 ± 2.26	49.92 ± 1.56	NS	***P* = 0.0274**	***P* < 0.0001**	NS
CD69+	20.87 ± 0.67	23.08 ± 1.01	20.16 ± 1.60	12.86 ± 1.11	***P* < 0.0001**	***P* = 0.0497**	***P* < 0.0001**	***P* = 0.0010**
CD25+CD69-	8.20 ± 0.44	8.82 ± 0.50	9.85 ± 0.46	9.39 ± 0.65	NS	***P* = 0.0475**	NS	NS
CD69+CD25+	8.28 ± 0.50	8.07 ± 0.85	6.40 ± 1.16	4.69 ± 0.59	***P* = 0.0003**	NS	***P* = 0.0062**	NS
CD69+CD25-	26.65 ± 2.56	28.72 ± 1.97	23.58 ± 1.98	17.23 ± 2.62	***P* = 0.0169**	NS	***P* = 0.0045**	NS
Mem. (CD62L+CD44-)	61.65 ± 2.25	78.81 ± 2.07	70.66 ± 2.53	36.89 ± 1.71	***P* < 0.0001**	***P* = 0.0047**	***P* < 0.0001**	***P* < 0.0001**
Naïve (CD62L-CD44+)	28.36 ± 2.27	11.97 ± 2.00	23.31 ± 5.22	47.44 ± 2.50	***P* < 0.0001**	***P* = 0.0192**	***P* < 0.0001**	***P* = 0.0004**
Follicular Helper[3]	16.18 ± 1.07	24.35 ± 2.64	18.44 ± 2.69	2.24 ± 0.26	***P* < 0.0001**	***P* = 0.0086**	***P* < 0.0001**	***P* = 0.0007**
CD8+	25.96 ± 1.80	19.86 ± 1.45	26.10 ± 1.66	32.31 ± 1.28	***P* = 0.0055**	***P* = 0.0134**	***P* < 0.0001**	***P* = 0.0113**
CD69+	10.67 ± 0.57	10.65 ± 0.70	9.89 ± 1.18	7.27 ± 0.42	***P* < 0.0001**	NS	***P* = 0.0002**	***P* = 0.0481**
CD11b+	8.19 ± 0.49	14.77 ± 0.82	11.63 ± 1.03	11.29 ± 0.75	***P* = 0.0013**	***P* = 0.0117**	***P* = 0.0031**	NS
Number of cells	9494 ± 1292	15379 ± 1015	16034 ± 1481	16885 ± 2241	***P* = 0.0002**	NS	NS	NS
Neutrophils[4]	2.49 ± 0.38	5.40 ± 0.43	3.15 ± 0.23	4.15 ± 0.60	***P* = 0.0383**	***P* = 0.0020**	NS	NS
Inflammatory Monocytes[5]	1.03 ± 0.08	2.18 ± 0.20	1.20 ± 0.11	1.56 ± 0.13	***P* = 0.0345**	***P* = 0.0036**	***P* = 0.0291**	NS
Resident Monocytes[6]	0.79 ± 0.07	1.04 ± 0.06	0.82 ± 0.14	0.98 ± 0.09	NS	NS	NS	NS
Macrophages[7]	1.46 ± 0.14	2.29 ± 0.15	1.75 ± 0.16	2.16 ± 0.19	***P* = 0.0095**	NS	NS	NS
CD11c+	8.37 ± 0.48	9.52 ± 0.68	8.76 ± 0.93	7.83 ± 0.71	NS	NS	NS	NS
NK1.1+	2.46 ± 0.15	2.28 ± 0.15	2.41 ± 0.27	3.05 ± 0.27	NS	NS	***P* = 0.0081**	NS

Table 11. Splenic cell populations in B6, B6.*Sle1*, B6.*Sles1*^{129}, and B6.*Sle1Sles1* 12 month females

[1] Ten to eleven color flow cytometry was completed on splenocytes as detailed in Materials and Methods. Shown values represent mean ± SEM. Indented subsets indicate that the listed percentages are of the indicated parent population. All other percentages are of live cells, as determined by forward and side scatter profiles. NS = not significant.

[2] $B220^{+}CD23^{+}CD21^{+}IgM^{+}$

[3] $CD3^{+}CD4^{+}ICOS^{+}CXCR5^{+}$

[4] $CD11b^{+}Gr1^{+}SSC^{hi}$

[5] $CD11b^{+}Gr1^{+}Neu7/4^{+}SSC^{lo}$

[6] $CD11b^{+}Gr1^{-}Neu7/4^{+}$

[7] $CD11b^{+}F4/80^{+}$

be responsible for this intermediate phenotype of *Sles1*^{129} and possibly contribute to the canonical *Sles1* phenotype.

Sles1^{129} Does Not Suppress *Sle1*-mediated Disease in Male Mice with *Yaa*

To investigate whether the phenotype of *Sles1*^{129} could be influenced by enhanced innate immune stimulation, we also comprehensively evaluated *Sle1*-mediated disease in age- and sex-matched 4-6 month old B6.yaa, B6.*Sle1yaa*, B6.*Sle1Sles1*^{129}*yaa* and B6.*Sle1Sles1yaa* male mice. Like in the female B6.*Sle1* model above, we assayed humoral autoimmunity, splenomegaly, and splenic cell population markers.

Sle1-mediated humoral autoimmunity was determined through ELISAs detecting antinuclear IgG at various ages. In 4 month old males, B6.*Sle1yaa* and B6.*Sle1Sles1*^{129}*yaa* mice had comparable ANA levels (182.1 ± 42.80 vs. 310.4 ± 136.9) while B6.*Sle1Sles1yaa* mice had dramatically lower ANA levels than either diseased group (14.42 ± 5.49, both $p < 0.0001$) (Figure 36A). Similarly, in 6 month old males, B6.*Sle1yaa* and B6.*Sle1Sles1*^{129}*yaa* mice again had comparable ANA levels (619.9 ± 134.5 vs. 611.5 ± 160.9) while B6.*Sle1Sles1yaa* mice again had dramatically lower ANA levels (68.76 ± 46.20, both $p < 0.0001$)

(Figure 36B). These results indicate that, in contrast to the B6.*Sle1* female data, *Sles1*^{129} has no suppressive capacity for ANAs on the male *yaa* model.

As shown in Figure 37, the comparison of 6 month old mouse spleen weights demonstrated a similar pattern. While B6.*Sle1Sles1*^{129}*yaa* mice had statistically comparable degrees of splenomegaly as B6.*Sle1yaa* mice (481.8 ± 51.76 mg vs. 669.8 ± 104.7 mg), B6.*Sle1Sles1yaa* mice had much smaller spleens (105.2 ± 15.52 mg, $p = 0.0002$ and $p < 0.0001$ respectively) (Figure 37). There was a slight non-significant trend towards reduced splenomegaly in B6.*Sle1Sles1*^{129}*yaa* mice, compared to B6.*Sle1yaa* mice. This data confirms that *Sles*^{129} does not recapitulate the canonical *Sles1* phenotype.

Extensive 10-12 color flow cytometry analysis was completed on 6 month old male splenocytes to fully evaluate the suppressive capacity of *Sles1*^{129} in sub-phenotypes (for details, see *Materials and Methods*). Of the 25 splenic cell parameters with quantitative differences between B6.*Sle1yaa* and B6.*Sle1Sles1yaa* mice, 24 were also significantly different between B6.*Sle1Sles1yaa* and B6.*Sle1Sles1*^{129}*yaa*, while only one parameter was significantly different between B6.*Sle1yaa* and B6.*Sle1Sles1*^{129}*yaa* (Table 12).

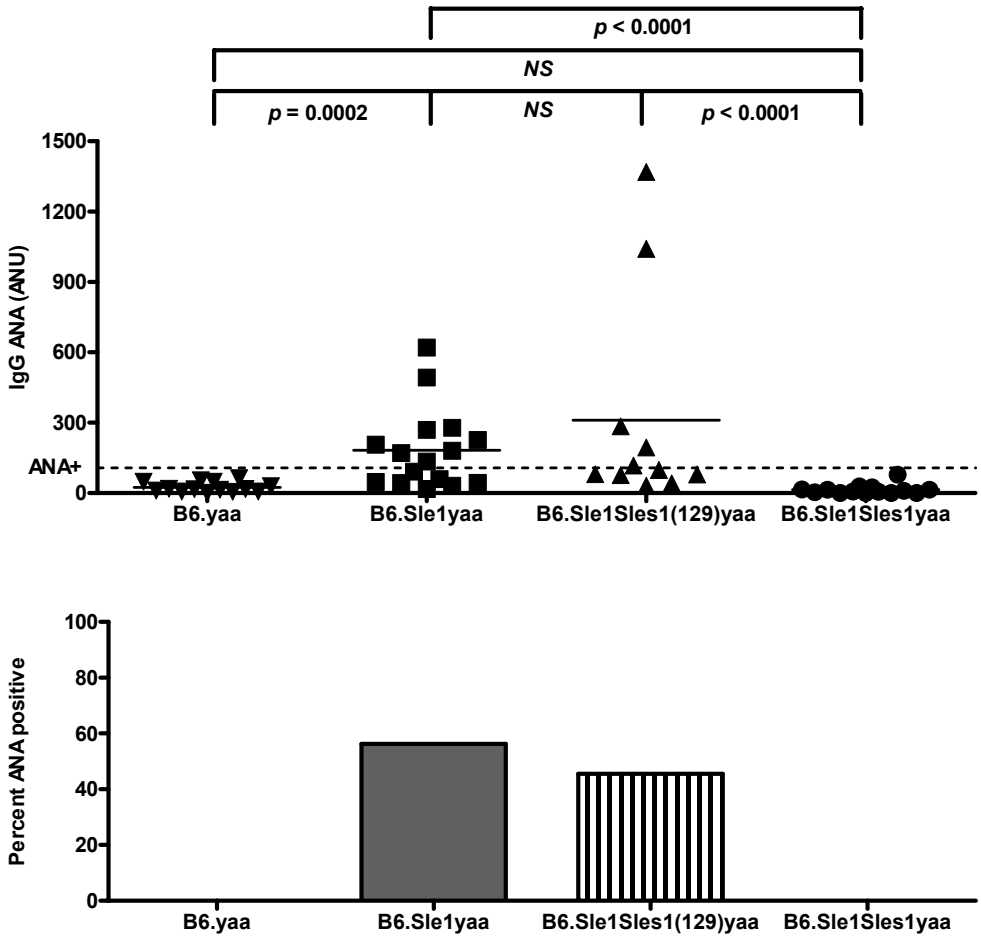

Figure 36A. *Sle1*-mediated humoral autoimmunity is not suppressed in 4 month B6.*Sle1Sles1*^{129}*yaa* males. Top panel shows IgG ANA levels and bottom panel shows penetrance of ANA positivity. Mice were considered ANA positive when the level was 4 standard deviations above the B6.yaa group mean. n = 11-16 mice per genotype.

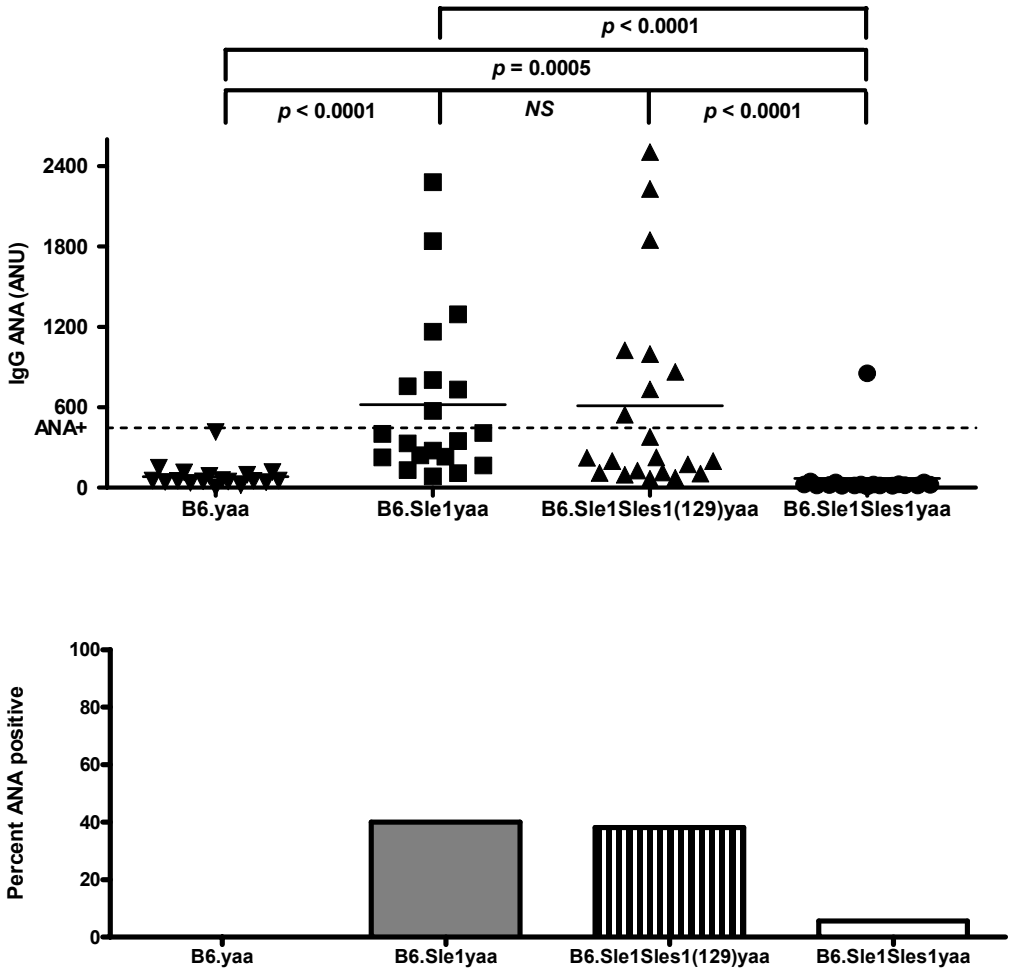

Figure 36A. *Sle1*-mediated humoral autoimmunity is not suppressed in 6 month B6.*Sle1Sles1*^{129}*yaa* males. Top panel shows IgG ANA levels and bottom panel shows penetrance of ANA positivity. Mice were considered ANA positive when the level was 4 standard deviations above the B6.yaa group mean. n = 18-21 mice

Sle1yaa induces hyper-activation of lymphocytes, as shown by increased expression of the activation marker CD86 on follicular B cells ($B220^+CD23^+CD21^+IgM^+$) and activation marker CD69 on helper T cells ($CD3^+CD4^+$). Figure 38 demonstrates that while the percentage of $CD86^+$ follicular B cells is statistically indistinguishable between B6.*Sle1yaa* (12.23 ± 1.38), and B6.*Sle1Sles1*^{129}*yaa* mice (14.09 ± 1.36), B6.*Sle1Sles1yaa* mice have significantly less activated follicular B cells (6.96 ± 0.53, $p = 0.0095$ and $p = 0.0002$, respectively) (Table 12). This is also evident in the helper T cell compartment. B6.*Sle1yaa* and B6.*Sle1Sles1*^{129}*yaa* mice have equivalent percentages (26.77 ± 1.34 vs. 31.31 ± 2.70) of $CD69^+$ helper T cells, while B6.*Sle1Sles1yaa* mice have far less activated helper T cells (13.34 ± 1.43, $p < 0.0001$ and $p = 0.0002$, respectively) (Figure 39A and Table 12). These phenotypes are also reflected in the cell-surface densities of activation markers as determined by MFIs on follicular B cells (bottom panel of Figure 38) and helper T cells (Figure 39A, right panel). Therefore, *Sles1*^{129} is not sufficient to restore normal lymphocyte activation levels in B6.*Sle1yaa* mice, unlike *Sles1.*

Sle1yaa also mediates striking changes in subpopulations of helper T cells, reflecting the hyperactivity of this cellular compartment. Specifically, there is an increase in memory helper T cells

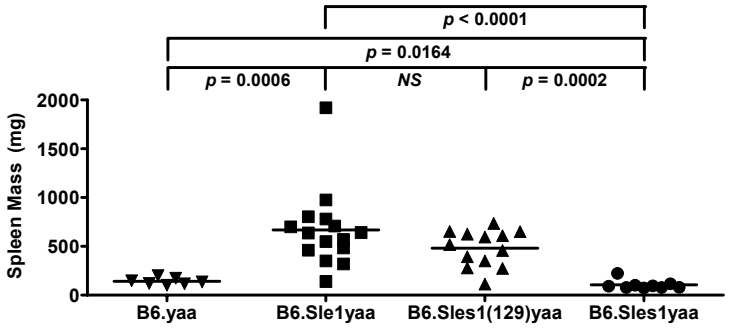

Figure 37. *Sle1*-mediated splenomegaly is not suppressed in 6 month B6.*Sle1Sles1*^{129}*yaa* males. n = 7-15 mice per genotype.

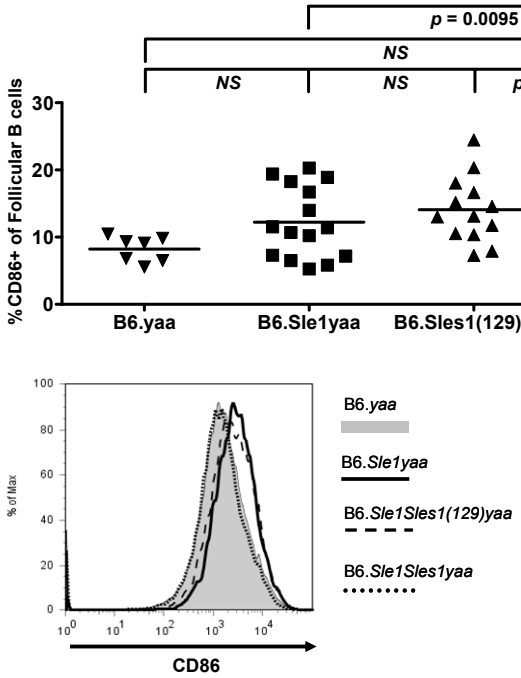

Figure 38. *Sles1*-mediated follicular B cell hypo-activation is not recapitulated in 6 month B6.*Sle1Sles1*^{129}*yaa* males. Top panel shows percentages of follicular B cells (B220+CD23+CD21+IgM+) that are CD86+. Bottom panel is a representative CD86 histogram overlay of follicular B cells. n = 7-15 mice per genotype.

($CD62L^{lo}CD44^{hi}CD4^{+}CD3^{+}$) and a corresponding decrease in naïve helper T cells ($CD62L^{hi}CD44^{lo}CD4^{+}CD3^{+}$), as well as increase in follicular helper T cells ($ICOS^{+}CXCR5^{+}CD4^{+}CD3+$). B6.*Sle1Sles1*^{129}*yaa* mice had comparable percentages of memory helper T cells as B6.*Sle1yaa* mice (69.11 ± 4.51 vs. 72.49 ± 3.84). Both of these groups had nearly 3-fold higher percentages of memory helper T cells than B6.*Sle1Sles1yaa* mice (26.09 ± 3.29, $p = 0.0002$ and $p < 0.0001$, respectively (Figure 39B and Table 12). There is also a marked increase in the percentage of follicular helper T cells in B6.*Sle1yaa* and B6.*Sle1Sles1*^{129}*yaa* but not in B6.*Sle1Sles1yaa* splenocytes (13.31 ± 1.71 and 14.48 ± 1.58 vs. 4.03 ± 1.02, both $p = 0.0003$) (Figure 39C and Table 12). This is also reflected in the cell-surface densities of ICOS, CXCR5 and PD-1 (bottom panel of Figure 39C). Thus, B6.*Sle1Sles1yaa* mice, but not B6.*Sle1Sles1*^{129}*yaa* mice, can reduce the *Sle1*-mediated skewing of helper T cell sub-populations proportions. The addition of *yaa* to B6.*Sle1* results in extreme monocytosis as measured by the significant increase in the percentage of $CD11b^{+}$ splenocytes. This phenotype is corrected by B6.*Sle1Sles1yaa* mice, compared to B6.*Sle1*yaa mice (10.96 ± 0.77 vs. 26.60 ± 4.23, $p = 0.0002$). However, B6.*Sle1Sles1*^{129}*yaa* mice do not have reduced monocytosis (20.60 ± 3.69, $p = 0074$ vs. B6.*Sle1Sles1yaa*) (Figure 40A and Table 12). We also looked more carefully at the monocyte

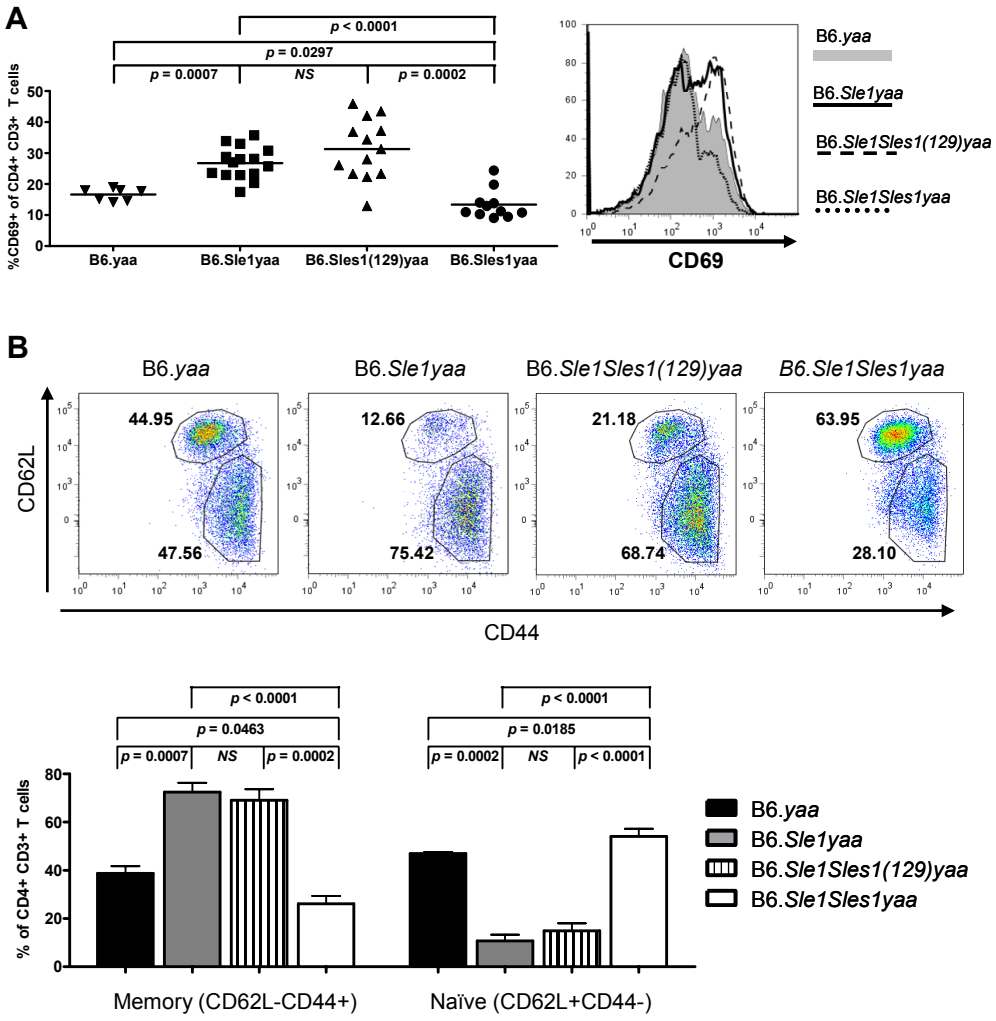

Figure 39A-B. *Sle1*-mediated T cell activation is not suppressed in 6 month B6.*Sle1Sles1*^{129}*yaa* males. A. Left panel, percentages of CD4+ CD3+ T cells that are CD69+. Right panel, representative CD69 histogram overlay of CD4+ CD3+ T cells. B. Top, representative dot plots of memory vs naïve CD4+CD3+ T cells. Bottom panel, percentages of CD4+CD3+ T cells that are memory (left) and naïve (right). n = 8-18 mice per genotype.

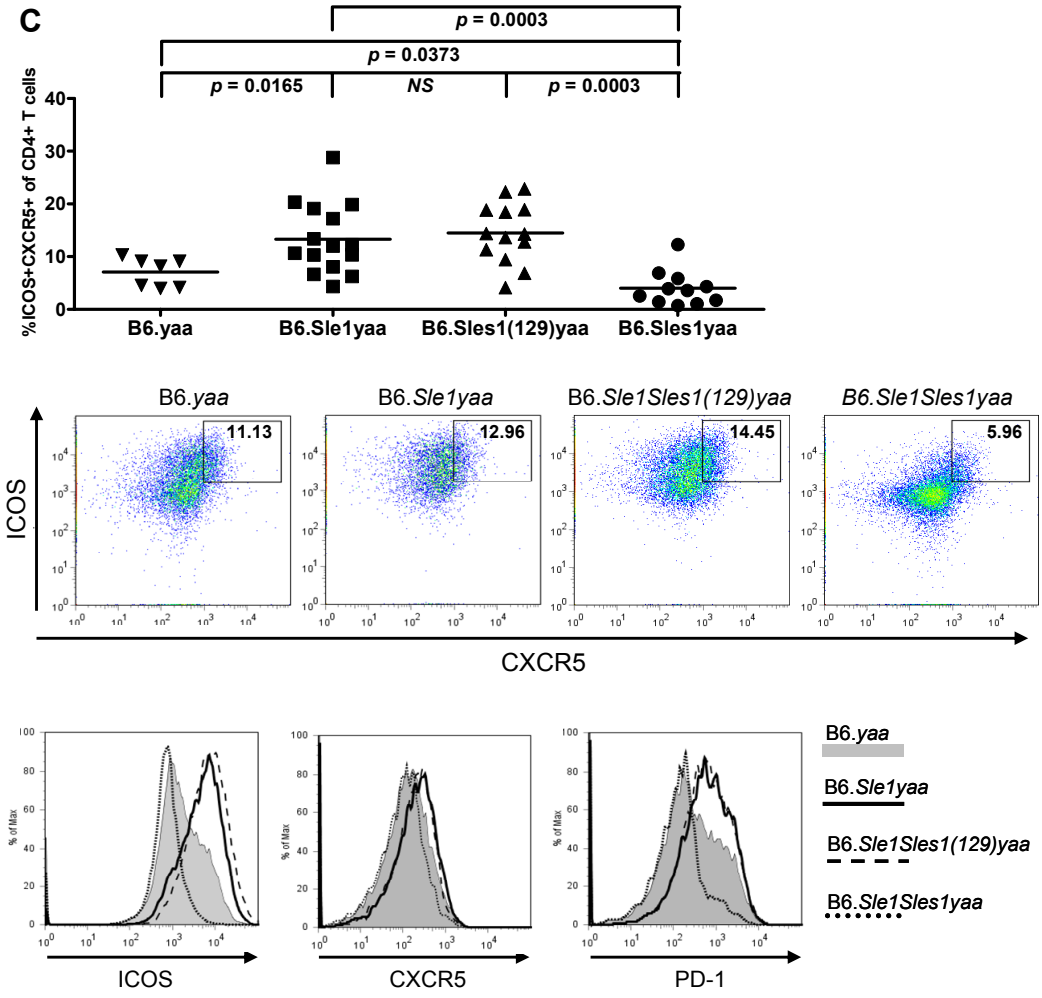

Figure 39C. *Sle1*-mediated follicular helper T cell expansion is not suppressed in 6 month B6.*Sle1Sles1*^{129}*yaa* males. Top panel, percentages of CD4+ CD3+ T cells are follicular helper T cells (ICOS+CXCR5+). Middle, representative dot plots of follicular helper CD4+CD3+ T cells. Bottom, representative histogram overlay of CD4+ CD3+ T cells showing expression of ICOS (left), CXCR5 (middle) and PD-1 (right). n = 8-18 mice per genotype.

compartment where B6.*Sle1yaa* and B6.*Sle1Sles1*^{129}*yaa* had similar percentages of inflammatory monocytes (Gr1^{+}Neu7/4^{+}SSC^{lo}), neutrophils (Gr1^{+}SSC^{hi}) and macrophages (F4/80^{+}) within the CD11b^{+} cell population. There is a non-significant trend towards increased proportion of neutrophils in B6.*Sle1Sles1*^{129}*yaa*, compared to B6.*Sle1yaa* mice Figure 40B and Table 12).

B6.*Sle1yaa* six month old male mice also have GN as determined by the blinded examination of stained longitudinal kidney sections by an independent investigator. B6.*Sle1Sle1yaa* and B6.*Sle1Sles1*^{129}*yaa* mice had similar overall pathology score (3.40 ± 0.37 vs. 3.20 ± 0.34), while B6.*Sle1Sles1yaa* mice had significantly less kidney damage than both diseased groups (0.50 ± 0.16, $p = 0.0109$ and $p = 0.0119$, respectively) (Figure 41). Therefore, *Sles1*^{129}, unlike *Sles1,* is not sufficient to prevent *Sle1*-mediated GN.

In conclusion, B6.*Sle1Sles1*^{129}*yaa* male mice consistently failed to recapitulate the canonical suppressive *Sles1* effect in all sub-phenotypes analyzed. This conflicts with the data from the B6.*Sle1* female model, in which *Sles1*^{129} demonstrated an intermediate suppressive phenotype, suggesting that any *Sles1* 129-derived suppressive modifiers are influenced by innate immune stimulation, such as is provided by *yaa*. Also, as *Sles1* remains fully suppressive even in the context of *yaa*,

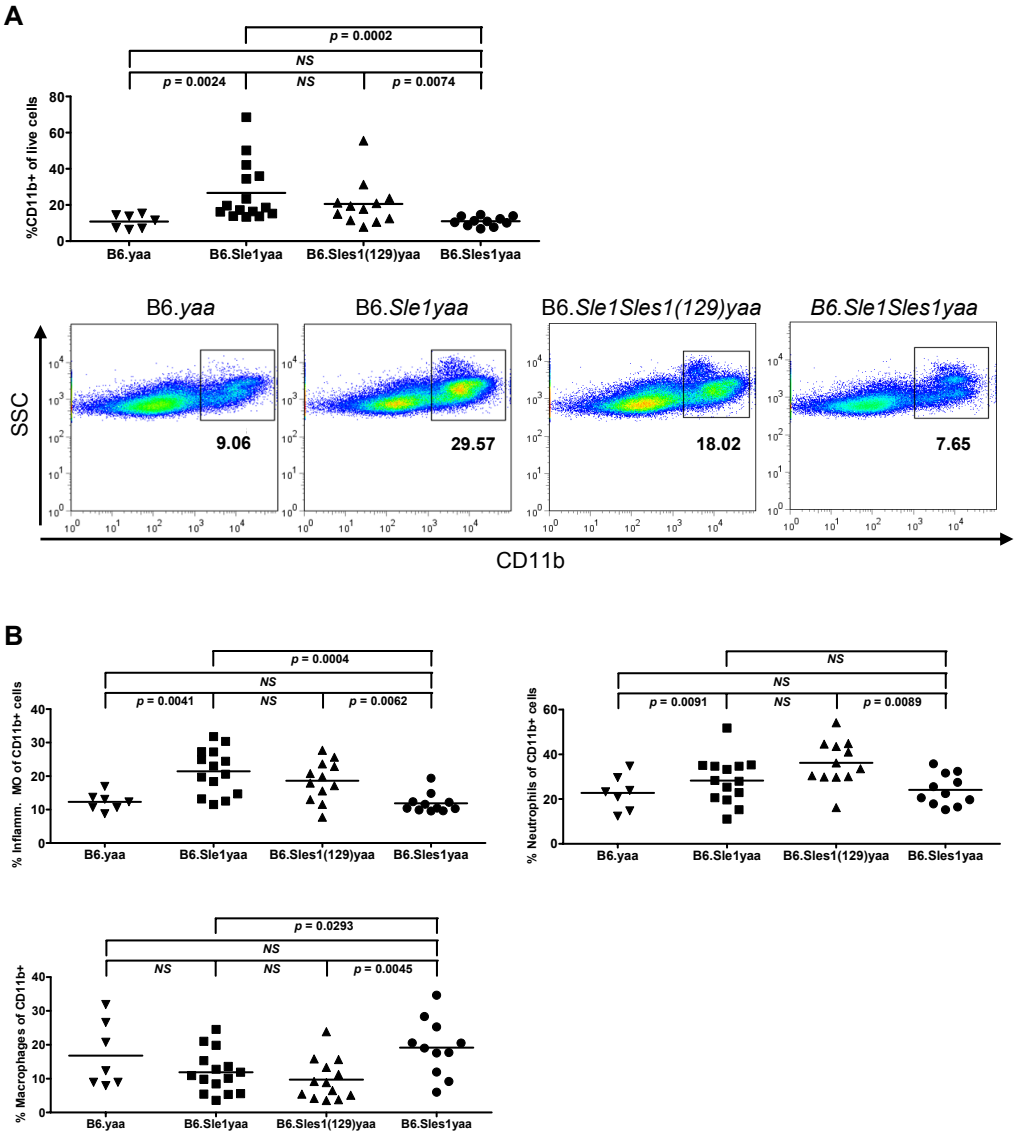

Figure 40. *Sle1yaa*-mediated monocytosis is not suppressed in 6 month B6.*Sle1Sles1*^{129}*yaa* males. **A.** Top panel, percentages of CD11b+ (of live). Bottom panel, representative dot plots of CD11b+ cells (of live). B. Percentages of inflammatory monocytes ($Gr1^+Neu7/4^+SSC^{lo}$), neutrophils ($Gr1^+SSC^{hi}$) and macrophages ($F4/80^+$) gated through live $CD19/3^-$ $CD11b^+$ cells. n = 8-18 mice per genotype.

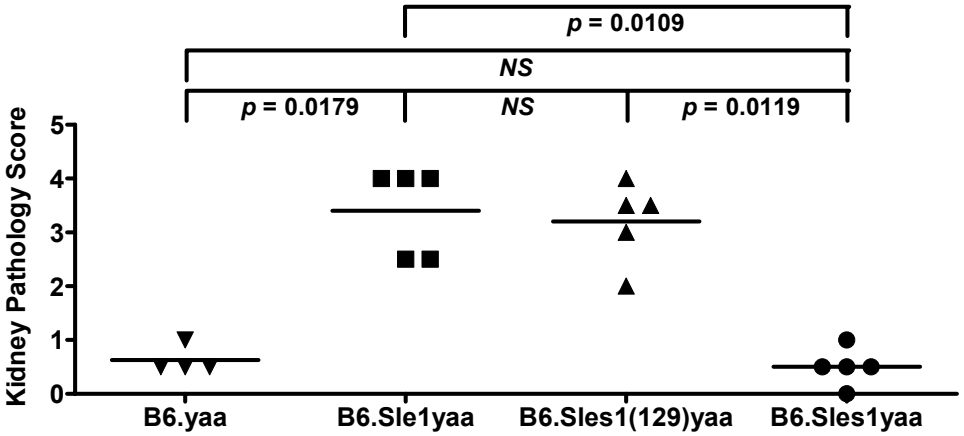

Figure 41. *Sle1yaa*-mediated glomerulnephritis is not suppressed in 6 month B6.*Sle1Sles1*^{129}*yaa* males. Stained longitudinal kidney sections were blind examined for evidence of disease pathology in the glomeruli, tubules or interstitial areas by Dr. Xin J. Zhou (Department of Pathology, UTSW). The GN severity was graded on a scale of 0 to 4, where 0 indicates normal and 4 indicates significant evidence of disease. See *Materials and Methods* sections for more details.

Table 12. Splenic cell populations in B6.yaa, B6.*Sle1yaa*, B6.*Sle1Sles1*^{129}*yaa*, and B6.*Sle1Sles1yaa* 6 month males

Population[1]	B6.*yaa* (n=7)	B6.*Sle1yaa* (n=15)	B6.*Sle1Sles1*^{129}*yaa* (n=12-13)	B6.*Sle1Sles1yaa* (n=11)	B6.*yaa* vs. B6.*SleSles1yaa*	B6.*Sle1yaa* vs. B6.*SleSles1*^{129}*yaa*	B6.*Sle1yaa* vs B6.*Sle1Sles1yaa*	B6.*Sle1Sles1*^{129}*yaa* vs B6.*Sle1Sles1yaa*
B220/CD19+	46.51 ± 3.19	25.38 ± 2.82	26.28 ± 240	42.60 ± 0.88	NS	NS	***P* = 0.0008**	***P* < 0.0001**
Number of cells	52038 ± 3571	28399 ± 3158	29398 ± 2680	47425 ± 1161	***P* = 0.0019**	NS	***P* = 0.0011**	***P* = 0.0001**
CD86+	13.18 ± 0.79	15.72 ± 0.88	21.07 ± 2.19	10.67 ± 0.69	***P* = 0.0463**	NS	***P* = 0.0005**	***P* = 0.0001**
T1 ($CD23^-CD21^-IgM^+$)	8.19 ± 0.74	9.58 ± 1.29	9.45 ± 0.77	5.70 ± 0.66	***P* = 0.0297**	NS	***P* = 0.0147**	***P* = 0.0038**
T2 ($CD23^+CD21^{hi}IgM^{hi}$)	2.24 ± 0.20	1.97 ± 0.35	1.96 ± 0.35	4.42 ± 0.79	***P* = 0.0236**	NS	***P* = 0.0026**	***P* = 0.0010**
Follicular[2]	54.66 ± 4.10	37.94 ± 4.20	39.17 ± 2.96	62.41 ± 2.01	NS	NS	***P* = 0.0002**	***P* = 0.0002**
CD86+	8.24 ± 0.72	12.23 ± 1.38	14.09 ± 1.36	6.96 ± 0.53	NS	NS	***P* = 0.0095**	***P* = 0.0006**
MZ ($CD23^-CD21^+IgM^+$)	1.76 ± 0.16	1.26 ± 0.33	1.93 ± 0.39	3.85 ± 0.50	***P* = 0.0112**	NS	***P* = 0.0011**	***P* = 0.0138**
B1a ($CD5^+CD23^-B220^+$)	1.22 ± 0.20	1.91 ± 0.33	1.80 ± 0.36	0.79 ± 0.09	NS	NS	***P* = 0.0170**	***P* = 0.0008**
B1b ($CD5^-CD23^-B220^{lo}$)	4.35 ± 0.17	5.93 ± 0.60	4.59 ± 0.52	2.95 ± 0.33	***P* = 0.0043**	NS	***P* = 0.0002**	***P* = 0.0091**
B2 ($CD5^-CD23^+B220^+$)	30.93 ± 2.84	16.95 ± 1.30	15.33 ± 1.40	34.08 ± 1.09	NS	NS	***P* < 0.0001**	***P* < 0.0001**
Plasma ($CD19^-CD138^+$)	1.41 ± 0.16	2.76 ± 0.25	3.90 ± 0.52	1.24 ± 0.11	NS	NS	***P* < 0.0001**	***P* = 0.0002**
CD3+	31.87 ± 1.85	19.28 ± 1.85	18.41 ± 2.15	36.79 ± 1.73	***P* = 0.0373**	NS	***P* < 0.0001**	***P* = 0.0001**
Number of cells	32184 ± 1863	19474 ± 1862	18594 ± 2171	37155 ± 1743	***P* = 0.0039**	NS	***P* < 0.0001**	***P* = 0.0001**
CD4+	53.14 ± 0.61	59.58 ± 2.89	65.79 ± 1.42	53.54 ± 1.20	NS	NS	NS	***P* = 0.0001**
CD69+	16.66 ± 0.73	26.77 ± 1.34	31.31 ± 2.70	13.34 ± 1.43	***P* = 0.0297**	NS	***P* < 0.0001**	***P* = 0.0002**
CD25+CD69-	10.89 ± 1.31	10.40 ± 0.81	10.41 ± 0.66	8.67 ± 0.74	NS	NS	NS	NS
CD69+CD25+	3.45 ± 0.55	6.27 ± 0.69	7.99 ± 0.76	2.78 ± 0.58	NS	NS	***P* = 0.0031**	***P* = 0.0004**
CD69+CD25-	8.88 ± 0.73	16.03 ± 1.9	21.14 ± 2.06	7.88 ± 1.70	NS	***P* = 0.0427**	***P* = 0.0026**	***P* = 0.0006**
Mem. (CD62L+CD44-)	38.74 ± 2.98	72.49 ± 3.84	69.11 ± 4.51	26.09 ± 3.29	***P* = 0.0463**	NS	***P* < 0.0001**	***P* = 0.0002**
Naïve (CD62L-CD44+)	46.94 ± 0.71	10.70 ± 2.63	14.90 ± 3.15	54.07 ± 2.93	***P* = 0.0185**	NS	***P* < 0.0001**	***P* < 0.0001**
Follicular Helper[3]	7.07 ± 1.03	13.31 ± 1.71	14.48 ± 1.58	4.03 ± 1.02	***P* = 0.0373**	NS	***P* = 0.0003**	***P* = 0.0003**
CD8+	32.49 ± 0.86	22.86 ± 1.44	20.04 ± 1.50	35.98 ± 1.82	***P* = 0.0373**	NS	***P* = 0.0002**	***P* = 0.0001**
CD69+	6.99 ± 0.28	13.79 ± 1.20	13.40 ± 1.65	4.98 ± 0.44	***P* = 0.0066**	NS	***P* < 0.0001**	***P* < 0.0001**
CD11b+	10.86 ± 1.44	26.60 ± 4.23	20.60 ± 3.69	10.96 ± 0.77	NS	NS	***P* = 0.0002**	***P* = 0.0074**
Number of cells	10729 ± 1426	26289 ± 4184	20354 ± 3648	9756 ± 974.2	***P* = 0.0024**	NS	***P* < 0.0001**	***P* = 0.0035**
Neutrophils[4]	2.46 ± 0.33	7.53 ± 1.53	8.39 ± 1.86	2.84 ± 0.26	NS	NS	***P* = 0.0035**	***P* = 0.0043**
Inflammatory Monocytes[5]	1.38 ± 0.19	6.10 ± 1.37	4.00 ± 0.85	1.45 ± 1.78	NS	NS	***P* = 0.0006**	***P* = 0.0010**
Resident Monocytes[6]	0.93 ± 0.16	2.10 ± 0.31	2.70 ± .74	1.22 ± 0.10	NS	NS	NS	NS
Macrophages[7]	2.35 ± 0.83	3.36 ± 0.79	1.94 ± 0.38	2.35 ± 0.42	NS	NS	NS	NS
CD11c+	7.30 ± 1.12	9.99 ± 0.91	7.70 ± 0.99	5.12 ± 0.80	NS	NS	***P* = 0.0009**	NS
NK1.1+	2.71 ± 0.21	2.02 ± 0.26	1.78 ± 0.17	2.50 ± 0.11	NS	NS	***P* = 0.0379**	***P* = 0.0077**

Table 12. Splenic cell populations in B6.*yaa*, B6.*Sle1yaa*, B6.*Sle1Sles1*^{129}*yaa*, and B6.*Sle1Sles1yaa* 6 month males

[1] Ten to eleven color flow cytometry was completed on splenocytes as detailed in Materials and Methods. Shown values represent mean ± SEM. Indented subsets indicate that the listed percentages are of the indicated parent population. All other percentages are of live cells, as determined by forward and side scatter profiles. NS = not significant.

[2] $B220^+CD23^+CD21^+IgM^+$

[3] $CD3^+CD4^+ICOS^+CXCR5^+$

[4] $CD11b^+Gr1^+SSC^{hi}$

[5] $CD11b^+Gr1^+Neu7/4^+SSC^{lo}$

[6] $CD11b^+Gr1^-Neu7/4^+$

[7] $CD11b^+$F4/80+

any 129-derived suppressive modifiers, possibly shared by NZW, likely only play a minor contributory role in suppressing *Sle1*-mediated autoimmunity.

Sles1^{B6} is not sufficient to promote autoimmunity on a 129 background

As our preliminary studies had suggested that *Sles1*^{129} was a suppressive allele, complementing the extremely potent *Sles1* derived from NZW [35], we also investigated whether *Sles1*^{129} was the major autoimmunity modifier loci in the 129 genome. To do this, we generated 129 congenic mice with the B6-derived non-suppressive allele of *Sles1* in a similar fashion to our other congenic mice (see Generation of B6.*Sle1Sles1*^{129}*yaa* Congenic Strain section above). We comprehensively evaluated *Sle1b*-mediated disease in age- and sex-matched 129, (129xB6.*Sle1*)F1, and 129.*Sles1*^{B6} female mice. In addition to assaying humoral autoimmunity and splenomegaly, flow cytometry characterization of splenic cell populations was completed. Suppression of *Sle1*-mediated humoral autoimmunity was determined through ELISAs detecting antinuclear IgG at various ages. In 9 month old females, 129.*Sles1*^{B6} mice demonstrated slightly reduced ANA levels, compared to 129 mice (42.48 ± 10.51 vs. 80.21 ± 14.06, p = 0.0370),

while (129xB6.*Sle1*)F1 mice had dramatically higher ANA levels (999.5 ± 242.8, $p = 0.0049$ and $p = 0.0284$, respectively) (Figure 42A). A similar pattern was seen in 12 month old females, where (129xB6.*Sle1*)F1 mice had markedly increased ANA levels (2841 ± 313.0), compared to the approximately equivalent ANA levels of 129 and 129.*Sles1*^{B6} mice (14.11 ± 5.04 and 62.58 ± 23.81, $p < 0.0001$ for both vs. (129xB6.*Sle1*(F1)) (Figure 42B). In addition, the simultaneous assaying of B6, B6.*Sle1* and B6.*Sle1Sles1* age- and sex- matched sera indicate that the 129-derived series of mice have roughly comparable ANA levels and that the (129xB6.*Sle1*)F1 mice are an legitimate model of autoimmune disease (Figure 42A-B). This data indicates that *Sles1*^{B6} is not sufficient to break tolerance to anti-nuclear antigens in 129 mice.

As shown in Figure 43, the comparison of 12 month old mouse spleen weights demonstrated a similar pattern. (129xB6.*Sle1*)F1 mice developed significant splenomegaly, compared to both 129 and 129.*Sles1*^{B6} mice (190.4 ± 21.63 mg vs. 61.71 ± 4.08 mg and 73.14 ± 6.55 mg, both $p < 0.0001$). However, there was a small, but significant, increase in spleen weight in 129.*Sles1*^{B6} mice, when compared to 129 mice ($p < 0.0001$). These results suggest that although a *Sles1* gene may play a very minor role in the suppression of autoimmunity in the 129

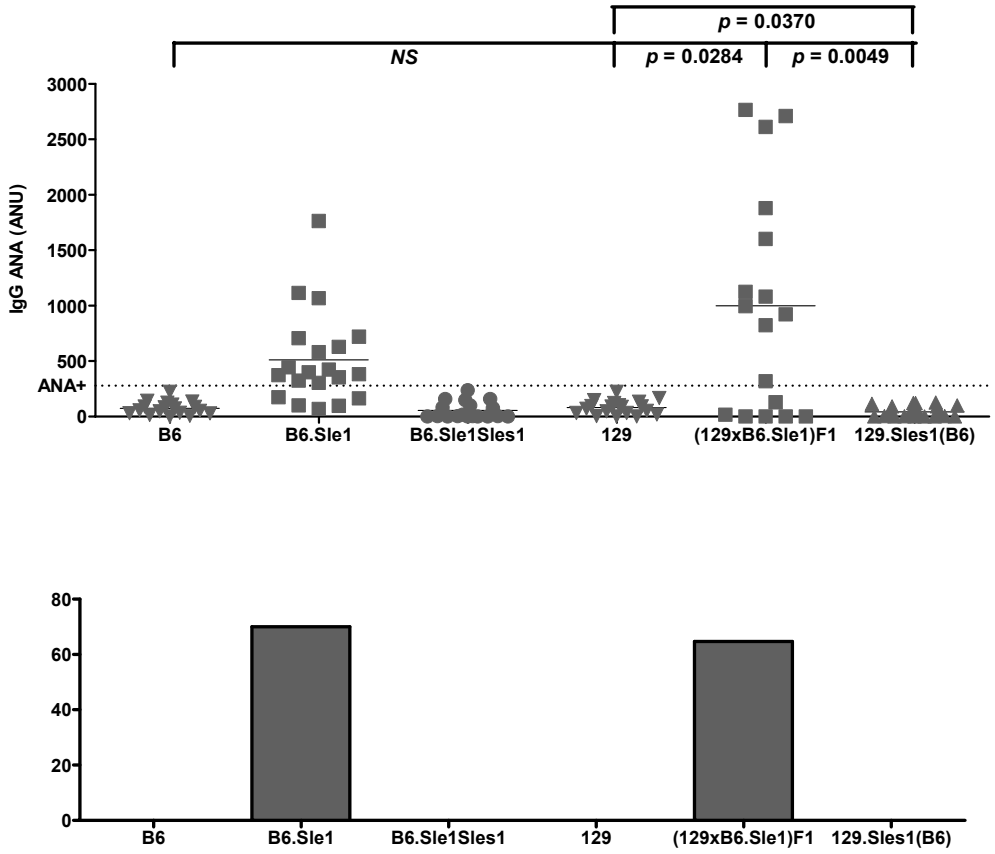

Figure 42A. *Sles1*^{B6} is not sufficient for 9 month female 129 mice to develop humoral autoimmunity. Top panel shows IgG ANA levels and bottom panel shows penetrance of ANA positivity. Mice were considered ANA positive when the level was 4 standard deviations above the B6 group mean. n = 17-22 mice per genotype.

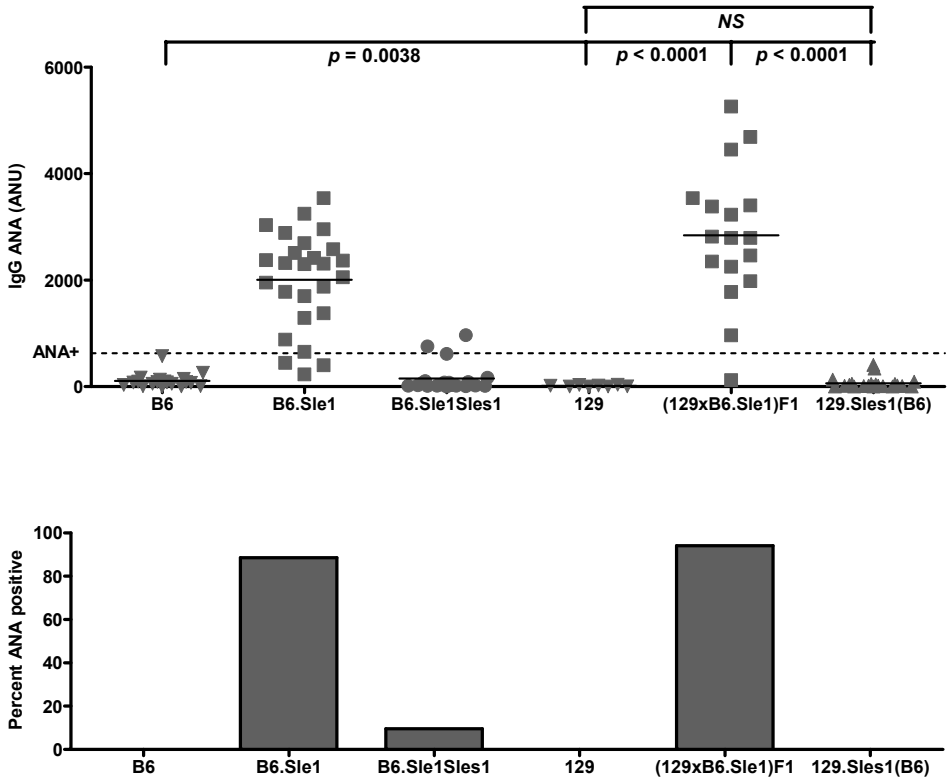

Figure 42B. *Sles1*^{B6} is not sufficient for 12 month female 129 mice to develop humoral autoimmunity. Top panel shows IgG ANA levels and bottom panel shows penetrance of ANA positivity. Mice were considered ANA positive when the level was 4 standard deviations above the B6 group mean. n = 8-26 mice per genotype.

mouse strain, it is not a major contributor to the development of splenomegaly.

Extensive 10-12 color flow cytometry analysis was completed on splenocytes from 12 month old female to fully evaluate the suppressive capacity of *Sles1*^{B6} in sub-phenotypes (for details, see *Materials and Methods*). Of the 12 splenic cell parameters with quantitative differences between 129 and (129xB6.*Sle1*)F1 mice, nine were also significantly different between (129xB6.*Sle1*)F1 and 129.*Sles1*^{B6} mice, while just three were significantly different between 129 and 129.*Sles1*^{B6} mice (Table 13). This is consistent with the ANA and splenomegaly data, which demonstrate that *Sles1*^{B6} is not sufficient to promote autoimmunity on a 129 background.

Surprisingly, (129xB6.*Sle1*)F1 mice had fewer activated follicular B cells ($B220^+CD23^+CD21^+IgM^+$), compared to 129 mice (2.78 ± 0.25 vs. 4.42 ± 0.59, $p = 0.0152$), despite displaying other autoimmunity phenotypes. 129.*Sles1*^{B6} mice had intermediate percentages of $CD86^+$ activated follicular B cells (3.63 ± 0.50) which were not significantly different from either 129 or (129xB6.*Sle1)*F1 mice (Figure 44 and Table 13). This data does support a small effect of *Sles1*^{B6} on the 129 genome though.

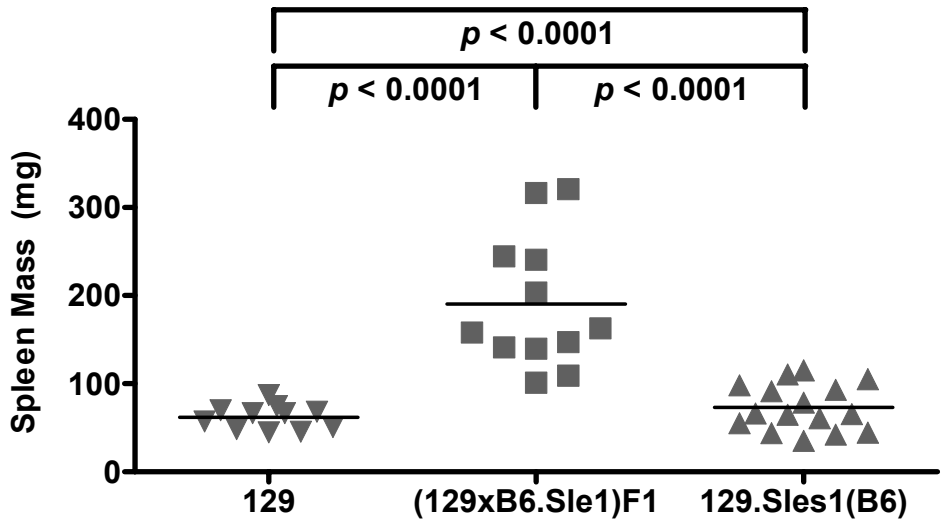

Figure 43. Despite a mild increase in spleen mass, *Sles1*^{B6} is not sufficient for 12 month female 129 mice to develop the degree of splenomegaly seen in (129xB6.*Sle1*) F1 females. n = 11-16 mice per genotype.

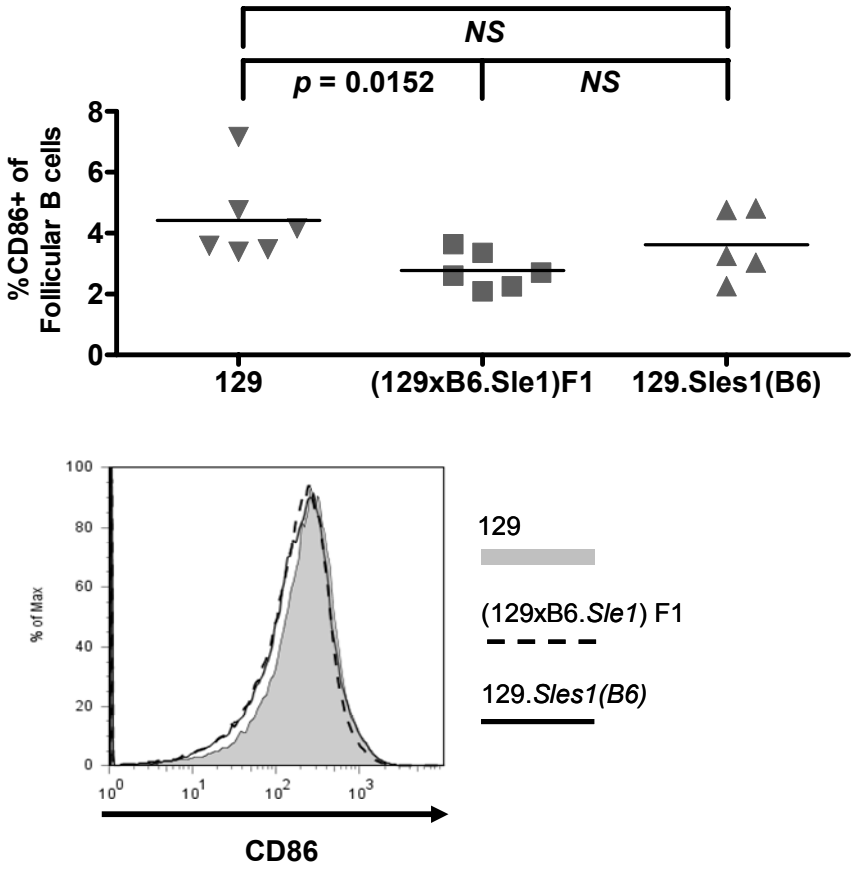

Figure 44. 129.*Sles1*^{B6} 12 month females have levels of B cell activation indistinguishable between 129 and (129xB6.*Sle1*) F1 mice. Top panel shows percentages of follicular B cells (B220+CD23+CD21+IgM+) that are CD86+. Bottom panel is a representative CD86 histogram overlay of follicular B cells. n = 5-6 mice per genotype.

(129xB6.*Sle1*)F1 *mice* also have striking changes in the helper T cell ($CD4^+CD3^+$) compartment, including hyper-activation and sub-population proportions. (129xB6.*Sle1*)F1 mice have an approximately 2-fold increase in the percentage of activated $CD69^+$ helper T cells than 129 and 129.*Sles1*^{B6} mice (27.58 ± 3.24 vs. 11.33 ± 0.86 and 14.40 ± 1.34, p = 0.0022 and p = 0.0043, respectively) (Figure 45 and Table 13). This is also illustrated by the cell-surface density of CD69, as determined by MFIs, on helper T cells (Figure 45A, right panel).

(129xB6.*Sle1*)F1 mice also display an increase in memory helper T cells ($CD62L^{lo}CD44^{hi}CD4^+CD3^+$), a corresponding decrease in naïve helper T cells ($CD62L^{hi}CD44^{lo}CD4^+CD3^+$), and an increase in follicular helper T cells ($ICOS^+CXCR5^+CD4^+CD3^+$). While (129xB6.*Sle1)F1* mice have significantly more memory helper T cells than either 129 or 129.*Sles1*^{B6} mice (65.44 ± 2.71 vs. 36.22 ± 1.92 and 46.83 ± 2.56, p = 0.0022 and p = 0.0043, respectively), 129.*Sles1*^{B6} mice have an intermediate mean percentage of memory helper T cells (p = 0.0173 vs. 129 and p = 0.0043 vs. (129xB6.*Sle1*)F1) (Figure 45B and Table 13). (129xB6.*Sle1)F1* mice also have significantly more follicular helper T cells than either 129 or 129.*Sles1*^{B6} mice (18.95 ± 1.59 vs. 8.25 ± 1.41 and 9.88 ± 0.94, p = 0.0022 and p = 0.0043, respectively) (Figure 45C and Table 13). This is also reflected in the cell-surface densities of ICOS, and PD-1,

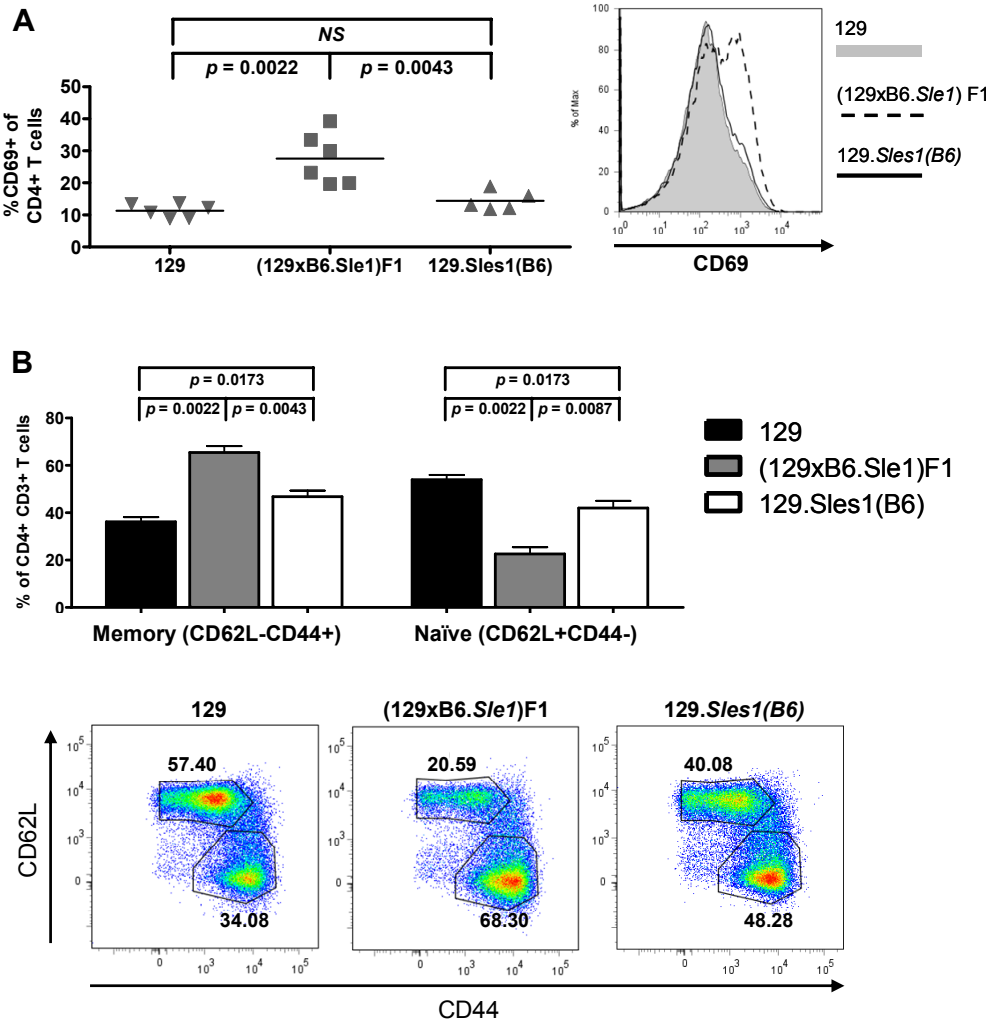

Figure 45A-B. Compared to (129xB6.*Sle1*) F1 12 month old females, *Sles1*^{B6} is not sufficient for 129 mice to have increased T cell activation, but does mediate a partial the increase in memory CD4+ T cells. **A.** Left panel, percentages of CD4+ CD3+ T cells that are CD69+. Right panel, representative CD69 histogram overlay of CD4+ CD3+ T cells. **B.** Top, representative dot plots of memory vs naïve CD4+CD3+ T cells. Bottom panel, percentages of CD4+CD3+ T cells that are memory (left) and naïve (right). n = 5-6 mice per genotype.

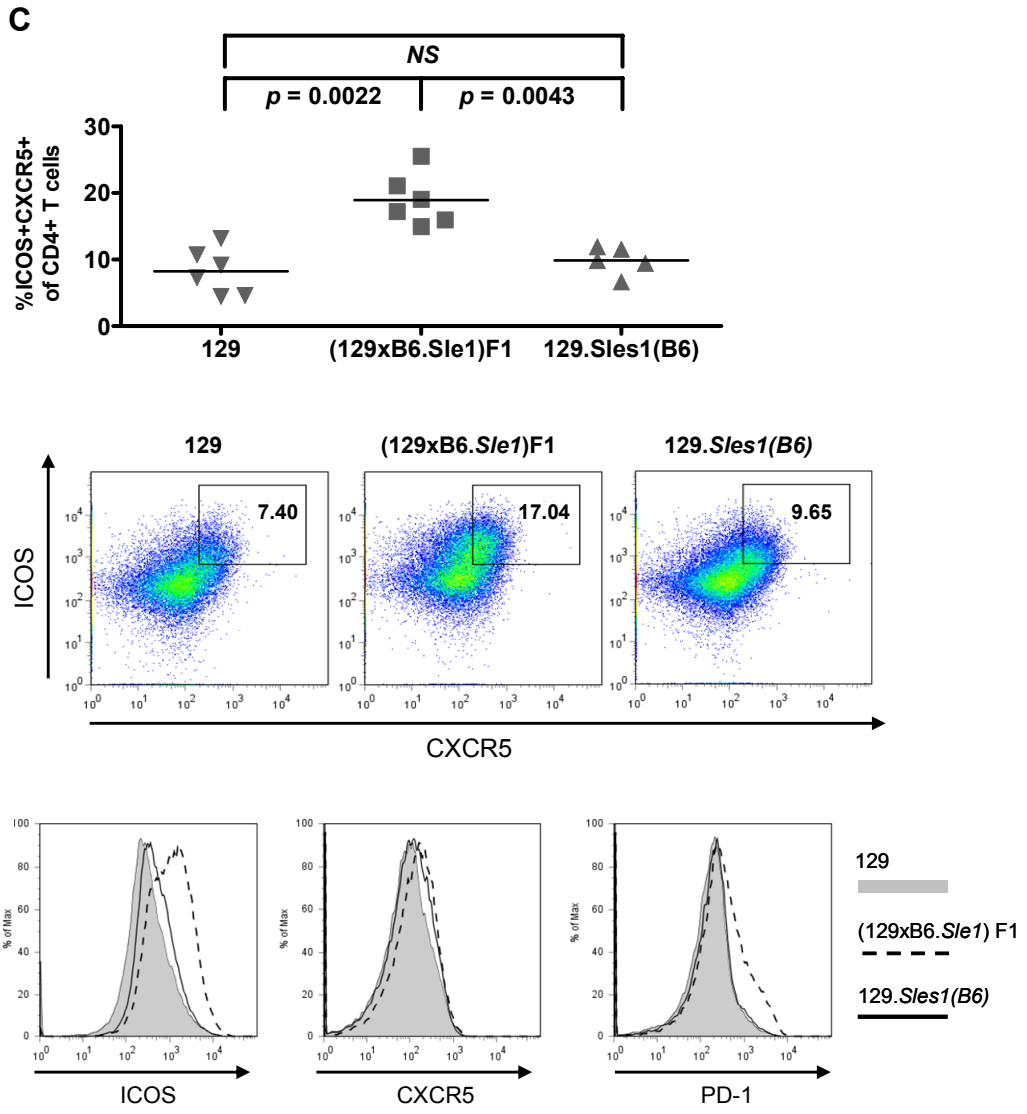

Figure 45C. *Sles1*^{B6} is not sufficient for 12 month female 129 mice to develop an expanded follicular helper T cell population. Top panel, percentages of CD4+ CD3+ T cells are follicular helper T cells (ICOS+CXCR5+). Middle, representative dot plots of follicular helper CD4+CD3+ T cells. Bottom, representative histogram overlay of CD4+ CD3+ T cells showing expression of ICOS (left), CXCR5 (middle) and PD-1 (right). n = 5-6 mice per genotype.

and to a lesser degree in CXCR5, (Figure 45C, bottom panel). Together, this data indicates that *Sles1*^{B6} is sufficient to mediate a moderate increase in memory helper T cells, but not increases in activated or follicular helper T cells. This also supports the presence of weak 129-derived *Sles1* modifier loci.

Monocytosis, defined by a significant increase in the percentage of CD11b^{+} cells, was only detected in 129.*Sles1*^{B6} mice, compared to (129xB6.*Sle1*)F1 mice (9.29 ± 0.80 vs. 6.29 ± 0.72, p = 0.0303) (Figure 46 and Table 13). This was unexpected since monocytosis typically correlates with autoimmunity, and thus should have been present in (129xB6.*Sle1*)F1 mice, rather than 129.*Sles1*^{B6} mice. These results support a non-critical role of the myeloid compartment in the development of ANAs and the existence of 129-derived modifier loci in the *Sles1* interval affecting monocytosis.

In conclusion, *Sles1*^{B6} is not sufficient for 129 mice to develop autoimmunity, but may be sufficient for small changes in sub-phenotypes like splenomegaly, proportion of memory helper T cells, and monocytosis. This is not surprising as the recent analysis of the B6.*Sle1Sles1*^{129} congenic mice demonstrate that *Sles1*^{129} is not suppressive on a B6 background and thus the *Sles1* region probably does not play a major role in the maintenance of tolerance in the 129 mouse strain.

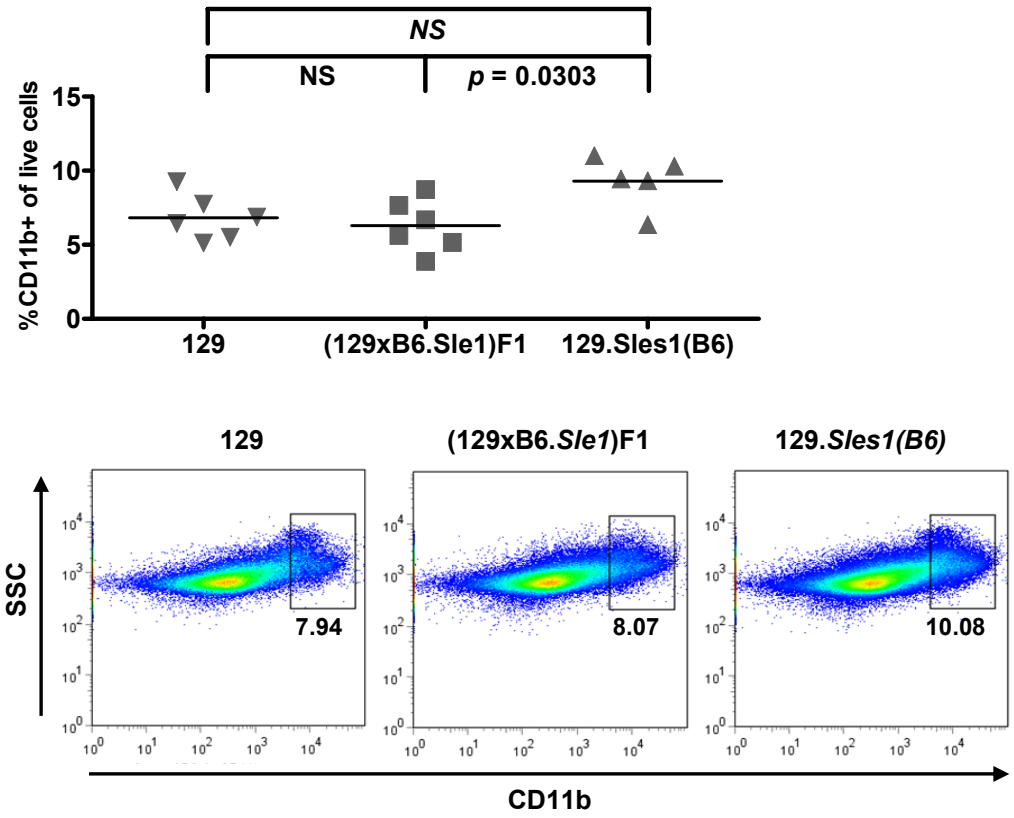

Figure 46. *Sles1*^{B6} is sufficient for 12 month female 129 mice to develop slight monocytosis. Top panel, percentages of CD11b+ cells (of live). Bottom panel, representative dot plots of CD11b+ cells (of live). n = 5-6 mice per genotype.

Table 13. Splenic cell populations in 129, (129xB6.*Sle1*) F1, and 129.*Sles1*^{B6} 12 month females

Population[1]	129 (n=6)	(129xB6.*Sle1*)F1 (n=6)	129.*Sles1*(B6) (n=5)	129 vs (129xB6.*Sle1*) F1	(129xB6.*Sle1*) F1) vs 129.*Sles1(B6)*	129 vs 129.*Sles1(B6)*
B220/CD19+	54.56 ± 1.30	61.78 ± 1.61	50.49 ± 1.48	***P* = 0.0087**	***P* = 0.0043**	NS
Number of cells	53919 ± 1280	61049 ± 1592	49487 ± 1458	***P* = 0.0087**	***P* = 0.0043**	NS
CD86+	10.07 ± 0.74	6.15 ± 0.76	11.37 ± 1.38	***P* = 0.0152**	***P* = 0.0303**	NS
T1 ($CD23^-CD21^-IgM^+$)	8.96 ± 0.88	5.72 ± 0.76	9.54 ± 0.45	***P* = 0.0411**	***P* = 0.0173**	NS
T2 ($CD23^+CD21^{hi}IgM^{hi}$)	1.94 ± 0.36	1.80 ± 0.30	1.07 ± 0.09	NS	***P* = 0.0303**	***P* = 0.0173**
Follicular[2]	40.90 ± 2.49	47.10 ± 2.01	35.29 ± 0.90	NS	***P* = 0.0043**	NS
CD86+	4.42 ± 0.59	2.78 ± 0.25	3.63 ± 0.50	***P* = 0.0152**	NS	NS
MZ ($CD23^-CD21^+IgM^+$)	15.74 ± 0.88	11.28 ± 1.08	16.01 ± 1.16	***P* = 0.0152**	NS	NS
B1a ($CD5^+CD23^-B220^+$)	2.69 ± 0.55	3.27 ± 0.31	1.41 ± 0.10	NS	***P* = 0.0080**	NS
B1b ($CD5^-CD23^-B220^{lo}$)	6.14 ± 0.34	6.39 ± 0.42	6.98 ± 0.21	NS	NS	NS
B2 ($CD5^-CD23^+B220^+$)	22.48 ± 2.01	28.25 ± 2.14	18.75 ± 0.66	NS	***P* = 0.003**	NS
Plasma ($CD19^-CD138^+$)	1.16 ± 0.09	1.62 ± 0.20	1.41 ± 0.113	NS	NS	NS
CD3+	33.40 ± .78	26.01 ± 1.32	29.74 ± 2.50	***P* = 0.0022**	NS	NS
Number of cells	33580 ± 785.8	26149 ± 1326	29901 ± 2516	***P* = 0.0022**	NS	NS
CD4+	64.78 ± 0.94	62.88 ± 1.96	67.58 ± 1.90	NS	NS	NS
CD69+	11.33 ± 0.86	27.58 ± 3.24	14.40 ± 1.34	***P* = 0.0022**	***P* = 0.0043**	NS
CD62L+CD44-	53.99 ± 2.04	22.65 ± 2.81	42.02 ± 3.00	***P* = 0.0022**	***P* = 0.0087**	***P* = 0.0173**
CD62L-CD44+	36.22 ± 1.92	65.44 ± 2.71	46.83 ± 2.56	***P* = 0.0022**	***P* = 0.0043**	***P* = 0.0173**
Follicular Helper[3]	8.25 ± 1.41	18.95 ± 1.59	9.88 ± 0.94	***P* = 0.0022**	***P* = 0.0043**	NS
CD8+	29.34 ± 0.89	29.32 ± 1.92	25.74 ± 1.57	NS	NS	NS
CD69+	7.90 ± 0.31	12.95 ± 0.95	9.98 ± 0.50	***P* = 0.0022**	***P* = 0.0303**	***P* = 0.0043**
CD11b+	6.83 ± 0.62	6.29 ± 0.72	9.29 ± 0.80	NS	***P* = 0.0303**	NS
Number of cells	6607 ± 599.9	6090 ± 694.3	8995 ± 771.9	NS	***P* = 0.0303**	NS
Macrophages[4]	3.76 ± 0.55	2.32 ± 0.37	5.53 ± 0.60	NS	***P* = 0.0087**	NS
CD11c+	4.70 ± 0.32	4.34 ± 0.88	4.76 ± 0.23	NS	NS	NS
NK1.1+	1.08 ± 0.12	2.34 ± 0.35	1.16 ± 0.11	***P* = 0.0260**	***P* = 0.0303**	NS

Table 13. Splenic cell populations in 129, (129xB6.*Sle1*) F1. and 129.*Sles1*^{B6} 12 month females

[1] Ten to eleven color flow cytometry was completed on splenocytes as detailed in Materials and Methods. Shown values represent mean ± SEM. Indented subsets indicate that the listed percentages are of the indicated parent population. All other percentages are of live cells, as determined by forward and side scatter profiles. NS = not significant.

[2] $B220^+CD23^+CD21^+IgM^+$

[3] $CD3^+CD4^+ICOS^+CXCR5^+$

[4] $CD11b^+F4/80^+$

Preliminary analysis of (129xB6.Sle1) F2 mice

We also gauged the impact of either the *Sles1*^{B6} or *Sles1*^{129} allele on a mixed B6.*Sle1* and 129 genomic background by assaying humoral autoimmunity in 9 month old female (129xB6.*Sle1*) F2 mice, grouped by *Sles1* genotype. Although there were no statistically significant differences in ANA level between (129.xB6.*Sle1*) F2 mice homozygous for *Sles1*^{B6}, heterozygous for *Sles1* (B6/129) or homozygous for *Sles1*^{129} (564.5 ± 151.4, 708.6 ± 172.5, and 816.8 ± 181.6, respectively), there were subtle differences in ANA level distribution within each group (Figure 47). This data further supports that the *Sles1* region does not play a major role in the maintenance of tolerance in the 129 mouse strain.

Discussion

Reminiscent of the previous chapter, *Sles1*^{129} is partially suppressive in B6.*Sle1* females, but non-suppressive in B6.*Sle1yaa* males. This suggests that a 129-derived non-MHC Class II gene may be able to modify autoimmunity, but not in the context of heightened innate immune stimulation, such as is provided by *yaa*. The canonical *Sles1* phenotype is fully suppressive, even on a B6.*Sle1yaa* background, so it is unlikely that this undetermined modifier makes a major

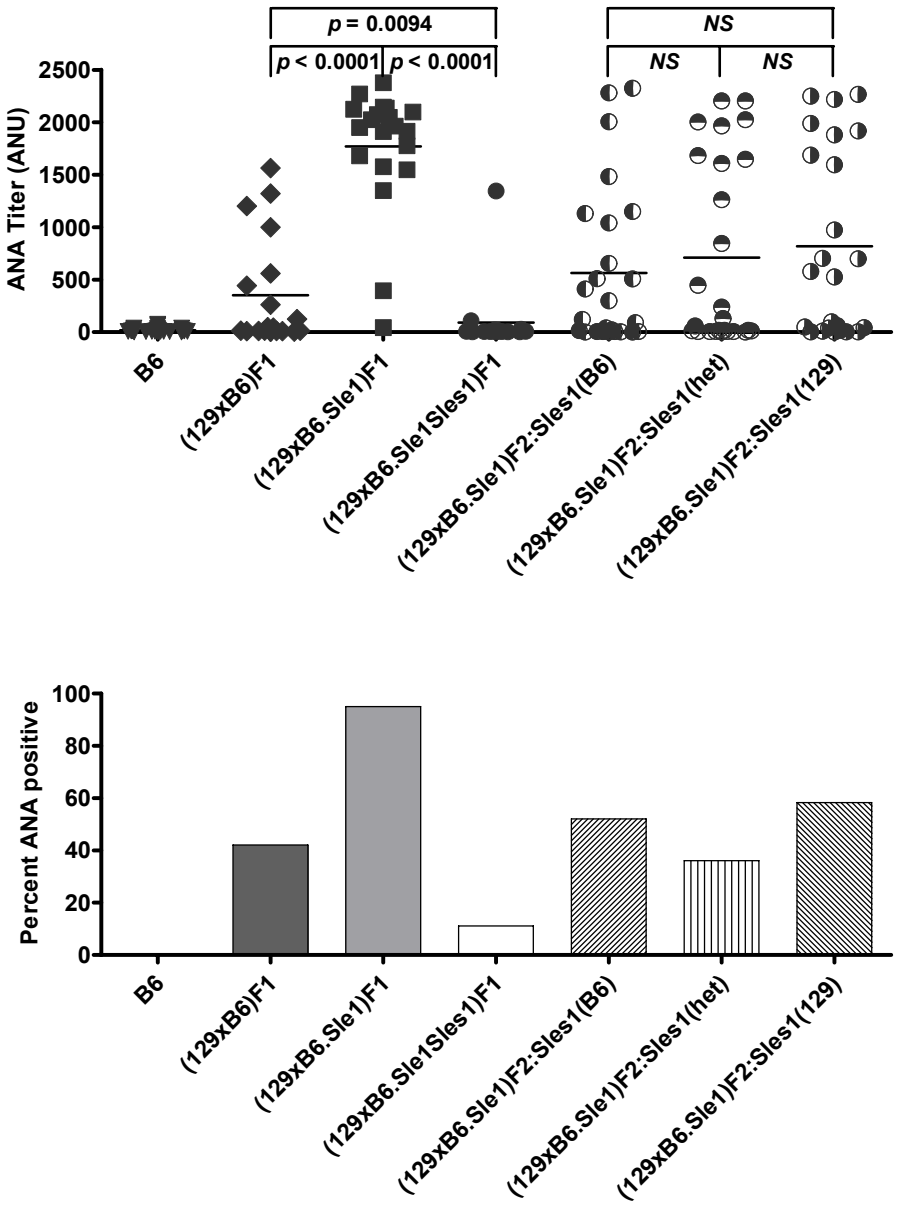

Figure 47. The genotype of *Sles1* has no significant impact on humoral autoimmunity in 9 month old female (129xB6.*Sle1*) F2 mice. Top panel shows IgG ANA levels and bottom panel shows penetrance of ANA positivity. Mice were considered ANA positive when the level was 4 standard deviations above the B6 group mean. n = 17-27 mice per genotype.

contribution to this process, and is thus probably not of significant interest for future *Sles1* studies. However, there are two SNPs which are polymorphic between B6 and 129 in the Mouse Phenome SNP Database (http://phenome.jax.org) which may suggest the identity of this 129-derived modifier locus: rs29534469 in intron 3 of *Btnl2* and rs33661800 in intron 2 of *H2-DMb2*. *Btnl2* has been discussed in an earlier section, but *H2-DMb2* is a specialized MHC Class II-like molecule which facilitates the loading of the peptides onto MHC Class II molecules. Although functional variation in either of these genes could conceivably affect autoimmunity, more experimentation would be needed to determine any effect of these intronic SNPs.

The B6.*Sle1Sles1*^{129} data contradicts the previous 129 complementation data. How is this discrepancy reconciled? First, both the B6 and 129 genomes have been shown to have loci that modify autoimmunity [31, 177-181], so it is likely that there are multiple, epistatic genes in both genomes that affect SLE. This theory is supported by the (129xB6.*Sle1*) F2 data which demonstrates that in the context of a randomly segregated mixed B6 and 129 genome, there is wide range of ANA levels independent of *Sles1* genotype. Secondly, *Sles1*^{129} does have a slight suppressive effect on females, as were used in the complementation experiment. Finally, the fact that *Sles1* heterozygotes

are now operating in a co-dominant fashion, versus previous recessive behavior, suggests the possibility that this inconsistency may have contributed to the misinterpretation of the 129 complementation data. Cumulatively, these factors likely account for the potent suppression of SLE seen in (129xB6.*Sle1Sles1*) F1, but not in (129xB6.*Sle1*) F1, female mice.

The data presented here confirms that both $Sles1^{129}$ and $Sles1^{B6}$ have non-suppressive phenotypes so their shared MHC Class II molecules can no longer be excluded from *Sles1* candidacy. As discussed earlier, the MHC Class II genes are the strongest genome-wide association with SLE [51, 52] which is not surprising considering their critical roles in lymphocyte development and the initiation of immune responses. It is of interest that the B6 haplotype does not generate *H2-Ea* molecules, due to a promoter defect, and $H2\text{-}Eb^{b}$ molecules remain in the cytoplasm as partially glycosylated precursors [159], while the NZW haplotype produce functional $H2\text{-}Ea^{z}$ and $H2\text{-}Eb^{z}$ molecules. However, $H2^{b}$ compensates for this with elevated *H2-Aa* and *H2-Ab* expression [182]. Various studies have inconsistently associated both $H2^{z}$ and $H2^{b}$ genes with autoimmunity susceptibility or resistance [155-158]. Differences in genetic backgrounds and/or congenic strain contamination probably accounts for this diverse results, which have failed to identify a

clear mechanism for either *H2*^{z} or *H2*^{b} in murine lupus. Nonetheless, the *H2* genes, along with *Btnl2*, are now the strongest candidates for the causal gene of *Sles1* (Figure 48).

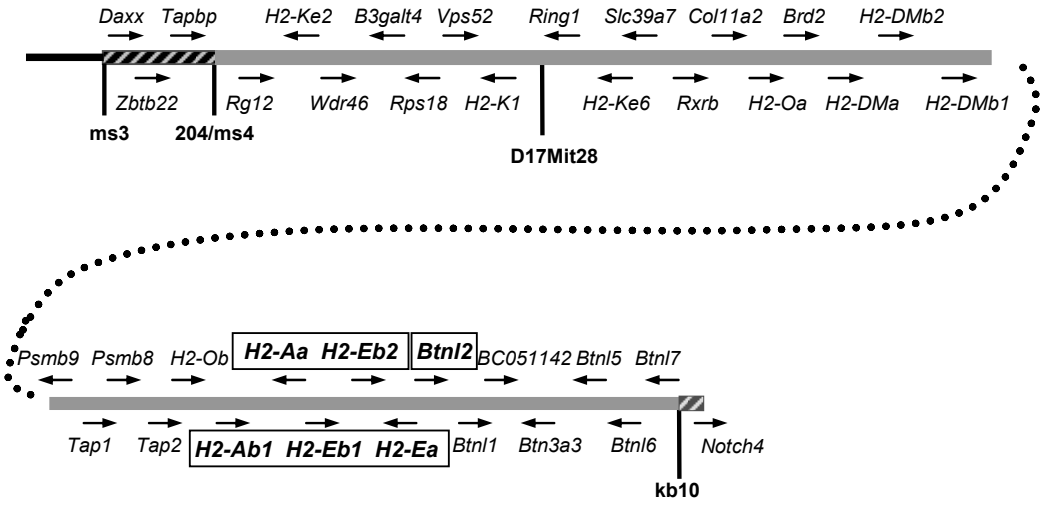

Figure 48. *Sles1* Strongest Candidate Gene Schematic
Detailed map of remaining non-*KB1* portion of *Sles1*$^{(28\text{-}83)}$ interval, showing microsatellite markers (heavy vertical lines) flanking breakpoint regions (hatched thick horizontal lines) and genes (italicized names). The strongest *Sles1* candidate genes are denoted by boxes. Transcription orientation is indicated by arrows. Gene information and marker location were obtained from Ensembl 52 (www.ensembl.org/Mus_musculus/) based on NCBI build m37.

CHAPTER SIX

Further characterization of *Sles1*

Introduction

Despite the many well-documented phenotypic changes between aged B6, B6.*Sle1* and B6.*Sle1Sles1* mice, there is minimal *Sles1* mechanistic data available. It is difficult to distinguish which of these differences result from causal genetics or late-stage autoimmune disease. To increase this body of knowledge, we phenotyped two month old, pre-diseased B6, B6.*Sle1* and B6.*Sle1Sles1* female mice. We also examined the cell-surface expression of MHC Class II molecules and *Ly108*, based on their strong candidacy as the underlying genetic lesions for *Sles1* and *Sle1b* [30, 31], respectively. Additionally, as follicular helper T cells have been associated with autoimmunity [183] and show a striking reduction in B6.*Sle1Sles1* mice, we looked more carefully at this lymphocyte population.

Results

Many components of the *Sles1* phenotype are detectable in two month old female mice

B6.*Sle1*, B6.*Sle1Sles1* and related mice are typically phenotyped between six and twelve months of age, at a relatively late stage of autoimmune disease. At this point, it is very difficult to distinguish between cellular differences caused by a specific genetic locus versus cellular differences that are secondary to increasing disease pathology. To gain a better understanding of possible *Sles1* mechanisms, unperturbed by rampant autoimmunity, two month old B6, B6.*Sle1* and B6.*Sle1Sles1* female mice splenocytes were phenotyped through extensive 10-12 color flow cytometry analysis (for details, see *Materials and Methods*).

Sle1 induces hyper-activation of lymphocytes, as shown by increased expression of the activation marker CD86 on follicular B cells ($B220^+CD23^+CD21^+IgM^+$) and activation marker CD69 on helper T cells ($CD3^+CD4^+$). Although there was no statistically significant increase in the percentage of activated follicular B cells in B6.*Sle1* mice, compared to B6 mice (3.04 ± 0.09 vs. 2.69 ± 0.45), B6.*Sle1Sles1* mice had fewer activated follicular B cells (1.97 ± 0.21, $p = 0.0079$ vs. B6.*Sle1*) (Figure 49 and Table 14). In contrast, there was no evidence of any differences in the percentage of activated helper T cells between any of the groups (Figure 50A and Table 14). These phenotypes are also reflected in the cell-surface density of these activation markers as determined by MFIs (right

panels of Figure 49 and 50A). This suggests that follicular B cells may be involved in early disease processes.

Sle1 also mediates an increase in memory helper T cells ($CD62L^{lo}CD44^{hi}CD4^{+}CD3^{+}$), a corresponding decrease in naïve helper T cells ($CD62L^{hi}CD44^{lo}CD4^{+}CD3^{+}$), and an increase in follicular helper T cells ($ICOS^{+}CXCR5^{+}CD4^{+}CD3^{+}$). B6 and B6.*Sle1Sles1* mice had approximately equivalent percentages of memory helper T cells (14.59 ± 1.20 and 13.00 ± 0.58), while B6.*Sle1* mice had slightly increased percentages of memory helper T cells (19.09 ± 1.20, p = 0.0079 vs. B6.*Sle1Sles1*). B6.*Sle1Sles1* had slightly increased percentages of follicular helper T cells, compared to B6 (3.24 ± 0.12 vs. 3.36 ± 0.25, p = 0.0079) and a non-significant trend towards fewer follicular helper T cell than B6.*Sle1* mice (4.39 ± 0.50). However, the quantitative difference between these groups is small and this is reflected in the representative histogram overlays of ICOS and CXCR5 in which it is difficult to distinguish the individual mice (Figure 50C, right panel). This trend towards a reduction in follicular helper T cells in B6.*Sle1Sles1* mice suggests that these cells may play a role in the initial stages of *Sle1*-mediated autoimmunity. Alternatively, this small difference maybe an early sign of a disparate development of follicular helper T cells over the lifetime of B6.*Sle1* mice, compared to B6.*Sle1Sles1* mice.

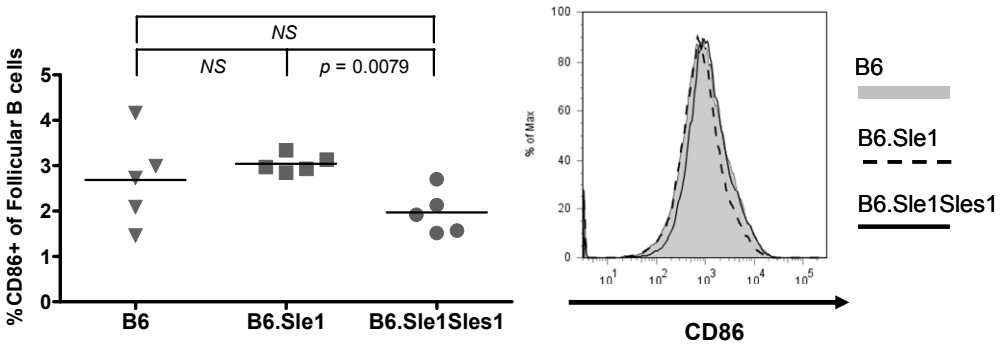

Figure 49. *Sles1*-mediated suppression of follicular B cell activation is evident in two month old females. Left panel, percentages of follicular B cells (define follicular) that are positive for CD86+. Right panel, representative histogram overlay of CD86 MFIs on follicular B cells. n = 5 mice per genotype.

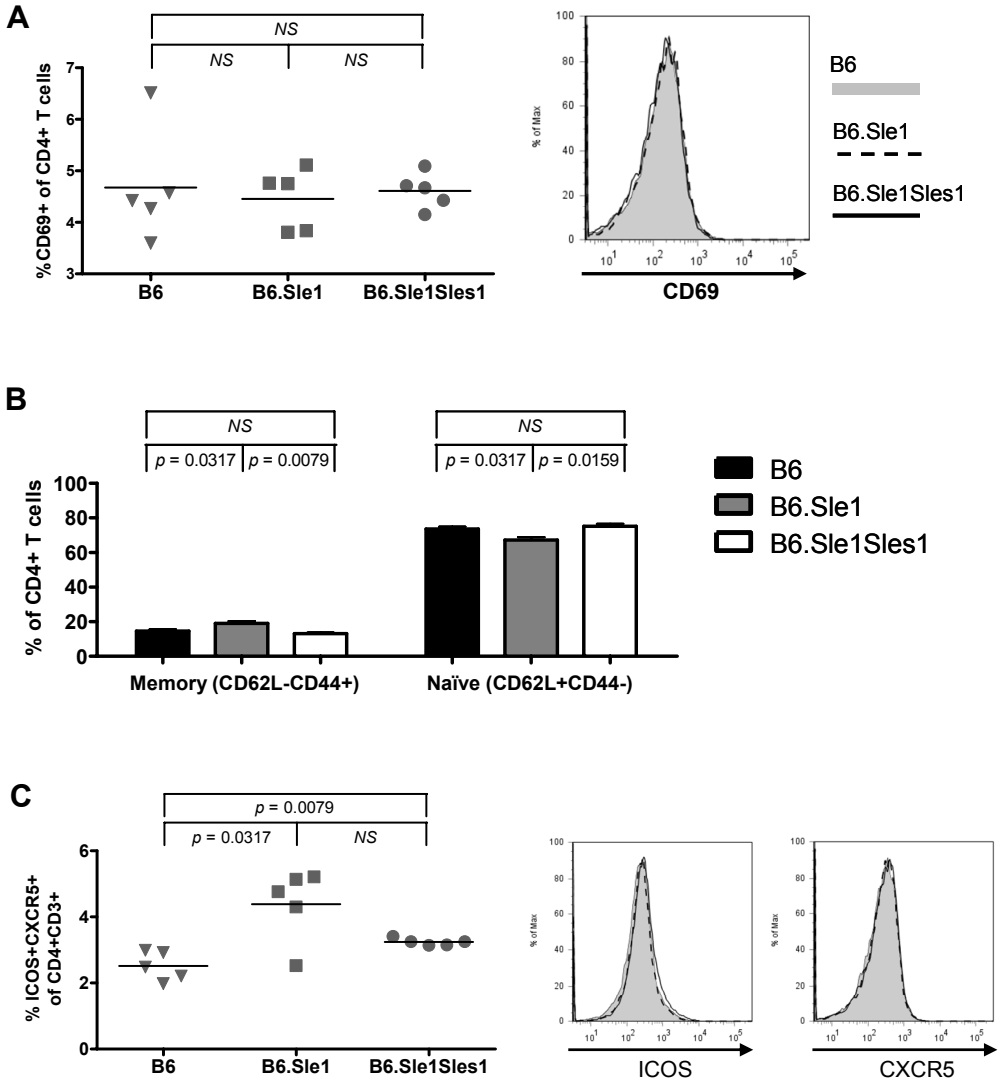

Figure 50. *Sle1*-mediated expansion of memory and follicular, but not activated helper T cells is slightly suppressed in two month B6.*Sle1Sles1* females. **A.** Left panel, percentages of $CD4^+$ $CD3^+$ T cells that are $CD69^+$. Right panel, representative CD69 histogram overlay of $CD4^+$ $CD3^+$ T cells. **B.** Top, percentages of $CD4^+CD3^+$ T cells that are memory (left) and naïve (right). Bottom, representative dot plots of memory vs. naïve $CD4^+CD3^+$ T cells. **C.** Left, percentages of $CD4^+$ $CD3^+$ T cells that are follicular helper T cells ($ICOS^+CXCR5^+$). Right, representative histogram overlay of $CD4^+$ $CD3^+$ T cells showing expression of ICOS (left) and CXCR5 (right). n = 5 mice per genotype.

Table 14. Splenic cell populations in B6, B6.*Sle1*, and B6.*Sle1Sles1* 2 month females

Population[1]	B6 (n=5)	B6.*Sle1* (n=5)	B6.*Sle1Sles1* (n=5)	B6 vs. B6.*Sle1Sles1*	B6 vs. B6.*Sle1*	B6.*Sle1* vs B6.*Sle1Sles1*
B220/CD19+	39.96 ± 1.21	43.95 ± 1.01	48.63 ± 1.36	***P* = 0.0079**	NS	NS
Number of cells	39176 ± 1185	43088 ± 990.9	47673 ± 1325	***P* = 0.0079**	NS	NS
CD86+	4.14 ± 0.66	3.92 ± 0.10	3.29 ± 0.36	NS	NS	NS
T1 ($CD23^-CD21^-IgM^+$)	4.59 ± 0.50	3.32 ± 0.27	3.92 ± 0.13	NS	NS	NS
T2 ($CD23^+CD21^{hi}IgM^{hi}$)	4.89 ± 0.78	3.47 ± 0.62	6.44 ± 0.32	NS	NS	***P* = 0.0079**
Follicular[2]	44.39 ± 1.26	42.43 ± 0.93	42.32 ± 0.92	NS	NS	NS
CD86+	2.69 ± 0.45	3.04 ± 0.09	1.97 ± 0.21	NS	NS	***P* = 0.0079**
MZ ($CD23^-CD21^+IgM^+$)	0.93 ± 0.21	0.40 ± 0.11	1.02 ± 0.12	NS	NS	***P* = 0.0159**
B1a ($CD5^+CD23^-B220^+$)	0.43 ± 0.03	0.54 ± 0.05	0.45 ± 0.04	NS	NS	NS
B1b ($CD5^-CD23^-B220^{lo}$)	3.89 ± 0.31	3.77 ± 0.30	4.02 ± 0.19	NS	NS	NS
B2 ($CD5^-CD23^+B220^+$)	33.63 ± 0.96	37.66 ± 1.06	42.11 ± 1.20	***P* = 0.0079**	NS	***P* = 0.0317**
CD3+	33.42 ± 0.97	30.24 ± 1.21	32.77 ± 1.00	NS	NS	NS
Number of cells	33650 ± 978.6	30444 ± 1213	32989 ± 1004	NS	NS	NS
CD4+	60.27 ± 0.63	56.18 ± 0.54	59.46 ± 0.65	NS	***P* = 0.0079**	***P* = 0.0079**
CD69+	4.67 ± 0.49	4.45 ± 0.26	4.61 ± 0.16	NS	NS	NS
CD62L+CD44-	73.63 ± 1.32	67.27 ± 1.64	75.18 ± 1.39	NS	***P* = 0.0317**	***P* = 0.0159**
CD62L-CD44+	14.59 ± 0.89	19.09 ± 1.20	13.00 ± 0.58	NS	***P* = 0.0317**	***P* = 0.0079**
Follicular Helper[3]	2.52 ± 0.20	4.39 ± 0.50	3.24 ± 0.05	***P* = 0.0079**	***P* = 0.0317**	NS
CD8+	30.63 ± 1.05	33.07 ± 0.71	31.15 ± 0.50	NS	NS	NS
CD69+	3.36 ± 0.25	3.33 ± 0.20	3.96 ± 0.12	NS	NS	***P* = 0.0317**
CD11b+	12.72 ± 0.75	14.68 ± 0.49	9.33 ± 0.60	***P* = 0.0159**	NS	***P* = 0.0079**
Number of cells	12991 ± 771.7	14986 ± 500.9	9514 ± 618.1	***P* = 0.0159**	NS	***P* = 0.0079**
Neutrophils[4]	3.31 ± 0.40	4.35 ± 0.34	1.84 ± 0.24	***P* = 0.0317**	NS	***P* = 0.0079**
Inflammatory MO[5]	1.68 ± 0.19	1.93 ± 0.25	1.27 ± 0.14	NS	NS	NS
Resident MO[6]	0.57 ± 0.07	0.71 ± 0.08	0.37 ± 0.02	***P* = 0.0317**	NS	***P* = 0.0079**
Macrophages[7]	2.15 ± 0.21	2.25 ± 0.08	1.74 ± 0.15	NS	NS	***P* = 0.0362**
CD11c+	4.68 ± 0.27	.95 ± 0.33	4.28 ± 0.17	NS	***P* = 0.0317**	***P* = 0.0159**

Table 14. Splenic cell populations in B6, B6.*Sle1*, and B6.*Sle1Sles1* 2 month old females

[1] Ten to eleven color flow cytometry was completed on splenocytes as detailed in Materials and Methods. Shown values represent mean ± SEM. Indented subsets indicate that the listed percentages are of the indicated parent population. All other percentages are of live cells, as determined by forward and side scatter profiles. NS = not significant.

[2] $B220^{+}CD23^{+}CD21^{+}IgM^{+}$

[3] $CD3^{+}CD4^{+}ICOS^{+}CXCR5^{+}$

[4] $CD11b^{+}Gr1^{+}SSC^{hi}$

[5] $CD11b^{+}Gr1^{+}Neu7/4^{+}SSC^{lo}$

[6] $CD11b^{+}Gr1^{-}Neu7/4^{+}$

[7] $CD11b^{+}F4/80^{+}$

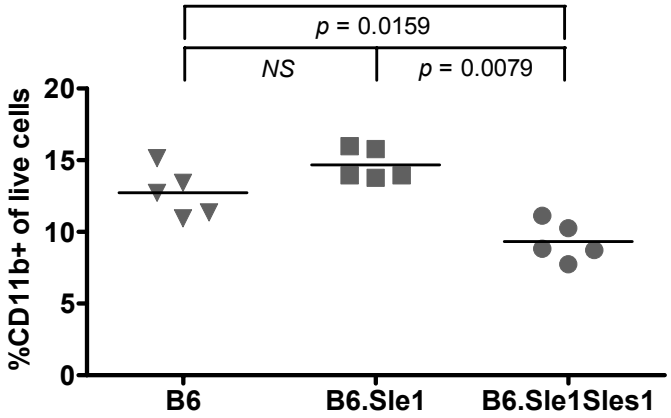

Figure 51. *Sles1*-mediated reduction of monocytes is significant in two month old females. n = 5 mice per genotype.

At two months of age, the mild expansion of the myeloid compartment observed in B6.*Sle1* mice was prevented in B6.*Sle1Sles1* mice. Moreover, there was a significant reduction in the percentage of $CD11b^+$ splenocytes between these two groups (14.68 ± 0.49 vs. 9.33 ± 0.60 for B6.*Sle1* and B6.*Sle1Sles1*, respectively, $p = 0.0079$.

Overall, 13 splenic cell parameters, representing the B, T and myeloid compartments had quantitative differences between B6.*Sle1* and B6.*Sle1Sles1* female mice at two months of age. Among these disparities, *Sles1* suppresses *Sle1*-mediated follicular B cell, but not overall B or helper T cell, hyper-activation and displays a non-significant trend towards a reduction in follicular helper T cells.

The ability of *Sles1 to* reduce the *Sle1*-mediated increase of peripheral lymphocytes *Ly108* expression in aged mice correlates with activation markers

Recent studies have strongly implicated *Ly108* as the causative gene for the autoimmune susceptibility loci [30, 31] and demonstrated that the SLE susceptibility *Sle1b* allele results in higher expression of an alternate isoform of *Ly108* on lymphocytes [31, 96]. To investigate whether *Sles1* alters this causal phenotype of *Sle1b*, we looked at the cell-

surface expression of Ly108, as determined by MFIs, on splenic B and T cells via flow cytometry analysis.

In 12 month old female mice, there was a significant reduction in overall cell surface *Ly108* in B6.*Sle1Sles1* mice, compared to B6.*Sle1* mice, in $CD4^+$ T cells (8964 ± 424.4 vs. 19574 ± 561.3, $p = 0.0238$), but not $B220^+$ B cells (5969 ± 101.8 vs. 6164 ± 79.15). This down-regulation of Ly108 on B6.*Sle1Sles1* T cells correlated with a lower density of the activation marker CD69 ($p = 0.0022$ vs. B6.*Sle1*, 342.8 ± 23.35 vs. 7849 ± 11.48). There was a concomitant decrease in cell surface CD86 on B6.*Sle1Sles1* B cells ($p = 0.0087$ vs. B6.*Sle1*, 2098 ± 109.4 vs. 1667 ± 66.98) (Figure 52A). A comparable pattern was seen in six month old male mice *yaa* mice. However, in this male group, *Sles1*-induced down-regulation of cell surface *Ly108* correlated with decreased cell-surface activation markers in both B and T lymphocytes (Figure 52B).

A recent report has also described *Sle1*-mediated *Ly108* expression dysregulation in the thymus affects thymocyte selection [106] Therefore, the overall *Ly108* cell surface expression was also assayed in pre-diseased two month old $CD4^+CD3^+$ thymocytes from B6, B6.*Sle1*, and B6.*Sle1Sles1* females. The densities of cell surface *Ly108*, and a related SLAM family member, *Ly9*, were indistinguishable between B6.*Sle1* and

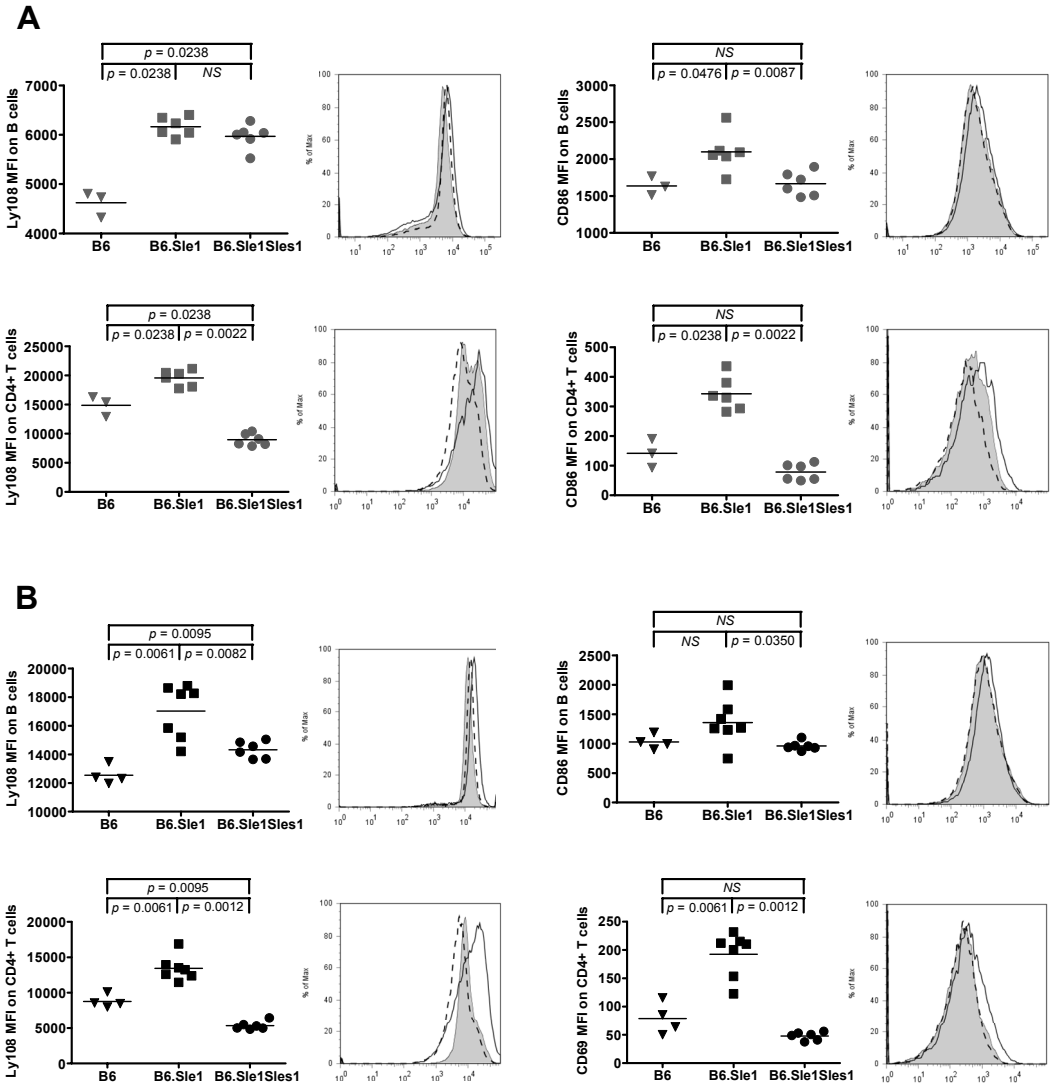

Figure 52. *Sles1* affects splenic B and CD4+ T cell expression of Ly108 in late-stage SLE, but correlates with activation. It is not known if *Sles1* affects Ly108 expression in peripheral lymphoid tissues during early phases of disease. Shaded histogram = B6, dotted line = B6.*Sle1*, and solid line = B6.*Sle1Sles1*. Top panel, expression of Ly108 (left) and CD86 (right) on B cells. Bottom panel, expression of Ly108 (left) and CD69 (right) on $CD4^+$ T cells. **A.** 12 month old females. **B.** 6 month old males with *yaa.* n = 4-8 mice per genotype.

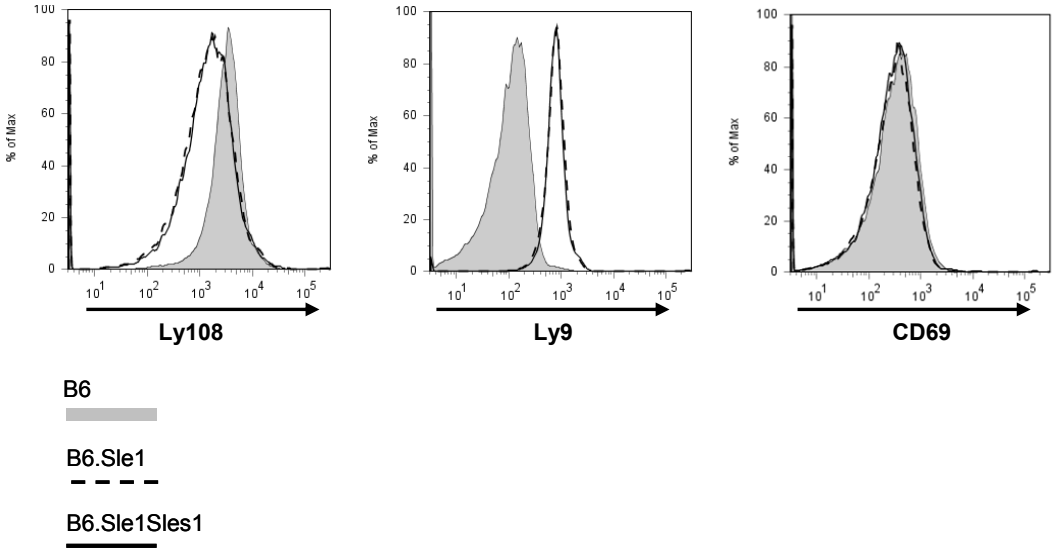

Figure 53. *Sles1* has no effect on *Sle1*-mediated dysregulation of Ly108 and Ly9 expression on CD4$^+$ T cells in the thymus of 2 month old female mice. n = 5 mice per genotype.

B6.*Sle1Sles1* mice. However, the B6 levels of overall *Ly10*8 were higher than in either B6.*Sle1* or B6.*Sle1Sles1*, while the reverse was true for *Ly9* (Figure 53).

Together, this data suggests that the *Sles1*-mediated down-regulation of *Ly108* is likely a secondary consequence of the *Sles1*-mediated suppression of lymphocyte activation occurring in the periphery after thymic selection. It is intriguing to note though that the dysregulation of *Ly108* cell surface levels by *Sle1* has opposing effects in thymocytes and peripheral lymphocytes. More experiments are needed to confirm this phenomenon, but if true, this could result in uncoupled signaling thresholds for central and peripheral tolerance. However, *Sle1b* has been shown to mediate differences in *Ly108* isoform usage which would not be detected by overall cell surface *Ly108* expression data.

Sles1 **mediates a B cell-specific down-regulation of cell surface MHC Class II**

As discussed earlier, the lack of a suppressive phenotype of *Sles1*^{129} does not support the exclusion of the *H2* gene family from consideration as a *Sles1* candidate gene. Therefore, flow cytometry was used to determine if *Sles1* affects the cell surface expression of MHC

Class II (MHCII) molecules on various splenic sub-populations of leukocytes.

In 12 month old female mice, there was no significant difference in the amount of cell-surface MHCII, as determined by MFIs, between B6, B6.*Sle1*, and B6.*Sle1Sles1* splenic dendritic cells ($CD11c^+$) (4870 ± 394.2 vs. 5071 ± 299.2 vs. 5241 ± 438.1, respectively). Nor was there a difference in MHCII expression on splenic macrophages ($F4/80^+CD11b^+$) between B6.*Sle1* and B6.*Sle1Sles1* mice (6407 ± 395.0 vs. 6980 ± 898.4). However, there was a small increase in the level of MHCII on macrophages in B6 mice (8684 ± 334.8, $p = 0.0238$ vs. B6.*Sle1*). However, B cells ($B220^+$) from B6.*Sle1Sles1* mice only displayed approximately one-fifth the level of MHC II molecules as compared with B6.*Sle1* mice (5491 ± 214.1 vs. 147056 ± 538.7, $p = 0.0022$) or B6 mice (8207 ± 641.4, $p = 0.0238$). B6.*Sle1Sles1* B cells displayed about two-thirds the level of CD86, an activation marker, compared with B6.*Sle1* B cells (1203 ± 51.89 vs. 1833 ± 67.45, $p = 0.0022$), but the levels of CD86 were similar to the B6 counterparts (1265 ± 54.41). These phenotypes are also reflected in representative histogram overlays of MHCII and CD86 on B cells, dendritic cells and macrophages (Figure 54A). The dramatic reduction of MHCII on B6.*Sle1Sles1* B cells only partially correlated with

activation, suggesting that this dysregulation was not merely a disease consequence and may reflect a causal *Sles1* phenotype.

To better distinguish between those possibilities, MHCII and CD86 cell surface levels were also determined in two month old splenocytes. Again, there were no significant differences in the level of MHCII on dendritic cells between B6, B6.*Sle1* and B6.*Sle1Sles1* mice (5744 ± 338.8 vs. 4819 ± 338.8 vs. 5533 ± 579.7).

In macrophages, B6.*Sle1* mice had slightly lower cell surface expression of MHCII, compared to B6 and B6.*Sle1Sles1* mice, although this difference was only statistically significant compared to B6 mice (3115 ± 442.7 vs. 4999 ± 609.4 and 4503 ± 594.0; B6 vs B6.*Sle1*, $p = 0.0317$). In B cells, B6.*Sle1Sles1* also had decreased levels of MHCII than either B6 or B6.*Sle1* (6366 ± 71.78 vs. 8084 ± 467.8 and 8859 ± 333.5, $p = 0.0079$ vs. B6 and $p = 0.0079$ vs. B6.*Sle1*). There was a non-significant slight increase in CD86 levels on B6.*Sle1* B cells, compared to B6 and B6.*Sle1Sles1* mice which were very similar (1430 ± 32.67 vs. 1222 ± 75.29 and 1251 ± 52.27). Therefore, at both time points, there was a B-cell specific down-regulation of MHCII in B6.*Sle1Sles1* mice compared to B6 mice, yet no difference in B cell CD86 expression. This suggests that polymorphisms in the NZW allele of *Sles1* result in allele-specific and tissue-specific regulation of MHCII expression.

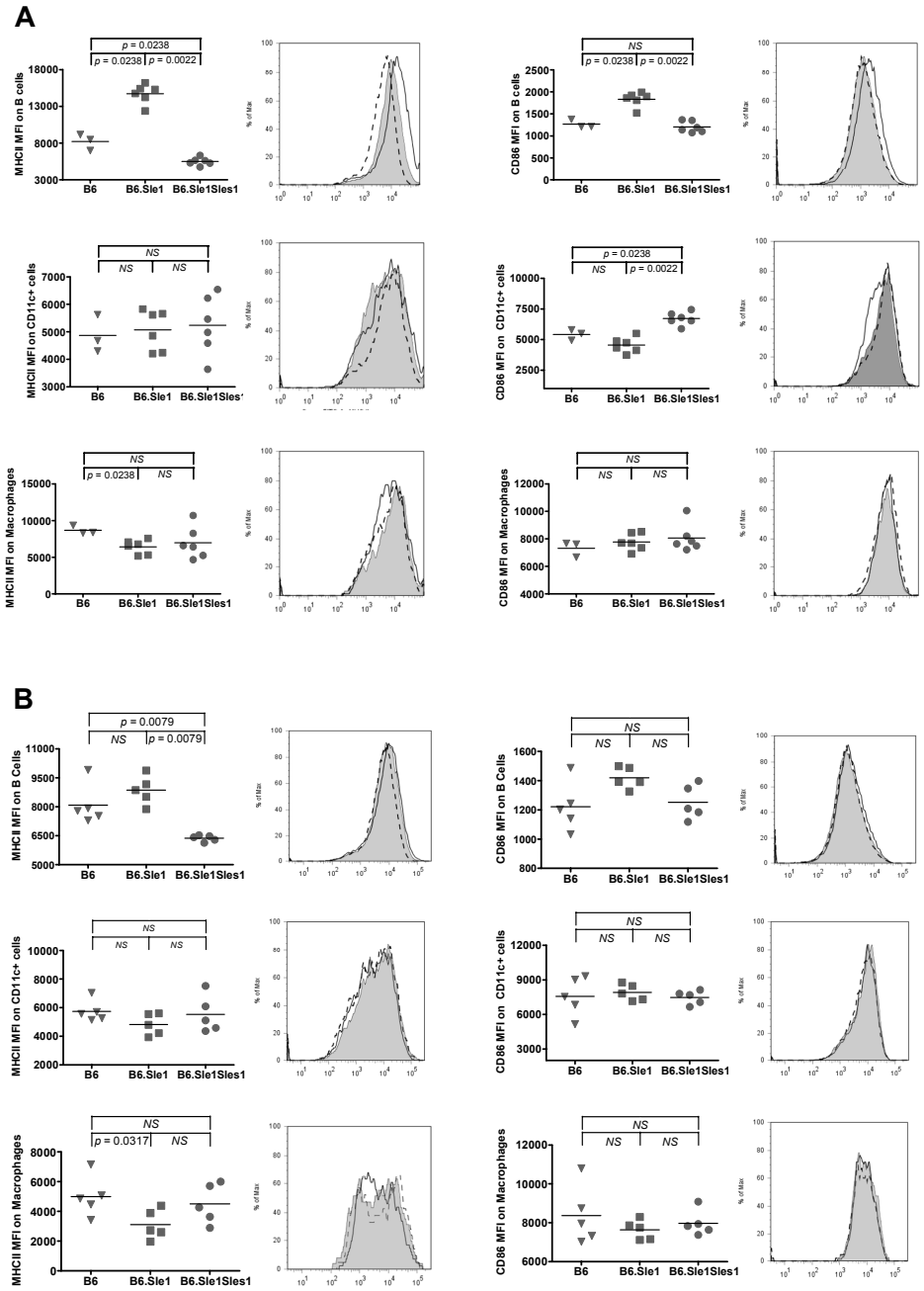

Figure 54. *Sles1* mediates a B cell-specific down-regulation of cell surface MHC II. Expression of MHCII (left) and CD86 (right) on splenic B cells (top), $CD11c^{+}$ dendritic cells (middle) and $F4/80^{+}CD11b^{+}$ macrophages (bottom). **A.** 12 month old females. **B.** 2 month old females. n = 5 mice per genotype.

The anti-MHCII clone (2G9) used recognizes epitopes on both I-A and I-E molecules on many, but not all, haplotypes. Our data demonstrating indistinguishable cell surface levels of MHCII on dendritic cells and macrophages from B6.*Sle1* and B6.*Sle1Sles1* mice suggests that 2G9 recognizes both $H2^b$ and $H2^z$ haplotypes equally (Figure 54). We also confirmed that 2G9 had a similar binding pattern for both B6.*Sle1* and B6.*Sle1Sles1* mice at multiple dilutions (data not shown). This data is consistent with equivalent binding by 2G9 of the both *b* and *z* haplotypes but more experiments are needed to demonstrate this clearly.

Sles1 mediates a contraction in the resident subpopulation of follicular helper T cells

Follicular helper T (T_{FH}) cells have a crucial role in the providing germinal center T-cell help for B cells (reviewed in [184]) and display a unique transcriptional profile including elevated ICOS, CXCR5, PD-1 [168, 169]. An expanded T_{FH} population was observed in *sanroque* murine model of autoimmunity caused by an ENU-induced polymorphism of a RING-type ubiquitin-ligase which normally degrades ICOS messenger RNA [185, 186]. Disease in this model was also shown to be dependent on germinal center formation and T_{FH} cells [183]. Finally, the adoptive

transfer of *sanroque* T_{FH} cells is sufficient to for the development of spontaneous germinal centers in B6 mice [183].

A marked reduction in the number of T_{FH}, as well as the down-regulation of ICOS, PD-1, and to a lesser extent, CXCR5, has also been observed in B6.*Sle1Sles1* mice earlier ([19] and within this report, Figures 8C, 13C, 34C, and 39C and 50C, and Tables 5-6, 11-12, and 14). A recent study by Fazilleau and colleagues has described that the strength of the TCR antigen receptor binding dictates the development of effector T_{FH} into three distinct functional subsets [187]. "Lymphoid" effector T_{FH} cells express CCR7, a homing molecule to the outer T cell zones of peripheral lymphoid tissues, as well as CD62L and low levels of CXCR5. "Emigrant" effector cells have down-regulated CCR7 and CD62L. Only the T_{FH} with the strongest MHC-TCR interaction developed into the "resident" T_{FH} effector cells, characterized within the T_{FH} compartment by significantly higher expression of PD-1, IL-4 and IL-21 and unique expression CD69, OX40 and Bcl-6 [187]. As MHCII expression differences between B6.*Sle1* and B6.*Sle1Sles1* mice (Figure 54) could contribute affect the strength of TCR-BCR interactions, we looked more carefully at the T_{FH} cellular compartment through flow cytometry analysis of splenocytes from our mouse models.

In both 12 month old and pre-diseased 2 month old females, there was no difference in the percentage of T_{FH} cells that displayed the "lymphoid" phenotype ($CD62L^{+}CXCR5^{lo}ICOS^{+}CD4^{+}CD3^{+}$) between B6, B6.*Sle1* and B6.*Sle1Sles1* (Figure 55A and C). However, 6 month old male B6.*Sle1yaa* mice had dramatically fewer "lymphoid" effector T_{FH} cells than B6.*Sle1Sles1yaa* mice (3.46 ± 1.59 vs. 26 ± 4.11, $p = 0.0012$ vs. B6.*Sle1Sles1*). Additionally, B6.*yaa* mice had an intermediate phenotype (19.75 ± 4.93, $p = 0.0061$ vs B6.*Sle1yaa* and $p = 0.0381$ vs. B6.*Sle1Sles1yaa*) (Figure 55B). A similar pattern was seen in the percentages of "emigrant" effector T_{FH} cells ($CD62L^{lo+}CXCR5^{lo}ICOS^{+}CD4^{+}CD3^{+}$) in which B6.*Sle1Sles1* mice had increased percentages of this subset, compared to B6.*Sle1* in 12 month females (Figure 55A), 2 month females (Figure 55C) and 6 month males also carrying *yaa* (Figure 55B).

However, the opposite effect was seen in the "resident" T_{FH} cell compartment ($CD62L^{lo}CXCR5^{hi}ICOS^{+}CD4^{+}CD3^{+}$). In 12 month old female mice, there was an approximately 3-fold reduction in the percentage of "resident" T_{FH} cells in B6.*Sle1Sles1* mice, compared to B6 and B6.*Sle1* mice (14.85 ± 4.24 vs. 41.70 ± 2.45 and 50.80 ± 1.33, $p = 0.0200$ vs B6 and $p = 0.0007$ vs. B6.*Sle1*) (Figure 55A).

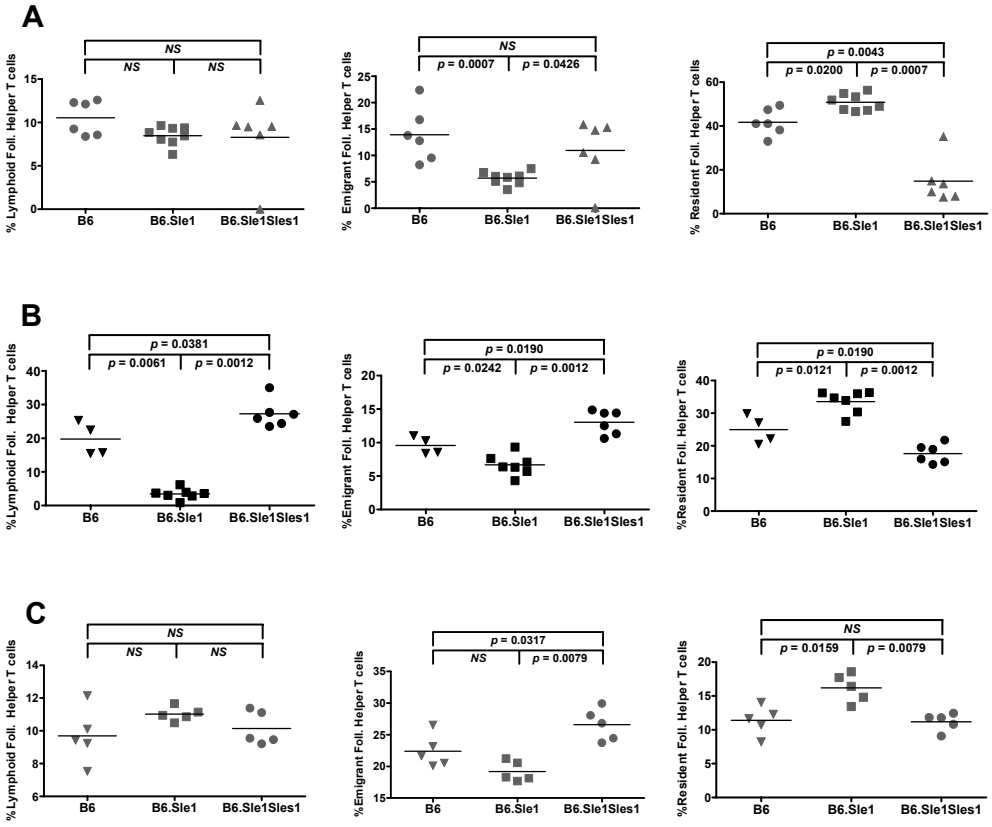

Figure 55. *Sles1* mediates changes in sub-populations of follicular helper T cells. Percentages of follicular helper T cells that are lymphoid (left, $CD62L^{+}CXCR5^{lo}ICOS^{+}$), emigrant (middle, $CD62L^{lo}CXCR5^{lo}ICOS^{+}$) and resident (right, $CD62L^{lo}CXCR5^{hi}ICOS^{+}$). **A.** 12 month old females. **B.** 6 month old males with *yaa*. **C.** 2 month old females. n = 5 mice per genotype.

In 6 month old males, a smaller yet significant decrease in this compartment was also observed in B6.*Sle1Sles1yaa* mice, compared to B6.*yaa* and B6.*Sle1ya*a mice (17.60 ± 1.19 vs. 24.94 ± 2.17 and 33.57 ± 1.28, p = 0.0121 vs B6.*yaa* and p = 0.0012 vs. B6.*Sle1ya*a) (Figure 55B). Finally, in 2 month old females, B6.*Sle1* mice had elevated percentages of "resident" T_{FH} cells, compared to B6 and B6.*Sle1Sles1* mice (16.20 ± 0.93 vs. 11.39 ± 0.96 and 11.18 ± 0.56, p = 0.0159 vs B6 and p = 0.0079 vs. B6.*Sle1Sles1*). In contrast to the older mice, there were no significant differences in this compartment between B6 and B6.*Sle1Sles1* two month old mice.

Overall, these results are consistent with a scenario of B6.*Sle1* T_{FH} cells having stronger engagement of the TCR, driving the development of "resident" T_{FH} cells at the expense of "lymphoid" and "emigrant" cells, while *Sles1* is sufficient to correct this phenotype, even in pre-diseased young mice.

Discussion

In young B6.*Sle1Sles1* female mice, there was evidence of fewer activated follicular B cells and memory helper T cells, but no evidence of a reduction in overall lymphocyte activation, compared to B6.*Sle1* mice. There was also a slight trend towards decreased percentages of T_{FH} cells

and a significant reduction in the "resident" effector T_{FH} cell subset in the B6.*Sle1Sles1* females. This is conceivably consistent with *Sles1* functioning by altering B cell-T cell interactions in the germinal centers of the spleen. However, it is also possible that the phenotype of *Sles1* is mediated by one of the other dysregulated splenic populations, such as the surprising and unexplained increase in monocytes in B6.*Sle1Sles1* mice, when compared to B6.*Sle1* mice. Overall, despite limited disease at two months, it is still difficult to distinguish causal and secondary phenotypes. However, by comparing the expression of *Ly108* and activation markers on B cells and helper T cells in both aged and young mice, it does seem likely that the *Sles1*-mediated down-regulation of *Ly108* is a resulting consequence of the *Sles1*-mediated suppression of lymphocyte activation.

As the *H2* genes are among remarkably polymorphic, it is not surprising that that variability also extends to the promoter regions of these genes [188-190]. The control of MHCII expression is also extremely complex with numerous regulatory motifs identified (reviewed in [188, 190]), even in locations relatively far upstream [191, 192]. Polymorphisms in the $H2^b$ haplotype result in no cell surface expression of *H2-Ea* or *H2-Eb* [159], but increased expression of *H2-Aa*, particularly in stimulated B cells, and increased expression of *H2-Ab* in macrophages [182]. The

latter effect is especially interesting because it is mediated by a single SNP [182]. Little is known about specific expression of the *H2*^{z} haplotype, other than it produces functional *H2-Ea* and *H2-Eb* molecules, but an allele-specific and tissue-specific regulation of *H2*^{z} would not be unusual for this gene family.

Attempts have been made to determine functional consequences of these allele-specific H2 expression differences. The *H2*^{b} haplotype has historically been associated with a suppressive effect in several models of autoimmunity. However, many of these studies have compared haplotypes through the use of different strains and/or F1 hybrids so it is likely that genomic background gene-gene interactions and/or other nearby immunomodulatory genes may have contributed to the experimental outcome [193-196]. Other studies using *H2-Ea* transgenic mice have demonstrated a protective effect of *H2-Ea* molecules, which are not present in B6 mice, in murine lupus [197-200]. Martinez-Soria and collegues have recently demonstrated that in a BSXB model of SLE this phenomenon is a due to peptides derived from the over-expression of transgenic *H2-Ea* competing with pathogenic or self peptides for binding to I-A molecules [201]. In a different approach, Zhang and colleagues used a spontaneous intra-*H2* recombination to show that *H2-Ea* prevented disease in dose- and *H2-A*-haplotype-dependent manner. Further, the

haplotype of the *H2-A* molecules, but not the *H2-Ea* molecule, influenced the potential of dendritic cells to present self-antigens [155]. It should be noted that all these recombinant intervals extended significantly in both directions, which considering the density of immuno-modulating genes in this region introduces the possibility of other gene-gene interactions contributing to these results. Together, this data suggests that the *H2-A* genes are more likely than *H2-Ea* gene to be responsible for any *b*- and *z*-haplotype specific effects on autoimmunity.

There was repeated evidence of a *Sles1*-mediated reduction of both overall T_{FH} cells and the "resident" T_{FH} subset. This subset has recently been shown to differentiate from the T cells with the strongest MHC-TCR interaction and is characterized by significantly higher expression of PD-1, IL-4 and IL-21 and unique expression CD69, OX40 and Bcl-6 [187]. This could explain the dramatic down-regulation of cell surface PD-1 in B6.*Sle1Sles1* mice, compared to B6.*Sle1* mice, as seen in representative histogram overlays of CD4+ T cells (see Figures 8C, 13C, 34C and 39C). Overall, these results are consistent with a scenario of B6.*Sle1* T_{FH} cells having stronger engagement of the TCR, driving the development of "resident" T_{FH} cells at the expense of "lymphoid" and "emigrant" cells. *Sles1* is sufficient to correct this phenotype, even in pre-diseased young mice. This could conceivably be a consequence of allele-

specific MHCII expression differences, although there are numerous molecules which also influence MHC-TCR interactions.

CHAPTER SEVEN

Discussion

The identification of the causative gene of *Sles1* has been and continues to be a daunting task, particularly due to the high density of immuno-modulatory genes within the *Sles1* interval and numerous phenotypic differences between B6.*Sle1* and B6.*Sle1Sles1* mice. Nonetheless, careful review of the data presented in this manuscript provides some insight into the best candidate genes and their possible mechanism of suppression.

A series of mouse strains have been constructed with a variety of suppressive and non-suppressive variants of *Sles1* on the B6.Sle1 and B6.*Sle1yaa* backgrounds. A summary of the phenotypic data for each of these strains is shown in Table 15 and reveals several interesting trends, despite slight variations between individual strains. First, the partial suppression of autoimmunity in B6.*Sle1KB1* and B6.*Sle1Sles1*^{129} females provides clear evidence of multiple epistatic genes within the *Sles1* interval. Secondly, the amplifying effect of *yaa* is sufficient to abrogate any potential suppressive loci in the B6.*Sle1KB1* and B6.*Sle1Sles1*^{129} mice which is another layer of epistatic interaction. Finally, both *Sles1* heterozygotes display an interesting phenotype on the B6.*Sle1yaa*

Table 15. Summary of component phenotypes of experimental mouse strains.

Genotype	ANAs	Splenomegaly	Foll. B cell Activation	CD4+ T cell Activation	Memory T cell Expansion	Foll. T cell Expansion	Monocytosis	GN
Females								
B6	-	-	-	+	+	+	-	n/a
B6.*Sle1*	+++	+++	+++	+++	+++	+++	+++	n/a
B6.*Sle1KB1*	+++	++	+++	+++	+++	++	++	n/a
B6.*Sle1Sles1*^{129}	+++	++	-	++	++	++	+	n/a
B6.*Sle1Sles1*^{het}	+	++	+	+	+	+	+	n/a
B6.*Sle1Sles1*	-	-	-	-	-	-	+	n/a
B6.*Sle1(81-22)*^{het}	+	-	-	+	+	+	+	n/a
B6.*Sle1(81-22)*	-	-	-	-	-	-	+	n/a
Males								
B6.*yaa*	+	+	+	+	+	+	-	-
B6.*Sle1yaa*	+++	+++	++	+++	+++	+++	+++	+++
B6.*Sle1KB1yaa*	++++	+++	++	+++	++++	+++	++	+++
B6.*Sle1Sles1*^{129}*yaa*	+++	++	++	+++	+++	+++	+++	+++
B6.*Sle1Sles1*^{het}*yaa*	+	+++	+++	+++	++	++	+	+
B6.*Sle1Sles1yaa*	-	-	-	-	-	-	-	-
B6.*Sle1(81-22)*^{het}*yaa*	+	+++	+++	+++	++	++	+	++
B6.*Sle1(81-22)yaa*	-	-	-	-	-	-	-	-

background. Here, both B6.*Sle1Sles1*^{het}*yaa* and B6.*Sle1(81-22)*^{het}*yaa* have very low ANA levels and monocytosis and intermediate expansions of the memory and follicular helper T cell compartments, yet severe splenomegaly and lymphocyte hyper-activation. This indicates that a surprising degree of immune dysfunction can be tolerated before significant production of ANAs occurs.

Further characterization of phenotypic differences between B6.*Sle1* and B6.*Sle1Sles1* mice have also suggested a possible role of T_{FH} in the development of *Sle1*-mediated autoimmnity. This is supported by the dramatic reduction of T_{FH} in B6.*Sle1Sles1* mice, compared to B6.*Sle1* mice in aged females and *yaa* males. Additionally, within the T_{FH} compartment, B6.*Sle1Sles1* mice have a specific decrease in resident T_{FH} which express a unique set of molecules to efficiently provide help to follicular B cells.

The fine-mapping of the suppressive *Sles1* phenotype to the proximal non-*KB1* portion of *Sles1*$^{(28\text{-}83)}$ in conjunction with genomic and expression data has identified *Btnl2* as a strong candidate for *Sles1*. Meanwhile, the non-suppressive phenotype of B6.*Sle1Sles1*^{129} and the observation of a *Sles1*-mediated down-regulation of surface MHCII specifically on B cells support the *H2* gene cluster as candidates for *Sles1*.

We will discuss these candidates and possible mechanisms for suppression in more detail below.

Btnl2 has been demonstrated to function as a negative regulator of T cell activation [174, 175]. In order for the NZW allele of *Btnl2* to be suppressive of autoimmunity then, one would expect increased *Btnl2* activity either through gain-of-function polymorphisms or increased expression. We have identified three non-synonymous polymorphisms in the putative receptor-binding domains of the NZW allele of *Btnl2*, but it remains to be seen, what, if any, effect these SNPs have on *Btnl2* activity. Alternatively, reduced expression of *Btnl2* in the thymus might result in increased thymocyte sensitivity to antigen and possibly affect central tolerance. This scenario is particularly interesting in light of recent work demonstrating that the autoimmune-prone *Sle1b* allele results in increased usage of the *Ly108-1* isoform in thymocytes resulting in decreased antigen sensitivity and inefficient negative selection [106]. In support of this model, we have preliminarily demonstrated a non-significant trend towards down-regulation of thymic *Btnl2* in B6.*Sle1Sles1* mice, compared to B6.*Sle1*mice. Therefore, *Sles1*-mediated decreased *Btnl2* inhibition of thymocytes, resulting in increased sensitivity, compensates for the *Sle1b*-mediated decrease in thymocyte sensitivity through the increased usage of the *Ly108-1* isoform (Figure 56A).

In another scenario, the *Sles1* specific down-regulation of MHCII on B cells may be responsible for the observed suppressive phenotype. Because B cells are an antigen-presenting cell unique to the periphery, it is possible that TCRs that are positively selected in the thymus fail to have quality B cell interactions due to the NZW-mediated reduction of surface MHCII. This could conceivably suppress *Sle1*-mediated autoimmunity through limiting T cell help to autoreactive B cells (Figure 56B).

The recently discovered role of TCR-MHC interactions in the determination of subsets of T_{FH} cells suggests another possible mechanism of *Sles1*-mediated suppression. In this scenario, the reduction of surface MHCII on B6.*Sle1Sles1* B cells results in inferior TCR-MHC interactions and a consequent reduction in overall T_{FH} cells, as well as the "resident" effector T_{FH} subpopulation. This is consistent with B6.*Sle1Sles1* phenotypic data. Moreover, this reduction in T_{FH} would probably have a potent effect on the local cytokine milieu of splenic germinal centers as a study examining lymph nodes demonstrated that virtually all IL-4 secreting T cells were T_{FH} cells [202].

This hypothesis is particularly appealing due a recent study suggesting a possible link between the SLAM family, including *Ly108*, and the *sanroqu*e model of murine autoimmunity which is driven by T_{FH} cells. *Sanroque* mice that are deficient for the T cell SLAM family adapter

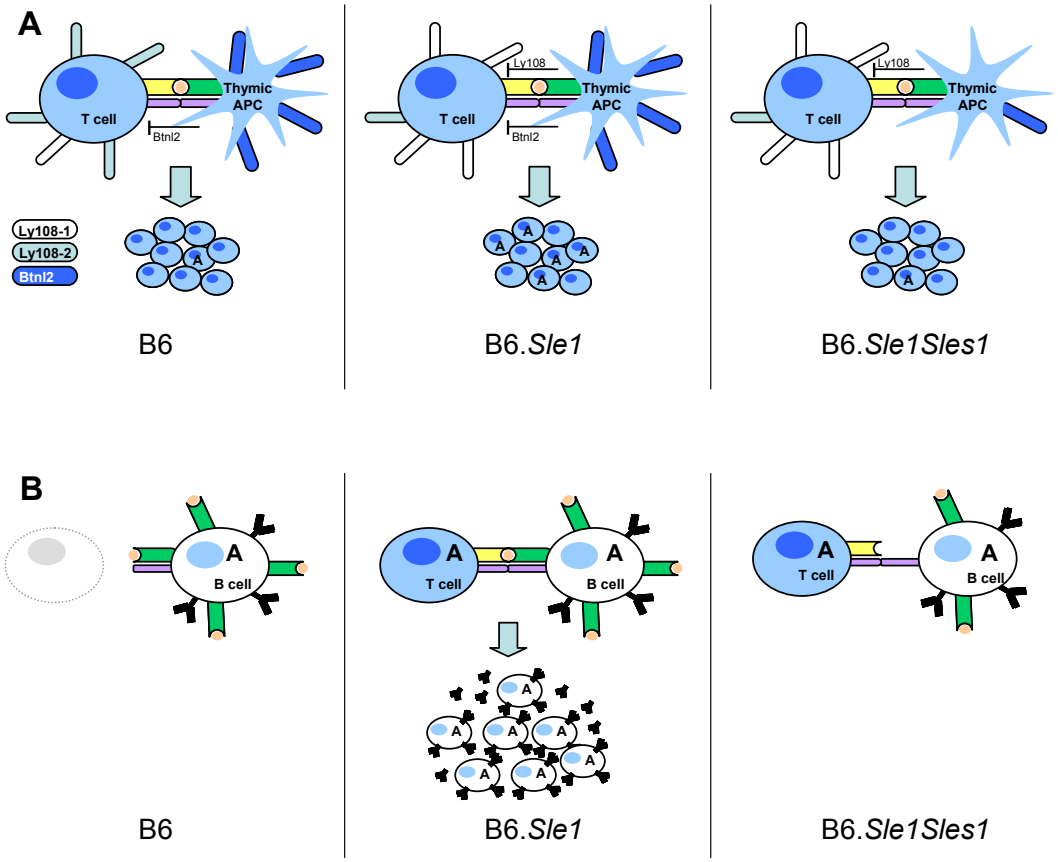

Figure 56A-B. Possible mechanisms of *Sles1* candidate genes
A. During thymocyte development, normal negative selection limits the further development of auto-reactive T cells in B6 mice. Elevated expression of the *Ly108-1* isoform in B6.*Sle1b* thymocytes increases the signaling threshold and resulting in more auto-reactive T cells escaping to the periphery. Reduced levels of *Btnl2* on B6.*Sle1Sles1* thymic APCs decreases the signaling threshold in thymocytes, compensating for the effect of *Ly108-1*.
B. In the periphery, effective negative selection limits auto-reactive T cells in B6 mice, but not in B6.Sle1 mice, allowing for the activation of auto-reactive B cells. Reduced levels of MHCII on the surface of B6.*Sle1Sles1* B cells result in inadequate T cell: B cell interactions.

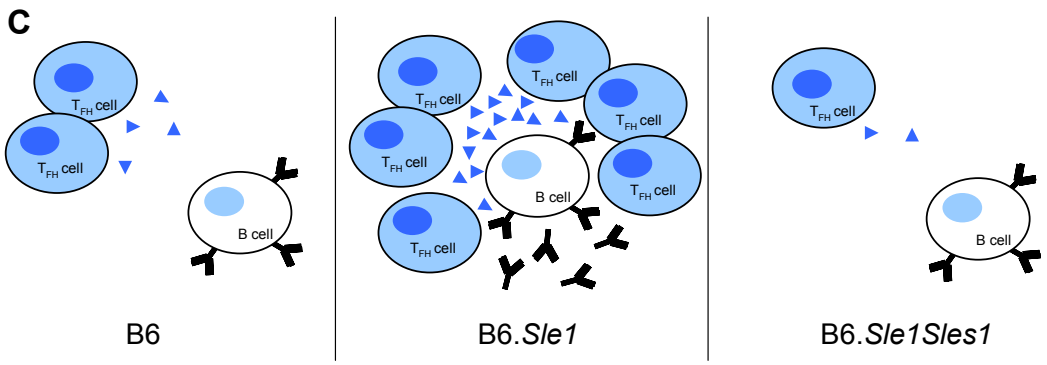

Figure 56C. Possible mechanisms of *Sles1* candidate genes
Normal levels of T_{FH} cells secrete limited cytokines in B6 mice. B6.*Sle1* mice have increased numbers of T_{FH} cells, either as a result general lymphocyte hyper-activation or through a interaction between *Ly108-1*and the SAP-dependent, but unknown, T_{FH} development pathway, which produce sufficient cytokines to assist B cells in antibody production. B6.*Sle1Sles1* mice have dramatically reduced percentages of T_{FH} cells, possible as a result of inadequate TCR-MHC interactions due to reduced B cells levels of MHCII (as shown in panel B) which have been demonstrated to influence T_{FH} development. This results in a cytokine environment that dose not assist B cells in antibody production.

molecule, SAP, had dramatically reduced numbers of T_{FH} cells and did not develop autoimmunity [183]. Despite the demonstration that SAP-mediated development of T_{FH} is intact in $SLAM^{-/-}$ mice [203], it is possible that subtle variations in SLAM family genes, like the *Sle1b* preferential use of the *Ly108-1* isoform, may affect the T_{FH} compartment in a less perturbed mouse model. Therefore, the B-cell specific down-regulation of MHCII may rebalance TCR-MHC interactions, heightened through *Sle1b*-mediated increased expression of *Ly108-1,* and consequently inhibit the development of T_{FH} cells and an autoimmune-prone cytokine environment (Figure 56C).

However, a continuing inconsistency is the lack of IgM ANAs in B6.*Sle1Sles1* mice [35] which argue for a B cell-intrinsic suppressive mechanism. Neither of the proposed *Sles1* candidate genes directly address this phenomenon, but it is most conceivable that a severely altered cytokine environment, caused by the *Sles1*-mediated significant reduction in T_{FH} cells, could impact the production of IgM ANAs. It is also possible that a *Sles1*-mediated change in MHC Class II expression could directly affect B cells in a currently unidentified pathway.

Recent high-density SNP screens of the extended human HLA region suggest multiple disease susceptibility loci [151, 152], so it possible that the suppressive phenotype of *Sles1* is a cumulative effect of both

Btnl2 and *H2*, or even other undetermined genes. It should also be noted that there are four other relatively uncharacterized butyrophilin-like genes and one butyrophilin gene located in the minimal *Sles1* interval, between *Btnl2* and the *KB1* recombinant breakpoint. Additionally, there are MHC Class II accessory genes, such as *H2-O* and *H2-Dm*, in the minimal Sles1 interval. These molecules could affect MHC Class II peptide binding, stability and transport to the cell surface (reviewed in [204]). Therefore, polymorphisms in these genes could alternatively account for the NZW-specific reduction of surface MHC Class II molecules.

Conclusions and Future Directions

The data presented in this manuscript further illustrates the complex gene-gene and gene-environment interactions that influence the development of SLE. These results also present a spectrum of suppression from *Sles1* variants and their interaction with *yaa*, which suggests that even in the context of strong innate stimulation, the cumulative immuno-regulation of an individual immune system may reach discrete levels of autoimmunity. For example, the B6.*Sle1*^{KB1} and B6.*Sle1Sles1*^{129} mouse strains display partial autoimmunity, but are driven to severe autoimmunity by *yaa*, while the B6.*Sle1Sles1* mice are completely resistant to SLE. Also, the B6.*Sle1Sles1*^{het} and B6.*Sle1(81-*

22)^{het} strains display only slight autoimmunity, but when *yaa* is introduced, they exhibit significant lymphocyte activation, yet do not produce high ANA levels. This seems to mimic human SLE where disease progression is highly variable.

The identification of the causal gene and mechanism of the potent suppressive phenotype of *Sles1* will provide significant insight into how immune dysregulation does or does not develop into autoimmunity. The *Sles1*$^{(28\text{-}83)}$ murine interval is very similar to the syntenic human interval, the latter located on chromosome 6, so it is likely that knowledge gained from this research will possibly identify novel therapeutic pathways for human SLE. This is less likely if our model of the Sles1 candidate gene Btnl2 operating at the level of central tolerance is true, as human SLE patients are not identified until after thymocyte education is complete. However, if the *H2* genes are the causative *Sles1* genes, it would probably be possible to mimic their mechanism of suppression in a clinical setting.

Two strategies are currently underway to improve our understanding of the *Sles1* interval. For the BAC rescue strategy, illustrated in Figure 57, non-suppressive B6-derived BACs that cumulatively span across the *H2* and butyrophiliin-like gene complex regions have been individually introduced on a B6.*Sle1Sles1*^{het}*yaa* background. If the causal gene of *Sles1* is represented by one of the

BACs, the addition of its B6-derived non-suppressive allele will drive a significant increase in autoimmunity in B6.*Sle1Sles1*^{het} *yaa* mice. Any individual effects of the *H2* complex and the butryophilin-like gene family will be determined through the comparison of the overlapping BACs in that area. Secondly, the effect of MHC II gene dose is also being studied through the generation of a series of mouse strains with one, two, and three copies of the *H2* genes. These strains are being derived from commercially available *H2*$^{-/-}$ mice [205], as well as our B6.*Sle1Sles1*^{129} congenic and B6-derived BAC lines as shown in Figure 58.

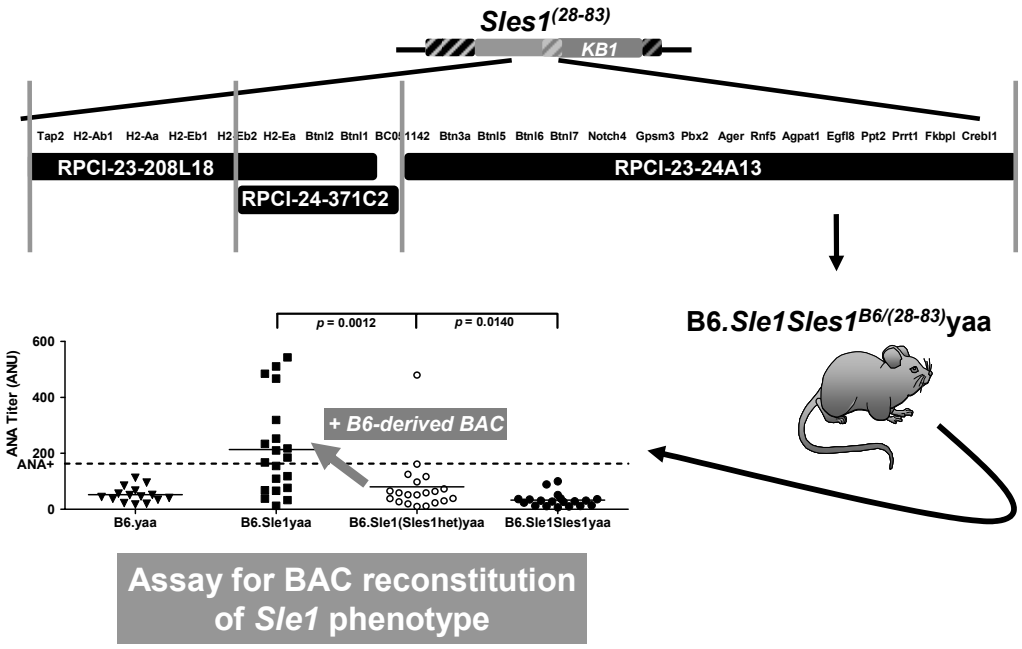

Figure 57. Pending *Sles1* causal gene identification strategy: BAC rescue. Three B6-derived BACs spanning the region of *Sles1* with the strongest candidate genes, *H1-Ab1, H2-Aa* and *Btnl2,* will be individually introduced onto the B6.*Sle1Sles1*^{het}*yaa* background. If the causal gene of *Sles1* is represented by one of the BACs, the addition of its B6-derived non-suppressive allele will drive a significant increase in autoimmunity in B6.*Sle1Sles1*^{het}*yaa* mice. Any individual effects of the MHC II complex and the butyrophilin-like gene family will be determined through the comparison of the overlapping BACs, RPCI-23-208L18 and RPC1-24-371C2.

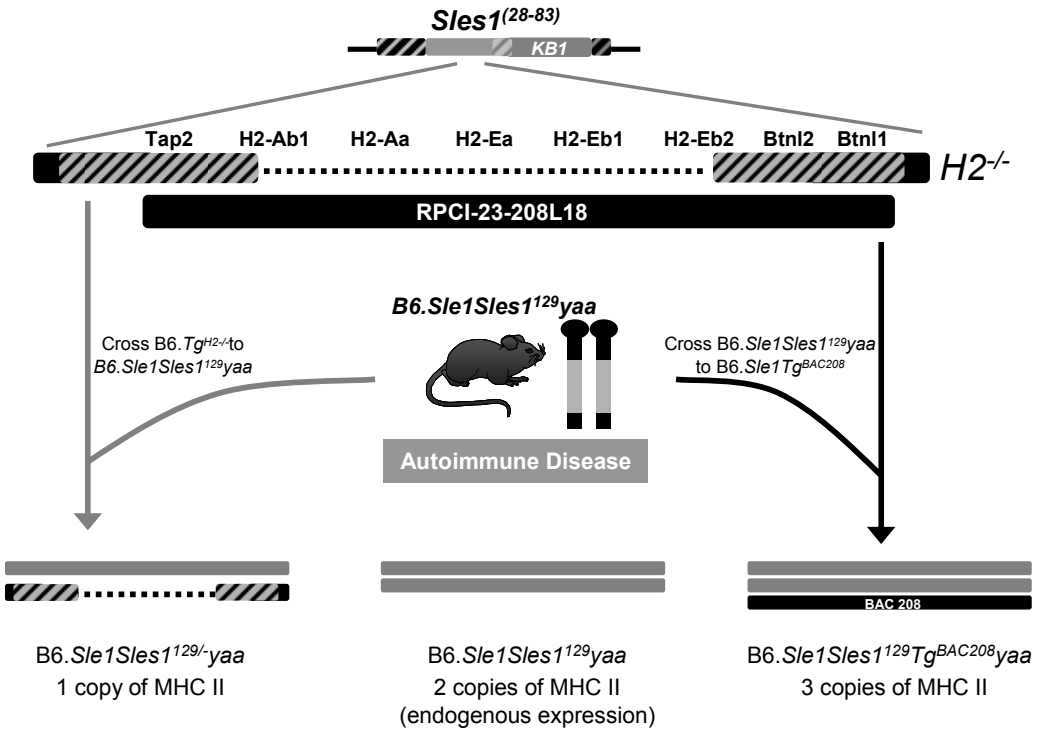

Figure 58. Pending *Sles1* causal gene identification strategy: Varying MHC II copy number. *H2-/-* mice, with flanking regions of contaminating 129 genome, will be crossed to autoimmune-prone B6.*Sle1Sles1*^{129}*yaa* mice to generate mice with only one copy of MHC II. The B6-derived BAC 208, representing the MHC Class II complex and *Btnl2* will be separately introduced onto autoimmune-prone B6.*Sle1Sles1*^{129}*yaa,* generating mice with three copies of MHC II. This strategy will identify the effect of varying MHC II copy numbers on spontaneous autoimmunity.

BIBLIOGRAPHY

[1] D'Cruz DP, Khamashta MA, Hughes GR. Systemic lupus erythematosus. Lancet 2007 Feb 17;369(9561):587-96.

[2] Pons-Estel GJ, Alarcon GS, Scofield L, Reinlib L, Cooper GS. Understanding the Epidemiology and Progression of Systemic Lupus Erythematosus. Semin Arthritis Rheum 2009 Jan 9.

[3] Hochberg MC. Updating the American College of Rheumatology revised criteria for the classification of systemic lupus erythematosus. Arthritis Rheum 1997 Sep;40(9):1725.

[4] Tan EM, Cohen AS, Fries JF, Masi AT, McShane DJ, Rothfield NF, et al. The 1982 revised criteria for the classification of systemic lupus erythematosus. Arthritis Rheum 1982 Nov;25(11):1271-7.

[5] Lau CS, Yin G, Mok MY. Ethnic and geographical differences in systemic lupus erythematosus: an overview. Lupus 2006;15(11):715-9.

[6] Bernatsky S, Boivin JF, Joseph L, Manzi S, Ginzler E, Gladman DD, et al. Mortality in systemic lupus erythematosus. Arthritis Rheum 2006 Aug;54(8):2550-7.

[7] Urowitz MB, Gladman DD, Tom BD, Ibanez D, Farewell VT. Changing patterns in mortality and disease outcomes for patients with systemic lupus erythematosus. J Rheumatol 2008 Nov;35(11):2152-8.

[8] Zhu X, Tang H, Risch N. Admixture mapping and the role of population structure for localizing disease genes. Adv Genet 2008;60:547-69.

[9] Andrews BS, Eisenberg RA, Theofilopoulos AN, Izui S, Wilson CB, McConahey PJ, et al. Spontaneous murine lupus-like syndromes. Clinical and immunopathological manifestations in several strains. J Exp Med 1978 Nov 1;148(5):1198-215.

[10] Santiago-Raber ML, Laporte C, Reininger L, Izui S. Genetic basis of murine lupus. Autoimmun Rev 2004 Jan;3(1):33-9.

[11] Watanabe-Fukunaga R, Brannan CI, Copeland NG, Jenkins NA, Nagata S. Lymphoproliferation disorder in mice explained by defects in Fas antigen that mediates apoptosis. Nature 1992 Mar 26;356(6367):314-7.

[12] Watson ML, Rao JK, Gilkeson GS, Ruiz P, Eicher EM, Pisetsky DS, et al. Genetic analysis of MRL-lpr mice: relationship of the Fas apoptosis gene to disease manifestations and renal disease-modifying loci. J Exp Med 1992 Dec 1;176(6):1645-56.

[13] Castro JE, Listman JA, Jacobson BA, Wang Y, Lopez PA, Ju S, et al. Fas modulation of apoptosis during negative selection of thymocytes. Immunity 1996 Dec;5(6):617-27.

[14] Fortner KA, Budd RC. The death receptor Fas (CD95/APO-1) mediates the deletion of T lymphocytes undergoing homeostatic proliferation. J Immunol 2005 Oct 1;175(7):4374-82.

[15] Izui S, Kelley VE, Masuda K, Yoshida H, Roths JB, Murphy ED. Induction of various autoantibodies by mutant gene lpr in several strains of mice. J Immunol 1984 Jul;133(1):227-33.

[16] Deane JA, Pisitkun P, Barrett RS, Feigenbaum L, Town T, Ward JM, et al. Control of toll-like receptor 7 expression is essential to restrict autoimmunity and dendritic cell proliferation. Immunity 2007 Nov;27(5):801-10.

[17] Fairhurst AM, Hwang SH, Wang A, Tian XH, Boudreaux C, Zhou XJ, et al. Yaa autoimmune phenotypes are conferred by overexpression of TLR7. Eur J Immunol 2008 Jul;38(7):1971-8.

[18] Pisitkun P, Deane JA, Difilippantonio MJ, Tarasenko T, Satterthwaite AB, Bolland S. Autoreactive B cell responses to RNA-related antigens due to TLR7 gene duplication. Science 2006 Jun 16;312(5780):1669-72.

[19] Subramanian S, Tus K, Li QZ, Wang A, Tian XH, Zhou J, et al. A Tlr7 translocation accelerates systemic autoimmunity in murine lupus. Proc Natl Acad Sci U S A 2006 Jun 27;103(26):9970-5.

[20] Izui S, Ibnou-Zekri N, Fossati-Jimack L, Iwamoto M. Lessons from BXSB and related mouse models. Int Rev Immunol 2000;19(4-5):447-72.

[21] Morel L, Wakeland EK. Susceptibility to lupus nephritis in the NZB/W model system. Curr Opin Immunol 1998 Dec;10(6):718-25.

[22] Morel L, Rudofsky UH, Longmate JA, Schiffenbauer J, Wakeland EK. Polygenic control of susceptibility to murine systemic lupus erythematosus. Immunity 1994 Jun;1(3):219-29.

[23] Morel L, Mohan C, Yu Y, Croker BP, Tian N, Deng A, et al. Functional dissection of systemic lupus erythematosus using congenic mouse strains. J Immunol 1997 Jun 15;158(12):6019-28.

[24] Morel L, Croker BP, Blenman KR, Mohan C, Huang G, Gilkeson G, et al. Genetic reconstitution of systemic lupus erythematosus immunopathology with polycongenic murine strains. Proc Natl Acad Sci U S A 2000 Jun 6;97(12):6670-5.

[25] Mohan C, Alas E, Morel L, Yang P, Wakeland EK. Genetic dissection of SLE pathogenesis. Sle1 on murine chromosome 1 leads to a selective loss of tolerance to H2A/H2B/DNA subnucleosomes. J Clin Invest 1998 Mar 15;101(6):1362-72.

[26] Sobel ES, Satoh M, Chen Y, Wakeland EK, Morel L. The major murine systemic lupus erythematosus susceptibility locus Sle1 results in abnormal functions of both B and T cells. J Immunol 2002 Sep 1;169(5):2694-700.

[27] Xie C, Patel R, Wu T, Zhu J, Henry T, Bhaskarabhatla M, et al. PI3K/AKT/mTOR hypersignaling in autoimmune lymphoproliferative disease engendered by the epistatic interplay of Sle1b and FASlpr. Int Immunol 2007 Apr;19(4):509-22.

[28] Croker BP, Gilkeson G, Morel L. Genetic interactions between susceptibility loci reveal epistatic pathogenic networks in murine lupus. Genes Immun 2003 Dec;4(8):575-85.

[29] Morel L, Blenman KR, Croker BP, Wakeland EK. The major murine systemic lupus erythematosus susceptibility locus, Sle1, is a cluster of

functionally related genes. Proc Natl Acad Sci U S A 2001 Feb 13;98(4):1787-92.

[30] Chan A, Li Q, Tian XH, Liang C, Zeng Z, Kaufman K, et al. Multiple members of the SLAM/CD2 gene cluster mediate susceptibility to systemic autoimmunity in mice and humans. . Genes and Immunity;Submitted.

[31] Wandstrat AE, Nguyen C, Limaye N, Chan AY, Subramanian S, Tian XH, et al. Association of extensive polymorphisms in the SLAM/CD2 gene cluster with murine lupus. Immunity 2004 Dec;21(6):769-80.

[32] Chan AY, Westcott JM, Mooney JM, Wakeland EK, Schatzle JD. The role of SAP and the SLAM family in autoimmunity. Curr Opin Immunol 2006 Dec;18(6):656-64.

[33] Morel L, Tian XH, Croker BP, Wakeland EK. Epistatic modifiers of autoimmunity in a murine model of lupus nephritis. Immunity 1999 Aug;11(2):131-9.

[34] Morel L, Mohan C, Yu Y, Schiffenbauer J, Rudofsky UH, Tian N, et al. Multiplex inheritance of component phenotypes in a murine model of lupus. Mamm Genome 1999 Feb;10(2):176-81.

[35] Subramanian S, Yim YS, Liu K, Tus K, Zhou XJ, Wakeland EK. Epistatic suppression of systemic lupus erythematosus: fine mapping of Sles1 to less than 1 mb. J Immunol 2005 Jul 15;175(2):1062-72.

[36] Banchereau J, Pascual V. Type I interferon in systemic lupus erythematosus and other autoimmune diseases. Immunity 2006 Sep;25(3):383-92.

[37] Baechler EC, Batliwalla FM, Karypis G, Gaffney PM, Ortmann WA, Espe KJ, et al. Interferon-inducible gene expression signature in peripheral blood cells of patients with severe lupus. Proc Natl Acad Sci U S A 2003 Mar 4;100(5):2610-5.

[38] Nikpour M, Dempsey AA, Urowitz MB, Gladman DD, Barnes DA. Association of a gene expression profile from whole blood with disease activity in systemic lupus erythaematosus. Ann Rheum Dis 2008 Aug;67(8):1069-75.

[39] Hua J, Kirou K, Lee C, Crow MK. Functional assay of type I interferon in systemic lupus erythematosus plasma and association with anti-RNA binding protein autoantibodies. Arthritis Rheum 2006 Jun;54(6):1906-16.

[40] Fairhurst AM, Mathian A, Connolly JE, Wang A, Gray HF, George TA, et al. Systemic IFN-alpha drives kidney nephritis in B6.Sle123 mice. Eur J Immunol 2008 Jul;38(7):1948-60.

[41] Santiago-Raber ML, Baccala R, Haraldsson KM, Choubey D, Stewart TA, Kono DH, et al. Type-I interferon receptor deficiency reduces lupus-like disease in NZB mice. J Exp Med 2003 Mar 17;197(6):777-88.

[42] Christensen SR, Shupe J, Nickerson K, Kashgarian M, Flavell RA, Shlomchik MJ. Toll-like receptor 7 and TLR9 dictate autoantibody specificity and have opposing inflammatory and regulatory roles in a murine model of lupus. Immunity 2006 Sep;25(3):417-28.

[43] Komatsuda A, Wakui H, Iwamoto K, Ozawa M, Togashi M, Masai R, et al. Up-regulated expression of Toll-like receptors mRNAs in peripheral blood mononuclear cells from patients with systemic lupus erythematosus. Clin Exp Immunol 2008 Jun;152(3):482-7.

[44] Poovassery JS, Vanden Bush TJ, Bishop GA. Antigen Receptor Signals Rescue B Cells from TLR Tolerance. J Immunol 2009 Jul 31.

[45] Green NM, Laws A, Kiefer K, Busconi L, Kim YM, Brinkmann MM, et al. Murine B cell response to TLR7 ligands depends on an IFN-beta feedback loop. J Immunol 2009 Aug 1;183(3):1569-76.

[46] Thibault DL, Graham KL, Lee LY, Balboni I, Hertzog PJ, Utz PJ. Type I IFN receptor controls B cell expression of nucleic acid sensing toll-like receptors and autoantibody production in a murine model of lupus. Arthritis Res Ther 2009 Jul 22;11(4):R112.

[47] Cunninghame Graham DS, Akil M, Vyse TJ. Association of polymorphisms across the tyrosine kinase gene, TYK2 in UK SLE families. Rheumatology (Oxford) 2007 Jun;46(6):927-30.

[48] Hellquist A, Jarvinen TM, Koskenmies S, Zucchelli M, Orsmark-Pietras C, Berglind L, et al. Evidence for Genetic Association and

Interaction Between the TYK2 and IRF5 Genes in Systemic Lupus Erythematosus. J Rheumatol 2009 Jun 30.

[49] Sigurdsson S, Nordmark G, Goring HH, Lindroos K, Wiman AC, Sturfelt G, et al. Polymorphisms in the tyrosine kinase 2 and interferon regulatory factor 5 genes are associated with systemic lupus erythematosus. Am J Hum Genet 2005 Mar;76(3):528-37.

[50] Suarez-Gestal M, Calaza M, Endreffy E, Pullmann R, Ordi-Ros J, Domenico Sebastiani G, et al. Replication of recently identified systemic lupus erythematosus genetic associations: a case-control study. Arthritis Res Ther 2009;11(3):R69.

[51] Harley JB, Alarcon-Riquelme ME, Criswell LA, Jacob CO, Kimberly RP, Moser KL, et al. Genome-wide association scan in women with systemic lupus erythematosus identifies susceptibility variants in ITGAM, PXK, KIAA1542 and other loci. Nat Genet 2008 Feb;40(2):204-10.

[52] Hom G, Graham RR, Modrek B, Taylor KE, Ortmann W, Garnier S, et al. Association of systemic lupus erythematosus with C8orf13-BLK and ITGAM-ITGAX. N Engl J Med 2008 Feb 28;358(9):900-9.

[53] Richter MF, Dumenil G, Uze G, Fellous M, Pellegrini S. Specific contribution of Tyk2 JH regions to the binding and the expression of the interferon alpha/beta receptor component IFNAR1. J Biol Chem 1998 Sep 18;273(38):24723-9.

[54] Shaw MH, Boyartchuk V, Wong S, Karaghiosoff M, Ragimbeau J, Pellegrini S, et al. A natural mutation in the Tyk2 pseudokinase domain underlies altered susceptibility of B10.Q/J mice to infection and autoimmunity. Proc Natl Acad Sci U S A 2003 Sep 30;100(20):11594-9.

[55] Spach KM, Noubade R, McElvany B, Hickey WF, Blankenhorn EP, Teuscher C. A single nucleotide polymorphism in Tyk2 controls susceptibility to experimental allergic encephalomyelitis. J Immunol 2009 Jun 15;182(12):7776-83.

[56] Abelson AK, Delgado-Vega AM, Kozyrev SV, Sanchez E, Velazquez-Cruz R, Eriksson N, et al. STAT4 Associates with SLE through two independent effects that correlate with gene expression and act additively with IRF5 to increase risk. Ann Rheum Dis 2008 Dec 9.

[57] Ji JD, Lee WJ, Kong KA, Woo JH, Choi SJ, Lee YH, et al. Association of STAT4 polymorphism with rheumatoid arthritis and systemic lupus erythematosus: a meta-analysis. Mol Biol Rep 2009 May 29.

[58] Kariuki SN, Kirou KA, MacDermott EJ, Barillas-Arias L, Crow MK, Niewold TB. Cutting edge: autoimmune disease risk variant of STAT4 confers increased sensitivity to IFN-alpha in lupus patients in vivo. J Immunol 2009 Jan 1;182(1):34-8.

[59] Namjou B, Sestak AL, Armstrong DL, Zidovetzki R, Kelly JA, Jacob N, et al. High-density genotyping of STAT4 reveals multiple haplotypic associations with systemic lupus erythematosus in different racial groups. Arthritis Rheum 2009 Mar 30;60(4):1085-95.

[60] Sigurdsson S, Nordmark G, Garnier S, Grundberg E, Kwan T, Nilsson O, et al. A risk haplotype of STAT4 for systemic lupus erythematosus is over-expressed, correlates with anti-dsDNA and shows additive effects with two risk alleles of IRF5. Hum Mol Genet 2008 Sep 15;17(18):2868-76.

[61] Yang W, Ng P, Zhao M, Hirankarn N, Lau CS, Mok CC, et al. Population differences in SLE susceptibility genes: STAT4 and BLK, but not PXK, are associated with systemic lupus erythematosus in Hong Kong Chinese. Genes Immun 2009 Feb 19.

[62] Taylor KE, Remmers EF, Lee AT, Ortmann WA, Plenge RM, Tian C, et al. Specificity of the STAT4 genetic association for severe disease manifestations of systemic lupus erythematosus. PLoS Genet 2008 May;4(5):e1000084.

[63] Jacob CO, Zang S, Li L, Ciobanu V, Quismorio F, Mizutani A, et al. Pivotal role of Stat4 and Stat6 in the pathogenesis of the lupus-like disease in the New Zealand mixed 2328 mice. J Immunol 2003 Aug 1;171(3):1564-71.

[64] Xu Z, Duan B, Croker BP, Morel L. STAT4 deficiency reduces autoantibody production and glomerulonephritis in a mouse model of lupus. Clin Immunol 2006 Aug;120(2):189-98.

[65] Tyler DR, Persky ME, Matthews LA, Chan S, Farrar JD. Pre-assembly of STAT4 with the human IFN-alpha/beta receptor-2 subunit is mediated by the STAT4 N-domain. Mol Immunol 2007 Mar;44(8):1864-72.

[66] Armstrong DL, Reiff A, Myones BL, Quismorio FP, Jr., Klein-Gitelman M, McCurdy D, et al. Identification of new SLE-associated genes with a two-step Bayesian study design. Genes Immun 2009 Jul;10(5):446-56.

[67] Ferreiro-Neira I, Calaza M, Alonso-Perez E, Marchini M, Scorza R, Sebastiani GD, et al. Opposed independent effects and epistasis in the complex association of IRF5 to SLE. Genes Immun 2007 Jul;8(5):429-38.

[68] Lee YH, Song GG. Association between the rs2004640 functional polymorphism of interferon regulatory factor 5 and systemic lupus erythematosus: a meta-analysis. Rheumatol Int 2009 Aug;29(10):1137-42.

[69] Graham RR, Kozyrev SV, Baechler EC, Reddy MV, Plenge RM, Bauer JW, et al. A common haplotype of interferon regulatory factor 5 (IRF5) regulates splicing and expression and is associated with increased risk of systemic lupus erythematosus. Nat Genet 2006 May;38(5):550-5.

[70] Graham RR, Kyogoku C, Sigurdsson S, Vlasova IA, Davies LR, Baechler EC, et al. Three functional variants of IFN regulatory factor 5 (IRF5) define risk and protective haplotypes for human lupus. Proc Natl Acad Sci U S A 2007 Apr 17;104(16):6758-63.

[71] Kozyrev SV, Lewen S, Reddy PM, Pons-Estel B, Witte T, Junker P, et al. Structural insertion/deletion variation in IRF5 is associated with a risk haplotype and defines the precise IRF5 isoforms expressed in systemic lupus erythematosus. Arthritis Rheum 2007 Apr;56(4):1234-41.

[72] Sigurdsson S, Goring HH, Kristjansdottir G, Milani L, Nordmark G, Sandling JK, et al. Comprehensive evaluation of the genetic variants of interferon regulatory factor 5 (IRF5) reveals a novel 5 bp length polymorphism as strong risk factor for systemic lupus erythematosus. Hum Mol Genet 2008 Mar 15;17(6):872-81.

[73] Mancl ME, Hu G, Sangster-Guity N, Olshalsky SL, Hoops K, Fitzgerald-Bocarsly P, et al. Two discrete promoters regulate the alternatively spliced human interferon regulatory factor-5 isoforms.

Multiple isoforms with distinct cell type-specific expression, localization, regulation, and function. J Biol Chem 2005 Jun 3;280(22):21078-90.

[74] Lau CM, Broughton C, Tabor AS, Akira S, Flavell RA, Mamula MJ, et al. RNA-associated autoantigens activate B cells by combined B cell antigen receptor/Toll-like receptor 7 engagement. J Exp Med 2005 Nov 7;202(9):1171-7.

[75] Busconi L, Bauer JW, Tumang JR, Laws A, Perkins-Mesires K, Tabor AS, et al. Functional outcome of B cell activation by chromatin immune complex engagement of the B cell receptor and TLR9. J Immunol 2007 Dec 1;179(11):7397-405.

[76] Leadbetter EA, Rifkin IR, Hohlbaum AM, Beaudette BC, Shlomchik MJ, Marshak-Rothstein A. Chromatin-IgG complexes activate B cells by dual engagement of IgM and Toll-like receptors. Nature 2002 Apr 11;416(6881):603-7.

[77] Viglianti GA, Lau CM, Hanley TM, Miko BA, Shlomchik MJ, Marshak-Rothstein A. Activation of autoreactive B cells by CpG dsDNA. Immunity 2003 Dec;19(6):837-47.

[78] Uccellini MB, Busconi L, Green NM, Busto P, Christensen SR, Shlomchik MJ, et al. Autoreactive B cells discriminate CpG-rich and CpG-poor DNA and this response is modulated by IFN-alpha. J Immunol 2008 Nov 1;181(9):5875-84.

[79] Pawar RD, Ramanjaneyulu A, Kulkarni OP, Lech M, Segerer S, Anders HJ. Inhibition of Toll-like receptor-7 (TLR-7) or TLR-7 plus TLR-9 attenuates glomerulonephritis and lung injury in experimental lupus. J Am Soc Nephrol 2007 Jun;18(6):1721-31.

[80] Kwok SK, Lee JY, Park SH, Cho ML, Min SY, Kim HY, et al. Dysfunctional interferon-alpha production by peripheral plasmacytoid dendritic cells upon Toll-like receptor-9 stimulation in patients with systemic lupus erythematosus. Arthritis Res Ther 2008;10(2):R29.

[81] Lartigue A, Courville P, Auquit I, Francois A, Arnoult C, Tron F, et al. Role of TLR9 in anti-nucleosome and anti-DNA antibody production in lpr mutation-induced murine lupus. J Immunol 2006 Jul 15;177(2):1349-54.

[82] Tao K, Fujii M, Tsukumo S, Maekawa Y, Kishihara K, Kimoto Y, et al. Genetic variations of Toll-like receptor 9 predispose to systemic lupus erythematosus in Japanese population. Ann Rheum Dis 2007 Jul;66(7):905-9.

[83] Wu X, Peng SL. Toll-like receptor 9 signaling protects against murine lupus. Arthritis Rheum 2006 Jan;54(1):336-42.

[84] Yu P, Wellmann U, Kunder S, Quintanilla-Martinez L, Jennen L, Dear N, et al. Toll-like receptor 9-independent aggravation of glomerulonephritis in a novel model of SLE. Int Immunol 2006 Aug;18(8):1211-9.

[85] Yeo SJ, Yoon JG, Yi AK. Myeloid differentiation factor 88-dependent post-transcriptional regulation of cyclooxygenase-2 expression by CpG DNA: tumor necrosis factor-alpha receptor-associated factor 6, a diverging point in the Toll-like receptor 9-signaling. J Biol Chem 2003 Oct 17;278(42):40590-600.

[86] Gottipati S, Rao NL, Fung-Leung WP. IRAK1: a critical signaling mediator of innate immunity. Cell Signal 2008 Feb;20(2):269-76.

[87] Deng C, Radu C, Diab A, Tsen MF, Hussain R, Cowdery JS, et al. IL-1 receptor-associated kinase 1 regulates susceptibility to organ-specific autoimmunity. J Immunol 2003 Mar 15;170(6):2833-42.

[88] Jacob CO, Zhu J, Armstrong DL, Yan M, Han J, Zhou XJ, et al. Identification of IRAK1 as a risk gene with critical role in the pathogenesis of systemic lupus erythematosus. Proc Natl Acad Sci U S A 2009 Mar 27.

[89] Ehlers M, Fukuyama H, McGaha TL, Aderem A, Ravetch JV. TLR9/MyD88 signaling is required for class switching to pathogenic IgG2a and 2b autoantibodies in SLE. J Exp Med 2006 Mar 20;203(3):553-61.

[90] Sadanaga A, Nakashima H, Akahoshi M, Masutani K, Miyake K, Igawa T, et al. Protection against autoimmune nephritis in MyD88-deficient MRL/lpr mice. Arthritis Rheum 2007 May;56(5):1618-28.

[91] Silver KL, Crockford TL, Bouriez-Jones T, Milling S, Lambe T, Cornall RJ. MyD88-dependent autoimmune disease in Lyn-deficient mice. Eur J Immunol 2007 Oct;37(10):2734-43.

[92] Croker BA, Lawson BR, Rutschmann S, Berger M, Eidenschenk C, Blasius AL, et al. Inflammation and autoimmunity caused by a SHP1 mutation depend on IL-1, MyD88, and a microbial trigger. Proc Natl Acad Sci U S A 2008 Sep 30;105(39):15028-33.

[93] Groom JR, Fletcher CA, Walters SN, Grey ST, Watt SV, Sweet MJ, et al. BAFF and MyD88 signals promote a lupuslike disease independent of T cells. J Exp Med 2007 Aug 6;204(8):1959-71.

[94] Herlands RA, Christensen SR, Sweet RA, Hershberg U, Shlomchik MJ. T cell-independent and toll-like receptor-dependent antigen-driven activation of autoreactive B cells. Immunity 2008 Aug;29(2):249-60.

[95] Lech M, Kulkarni OP, Pfeiffer S, Savarese E, Krug A, Garlanda C, et al. Tir8/Sigirr prevents murine lupus by suppressing the immunostimulatory effects of lupus autoantigens. J Exp Med 2008 Aug 4;205(8):1879-88.

[96] Kumar KR, Li L, Yan M, Bhaskarabhatla M, Mobley AB, Nguyen C, et al. Regulation of B cell tolerance by the lupus susceptibility gene Ly108. Science 2006 Jun 16;312(5780):1665-9.

[97] Zhong MC, Veillette A. Control of T lymphocyte signaling by Ly108, a signaling lymphocytic activation molecule family receptor implicated in autoimmunity. J Biol Chem 2008 Jul 11;283(28):19255-64.

[98] Peck SR, Ruley HE. Ly108: a new member of the mouse CD2 family of cell surface proteins. Immunogenetics 2000 Nov;52(1-2):63-72.

[99] Cunninghame Graham DS, Vyse TJ, Fortin PR, Montpetit A, Cai YC, Lim S, et al. Association of LY9 in UK and Canadian SLE families. Genes Immun 2008 Mar;9(2):93-102.

[100] Limaye N, Belobrajdic KA, Wandstrat AE, Bonhomme F, Edwards SV, Wakeland EK. Prevalence and evolutionary origins of autoimmune susceptibility alleles in natural mouse populations. Genes Immun 2008 Jan;9(1):61-8.

[101] Sayos J, Wu C, Morra M, Wang N, Zhang X, Allen D, et al. The X-linked lymphoproliferative-disease gene product SAP regulates signals induced through the co-receptor SLAM. Nature 1998 Oct 1;395(6701):462-9.

[102] Takei M, Ishiwata T, Mitamura K, Fujiwara S, Sasaki K, Nishi T, et al. Decreased expression of signaling lymphocytic-activation molecule-associated protein (SAP) transcripts in T cells from patients with rheumatoid arthritis. Int Immunol 2001 Apr;13(4):559-65.

[103] Qi H, Cannons JL, Klauschen F, Schwartzberg PL, Germain RN. SAP-controlled T-B cell interactions underlie germinal centre formation. Nature 2008 Oct 9;455(7214):764-9.

[104] Jennings P, Chan A, Schwartzberg P, Wakeland EK, Yuan D. Antigen-specific responses and ANA production in B6.Sle1b mice: a role for SAP. J Autoimmun 2008 Dec;31(4):345-53.

[105] Komori H, Furukawa H, Mori S, Ito MR, Terada M, Zhang MC, et al. A signal adaptor SLAM-associated protein regulates spontaneous autoimmunity and Fas-dependent lymphoproliferation in MRL-Faslpr lupus mice. J Immunol 2006 Jan 1;176(1):395-400.

[106] Batteux F, Wang A, Tus K, Westcott JM, Chan A, Schatzle JD, et al. Regulation of the thymic selection by the lupus susceptibility gene Ly108. Immunity;Accepted with revisions.

[107] Cornall RJ, Cyster JG, Hibbs ML, Dunn AR, Otipoby KL, Clark EA, et al. Polygenic autoimmune traits: Lyn, CD22, and SHP-1 are limiting elements of a biochemical pathway regulating BCR signaling and selection. Immunity 1998 Apr;8(4):497-508.

[108] Hibbs ML, Tarlinton DM, Armes J, Grail D, Hodgson G, Maglitto R, et al. Multiple defects in the immune system of Lyn-deficient mice, culminating in autoimmune disease. Cell 1995 Oct 20;83(2):301-11.

[109] Whyburn LR, Halcomb KE, Contreras CM, Lowell CA, Witte ON, Satterthwaite AB. Reduced dosage of Bruton's tyrosine kinase uncouples B cell hyperresponsiveness from autoimmunity in lyn-/- mice. J Immunol 2003 Aug 15;171(4):1850-8.

[110] Flores-Borja F, Kabouridis PS, Jury EC, Isenberg DA, Mageed RA. Altered lipid raft-associated proximal signaling and translocation of CD45 tyrosine phosphatase in B lymphocytes from patients with systemic lupus erythematosus. Arthritis Rheum 2007 Jan;56(1):291-302.

[111] Liossis SN, Solomou EE, Dimopoulos MA, Panayiotidis P, Mavrikakis MM, Sfikakis PP. B-cell kinase lyn deficiency in patients with systemic lupus erythematosus. J Investig Med 2001 Mar;49(2):157-65.

[112] Lu R, Vidal GS, Kelly JA, Delgado-Vega AM, Howard XK, Macwana SR, et al. Genetic associations of LYN with systemic lupus erythematosus. Genes Immun 2009 Jul;10(5):397-403.

[113] Hatta Y, Tsuchiya N, Matsushita M, Shiota M, Hagiwara K, Tokunaga K. Identification of the gene variations in human CD22. Immunogenetics 1999 Apr;49(4):280-6.

[114] Lajaunias F, Ibnou-Zekri N, Fossati Jimack L, Chicheportiche Y, Parkhouse RM, Mary C, et al. Polymorphisms in the Cd22 gene of inbred mouse strains. Immunogenetics 1999 Oct;49(11-12):991-5.

[115] Law CL, Torres RM, Sundberg HA, Parkhouse RM, Brannan CI, Copeland NG, et al. Organization of the murine Cd22 locus. Mapping to chromosome 7 and characterization of two alleles. J Immunol 1993 Jul 1;151(1):175-87.

[116] O'Keefe TL, Williams GT, Davies SL, Neuberger MS. Hyperresponsive B cells in CD22-deficient mice. Science 1996 Nov 1;274(5288):798-801.

[117] O'Keefe TL, Williams GT, Batista FD, Neuberger MS. Deficiency in CD22, a B cell-specific inhibitory receptor, is sufficient to predispose to development of high affinity autoantibodies. J Exp Med 1999 Apr 19;189(8):1307-13.

[118] Mary C, Laporte C, Parzy D, Santiago ML, Stefani F, Lajaunias F, et al. Dysregulated expression of the Cd22 gene as a result of a short interspersed nucleotide element insertion in Cd22a lupus-prone mice. J Immunol 2000 Sep 15;165(6):2987-96.

[119] Suzuki J, Nakano S, Nakairi Y, Mitsuo A, Amano H, Morimoto S, et al. CD19/22 balance relates to improvement of disease activity in systemic lupus erythematosus. Mod Rheumatol 2006;16(4):235-8.

[120] Dorner T, Kaufmann J, Wegener WA, Teoh N, Goldenberg DM, Burmester GR. Initial clinical trial of epratuzumab (humanized anti-CD22 antibody) for immunotherapy of systemic lupus erythematosus. Arthritis Res Ther 2006;8(3):R74.

[121] Jacobi AM, Goldenberg DM, Hiepe F, Radbruch A, Burmester GR, Dorner T. Differential effects of epratuzumab on peripheral blood B cells of patients with systemic lupus erythematosus versus normal controls. Ann Rheum Dis 2008 Apr;67(4):450-7.

[122] Tsui HW, Siminovitch KA, de Souza L, Tsui FW. Motheaten and viable motheaten mice have mutations in the haematopoietic cell phosphatase gene. Nat Genet 1993 Jun;4(2):124-9.

[123] Pao LI, Lam KP, Henderson JM, Kutok JL, Alimzhanov M, Nitschke L, et al. B cell-specific deletion of protein-tyrosine phosphatase Shp1 promotes B-1a cell development and causes systemic autoimmunity. Immunity 2007 Jul;27(1):35-48.

[124] Matsuda A, Matsuzawa S, Nakamura K, Mizuno Y, Kikuchi K. Alterations in activity of protein tyrosine phosphatase SH-PTP1 in autoimmune MRL/mpj-lpr/lpr mice. J Biochem 1996 Feb;119(2):329-33.

[125] Huck S, Le Corre R, Youinou P, Zouali M. Expression of B cell receptor-associated signaling molecules in human lupus. Autoimmunity 2001 May;33(3):213-24.

[126] Kono H, Kyogoku C, Suzuki T, Tsuchiya N, Honda H, Yamamoto K, et al. FcgammaRIIB Ile232Thr transmembrane polymorphism associated with human systemic lupus erythematosus decreases affinity to lipid rafts and attenuates inhibitory effects on B cell receptor signaling. Hum Mol Genet 2005 Oct 1;14(19):2881-92.

[127] Blank MC, Stefanescu RN, Masuda E, Marti F, King PD, Redecha PB, et al. Decreased transcription of the human FCGR2B gene mediated by the -343 G/C promoter polymorphism and association with systemic lupus erythematosus. Hum Genet 2005 Jul;117(2-3):220-7.

[128] Bolland S, Ravetch JV. Spontaneous autoimmune disease in Fc(gamma)RIIB-deficient mice results from strain-specific epistasis. Immunity 2000 Aug;13(2):277-85.

[129] Bolland S, Yim YS, Tus K, Wakeland EK, Ravetch JV. Genetic modifiers of systemic lupus erythematosus in FcgammaRIIB(-/-) mice. J Exp Med 2002 May 6;195(9):1167-74.

[130] Sharpe AH, Wherry EJ, Ahmed R, Freeman GJ. The function of programmed cell death 1 and its ligands in regulating autoimmunity and infection. Nat Immunol 2007 Mar;8(3):239-45.

[131] Lee YH, Woo JH, Choi SJ, Ji JD, Song GG. Association of programmed cell death 1 polymorphisms and systemic lupus erythematosus: a meta-analysis. Lupus 2009 Jan;18(1):9-15.

[132] Liu JL, Zhang FY, Liang YH, Xiao FL, Zhang SQ, Cheng YL, et al. Association between the PD1.3A/G polymorphism of the PDCD1 gene and systemic lupus erythematosus in European populations: a meta-analysis. J Eur Acad Dermatol Venereol 2009 Apr;23(4):425-32.

[133] Prokunina L, Castillejo-Lopez C, Oberg F, Gunnarsson I, Berg L, Magnusson V, et al. A regulatory polymorphism in PDCD1 is associated with susceptibility to systemic lupus erythematosus in humans. Nat Genet 2002 Dec;32(4):666-9.

[134] Bertsias GK, Nakou M, Choulaki C, Raptopoulou A, Papadimitraki E, Goulielmos G, et al. Genetic, immunologic, and immunohistochemical analysis of the programmed death 1/programmed death ligand 1 pathway in human systemic lupus erythematosus. Arthritis Rheum 2009 Jan;60(1):207-18.

[135] Nishimura H, Nose M, Hiai H, Minato N, Honjo T. Development of lupus-like autoimmune diseases by disruption of the PD-1 gene encoding an ITIM motif-carrying immunoreceptor. Immunity 1999 Aug;11(2):141-51.

[136] Ding H, Wu X, Wu J, Yagita H, He Y, Zhang J, et al. Delivering PD-1 inhibitory signal concomitant with blocking ICOS co-stimulation suppresses lupus-like syndrome in autoimmune BXSB mice. Clin Immunol 2006 Feb-Mar;118(2-3):258-67.

[137] Hasegawa K, Martin F, Huang G, Tumas D, Diehl L, Chan AC. PEST domain-enriched tyrosine phosphatase (PEP) regulation of effector/memory T cells. Science 2004 Jan 30;303(5658):685-9.

[138] Lee YH, Rho YH, Choi SJ, Ji JD, Song GG, Nath SK, et al. The PTPN22 C1858T functional polymorphism and autoimmune diseases--a meta-analysis. Rheumatology (Oxford) 2007 Jan;46(1):49-56.

[139] Orru V, Tsai SJ, Rueda B, Fiorillo E, Stanford SM, Dasgupta J, et al. A loss-of-function variant of PTPN22 is associated with reduced risk of systemic lupus erythematosus. Hum Mol Genet 2009 Feb 1;18(3):569-79.

[140] Zikherman J, Hermiston M, Steiner D, Hasegawa K, Chan A, Weiss A. PTPN22 deficiency cooperates with the CD45 E613R allele to break tolerance on a non-autoimmune background. J Immunol 2009 Apr 1;182(7):4093-106.

[141] Arechiga AF, Habib T, He Y, Zhang X, Zhang ZY, Funk A, et al. Cutting edge: The PTPN22 allelic variant associated with autoimmunity impairs B cell signaling. J Immunol 2009 Mar 15;182(6):3343-7.

[142] Bansal-Pakala P, Jember AG, Croft M. Signaling through OX40 (CD134) breaks peripheral T-cell tolerance. Nat Med 2001 Aug;7(8):907-12.

[143] Lathrop SK, Huddleston CA, Dullforce PA, Montfort MJ, Weinberg AD, Parker DC. A signal through OX40 (CD134) allows anergic, autoreactive T cells to acquire effector cell functions. J Immunol 2004 Jun 1;172(11):6735-43.

[144] Cunninghame Graham DS, Graham RR, Manku H, Wong AK, Whittaker JC, Gaffney PM, et al. Polymorphism at the TNF superfamily gene TNFSF4 confers susceptibility to systemic lupus erythematosus. Nat Genet 2008 Jan;40(1):83-9.

[145] Delgado-Vega AM, Abelson AK, Sanchez E, Witte T, D'Alfonso S, Galeazzi M, et al. Replication of the TNFSF4 (OX40L) promoter region association with systemic lupus erythematosus. Genes Immun 2008 Dec 18.

[146] Patschan S, Dolff S, Kribben A, Durig J, Patschan D, Wilde B, et al. CD134 expression on CD4+ T cells is associated with nephritis and disease activity in patients with systemic lupus erythematosus. Clin Exp Immunol 2006 Aug;145(2):235-42.

[147] Aten J, Roos A, Claessen N, Schilder-Tol EJ, Ten Berge IJ, Weening JJ. Strong and selective glomerular localization of CD134 ligand and TNF receptor-1 in proliferative lupus nephritis. J Am Soc Nephrol 2000 Aug;11(8):1426-38.

[148] Lee YH, Nath SK. Systemic lupus erythematosus susceptibility loci defined by genome scan meta-analysis. Hum Genet 2005 Dec;118(3-4):434-43.

[149] Shiina T, Hosomichi K, Inoko H, Kulski JK. The HLA genomic loci map: expression, interaction, diversity and disease. J Hum Genet 2009;54(1):15-39.

[150] Fernando MM, Stevens CR, Walsh EC, De Jager PL, Goyette P, Plenge RM, et al. Defining the role of the MHC in autoimmunity: a review and pooled analysis. PLoS Genet 2008 Apr;4(4):e1000024.

[151] Barcellos LF, May SL, Ramsay PP, Quach HL, Lane JA, Nititham J, et al. High-density SNP screening of the major histocompatibility complex in systemic lupus erythematosus demonstrates strong evidence for independent susceptibility regions. PLoS Genet 2009 Oct;5(10):e1000696.

[152] Rioux JD, Goyette P, Vyse TJ, Hammarstrom L, Fernando MM, Green T, et al. Mapping of multiple susceptibility variants within the MHC region for 7 immune-mediated diseases. Proc Natl Acad Sci U S A 2009 Nov 3;106(44):18680-5.

[153] Flavell RA, Allen H, Burkly LC, Sherman DH, Waneck GL, Widera G. Molecular biology of the H-2 histocompatibility complex. Science 1986 Jul 25;233(4762):437-43.

[154] Vyse TJ, Halterman RK, Rozzo SJ, Izui S, Kotzin BL. Control of separate pathogenic autoantibody responses marks MHC gene contributions to murine lupus. Proc Natl Acad Sci U S A 1999 Jul 6;96(14):8098-103.

[155] Zhang D, Fujio K, Jiang Y, Zhao J, Tada N, Sudo K, et al. Dissection of the role of MHC class II A and E genes in autoimmune susceptibility in murine lupus models with intragenic recombination. Proc Natl Acad Sci U S A 2004 Sep 21;101(38):13838-43.

[156] Vyse TJ, Rozzo SJ, Drake CG, Appel VB, Lemeur M, Izui S, et al. Contributions of Ea(z) and Eb(z) MHC genes to lupus susceptibility in New Zealand mice. J Immunol 1998 Mar 15;160(6):2757-66.

[157] Gubbels MR, Jorgensen TN, Metzger TE, Menze K, Steele H, Flannery SA, et al. Effects of MHC and gender on lupus-like autoimmunity in Nba2 congenic mice. J Immunol 2005 Nov 1;175(9):6190-6.

[158] Rozzo SJ, Vyse TJ, David CS, Palmer E, Izui S, Kotzin BL. Analysis of MHC class II genes in the susceptibility to lupus in New Zealand mice. J Immunol 1999 Mar 1;162(5):2623-30.

[159] Jones PP, Murphy DB, McDevitt HO. Variable synthesis and expression of E alpha and Ae (E beta) Ia polypeptide chains in mice of different H-2 haplotypes. Immunogenetics 1981;12(3-4):321-37.

[160] Wu T, Qin X, Kurepa Z, Kumar KR, Liu K, Kanta H, et al. Shared signaling networks active in B cells isolated from genetically distinct mouse models of lupus. J Clin Invest 2007 Aug;117(8):2186-96.

[161] Mihaylova N, Voynova E, Tchorbanov A, Dolashka-Angelova P, Bayry J, Devreese B, et al. Simultaneous engagement of FcgammaIIb and CD22 inhibitory receptors silences targeted B cells and suppresses autoimmune disease activity. Mol Immunol 2009 Feb 23.

[162] Isnardi I, Ng YS, Srdanovic I, Motaghedi R, Rudchenko S, von Bernuth H, et al. IRAK-4- and MyD88-dependent pathways are essential for the removal of developing autoreactive B cells in humans. Immunity 2008 Nov;29(5):746-57.

[163] Lajaunias F, Ida A, Kikuchi S, Fossati-Jimack L, Martinez-Soria E, Moll T, et al. Differential control of CD22 ligand expression on B and T lymphocytes, and enhanced expression in murine systemic lupus. Arthritis Rheum 2003 Jun;48(6):1612-21.

[164] Karassa FB, Trikalinos TA, Ioannidis JP. Role of the Fcgamma receptor IIa polymorphism in susceptibility to systemic lupus erythematosus and lupus nephritis: a meta-analysis. Arthritis Rheum 2002 Jun;46(6):1563-71.

[165] Liang Z, Xie C, Chen C, Kreska D, Hsu K, Li L, et al. Pathogenic profiles and molecular signatures of antinuclear autoantibodies rescued from NZM2410 lupus mice. J Exp Med 2004 Feb 2;199(3):381-98.

[166] Kauppi L, Sajantila A, Jeffreys AJ. Recombination hotspots rather than population history dominate linkage disequilibrium in the MHC class II region. Hum Mol Genet 2003 Jan 1;12(1):33-40.

[167] Yu HX, Chia JM, Bourque G, Wong MV, Chan SH, Ren EC. A population-based LD map of the human chromosome 6p. Immunogenetics 2005 Sep;57(8):559-65.

[168] Chtanova T, Tangye SG, Newton R, Frank N, Hodge MR, Rolph MS, et al. T follicular helper cells express a distinctive transcriptional profile, reflecting their role as non-Th1/Th2 effector cells that provide help for B cells. J Immunol 2004 Jul 1;173(1):68-78.

[169] Kim CH, Lim HW, Kim JR, Rott L, Hillsamer P, Butcher EC. Unique gene expression program of human germinal center T helper cells. Blood 2004 Oct 1;104(7):1952-60.

[170] Zhang X, Schwartz JC, Almo SC, Nathenson SG. Crystal structure of the receptor-binding domain of human B7-2: insights into organization and signaling. Proc Natl Acad Sci U S A 2003 Mar 4;100(5):2586-91.

[171] Stammers M, Rowen L, Rhodes D, Trowsdale J, Beck S. BTL-II: a polymorphic locus with homology to the butyrophilin gene family, located at the border of the major histocompatibility complex class II and class III regions in human and mouse. Immunogenetics 2000 Apr;51(4-5):373-82.

[172] Sansom DM, Manzotti CN, Zheng Y. What's the difference between CD80 and CD86? Trends Immunol 2003 Jun;24(6):314-9.

[173] Hutloff A, Dittrich AM, Beier KC, Eljaschewitsch B, Kraft R, Anagnostopoulos I, et al. ICOS is an inducible T-cell co-stimulator structurally and functionally related to CD28. Nature 1999 Jan 21;397(6716):263-6.

[174] Nguyen T, Liu XK, Zhang Y, Dong C. BTNL2, a butyrophilin-like molecule that functions to inhibit T cell activation. J Immunol 2006 Jun 15;176(12):7354-60.

[175] Arnett HA, Escobar SS, Gonzalez-Suarez E, Budelsky AL, Steffen LA, Boiani N, et al. BTNL2, a butyrophilin/B7-like molecule, is a negative costimulatory molecule modulated in intestinal inflammation. J Immunol 2007 Feb 1;178(3):1523-33.

[176] Christensen SR, Kashgarian M, Alexopoulou L, Flavell RA, Akira S, Shlomchik MJ. Toll-like receptor 9 controls anti-DNA autoantibody production in murine lupus. J Exp Med 2005 Jul 18;202(2):321-31.

[177] Heidari Y, Bygrave AE, Rigby RJ, Rose KL, Walport MJ, Cook HT, et al. Identification of chromosome intervals from 129 and C57BL/6 mouse strains linked to the development of systemic lupus erythematosus. Genes Immun 2006 Oct;7(7):592-9.

[178] Heidari Y, Fossati-Jimack L, Carlucci F, Walport MJ, Cook HT, Botto M. A lupus-susceptibility C57BL/6 locus on chromosome 3 (Sle18) contributes to autoantibody production in 129 mice. Genes Immun 2009 Jan;10(1):47-55.

[179] Carlucci F, Cortes-Hernandez J, Fossati-Jimack L, Bygrave AE, Walport MJ, Vyse TJ, et al. Genetic dissection of spontaneous autoimmunity driven by 129-derived chromosome 1 Loci when expressed on C57BL/6 mice. J Immunol 2007 Feb 15;178(4):2352-60.

[180] Fossati-Jimack L, Cortes-Hernandez J, Norsworthy PJ, Cook HT, Walport MJ, Botto M. Regulation of B cell tolerance by 129-derived chromosome 1 loci in C57BL/6 mice. Arthritis Rheum 2008 Jul;58(7):2131-41.

[181] Bygrave AE, Rose KL, Cortes-Hernandez J, Warren J, Rigby RJ, Cook HT, et al. Spontaneous autoimmunity in 129 and C57BL/6 mice-

implications for autoimmunity described in gene-targeted mice. PLoS Biol 2004 Aug;2(8):E243.

[182] Janitz M, Mitchison A, Reiners-Schramm L, Lauster R. Polymorphic MHC class II promoters exhibit distinct expression pattern in various antigen-presenting cell lines. Tissue Antigens 1997 Feb;49(2):99-106.

[183] Linterman MA, Rigby RJ, Wong RK, Yu D, Brink R, Cannons JL, et al. Follicular helper T cells are required for systemic autoimmunity. J Exp Med 2009 Mar 16;206(3):561-76.

[184] Vinuesa CG, Tangye SG, Moser B, Mackay CR. Follicular B helper T cells in antibody responses and autoimmunity. Nat Rev Immunol 2005 Nov;5(11):853-65.

[185] Vinuesa CG, Cook MC, Angelucci C, Athanasopoulos V, Rui L, Hill KM, et al. A RING-type ubiquitin ligase family member required to repress follicular helper T cells and autoimmunity. Nature 2005 May 26;435(7041):452-8.

[186] Yu D, Tan AH, Hu X, Athanasopoulos V, Simpson N, Silva DG, et al. Roquin represses autoimmunity by limiting inducible T-cell co-stimulator messenger RNA. Nature 2007 Nov 8;450(7167):299-303.

[187] Fazilleau N, McHeyzer-Williams LJ, Rosen H, McHeyzer-Williams MG. The function of follicular helper T cells is regulated by the strength of T cell antigen receptor binding. Nat Immunol 2009 Apr;10(4):375-84.

[188] Handunnetthi L, Ramagopalan SV, Ebers GC, Knight JC. Regulation of major histocompatibility complex class II gene expression, genetic variation and disease. Genes Immun 2009 Nov 5.

[189] Mitchison NA, Mayer W. A survey of H2 gene sequences, including new wild-derived genes. Int J Immunogenet 2007 Feb;34(1):3-12.

[190] Muller-Hilke B, Mitchison NA. The role of HLA promoters in autoimmunity. Curr Pharm Des 2006;12(29):3743-52.

[191] Janitz M, Reiners-Schramm L, Lauster R. Expression of the H2-Ea gene is modulated by a polymorphic transcriptional enhancer. Immunogenetics 1998 Sep;48(4):266-72.

[192] Carson S, Wiles MV. Far upstream regions of class II MHC Ea are necessary for position-independent, copy-dependent expression of Ea transgene. Nucleic Acids Res 1993 May 11;21(9):2065-72.

[193] Baumgart M, Moos V, Schuhbauer D, Muller B. Differential expression of major histocompatibility complex class II genes on murine macrophages associated with T cell cytokine profile and protective/suppressive effects. Proc Natl Acad Sci U S A 1998 Jun 9;95(12):6936-40.

[194] Brunner M, Larsen S, Sette A, Mitchison A. Altered Th1/Th2 balance associated with the immunosuppressive/protective effect of the H-2Ab allele on the response to allo-4-hydroxyphenylpyruvate dioxygenase. Eur J Immunol 1995 Dec;25(12):3285-9.

[195] Hesse M, Bayrak S, Mitchison A. Protective major histocompatibility complex genes and the role of interleukin-4 in collagen-induced arthritis. Eur J Immunol 1996 Dec;26(12):3234-7.

[196] Mitchison NA, Brunner MC. Association of H2Ab with resistance to collagen-induced arthritis in H2-recombinant mouse strains: an allele associated with reduction of several apparently unrelated responses. Immunogenetics 1995;41(4):239-45.

[197] Iwamoto M, Ibnou-Zekri N, Araki K, Izui S. Prevention of murine lupus by an I-E alpha chain transgene: protective role of I-E alpha chain-derived peptides with a high affinity to I-Ab molecules. Eur J Immunol 1996 Feb;26(2):307-14.

[198] Merino R, Iwamoto M, Fossati L, Muniesa P, Araki K, Takahashi S, et al. Prevention of systemic lupus erythematosus in autoimmune BXSB mice by a transgene encoding I-E alpha chain. J Exp Med 1993 Oct 1;178(4):1189-97.

[199] Bohme J, Schuhbaur B, Kanagawa O, Benoist C, Mathis D. MHC-linked protection from diabetes dissociated from clonal deletion of T cells. Science 1990 Jul 20;249(4966):293-5.

[200] Lund T, O'Reilly L, Hutchings P, Kanagawa O, Simpson E, Gravely R, et al. Prevention of insulin-dependent diabetes mellitus in non-obese

diabetic mice by transgenes encoding modified I-A beta-chain or normal I-E alpha-chain. Nature 1990 Jun 21;345(6277):727-9.

[201] Martinez-Soria E, Santiago-Raber ML, Ho L, Moll T, Izui S. Protection of murine systemic lupus by the Ea transgene without expression of I-E heterodimers. J Immunol 2008 Sep 1;181(5):3651-7.

[202] Reinhardt RL, Liang HE, Locksley RM. Cytokine-secreting follicular T cells shape the antibody repertoire. Nat Immunol 2009 Apr;10(4):385-93.

[203] McCausland MM, Yusuf I, Tran H, Ono N, Yanagi Y, Crotty S. SAP regulation of follicular helper CD4 T cell development and humoral immunity is independent of SLAM and Fyn kinase. J Immunol 2007 Jan 15;178(2):817-28.

[204] Busch R, Rinderknecht CH, Roh S, Lee AW, Harding JJ, Burster T, et al. Achieving stability through editing and chaperoning: regulation of MHC class II peptide binding and expression. Immunol Rev 2005 Oct;207:242-60.

[205] Madsen L, Labrecque N, Engberg J, Dierich A, Svejgaard A, Benoist C, et al. Mice lacking all conventional MHC class II genes. Proc Natl Acad Sci U S A 1999 Aug 31;96(18):10338-43.